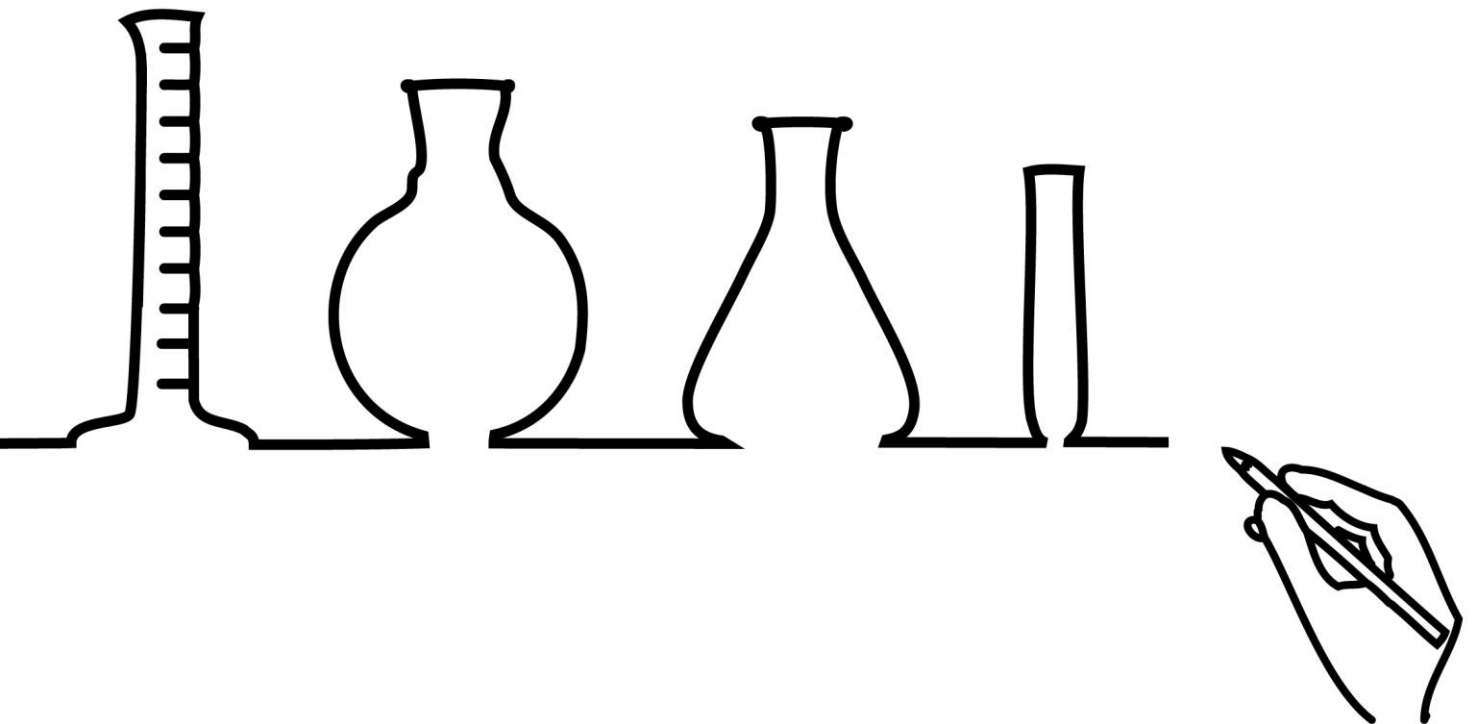




**Faculty of Sciences  
Department of Molecular Biology**

**$\rho$ SM19035:  
dissection of the plasmid  
partitioning machinery**



**Madrid 2014**

**Andrea VOLANTE**





Facultad de Ciencias  
Departamento de Biología Molecular  
Programa de Doctorado en Microbiología

# **pSM19035: dissection of the plasmid partitioning machinery**

–TESIS DOCTORAL–

Memoria presentada para optar al grado de Doctor en Ciencias

**Andrea Volante**

TUTOR ACADÉMICO:

Silvia Ayora

DIRECTOR:

Juan Carlos Alonso

Silvia Ayora

Consejo Superior de Investigaciones Científicas

Centro Nacional de Biotecnología

Madrid, 2014







# Contents

Contents.....	III
Index of Figures.....	VII
Index of Tables .....	IX
Abbreviations.....	XI
Abstract.....	1
Introduction .....	5
<b>1. Low-copy <i>Streptococcus pyogenes</i> pSM19035 plasmid.....</b>	<b>7</b>
1.1. The <i>segA</i> locus maximizes random segregation. ....	9
1.2. The <i>segB</i> loci promote better-than-random segregation. ....	10
1.2.1. The <i>segB1</i> encodes for a toxin-antitoxin system.....	10
1.2.2. The <i>segB2</i> encode for active partition system. ....	12
1.3. The <i>segC</i> locus synchronizes leading and lagging strand replication and avoids a replication fork collapse.....	13
1.4. The <i>segD</i> locus modulates the interplay between copy number fluctuation and plasmid better-than-random segregation.....	13
<b>2. Active partition systems.....</b>	<b>16</b>
2.1. Type I par system.....	18
2.1.1. Bacterial chromosomal par system. ....	21
2.1.2. The pSM19035 <i>par</i> system.....	22
2.2. Type II par system. ....	24
2.3. Type III par system.....	26
<b>3. Repression of transcription initiation in Bacteria.....</b>	<b>26</b>
3.1. Bacterial RNAP. ....	27
3.2. Transcription initiation at bacterial promoter .....	29
3.3. Regulation of Transcription initiation.....	30
3.4. The RHH superfamily of transcription factors .....	31
<b>Objectives.....</b>	<b>37</b>
<b>Materials and Methods .....</b>	<b>41</b>
<b>1. Materials .....</b>	<b>43</b>
1.1. Strains. ....	43
1.2. Plasmids.....	43
1.3. Reagents and Materials.....	47

1.4. Primers.....	49
1.5. Media.....	50
1.6. Buffers.....	50
<b>2. Methods.....</b>	<b>51</b>
2.1. Cells manipulation.....	51
2.1.1. Competent cells production.....	51
2.1.2. Bacterial Transformation.....	51
2.2. Protein purification.....	52
2.2.1. Protein overproduction.....	52
2.2.2. Protein purification.....	53
2.3. DNA manipulation.....	55
2.3.1. DNA isolation and quantification.....	55
2.3.2. DNA electrophoresis.....	55
2.3.3. Radioactive DNA labelling.....	55
2.3.4. Preparation and purification of DNA fragments.....	56
2.3.5. Site-specific mutagenesis.....	56
2.4. <i>In vitro</i> assays.....	56
2.4.1. Non-denaturing and denaturing protein electrophoresis.....	56
2.4.2. Homo- and hetero-oligomeric interactions between proteins.....	58
2.4.3. Limited proteolysis assay.....	58
2.4.4. Peptide mass fingerprinting MS.....	59
2.4.5. Western blotting analysis.....	59
2.4.6. Far western blotting analysis.....	59
2.4.7. Protein and DNA interactions.....	60
2.4.8. Transcription run-off experiment.....	61
2.4.9. ATPase assay.....	62
2.4.10. Electron Microscopy.....	63
2.5. <i>In vivo</i> assays.....	63
2.5.1. Plasmid stability.....	63
2.5.2. $\beta$ -Galactosidase assays.....	64
2.5.3. Fluorescence Microscopy.....	64
<b>Results.....</b>	<b>65</b>
<b>1. Chapter I: The pSM19035 plasmid partition system.....</b>	<b>67</b>
1.1. Molecular characterization of pSM19035 partition system.....	67



1.1.1.	$\omega_2$ protein forms a discrete complex on <i>parS</i> DNA. ....	67
1.1.2.	Protein $\delta_2$ forms diffuse complex on DNA. ....	67
1.1.3.	Proteins $\omega_2$ and $\delta_2$ bind <i>parS</i> DNA forming segresome and bridging complexes. ....	69
1.1.4.	The interaction of $\omega_2$ with $\delta_2$ markedly increases partition complex formation. ....	69
1.1.5.	Interaction of $\omega_2$ with $\delta_2$ discriminates between short–living and long–living partition complexes. ....	70
1.1.6.	Protein $\omega_2$ –bound to <i>parS</i> DNA promotes $\delta_2$ re–localization. ....	71
1.1.7.	Characterization of DNA binding domain of $\delta_2$ . ....	73
1.1.8.	$\delta_2$ – $\omega_2$ interacting domains. ....	84
1.2.	Cytological characterization of pSM19035 <i>par</i> system. ....	91
1.2.1.	Quantification of $\omega_2$ and $\delta_2$ molecules per cell. ....	91
1.2.2.	The $\delta_2$ DNA binding domain and its role in the plasmid stability. ....	92
1.2.3.	Protein $\delta_2$ facilitates plasmid pairing. ....	94
1.2.4.	Protein $\omega_2$ bound to <i>parS</i> stimulates $\delta_2$ disassembles from the nucleoid. ....	95
1.2.5.	Nucleoid bound $\delta$ :CFP <sub>2</sub> capture and tethers plasmid copies. ....	98
1.2.6.	The $\omega_2$ – <i>parS</i> complexes facilitate $\delta_2$ redistribution over the nucleoid. ....	98
<b>2.</b>	<b>Chapter II: Protein <math>\omega_2</math> regulates plasmid copy number, faithful partition and the toxin–antitoxin system. ....</b>	<b>103</b>
2.1.	Molecular characterization of $\omega_2$ transcriptional regulation. ....	103
2.1.1.	RNAP– $\sigma^A$ facilitates $\omega_2$ – <i>P<sub>ω</sub></i> DNA interaction. ....	103
2.1.2.	RNAP– $\sigma^A$ and $\omega_2$ can co–exist at <i>P<sub>ω</sub></i> DNA region. ....	105
2.1.3.	RNAP– $\sigma^A$ does not affect cooperative DNA binding of $\delta_2$ and $\omega_2$ . ....	107
2.1.4.	Protein $\omega_2$ affects <i>P<sub>ω</sub></i> utilization. ....	108
2.1.5.	Protein $\omega_2$ inhibits RNAP– $\sigma^A$ transition from close to open complex. ....	109
2.1.6.	Protein $\delta_2$ does not inhibits RNAP– $\sigma^A$ transition from RP <sub>C</sub> to RP <sub>INIT</sub> complex. ....	112
2.1.7.	Mapping $\omega_2$ –RNAP– $\sigma^A$ domains. ....	113
2.2.	Characterization of $\omega_2$ transcriptional regulation. ....	116
2.2.1.	Protein $\omega_2$ is a functional transcription repressor. ....	116
2.2.2.	Protein $\omega_2$ is functionally active in plasmid partition. ....	117
2.3.	Characterization of $\omega_2$ $\alpha_1$ – $\alpha_2$ domains for the repression of <i>P<sub>ω</sub></i> utilization. ....	117
	<b>Discussion</b> .....	<b>119</b>
<b>1.</b>	<b>The active partition systems of pSM19035. ....</b>	<b>122</b>
1.1.	The role of $\delta_2$ C–terminal region is essential for pSM19035 segregation. ....	122
1.2.	Protein $\omega_2$ interacts with the central domain of $\delta_2$ . ....	125

1.3. Molecular model explaining the pSM19035 plasmid partition system. ....	127
1.3.1. Formation of partition and dynamic complexes (PC1 and DC).....	127
1.3.2. Dynamics of PC, SC and BC formation and disassembly. ....	128
<b>2. The global <math>\omega_2</math> regulator.....</b>	<b>132</b>
2.1. The dual behaviour of the $\omega_2$ regulator.....	133
2.2. Interplay between the regulator and $\beta'$ subunits of RNAP- $\sigma$ . ....	137
<b>Conclusions .....</b>	<b>139</b>
<b>Acknowledgements.....</b>	<b>143</b>
<b>Appendixes.....</b>	<b>147</b>
<b>1. List of Publications.....</b>	<b>149</b>
<b>2. Playing with bioinformatics.....</b>	<b>150</b>
2.1. <i>In silico</i> analysis of $\omega_2$ and $\delta_2$ proteins. ....	150
2.2. <i>B. subtilis</i> RNA polymerase: 3D structure prediction. ....	153
<b>3. Resumen en Castellano. ....</b>	<b>156</b>
3.1. Introducción .....	156
3.2. Objetivos .....	157
3.3. Resultados y Discusión .....	157
3.4. Conclusiones. ....	158
<b>References .....</b>	<b>161</b>

# *Index of Figures*

Figure 1. Genome organization of plasmid pSM19035. ....	8
Figure 2. Genetic organization in plasmids of the <i>inc18</i> family. ....	9
Figure 3. The <i>segB</i> loci. ....	11
Figure 4. Conserved organization of the <i>segD</i> locus. ....	14
Figure 5. The model of copy number control of pSM19035. ....	15
Figure 6. Genetic arrangement of Type I, II and III segregation systems.....	17
Figure 7. Sequence alignment of relevant Walker box ATPases.....	20
Figure 8. Schematic representation of plasmid molecules separation during partition. ....	22
Figure 9. Important structural and functional features of RNAPs. ....	28
Figure 10. Summary of the intermediates in the process of initiation of RNA synthesis.....	31
Figure 11. The structure and DNA binding of ribbon–helix–helix $\omega_2$ protein.....	33
Figure 12. Models of two different nucleoprotein complexes at the DNA operators.....	34
Figure 13. Complexes formed by $\omega_2$ and $\delta_2$ binding to <i>parS</i> DNA. ....	67
Figure 14. The half–life of $\delta_2$ –DNA and $\delta_2$ D60A–DNA complexes.....	68
Figure 15. apo– $\delta_2$ facilitates $\omega_2$ – <i>parS</i> DNA complex formation. ....	70
Figure 16. $\delta_2$ – $\omega_2$ interaction enhances the half–life of the PC.....	70
Figure 17. Protein $\omega_2$ promotes $\delta_2$ redistribution. ....	71
Figure 18. DNase I footprinting shows that $\omega_2$ redistributes $\delta_2$ to form a SC. ....	72
Figure 19. The $\delta_2$ DNA binding domain maps to its C–terminus. ....	74
Figure 20. The conserved $\delta$ C–terminal domain. ....	76
Figure 21. The oligomeric state of $\delta$ mutants.....	77
Figure 22. Stimulation of the ATPase activity of $\delta_2$ variants by $\omega_2$ and <i>parS</i> DNA.....	77
Figure 23. $\delta_2$ variants with decreased binding to <i>parS</i> DNA. ....	78
Figure 24. $\delta_2$ variants with increased binding to <i>parS</i> DNA.....	79
Figure 25. EM visualization of protein–DNA complexes.....	82
Figure 26. Protein $\omega_2$ facilitates the loading of $\delta_2$ K242A onto <i>parS</i> DNA.....	84
Figure 27. A central domain of $\delta_2$ interacts with the $\omega_2$ and with itself. ....	85
Figure 28. The $\delta$ DNA binding domain is not essential for homodimer formation.....	87
Figure 29. The $\delta_2\Delta$ C255 and $\delta_2\Delta$ C227 form heterodimers in presence of $\omega_2$ . ....	88
Figure 30. The $\delta$ DNA binding domain is not essential for interaction with $\omega_2$ .....	89

Figure 31. Subcellular position of $\omega$ :YFP <sub>2</sub> foci in presence or absence of $\delta_2$ or $\delta_2$ D60A. ....	95
Figure 32. Subcellular localization of $\delta$ :GFP <sub>2</sub> or $\delta$ D60A:GFP <sub>2</sub> .....	96
Figure 33. Subcellular localization of $\delta$ :GFP <sub>2</sub> or $\delta$ D60A:GFP <sub>2</sub> foci in presence of $\omega_2$ or $\omega_2\Delta$ N19. .....	97
Figure 34. Subcellular localization of $\delta$ :CFP <sub>2</sub> and $\omega$ :YFP <sub>2</sub> . ....	98
Figure 35. Localization of induced $\delta$ :GFP <sub>2</sub> or $\delta$ D60A:GFP <sub>2</sub> .....	99
Figure 36. Localization of induced $\delta$ :GFP <sub>2</sub> or $\delta$ D60A:GFP <sub>2</sub> in the presence of $\omega_2$ or $\omega_2\Delta$ N19. .....	100
Figure 37. Cooperative binding of $\omega_2$ and RNAP- $\sigma^A$ to $P_\omega$ DNA. ....	104
Figure 38. Protein $\omega_2$ modulate RNAP- $\sigma^A$ to $P_\omega$ DNA.....	106
Figure 39. Cooperative binding of $\omega_2$ and RNAP- $\sigma^A$ to $P_\omega$ DNA. ....	107
Figure 40. RNAP- $\sigma^A$ transcription run-off experiments.....	109
Figure 41. Effect of $\omega_2$ on the formation of a RNAP- $\sigma^A$ -promoter RP <sub>O</sub> /RP <sub>INIT</sub> at $P_\omega$ . ....	110
Figure 42. The regulatory effect of $\omega_2$ on RNAP- $\sigma^A$ -promoter RP <sub>O</sub> at $P_\omega$ .....	111
Figure 43. RNAP- $\sigma^A$ -promoter RP <sub>O</sub> at $P_\omega$ is not affected by $\delta_2$ .....	113
Figure 44. RNAP- $\sigma^A$ retains $\omega_2$ .....	114
Figure 45. Far western blotting of $\omega_2$ , RNAP- $\sigma^A$ .....	115
Figure 46. Dynamics and models of pSM19035 plasmid partition complexes. ....	130
Figure 47. Schematic representation of cellular plasmid partition.....	131
Figure 48 Three-dimensional model of $\omega_2$ and RNAP- $\sigma^A$ bound to $P_\omega$ DNA.....	135
Figure 49. Structure predictions of $\omega$ N-terminal domain.....	151
Figure 50. The predictive docking between $\delta_2$ and the $\omega$ 1-13aa N-terminus. ....	152
Figure 51. The <i>B. subtilis</i> RNAP- $\sigma^A$ -promoter models. ....	153
Figure 52. The model of $\omega_2$ and RNAP- $\sigma^A$ at $P_\omega$ DNA. ....	154

# *Index of Tables*

Table 1. <i>E. coli</i> strains.....	43
Table 2. <i>B. subtilis</i> strains. ....	43
Table 3. Plasmids. ....	43
Table 4. Reactives and Materials .....	47
Table 5. Software and servers. ....	48
Table 6. Oligonucleotides. ....	49
Table 7. Media.....	50
Table 8. Buffers.....	50
Table 9. List of peptides matched to $\delta_2$ . ....	74
Table 10. Structural alignment of $\delta_2$ protein. ....	75
Table 11. Relative binding of $\delta_2$ or $\delta_2$ variants to DNA. ....	80
Table 12. EM data. ....	83
Table 13. Determination of $\omega_2$ and $\delta_2$ molecules per cell.....	91
Table 14. Effect of the pSM19035 Par system on plasmid stability.....	93
Table 15. <i>B. subtilis</i> RNA polymerase sub–units. ....	114
Table 16. The $\beta$ –galactosidase activity of $P_\delta$ . ....	116
Table 17. Plasmid stability ( $\omega_2$ ).....	117



# *Abbreviations*

2D-PAGE	Two-dimensional electrophoresis
aa	Amino acids
Ab	Antibody
AS	Ammonium sulphate
BN-PAGE	Blue Native electrophoresis
BSA	Bovine serum albumin
CBP	centromere binding protein
DAPI	4',6-diamidin-2-phenylindole
DNA	Deoxyribonucleic acid
DNaseI	Deoxyribonuclease I
dNTP	Deoxynucleotide Triphosphate
dPAGE	Denaturing electrophoresis
dsDNA	Double stranded DNA
DSS	Disuccinimidyl suberate, Suberic acid
DTT	Dithiothreitol
EDTA	Ethylene Diamine Tetra Acetic acid
EMSA	Electrophoretic mobility shift assay
FD	Free DNA
FWB	Far-western blotting
h	hour
HTH	<i>Helix turn helix</i>
IPTG	Isopropyl $\beta$ -D-1-thiogalactopyranoside
IR	Inverted Regions
Kb	Kilo-bases
Da	Kilo-Dalton
$K_{Dapp}$	Apparent dissociation constant
LB	Luria-Bertani culture media
MALDI-TOF-MS	matrix assisted laser desorption/ionization-time of flight-mass spectrometry
min	Minutes
MM	Molecular mass
Ni-NTA	Nickel-nitrilotriacetic acid
N-PAGE	Native PAGE
nsDNA	Non-sequence DNA
nt	Nucleotide
NTP	Nucleotide Triphosphate
OD	Optical Density
<i>orf</i>	Open reading frame

## Abbreviations

PAGE	Polyacrylamide gel electrophoresis
Par	Partitioning
pb	Base pair
PBS	Phosphate Buffered Saline
PCR	Polymerase chain reaction
PEI	Polyethyleneimine
ProK	Proteinase K
PVDF	Polyvinylidene fluoride
RHH	<i>Ribbon helix helix</i>
RNA	Ribonucleic acid
RNAP	RNA polymerase core
RNAP- $\sigma^A$	RNA polymerase holoenzyme ( $\sigma^A$ )
RP <sub>C</sub>	RNAP- $\sigma^A$ closed complex
RP <sub>e</sub>	RNAP elongation complex
RP <sub>I</sub>	RNAP- $\sigma^A$ intermediary complex
RP <sub>INIT</sub>	RNAP- $\sigma^A$ initiated complex
rpm	Revolutions per minute
RP <sub>O</sub>	RNAP- $\sigma^A$ open complex
SDS	Sodium dodecyl sulfate
SDS-PAGE	Polyacrylamide gel electrophoresis in presence of SDS
sec	Seconds
ssDNA	Single stranded DNA
TA	Toxin Antitoxin
TAE	Tris-acetate EDTA
TBE	Tris-borate EDTA
TBS	Tris-buffered saline
TEA	Tris-acetate EDTA
Tryp	Trypsin
TTBS	TBS tween 0.5%
WB	Western blotting



## *Abstract*



In Firmicutes, many plasmid-borne resistance genes are genetically linked with the  $\omega$  gene that encodes homodimeric  $\omega_2$  (ParB). Protein  $\omega_2$  is part of the partition system of low-copy-number pSM19035 together with homodimeric  $\delta_2$  (ParA), two or more *parS* sites and the host genome. Promoters of copy number control (*copS* gene) and of functions involved in accurate segregation ( $\delta$ ,  $\omega$ - $\varepsilon$ - $\zeta$  genes) overlap with the *parS* regions.

Protein  $\omega_2$  specifically binds to plasmid-borne *parS* DNA forming a short-lived complex (PC1,  $\omega_2$ -*parS*). In ATP-bound form,  $\delta_2$  is prone to nsDNA binding and mainly interacts with the host nucleoid forming a dynamic complex (DC,  $\delta_2$ -nsDNA). PC1, upon interaction with  $\delta_2$ , undergoes a structural transition that lead to long-lived (PC2, *parS*- $\omega_2$ ) and transient segregation complex (SC, *parS*- $\omega_2$ - $\delta_2$ ) formation.  $\omega_2$ -*parS* complex facilitates either DC positioning at PC2 or its re-location towards DC *in vivo*. The formation of quaternary complex of plasmid pairing/bridging complex (BC, *parS*- $\omega_2$ - $\delta_2$ - $\omega_2$ -*parS*) or plasmid-nucleoid (BC1, *parS*- $\omega_2$ - $\delta_2$ -non-*parS*) mediates direct plasmid positioning without the need of ATP hydrolysis. At stoichiometric  $\omega_2$ : $\delta_2$  ratios,  $\omega_2$ -bound to *parS* DNA facilitates  $\delta_2$  structural transitions that lead to ATP hydrolysis, disassembly from DNA, and unpairing. Cooperative  $\delta_2$  binding to different zones of the nucleoid generates a gradient to direct positioning and partition of the plasmid molecules. The iterative pairing and unpairing cycles may tether plasmids equidistantly on the nucleoid to ensure faithful plasmid segregation by a mechanism compatible with the “diffusion-ratchet” or “DNA relay” mechanisms.

Moreover,  $\omega_2$  binding to the promoter (*P*) of  $\omega\varepsilon\zeta$  operon ( $P_\omega$ ) facilitates cooperative recruitment of *Bacillus subtilis* hole RNA polymerase (RNAP- $\sigma^A$ ) to  $P_\omega$  DNA. Partial occupancy of the  $\omega_2$  operator sub-site increases the rate of isomerization of RNAP- $\sigma^A$  from close (RP<sub>C</sub>) to open complex (RP<sub>O</sub>) formation, and transcription initiation. Conversely, full operator occupancy, which leads to  $\omega_2$  wrapping on a nearly straight  $P_\omega$  DNA, facilitates RP<sub>C</sub> formation but precludes isomerization to RP<sub>O</sub> formation. The two activities of  $\omega_2$ , to act as a transcriptional activator and repressor, require its interaction with the N-terminal domain of  $\beta'$  subunit of RNAP- $\sigma^A$ . The stimulation and inhibition of RP<sub>O</sub> formation, by  $\omega_2$ , defines a poorly characterized mechanism by which  $\omega_2$  control copy number fluctuation, stable segregation of plasmids and indirectly antibiotic resistance genes.



## *Introduction*



## 1. Low-copy *Streptococcus pyogenes* pSM19035 plasmid.

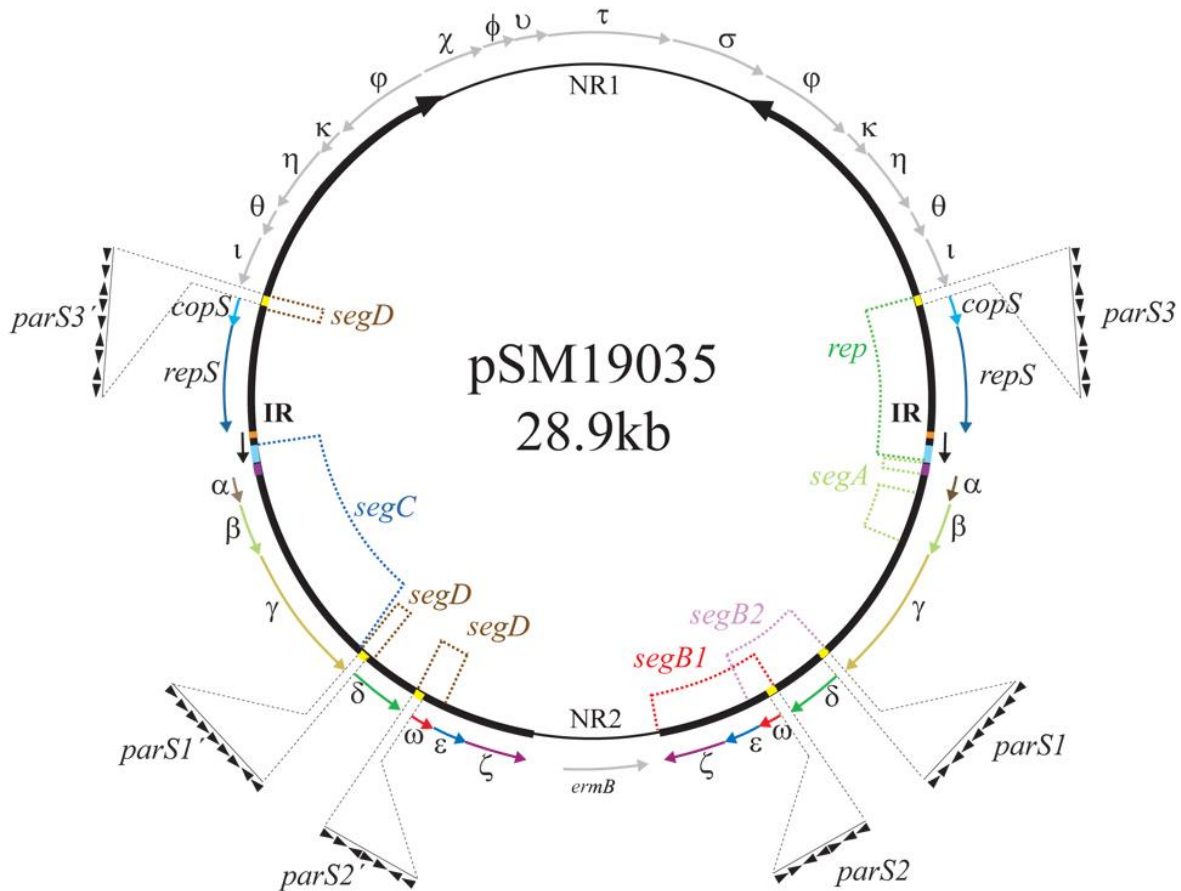
The broad host-range pSM19035 is a middle-size plasmid (~29 kb long) that presents less than 4 copies/cell (Fig. 1). It belongs to *inc18* group. pSM19035 is non-conjugative, but other members of the family mediate the horizontal gene transfer of a large range of antimicrobial resistance genes in Firmicutes (Novick 1987, Brantl, Behnke and Alonso 1990).

The pSM19035 was first isolated from infectious strains of *Streptococcus pyogenes* and it was linked to erythromycin and lincomycin resistance (Malke 1974). Other plasmids belonging to *inc18* group as pIP501 (*Streptococcus agalactiae*) (Horodniceanu et al. 1976), pAM $\beta$ 1, pW9-2, pRE25 (*Enterococcus faecalis*) (Dunny and Clewell 1975, Liu et al. 2013, Schwarz, Perreten and Teuber 2001), pIP186 and pVEF's (*Enterococcus faecium*) (Sletvold et al. 2007, Sletvold et al. 2010) were subsequently isolated and genetically linked to multiple antibiotic resistance genes.

The low-copy-number plasmids of the *inc18* family can be classified in three large groups according their genomic organization: (I) the non-self-transmissible plasmids in which inverted repeated regions (IR) implicated in replication and stable maintenance are separated by non-repeated regions (NR) (e.g. pSM10419, pSM19035 and pSM22095); (II) the non-self-transmissible (e.g. pVEF's) or self-transmissible (e.g. pRE25) plasmids that contains directed repeated (DR) regions separated by long NR segments and (III) the self-transmissible plasmids that neither contain IR nor DR (e.g. pAM $\beta$ 1 and pIP501). The plasmids *inc18* family replicate unidirectionally via the theta or circle-to-circle replication mode (Brantl et al. 1989, Brantl et al. 1990, Bruand, Ehrlich and Janniere 1991, Bruand et al. 1993, Bruand, Ehrlich and Janniere 1995). The low copy has a survival benefit by reducing the metabolic costs that the plasmid imposes on host cells, but by the other hand, it will drastically reduce the chances of plasmids transmission to daughter cells. Except for a few cases, the nucleotide sequences required for plasmid replication and stable segregation are highly conserved in this family (> 92% identity) (Brantl and Behnke 1992a) (see introduction, paragraph 1.4.) (Fig. 2).

Most of the information on the mechanisms of the stable maintenance of plasmids from the *inc18* family comes from studies on pSM19035. A very interesting property of this plasmid is the presence of extraordinarily long IR comprising over 80% of the plasmid genome (Behnke et al. 1979), a single IR contain six different loci (the *rep*, *segA*, *segB1*, *segB2*, *segC* and *segD*) required for the structural and segregational stability of pSM19035 (Volante 2014). The control of plasmid replication is a sophisticated system of ~2 kb in length. It contains the bipartite replication origin (*oriS* and the primosome assembly, *ssiA*), the structural gene (*rep*) that codes for a replication initiation protein (Rep), and genetic information for the control of the *rep gene*

(Cop protein, an antisense RNA [RNAIII] and a *cis-acting* element, see introduction, paragraph 1.4) (Brantl et al. 1990, Brantl and Wagner 1997) (Fig. 1).



**Figure 1. Genome organization of plasmid pSM19035.**

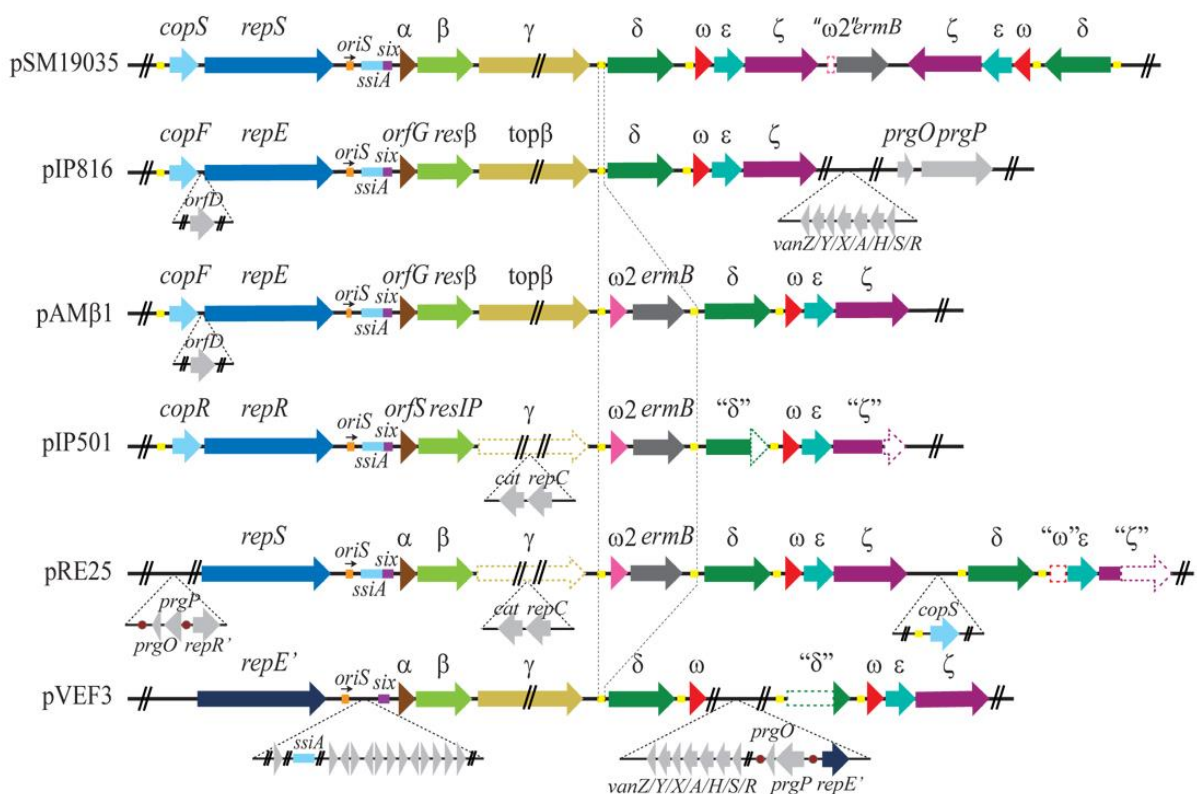
pSM19035 duplicated sequences (IR) are indicated by thick arrows and the unique NR1 and NR2 regions by thin lines. The upstream region of the promoters of the *copS*,  $\delta$  and  $\omega$  genes, which constitute the six *cis-acting* centromere-like *parS* sites (yellow boxes), are blown up. A *parS* site consists of a variable number of contiguous 7-bp heptad repeats (iterons) symbolized by  $\blacktriangleright$  (in direct) or  $\blacktriangleleft$  (invert orientation), and the number of repeats and their relative orientations are indicated. The colored outer thin arrows indicate the organization of the genes. For the sake of simplicity, the *rep* and *seg* loci are indicated only once although they are repeated twice. The leading strand replication origin (*oriS*, orange), the lagging strand replication origin (*ssiA*, light blue), the six sites (violet boxes), and the direction of replication (black arrows) are denoted. The plasmid region involved in replication is marked as *rep* (involving *CopS*, *RepS*, and *oriS* and *ssiA*). The regions involved in stable segregation are five: *segA* ( $\beta_2$  and six sites), *segB1* ( $\epsilon_2$  and  $\zeta$ ), *segB2* ( $\delta_2$ ,  $\omega_2$  and six *parS* sites), *segC* ( $\alpha$ ,  $\beta_2$ ,  $\gamma$  and *ssiA* and six sites) and *segD* ( $\omega_2$  and the  $P_{cop}$ ,  $P_\delta$  and  $P_\omega$  sites [denoted as yellow boxes]). The figure was taken from Volante et al, 2014 and modified.

Despite its low-copy-number, the pSM19035 is >100,000-fold more stable than expected for random segregation, revealing the presence of discrete regions outside the minimal replicon that contribute to the stabilization of the plasmid (*seg* loci). Three of them are systems directly involved to stable maintenance of low-copy numbers plasmids (*segA*, *segB1* and *segB2*). Another one processed the replication intermediates (*segC*) and two systems coordinate copy-number control, random segregation (*segD* and *segA*). The interplay between the different *seg* loci facilitates the separation of sister plasmids (Volante 2014).



### 1.1. The *segA* locus maximizes random segregation.

The *segA* locus encodes only the  $\beta$  gene and two inversely oriented *six* sites. The  $\beta$  protein, as a dimer ( $\beta_2$ ), is site-specific recombinase belonging to resolve/invertase family that show high levels of sequence identity (>91%) (Lioy et al. 2010a). The purified protein  $\beta_2$  acts as a repressor of its own synthesis and its role is essential in plasmid maintenance because catalyses the resolution of high order oligomers to monomers upon binding to 90 bp sites (*six*) (Rojo and Alonso 1994). The multimer resolution system (MRS) is important especially in the low-copy number plasmids because it will maximize the distribution of copies and consequently facilitate the efficiency of “passive” segregation of plasmids to daughter cells. Indeed, this system was demonstrated to stabilize the plasmid ~5-fold, (Ceglowski et al. 1993).



**Figure 2. Genetic organization in plasmids of the *inc18* family.**

The genomic organization at the *rep* and *seg* loci of the relevant pSM19035, pAM $\beta$ 1, pIP501, pRE25 and pVEF3 (as representative of the pVEF's series) plasmids is shown schematically. The conserved color code indicates that the gene products are highly conserved (> 89 % identity) within the family. The quotation marks surrounding a gene denote that this gene contains deletions and/or point mutations. Vertical broken lines link similar *parS* (light yellow boxes) sites. A double bar indicates that the corresponding gene/region is out of scale. In pRE25, the putative centromere sites of the second *par* system (*segE*) are indicated as brown circles. Genes are shown to scale. The figure was taken from Volante et al, 2014.

## 1.2. The *segB* loci promote better-than-random segregation.

The *segB* loci of pSM19035 assure better-than-random plasmid distribution. The region, encompassing the  $\delta$ ,  $\omega$ ,  $\varepsilon$ , and  $\zeta$  genes was further sub-divided in two discrete locus, *segB1* and *segB2* (Fig. 3) to distinguish between the partition and the toxin-antitoxin highly conserved systems in the *inc18* family plasmids (Fig. 2).

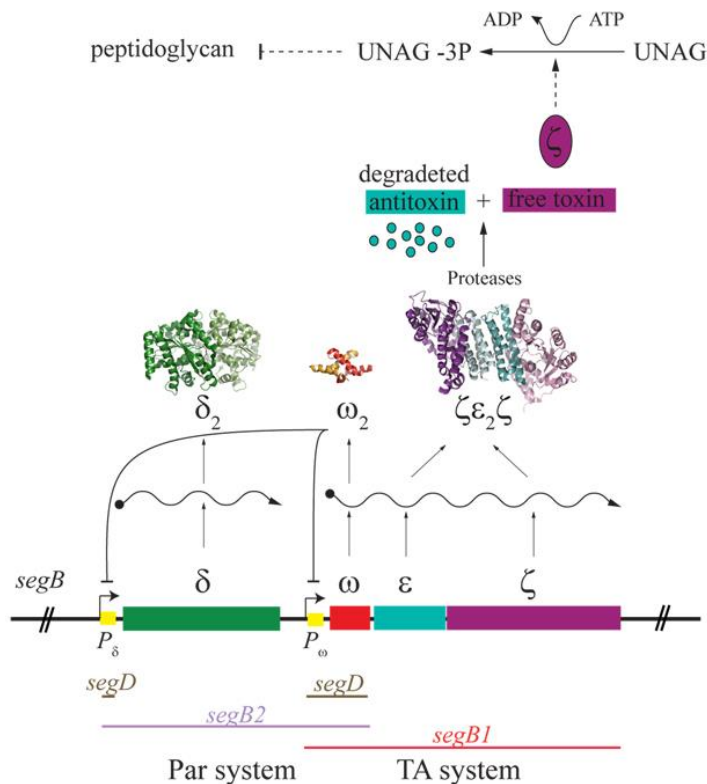
### 1.2.1. The *segB1* encodes for a toxin-antitoxin system.

Plasmid-encoded toxin-antitoxin (TA) systems participate in plasmid stabilization by a mechanism denoted as post-segregational killing (PSK). This relies on the difference in stability of the toxin and the antitoxin. The antitoxin interacts with the toxin and inactivates it. Cells that do not receive a plasmid copy during cell division stop its proliferation by the action of the free toxin, because the antitoxin is short living and cannot inactivate the toxin for long time. The overproduction of a toxin will not always result in cell death, but may lead instead to cell stasis as demonstrated for RelE or MazF toxin (Pedersen, Christensen and Gerdes 2002).

The *segB1* locus encodes a TA system. Three proteins compose the TA operon of pSM19035: the  $\omega_2$  global regulator, the  $\varepsilon_2$  labile antitoxin and the stable  $\zeta$  toxin. Indeed, the  $\varepsilon$ - $\zeta$  TA system stabilizes the plasmid >10,000-fold, by inhibiting the proliferation of plasmid-free cells (Ceglowski et al. 1993, Lioy et al. 2006).

Based on the molecular nature of the antitoxin and its mode of interaction with the toxin the TA modules are currently grouped into five classes (Unterholzner, Poppenberger and Rozhon 2013). According the new classification, *segB1* locus encodes for a genuine type II TA system present in the entire *inc18* group (Fig. 2 and 3) (Lioy et al. 2010a). Interesting, this TA system was also found in the chromosome of *S. pneumoniae* (known as PezAT) (Khoo et al. 2007) as well as in the chromosome of many bacteria of the *Enterococcus* genus. The *inc18* TA system is genetically linked to antibiotic resistance genes and facilitates the spread of the resistance to vancomycin, methicillin, gentamycin, erythromycin, linezolid, glycopeptide, and the multiresistant *cfr* locus among enterococci and staphylococci (Moritz and Hergenrother 2007, Zhu et al. 2008, Sletvold et al. 2008, Sletvold et al. 2010, Liu et al. 2013, Rosvoll et al. 2012). These genetic linkage was attributed to the plasmid-borne  $\zeta$ - $\varepsilon$  TA module. Unlike the majority of TA systems that are autogenously controlled, the expression of the  $\omega$ - $\zeta$ - $\varepsilon$  locus is regulated by the  $\omega_2$  transcriptional regulator (a 71 residues long peptide), which senses it, and also any decrease in plasmid copy number (*segD* locus, see introduction, 1.4.). The super-family of  $\zeta$  toxins are among the most abundant in bacteria of the Firmicutes Phylum (Leplae et al. 2011). So far, the mode of action produced by  $\zeta$  toxins is contended between bacteriostatic (Lioy et al.

2006, Lioy et al. 2012) or bactericide effects (Zielenkiewicz and Ceglowski 2005, Mutschler and Meinhart 2011).



**Figure 3. The *segB* loci.**

The Par system, composed by  $\delta$  (green) and  $\omega$  (red) genes, takes part in the active partitioning of pSM19035 before cell division. Whereas the  $\zeta$  (purple) and  $\epsilon$  (cyan) TA system, that is transcribed in the same operon  $\omega$ - $\epsilon$ - $\zeta$  with the antitoxin gene preceding the toxin gene, actuates as post-segregational control inhibiting the growth of plasmid-free descendent cells. Indeed, the Lon, ClpXP or ClpXA proteases usually degrade labile protein antitoxins and the toxin is free to phosphorylate the UNAG leading to unreactive UNAG-3P. The MurA does not recognize the UNAG-3P as substrate and the peptidoglycan biosynthesis is stopped. The *segD* locus has a central role by regulating the transcription of both systems. Genes are shown to scale.

The plasmid- or chromosomal-borne  $\zeta$ - $\epsilon$  TA complex consists of two monomeric long-living  $\zeta$  toxins (half-life ~80 min) separated by a dimeric short-living  $\epsilon$  ( $\epsilon_2$ ) antitoxin (half-life ~16 min) (Meinhart et al. 2001, Meinhart et al. 2003). The TA module is composed of two single molecules of toxin  $\zeta$  that are neutralized by the binding to antitoxin dimer  $\epsilon_2$  ( $\zeta\epsilon_2\zeta$ ) (Fig. 3). Toxin  $\zeta$  free in solution inhibits the first step of peptidoglycan biosynthesis by phosphorylating the 3'-OH group (3P) of the amino sugar moiety of uridine diphosphate-N-acetyl glucosamine (UNAG), leading to the accumulation of a fraction of unreactive UNAG-3P and thereby directly affecting the cell wall synthesis (Mutschler et al. 2011) (Fig. 3). Conditions that prevent  $\epsilon$ - $\zeta$  genes expression or promote the antitoxin  $\epsilon_2$  degradation, by the LonA and/or ClpXP protease, permit  $\zeta$  toxin to act freely to block cell proliferation in the large majority of the cells (Camacho et al. 2002, Lioy et al. 2006, Lioy et al. 2010b). At early times of expression, free  $\zeta$  or  $\zeta$ Y83C (a short-living variant with a half-life of ~28 min) also triggers a heterogeneous set of secondary responses that alter the expression of about 2% of total genes. In this step the expression of essential genes involved in cell membrane synthesis decrease, the expression of *relA*, as well as the synthesis of (p)ppGpp, increases and the GTP pool decreases (Lioy et al. 2006, Lioy et al. 2010b). The stable  $\zeta$  toxin induces a reversible inhibition of cell proliferation. At a later stage,  $\zeta$

decreases the macromolecule synthesis (DNA replication, RNA transcription and protein translation), the intracellular pool of ATP and inhibits the cell wall biosynthesis. A small fraction (20–30%) of the cell population can be stained with propidium iodine an indicator of cell death (Lioy et al. 2012). Subsequent expression of the  $\epsilon_2$  antitoxin specifically reverses  $\zeta$ -induced dormancy (Lioy et al. 2006). Although the TA system is the ultimate stabilization function of pSM19035, some cell escapes from its control: a subpopulation of cells shows a non-inheritable  $\zeta$  toxin tolerance with a frequency of 1 to  $5 \times 10^{-5}$  (Lioy et al. 2012). These cells are genetically insensitive to toxin action; hence, with this frequency, plasmid loss might occur. For this reason a further mechanisms as plasmid partitioning system are often present in concern with the TA systems.

### **1.2.2. The *segB2* encode for active partition system.**

In eukaryotic cells, the microtubule-based mitotic spindle apparatus that guides the separating chromosomes to different ends of the dividing cell drives chromosome segregation (McIntosh 2012). In contrast, how chromosome separation occurs in bacteria or plasmids is not well understood. Low-copy plasmids rely on a partitioning system to distribute newly replicated plasmids into the two nascent daughter cells (Nordstrom and Austin 1989, Ebersbach and Gerdes 2005). Accurate distribution of a newly replicated genome to daughter cells at cell division is a precise process; however, this process is prone to occasional error or inactivation of the system by spontaneous mutations. The plasmid partition ensures that each daughter cell receives at least one copy of the plasmid DNA by directing the active segregation of the plasmids to either side of the cell centre prior to cell division (Szardenings, Guymer and Gerdes 2011). The *segB2* locus encode for a genuine active partition system (*par*) that comprises two trans-acting proteins ( $\delta_2$  ATPase, and  $\omega_2$  acting as a centromeric binding protein, CBP) and six *parS* sites (see introduction, paragraph 2.1.2.) (Ceglowski et al. 1993, de la Hoz et al. 2000, de la Hoz et al. 2004) (Fig. 3). Interestingly, the *segB2* locus stabilizes the plasmid ~50-fold (Pratto et al. 2008). Some members of the *inc18* family encode a second ParAB-like system (*segE* locus). The *segE* locus (Figure 2, pIP816, pRE25 and the pVEF's series) comprises two *trans-acting* proteins (the putative PrgP ATPase, and the PrgO CBP), and two *cis-acting parS* sites, located upstream and downstream the *PrgPO* operon (Schwarz et al. 2001, Sletvold et al. 2008) (Fig. 2). The analysis of this *segE* locus, the mechanisms that underlie segregation of plasmids with two genuine partition systems (*segB2* and *segE*), and the interplay between them remains to be characterized.

### 1.3. The *segC* locus synchronizes leading and lagging strand replication and avoids a replication fork collapse.

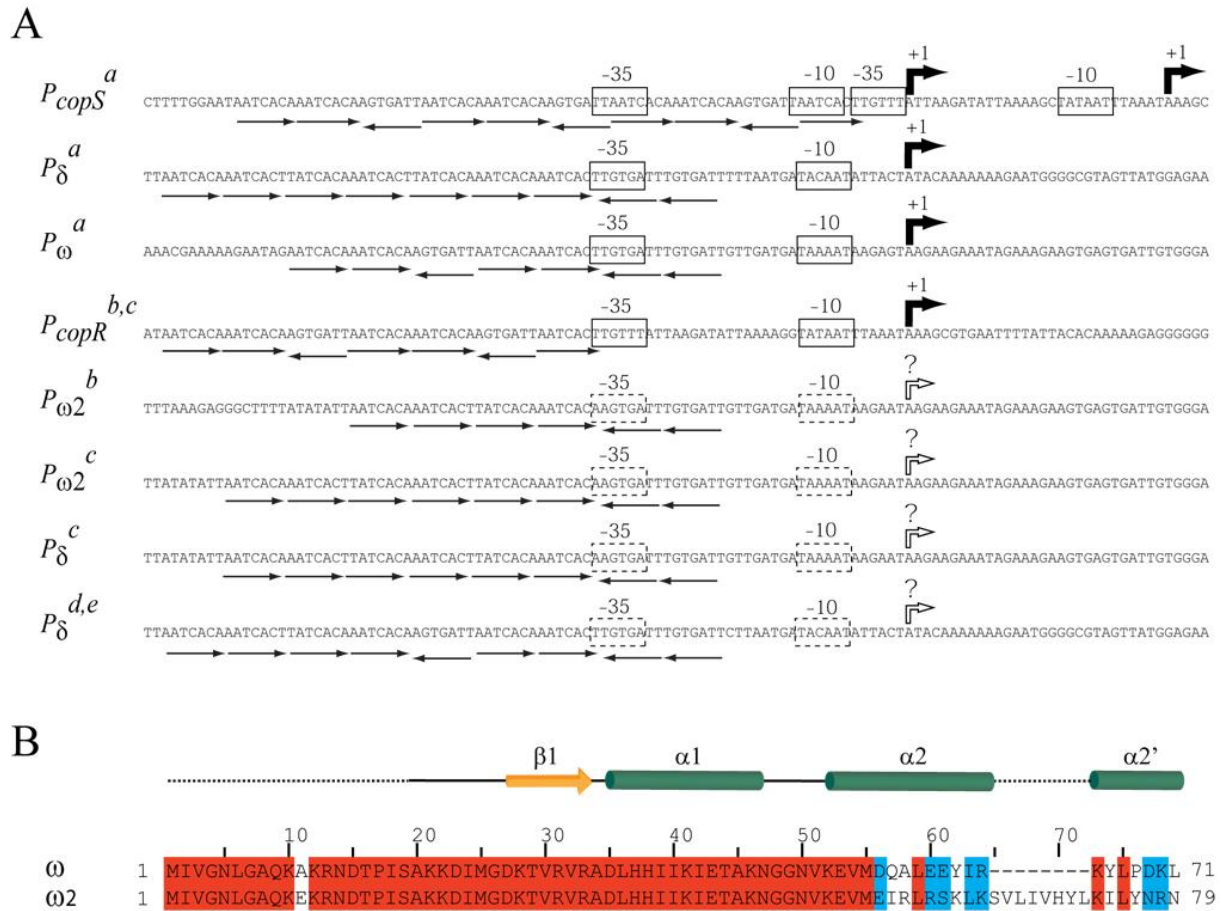
The *segC* locus comprises three trans-acting products ( $\alpha$ ,  $\beta$  and  $\gamma$  genes) and two *cis-acting* regions (*ssiA* and *six* sites). Open reading frame  $\alpha$  is conserved, but its nucleotide sequence has relative low levels of identity (<45%) among the *inc18* family (Lioy et al. 2010a). The function of *orfa*, which has different names (*orfG*, *orfS*, etc., among the group Fig. 2), is still unknown. The role of  $\beta_2$ , as site-specific recombinase, was briefly described as constituent of *segA* locus. Downstream of the  $\beta$  gene lays the  $\gamma$  gene that encodes for a type I topoisomerase. The product of recombination step is a catenate plasmid molecule that has to be unlinked by the  $\gamma$  protein.

The recombinase in concert with  $\gamma$  has a control over the replication of the plasmid, by mediating the process of inversion of DNA necessary to avoid collision being two replication forks moving in opposite direction initiated at the two inversely oriented *oriS* region. The topoisomerase  $\gamma$  may also contribute to decatenate the resolution products by acting at the single-stranded DNA present at the origin region as proposed in previous studies (López Torrejón 2002). It was observed that pAM $\beta$ 1 putative topoisomerase (top $\beta$ ) was dispensable for plasmid replication; nevertheless, the presence of DNA topoisomerase genes in plasmid genomes suggests a specific function(s) that cannot be fully accomplished by the host cell enzymes. In the absence of  $\gamma$ , a host-encoded topoisomerase should be responsible for resolving catenated plasmids (Bidnenko et al., 1998).

### 1.4. The *segD* locus modulates the interplay between copy number fluctuation and plasmid better-than-random segregation.

As previously introduced, the almost absolute plasmid stability of pSM19035 conferred by the *segA*, *segB1*, *segB2* and *segC* loci is achieved by the *segD* locus. The *segD* locus comprises the  $\omega_2$  transcriptional repressor and its cognate sites upstream the promoter regions of the *cop* ( $P_{copS}$ ),  $\delta$  ( $P_\delta$ ) and  $\omega$  ( $P_\omega$ ) genes (also termed *parS1* to *parS3* sites) that coordinate copy number fluctuation and better-than-random segregation function (de la Hoz et al. 2000)(Fig. 4A).

The sophisticated interplay between these functions not only stabilizes the plasmid but also contributes to minimize the metabolic cost to the host cell (Volante 2014). At present, the action of *segD* on pIP501 copy-number control has been inferred, but a sequence comparison of the replication and segregation regions of plasmids of the *inc18* family are >92% identical on the nucleotide level and reveal the same modular structure (*cop*, RNA III, *rep*) (Fig. 2)(Brantl and Behnke 1992b). Therefore, copy number control will occur in all *inc18* family plasmids similarly and at four levels (Fig. 5).

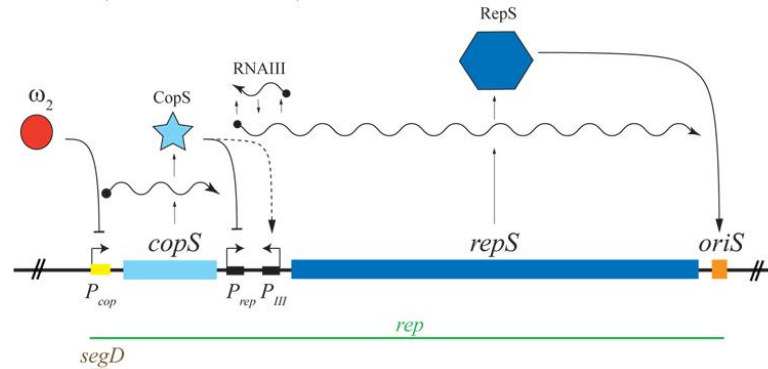


**Figure 4. Conserved organization of the *segD* locus.**

(A) The  $P_{copS}$ ,  $P_{\delta}$  and  $P_{\omega}$  regions of plasmid pSM19035<sup>a</sup>,  $P_{copR}$  or  $P_{copF}$  of pIP501<sup>b</sup> or pAM $\beta$ 1<sup>c</sup>,  $P_{\omega 2}$  of pIP501<sup>b</sup> or pAM $\beta$ 1<sup>c</sup>,  $P_{\delta}$  of pAM $\beta$ 1<sup>c</sup>, pRE25<sup>d</sup> and pVEF3<sup>e</sup> are indicated. The variable number of contiguous 7–bp heptad repeats (iterons), and their relative orientations ( $\rightarrow$  or  $\leftarrow$ ) are shown. The  $P_{\omega}$  region is highly conserved among plasmids of the *inc18* family. (B) Sequence alignment of the transcriptional repressors  $\omega$  and their highly relative  $\omega 2$ . The alignment was done using Clustal W2 and visualized using Jalview v 14.0. The identity residues and conserved are highlighted in red and blue respectively. The figure was taken from Volante et al, 2014.

Two negative regulators, Cop and RNAIII, and an IR structure limit the amounts of *repS* mRNA coding for the initiation protein, RepS (Brantl and Wagner 1994). Cop as a dual activity: it directly represses transcription of the *rep* mRNA by binding to its cognate site (Brantl and Wagner 1997), and it prevents convergent transcription from sense  $P_{rep}$  and antisense  $P_{III}$ , thereby indirectly increasing the amount of RNA III. The stable antisense RNA (RNA III) induces transcriptional attenuation within the leader region of *rep* mRNA (Heidrich and Brantl 2007). Deletion of one of the negative regulators (Cop or RNA III) causes a 10– to 20–fold increase in plasmid copy number, and a simultaneous deletion has no additive effect (Brantl and Behnke 1992a). The fourth element is  $\omega 2$ , it represses the levels of Cop and indirectly increases the supply of the *rep* mRNA (de la Hoz et al. 2000). In the presence of low levels of Cop, the levels of *rep* mRNA increases 20–fold (Brantl and Wagner 1994). Thus,  $\omega 2$ –mediated down regulation of Cop and indirectly it will increase the transcription of the *rep* (de la Hoz et al.

2000). Indeed, repression of Cop synthesis by  $\omega_2$  correlates with an increase in plasmid copy number and indirectly ensures stable plasmid maintenance. It is likely that the interplay of RNA III, Cop and  $\omega_2$  are part of a negative feedback control system of the minimal replicon of *inc18* plasmids.



**Figure 5. The model of copy number control of pSM19035.**

The promoters ( $P$ ) (small boxes), the replication origin *oriS* (orange box), the genes (rectangles), the mRNAs (wavy lines), CopS (cyan star), RepS (blue hexagon) and  $\omega_2$  (red ovals) are represented. The negative effect in plasmid replication by CopS is exerted at  $P_{rep}$  promoter, at the same time, CopS permits the increase the transcription of RNAIII. The negative regulation by RNAIII is induced by transcriptional attenuation of RepS. Genes are shown to scale. The figure inspired by Brantl S. and Wagner, E.G. (1997) was modified and adapted to pSM19035.

Protein  $\omega_2$  also regulates spatially and temporally transcription initiation at  $P_\delta$  and  $P_\omega$  and reduces the level of both  $\delta_2$  (ParA) and  $\omega_2$  (ParB) proteins required for active partitioning (de la Hoz et al. 2000, Pratto et al. 2008) (Fig. 4B and Fig. 5). In normal growing cells, the decrease in  $\omega_2$  concentrations results in a rapid increase in  $\delta_2:\omega_2$  ratios. Free  $\delta_2$  will bind, in a sequence independent manner, to chromosomal DNA serving as diffusion-ratchet for plasmid, however, any unbalanced  $\delta_2:\omega_2$  ratio markedly reduces the segregation stability of the plasmid (Pratto 2007). Protein  $\omega_2$  by repressing transcription initiation at  $P_\omega$  also regulates the expression of the  $\epsilon_2$  and  $\zeta$  proteins (Camacho et al. 2002, Meinhart et al. 2003, Liroy et al. 2006). When  $\omega_2$  is present at low levels, an increase of TA ratios that exceed a threshold value occurs in the cell. Any stochastic decrease of short half-living  $\epsilon_2$  antitoxin will indirectly raise the  $\zeta$  toxin that freely leads to a halt in cell proliferation. To overcome these disadvantages plasmid copy-number increases. Moreover, plasmids of the *inc18* family with RI encode for two copies of  $\omega$  gene (e.g., pSM19035, pRE25, pVEF3 with 100% identity among them). Those plasmids that encode for *ermB* also code for  $\omega_2$  protein (a 79 residues long peptide) (e.g., pIP501, pAM $\beta$ 1, pRE25) (Fig. 2 and Fig. 4B). The  $\omega_2$  gene is invariantly located upstream of the *ermB* gene (Volante 2014). Interesting, a fragment of last 26 codon of  $\omega_2$  was detected upstream of the *ermB* gene also in pSM19035. The genetic linkage between  $\omega_2$  and the erythromycin resistance

cassette remains to be unravelled, but suggests that both genes should be present in a common ancestor. The role of the *segD* locus in the spread of the *ermB* cassette is poorly understood.

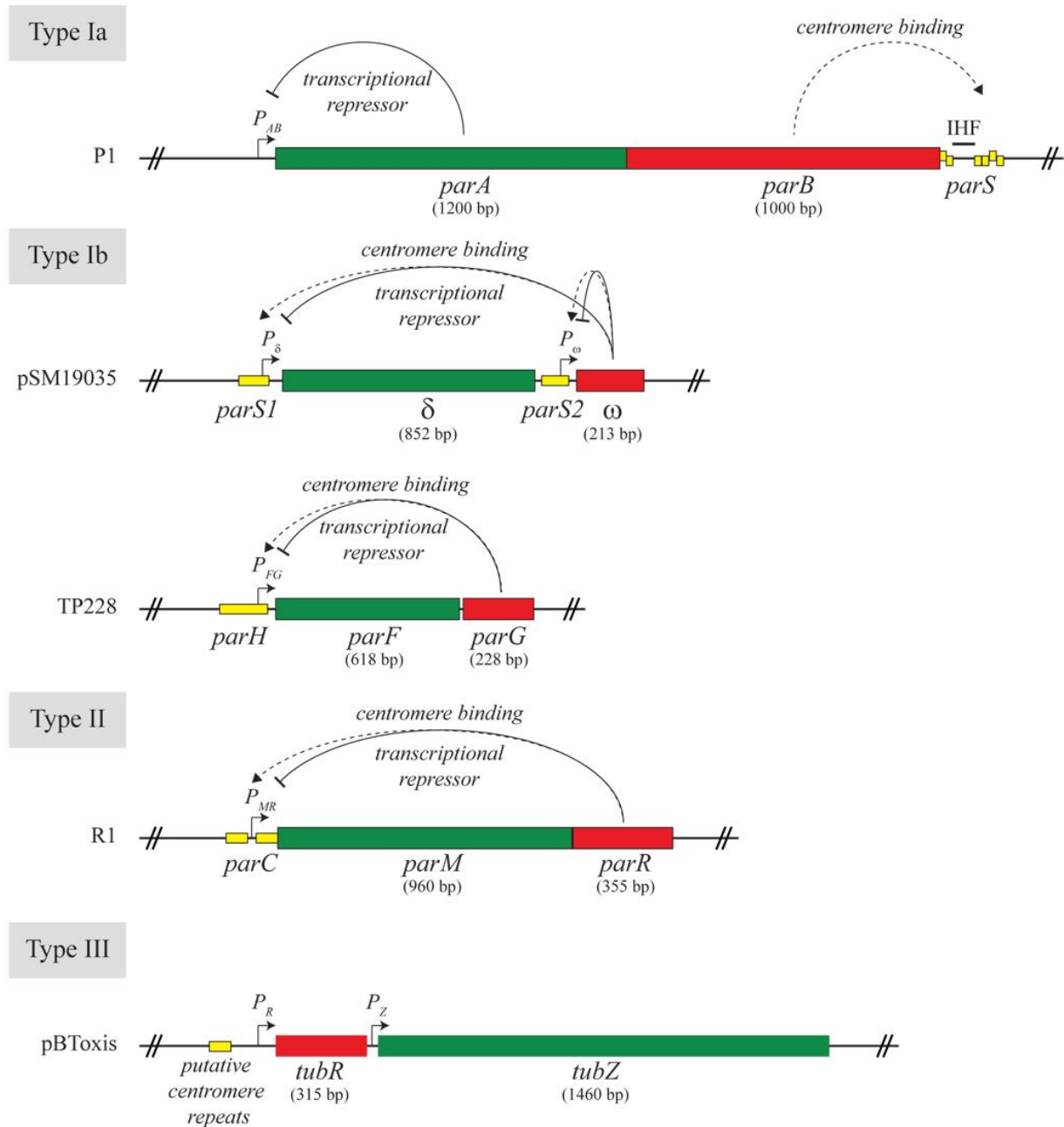
## **2. Active partition systems.**

Several mechanisms ensure that plasmids are stably maintained at a constant copy number within the host bacterial cells and are transmitted to the following generations (Salje 2010). High copy number plasmids, generally smaller than 10kbp that have 10 to 100 copies per cell, appear not to code for partition systems and their stable inheritance must be assured by the high number of copies of the plasmid molecules. The lack of partition systems led to the idea that they segregate by diffusing randomly through the cytoplasm, and the high number of copies was enough to ensure that every daughter cell receives at least one plasmid molecule (Durkacz and Sherratt 1973). While low copy number plasmids, to ensure their segregation, code for mechanisms that actively mediate the partition of the molecules among daughter cells.

In fact, on the basis of random segregation, the probability of plasmid-less cell appearance is  $2^{1-n}$  (where  $n$  is the plasmid copy number) (Summers 1991), what means that a plasmid existing in two copies per cell and lacking *seg* loci has a 50% chance of being inherited by the host progeny (as in the case of pSM19035). During evolution, plasmids have acquired or developed a number of features ensuring their stable maintenance in bacterial populations, to counteract the rule of copy number related loss-rate.

The use of an “*active*” partition system is the approach usually adopted by bacteria and low-copy plasmids for a stable maintenance. In eukaryotic cells, chromosome segregation is driven by the microtubule-based mitotic spindle in a process for which there is considerable mechanistic understanding (McIntosh 2012). In bacteria, plasmids coding for systems resembling the eukaryotic segregation machinery were also described: the type II (ParMR, ParM been an ATPase protein related to actin/hsp70 superfamily) and the type III (TubZR, TubZ been a tubulin-like GTPase related to the FtsZ/tubulin family) systems (Funnell 2005, Ebersbach, Sherratt and Gerdes 2005). The majority of plasmids and the bacterial chromosomes carry a partition locus of the ParAB type (Funnell 2005, Ebersbach et al. 2005). Much less is known in about the molecular basis of the ParAB system.





**Figure 6. Genetic arrangement of Type I, II and III segregation systems.**

The arrangement of representative Type Ia (P1 plasmid), Ib (pSM19035 and TP228), Type II (R1 plasmid) and Type III (pBTaxis plasmid) are shown. Plasmid names are given on the left and motor, centromere-binding protein and centromeric sites are given in red, green and yellow respectively. Binding of proteins to centromere and promoter regions is indicated. Genes are shown to scale with the size indicated below. *IHF* = Integration Host Factor binding site. The figure inspired by Saje J. (2010) was modified and adapted for this work.

The plasmid *par* systems studied to date require only three elements: a centromere-like region (*parS*), a DNA-binding adaptor protein (CBP), and a nucleotide-binding motor element that provides the force for plasmid movement. The Walker-type ParAB partition system requires the involvement of chromosomal DNA as the fourth elements. Moreover, they are also organized in operons or cassettes that can be easily moved from one plasmid to another without loss of functionality (Ebersbach and Gerdes 2005). Three major class of partitioning systems have been

classified based primarily on the type of NTPase present (Gerdes, Howard and Szardenings 2010).

The multiple *par* cassettes belonging to the three classes have been found and described from very diverse bacteria (Gerdes, Moller-Jensen and Bugge Jensen 2000), but most of them have very similar genetic organizations: the upstream gene in the operon usually encode for the motor proteins, whereas the downstream gene encodes the centromere-binding protein (Fig. 6). The centromere-like site is located either upstream or downstream of the *par* genes. These *cis-acting* centromeric regions are usually composed of repeated (in direct or inverted orientation) sequences. The single repeat length might vary from several to dozens of nucleotides repeated. Although only a single centromere site seems to be sufficient for partitioning (Williams, Macartney and Thomas 1998), in some plasmids multiple centromere sites were found scattered through the genomes (e.g. pSM19035).

All partition operons need to be auto-regulated at the transcriptional level. This function is carry out by the CBPs in the types Ib, II and III systems, and the NTPase in the type Ia systems (Fig. 6). Notably, the sequence and structures of CBPs are very divergent and only few domains for each type of partition system seem to be conserved. In fact, the CBP proteins of type Ia are larger and middle (182–336 residues) size CBPs than those encoded by Ib, II and III systems (46–113 residues). The large plasmid-encoded and middle size chromosomal-encoded CBPs contain the DNA-binding Helix-Turn-Helix motif (HTH). The small CBPs analysed so far, are much more variable in the primary amino acids sequence although structurally they are Ribbon-Helix-Helix (RHH) type proteins, with the  $\beta$ -strands from two monomers contacting the DNA major groove (Schreiter and Drennan 2007) (see introduction, paragraph 3.4.). A common feature of CBPs is the ability to bind to DNA repeats as a dimer (or oligomers), in the centromere to form large nucleoprotein complexes (segrosomes). This interacts with the motor stimulating the hydrolysis of the NTPs and producing the DNA movement to opposite poles of the cell such that each new daughter cell contains at least one plasmid upon cell division.

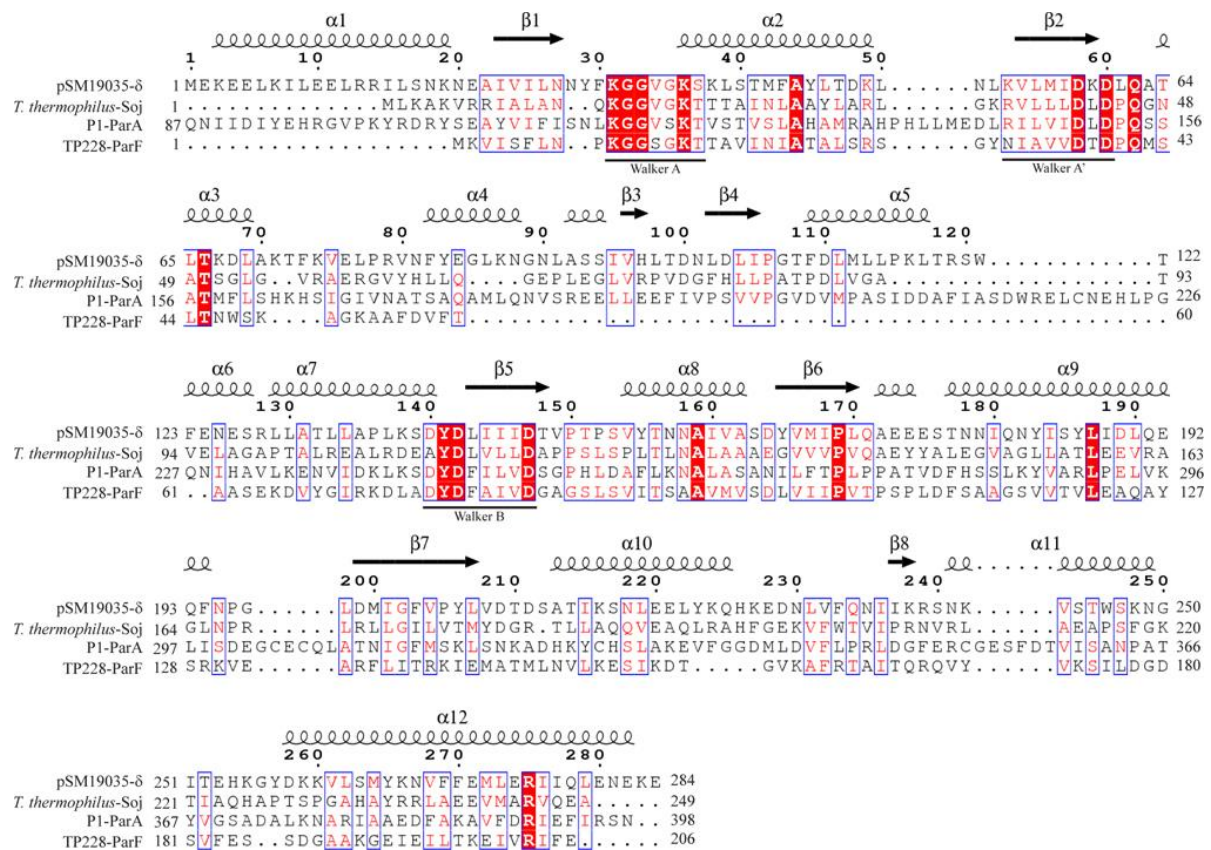
### **2.1. Type I *par* system.**

The type I of segregation system, the most prevalent class in the microbial world, contains an ATPase motor protein that belongs to the ParA/MinD family, an important group of proteins that are involved in divisome, chemotaxis or DNA partition machineries positioning and assembly (Lutkenhaus 2012).

The ParAB systems are sub-divided in two subfamilies (type Ia and Ib) based on the size or structure of the ParA ATPases and genetic organization of *par* operon. In both type the gene for

the Walker-type ATPase is located upstream of that for the CBP. However, the location of the centromere site differs: for the type Ia systems, the centromere-like sites are located downstream of *par* operon, whereas in the type Ib the centromere is found upstream and/or downstream the operon (Fig. 6). The ParAB of P1 and F for the type Ia and those of pSM19035, TP228 and pB171 are the best-studied plasmid partitioning systems up to date. The ParB proteins have not significant sequence identity or similarity between the type Ia and Ib.

The ParA-Ia proteins (e.g., P1-ParA or F-SopA; 251–420 residues) are characteristically larger than ParA-Ib plasmid encoded (e.g., TP228-ParF, pB171-ParA, pSM19035- $\delta_2$ ; 208–289 residues) and chromosomal encoded (ParA or Soj; 253–351 residues) (Bignell and Thomas 2001). The type Ia of ParA presents an extended N-terminal region of about 100 residues that contains a helix-turn-helix (HTH) DNA-binding motif. In fact, the ParA-Ia has two DNA binding characteristics: the binding of ATP without hydrolysis enables ParA·ATP\* to bind non-specific (ns) DNA (Vecchiarelli et al. 2010); whereas the ATP binding and hydrolysis enables ParA-ADP to bind the specific DNA sequences required for expression of the ParAB locus through its N-terminal HTH domain (Fig. 7) (Dunham et al. 2009). ParA-Ib proteins lack the specific HTH DNA binding motif and the need for the potential transition between the ATP to ATP\* stage is not obvious (Vecchiarelli, Mizuuchi and Funnell 2012). A further classification can be made based on ParA protein structures. The first group includes P1-ParA and pSM19035- $\delta_2$  ATPases that crystallize as dimers even in the apo form (Pratto et al. 2008, Dunham et al. 2009). The second group includes the type Ib TP228-ParF and chromosomal-encoded Soj ATPases that crystalize as monomers, and require ATP for dimerization (Leonard, Butler and Lowe 2005a, Schumacher et al. 2012). Anyway, the motor protein of ParAB system presents a “deviant” Walker A motif (KGGXXGKT) containing two conserved lysine (Fig. 7) (Leipe et al. 2002). Both residues are essential for ATP hydrolysis: the second lysine is common to all Walker A motifs and is also involved in the ATP binding (Motallebi-Veshareh, Rouch and Thomas 1990), while the amino terminal lysine is typical of deviant Walker A motif and seems to mediate the ATP dependent homo-dimer formation of some member of ParA/MinD family (Lutkenhaus and Sundaramoorthy 2003). This was first demonstrated for NifH (Schindelin et al. 1997), but has been subsequently shown for Soj (Leonard et al. 2005a) and MinD (Wu et al. 2011) and Get3 (Mateja et al. 2009).



**Figure 7. Sequence alignment of relevant Walker box ATPases.**

Boundaries of the secondary structure elements of pSM19035 protein  $\delta_2$  with Walker A, A' and B motifs are underlined. Secondary structure elements  $\alpha$ -helices (cylinders) and  $\beta$ -strands (arrows) are indicated and numbered sequentially. Identical residues are coloured white and red shaded and conserved residues are coloured red and boxed blue. The alignment was done using T-Coffee server. The identity range is between 14 and 25%..

The ParAs of type I have been shown to locate regularly on the nucleoid to allow the plasmid segregation. All the experimental evidences suggest that a common mechanism should be adopted to that purpose, but how it functions is controversial and is subject of considerable research and debate (Howard and Gerdes 2010). The biochemical and cytological data are consistent with, and provides a foundation for four mutually exclusive models. The first proposed models were the “filament pushing” (Leonard et al. 2005a, Schumacher et al. 2012) or the “filament-pulling” model by Ringgaard et al. (2009)). The “filament pushing” and “pulling model” are reminiscent of eukaryotic mitosis apparatus. In the “filament pushing” model ParA associates with itself in the form of ATP-bound dimers that polymerize into bundles in the absence of any support (Leonard et al. 2005a, Schumacher et al. 2012); whereas in the “pulling model” ParA associates with the nucleoid in the form of ATP-bound dimers that polymerize into a helical (Ringgaard et al. 2009) or linear (Ptacin et al. 2010) filament that is associated with nsDNA on the nucleoid. Once a growing ParA filament encounters a plasmid-bound ParB-parS nucleoprotein complex, ParB stimulates ParA ATP hydrolysis, thereby inducing filament disassembly. The depolymerizing (retracting) ParA filament pulls an attached plasmid until it

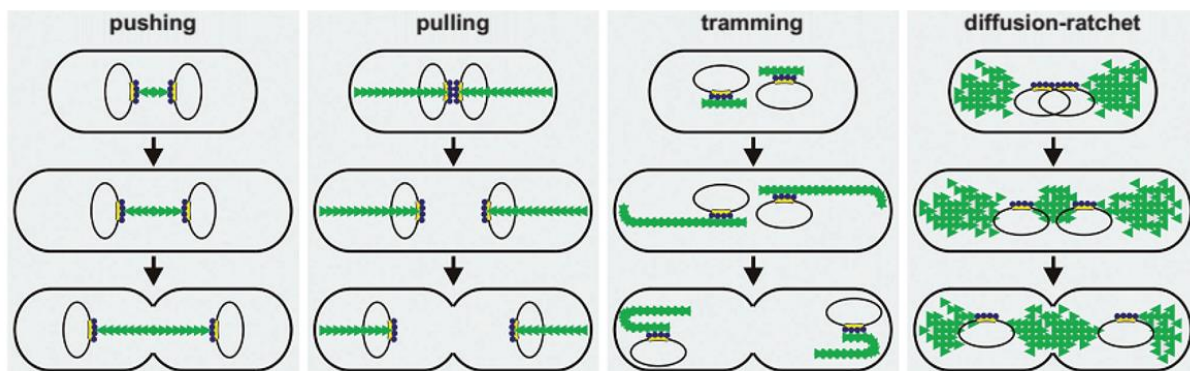
falls off or until the filament is completely disassembled. The ParA–ADP subunits dissociate from the nucleoid, are rejuvenated to the ATP–bound form in the cytoplasm and can then re–enter the process. Upon its release from a filament, a plasmid returns to diffusive motion again until it is contacted once more by a nascent ParA filament. The energetics of movement would be provided by insertion or removal of ParA molecules at the end of a filament to which the ParB–*parS* complexes are attached.

There are two “diffusion” models” proposed by Vecchiarelli et al. (2010) (“diffusion–ratchet model”, Fig. 8) and Jacobs–Wagner and co–workers (Schofield, Lim and Jacobs–Wagner 2010, Lim et al. 2014) (“DNA–relay model”). According to this model, the ParA–ATP dimers or small oligomers, independently bind the nucleoid. Once the ParA bound to chromosomal DNA is contacted by a ParB–*parS* nucleoprotein complex, the ATP hydrolysis is stimulated and ParA–ADP leaves the nsDNA and is free to diffuse in the cytoplasm. The rejuvenating slow transition from ADP to ATP of ParA generate a gradient of ParA associated with the nucleoid and simultaneously provides the motive force for plasmid cargo movement through transient ParB–plasmid and ParA interactions. This model assume that ParA is gradually distributed on the nucleoid rather than forms filaments, it relies on critical parameters that affect ParA activities: the kinetic of ATP/ADP transitions are responsible of two important states corresponding to DNA binding and non–binding forms respectively (Vecchiarelli et al. 2010, Hwang et al. 2013, Vecchiarelli, Hwang and Mizuuchi 2013). Alternatively, in the DNA–relay model ParA is bound to nsDNA and ParB to the *parS* site. When ParB intermittently binds to ParA, it usually catches the ParA–DNA complex when the complex is elastically stretched. The elasticity of the chromosome and the rate of ATP hydrolysis are critical for efficient ParA–dependent translocation of the ParB–*parS* complex, with it moving in the direction where the most ParA molecules are still bound to the chromosome (Lim et al. 2014).

### **2.1.1. Bacterial chromosomal par system.**

A large number of bacterial and archaeal chromosomes encode putative partitioning systems that appear to be hybrids of plasmid Type Ia and Ib systems: the chromosomal ParA proteins contain deviant Walker box motifs of the small Type Ib category and the corresponding chromosomal CBPs contain HTH motifs and are very similar to plasmid type Ia centromere–binding proteins (Gerdes et al. 2000). Notably, the *cis–acting* element, *parS*, occurs in several copies in the chromosome. The extent to which these systems are involved the partition of the chromosome are poorly understood. In some cases, these systems seem to be important only under specialized condition because its deletion did not produce significant effects under

laboratory growth conditions (Yamaichi and Niki 2000). For example, ParAB–*parS* system from *C. crescentus* is essential for life, deletion of *S. coelicolor par* system causes serious defect during the formation of spores and in *P. putida* the *parAB locus* plays a vital role during transition from exponential to stationary phase in minimal medium (Kim et al. 2000, Lewis et al. 2002). However, there are also few species in which these systems are known to be crucial for accurate chromosome segregation. This is the case of the best studied Soj/Spo0J system of *B. subtilis* (Ireton, Gunther and Grossman 1994, Pogliano, Sharp and Pogliano 2002, Gruber and Errington 2009), the ParAB–*parS* system from *C. crescentus* (Lin and Grossman 1998, Mohl and Gober 1997) and ParABI–*parSI* system from *V. cholera* (Fogel and Waldor 2006). In fact, genetic studies showing that mutation of the chromosomally encoded *B. subtilis* ParB homologue, *spo0J*, resulted in a 100–fold increase in the production of anucleate cells (Ireton et al. 1994). Soj, a “deviant Walker A” protein belonging to ParA/MinD family, together with Spo0J plays an important role in bringing together centromere sites that are far apart on the *B. subtilis* chromosome and organizing the origin region into a compact structure that facilitates separation of replicated origins. To do this, Spo0J, like its plasmid counterparts, binds a conserved DNA site, numerous copies of which are clustered about the *soj–spo0J* operon and the replicated chromosomal origins (Lee and Grossman 2006). The mechanism by which Soj or chromosomal ParAs led to DNA segregation is unclear but it seems to share many features with the type I of plasmid partition systems.



Dmowski M. & Jagura-Burdzy G. Pol J Microbiol. 2013;62(1):17-22. Review.

**Figure 8. Schematic representation of plasmid molecules separation during partition.**

The ParB–like proteins (blue circles) bind to the centromeric sequences (shown in yellow) on replicated plasmids. The polymerizing ParA–like protein (green triangles) interact with the ParB–DNA complex move the sister molecules toward bacterial cell poles. The figure was taken from Dmowski M. et Jagura–Burdzy G. (2013).

### 2.1.2. The pSM19035 *par* system.

The pSM19035 plasmid is the best–understood partition system of bacteria of Firmicute phylum: its segregation requires a ParAB–*parS* system composed by two *trans–acting* proteins, the ATPase  $\delta_2$  and the CBP called  $\omega_2$ , and six *cis–acting parS* DNA sites (Fig. 3). Although the

elements of this system are not organized in operon, the *parAB* arrangement of pSM19035 reminds to that of type Ib because  $\delta$  gene is similarly regulated by ParB  $\omega_2$  protein (Ceglowski and Alonso 1994, de la Hoz et al. 2000) (Fig. 6).

Protein  $\omega_2$  (71 residues long) which has an unstructured N-terminal domain (residues 1–19) and the ribbon–helix–helix (RHH) fold (residues 25–71) domain, specifically wraps the *parS* sites to generate a protein–DNA left-handed helix without any bending or twisting (Fig. 4B). This nucleoprotein structure formed by  $\omega_2$  protein does not spread significantly beyond the *parS* site. Conversely, the complexes formed by large CBPs such as P1–ParB, F–SopB or the medium-sized CBP Spo0J of *B. subtilis* that spread in a sequence-independent manner up to several kilobases upon binding to their cognate site(s) (Bouet and Lane 2009, Rodionov, Lobočka and Yarmolinsky 1999, Murray, Ferreira and Errington 2006).

The pSM19035–*parS* sites overlap the promoter region of *copS* genes and are composed by 9, 7 and 10 contiguous heptads of sequence 5'–<sup>A</sup>/TATCAC<sup>A</sup>/T–3' respectively, in direct (→→), inverted (→←) or divergent repeats (←→) orientation (Fig. 4A)(de la Hoz et al. 2000, de la Hoz et al. 2004). The affinities of  $\omega_2$  for the cognate sites  $P_{copS}$ ,  $P_{\omega}$  and  $P_{\delta}$  are similar with a  $K_{Dapp}$  values (equivalent to the  $\omega_2$  concentration required to protect 50% of the DNA) of  $5 \pm 1$  nM. Notably, the minimal cooperative high affinity binding sites for  $\omega_2$  are two contiguous heptads in direct (→→), inverted (→←) orientations with a  $K_{Dapp}$  of 20 and 90 nM, respectively (de la Hoz et al. 2004).

The RHH (or  $\beta\alpha\alpha$ ) domains of  $\omega$  dimers generate two-stranded antiparallel  $\beta$ -sheets that are responsible for making sequence-specific contacts with the major groove of *parS* DNA. In these promoter regions, specific interactions between base pairs of major groove and T29 and R31 located on the  $\omega$   $\beta$ -sheet are established. In particular, when the T29 residues of  $\omega$ , which binds specifically to the central G–C base pair of the heptads, is substituted for Alanine, the  $\omega_2$ T29A DNA specific binding is abolished in both *in vivo* and *in vitro* (Welfle et al. 2005, Weihofen et al. 2006). Moreover, the first 19 N-terminal residues of  $\omega$  is dispensable for regulation of plasmid copy number and of *par* and TA module expression (Welfle et al. 2005, Weihofen et al. 2006), but they are essential for active partitioning. This N-terminal domain of  $\omega_2$  interacts with the ParA  $\delta_2$  protein (Pratto et al. 2008, Pratto et al. 2009).

The motor  $\delta$  (284-residues long), which is a dimer in solution, is essential for accurate pSM19035 segregation. The crystal structure of  $\delta_2$  revealed that it shares sequence similarity with bacterial and archaeal Walker-box ATPases as *T. thermophilus* Soj, *P. furiosus* MinD as well as other members of ParA/MinD family (Fig 7). ATP binding to Walker box proteins typically leads to their dimerization through the formation of a nucleotide sandwich interaction

(Lutkenhaus and Sundaramoorthy 2003). However, biochemical data indicate that apo- $\delta$  is a dimer. The generality of this finding for Ib NTPases remains unknown. However, in the presence of ATP and  $Mg^{2+}$ ,  $\delta_2$  binds DNA in a sequence-independent manner forming discrete blobs rather than bundles or filaments in absence of DNA (Pratto et al. 2008, Pratto et al. 2009). A single substitution of Lysine 36 to Alanine (residues of Walker A motif that interacts directly with the  $\gamma$ -phosphate of ATP), prevents the binding of  $\delta_2K36A$  to ATP and subsequently even the DNA binding; whereas the substitution to Alanine of the Walker B Aspartate at position 60 ( $\delta_2D60A$ ) produces a hydrolysis-deficient version by preventing the nucleophile attack, that binds but does not hydrolyse ATP. Although these variants have different behaviours, both mutants impair the segregation of plasmids *in vivo*.

The  $\omega_2$ - $\delta_2$  interactions are key events of the partition mechanism, but *in vitro* analyses have shown the outcome to depend on the ratio of the two proteins. At low  $\omega_2$ : $\delta_2$  ratios (e.g., 1:3),  $\omega_2$  bound to *parS* does not stimulate the ATPase activity of  $\omega_2$  and it promotes plasmid pairing (Pratto et al. 2008). At equimolar  $\omega_2$ : $\delta_2$  ratios,  $\omega_2$  stimulates  $\delta_2$ -mediated ATP hydrolysis and promotes dislodging from the nucleoid and disassembling of the paired complexes (Pratto et al. 2008). Protein  $\delta_2$ , which fails to form genuine filaments; forms pseudo-filament on nsDNA in the presence of a very large excess of  $\omega_2$  (>1000-fold over its  $K_{Dapp}$ ) (Pratto et al. 2008). The  $\delta_2D60A$  variant presents a higher binding affinity for nsDNA and still is unable to polymerize on nsDNA. Protein  $\delta_2D60A$  interacts with  $\omega_2$  but it cannot hydrolyse ATP (Pratto et al. 2008). The crucial event in the partition process is the assembly of the segrosome that enables plasmid pairing and then separation. An important steps insight the partition systems of pSM19035 have been reported but the our understanding of how operate the mechanism of segregation still remain to be determined and compared with other types of *par* systems.

## 2.2. Type II par system.

Most of the knowledge of type II segregation system is due to extended studies on R1 *E. coli* and pSK41 *S. aureus* low copy number plasmids and it is currently the best characterized active partition system. The genetic organization of R1 type II system is similar to those of the type Ib systems where *parM* gene is located upstream of the *parR* gene and the *parC* centromeric site is located upstream the *parMR* genes. Moreover, the *parMR* cassettes is autoregulated by ParR protein (Jensen, Dam and Gerdes 1994)(Fig. 6). The R1 ParR protein, which has a RHH fold, forms dimers that bind cooperatively to the 10 repeats of the R1 *parC* region to generate a ParR-*parC* nucleoprotein complex (Breuner et al. 1996). ParM, specifically interacts with the ParR-



*parC* complex promoting the plasmid pairing (Jensen, Lurz and Gerdes 1998). Unlike ParA, ParM does not show any DNA-binding activity, underlying a different mechanism of partition. The motor ParM has a 3D structures very similar to that of actin, despite their low sequence alignment identity (<15%). Although a structural similarity between an actin-like protein and actin not always indicate filament formation as a mechanism of action, studies on the type II R1 *par* system provided key insights into this question. Specifically, the experiments show that the R1 ParM ATPase forms double stranded filamentous structures (van den Ent et al. 2002, Moller-Jensen et al. 2003). The R1 ParM filaments display a dynamic instability and bidirectional polymerization regulated by ATP hydrolysis (Garner, Campbell and Mullins 2004). In presence of ATP, short and unstable polymers were observed starting from 2.3  $\mu\text{M}$  of ParM, an *in vitro* protein concentration that is at least 5-fold lower than the one estimated in living cells (12–14  $\mu\text{M}$ ), these filaments were subsequently stabilized by the addition of ParR together with the centromere *parC in vitro* (Garner et al. 2007). Based on the evidences, the unstable polymerization model for *parMRC* system was formulated. The type II fundamental molecular mechanism for DNA segregation is thought to be based on bundles of actin-like ParM filaments that push ParR-*parC*-bound plasmids to opposite poles of the cell by a mechanism of insertional polymerization (Moller-Jensen et al. 2003) (“pushing model”, Fig. 8). A spindle-like model was also postulated for the ParAB-*parS* system (see above), but the data presented are inconsistent with the pushing model.

ParM filaments are dynamically unstable unless they are capped by the plasmid-bound ParR-*parC* nucleoprotein complex, and they thus use cycles of growing and shrinking to search the cell space for plasmids (Garner et al. 2007). Only when they are capped by the ParR-*parC* complexes at both ends do the filaments become stabilized; their subsequent bidirectional elongation ensures that the filament-bound plasmids move to opposite poles.

The last structural studies on pSK41 type II system have led to a near atomic level understanding of this process. The crystal structure of pSK41 ParR reveals that the protein forms dimers with a RHH DNA-binding domain at the N-terminus and a disordered C-terminal tail that was previously reported to interact with ParM (Popp et al. 2007). The co-crystal of pSK41 ParR with *parC* DNA uncovered the ParR-*parC* complex arrangement: multiple ParR dimers wrap the *parC* DNA generating a protein-DNA super helix structure, with the C-terminal domain facing into the centre of it (Schumacher et al. 2007a). Moreover, the pore of ParR-*parC* is suitable for ParM filament interaction (Schumacher, Mansoor and Funnell 2007b). pSK41 ParM forms polymers in the presence of GTP, ATP and its analogues but not in the presence of ADP or GDP, and its structure revealed a fold similar to R1 ParM. pSK41 ParM, which forms a

single stranded filaments rather than double stranded filaments (Popp et al. 2010), might promote accurate plasmid segregation by a mechanism different than R1 ParM. This remains to be determined.

### 2.3. Type III par system.

Type III partition systems are the most recently discovered of the plasmid partition systems. The best understood type III system is that encoded on the *B. thuringiensis* pBtoxis plasmid. This *par* system encodes an upstream gene called *tubR* and downstream gene *tubZ* (Larsen et al. 2007). A possible centromere site for pBtoxis *par* system has been identified upstream the *tubR* gene (Tang et al. 2007) (Fig.6). The genetic organization is distinct from the type I and II *par* systems. The structure of TubR revealed the protein forms dimer that contains a winged-THH domain with similarity to the ArsR family of transcriptional repressors. Moreover, biochemical studies also demonstrated that TubR uses residues in its wing and the helix preceding its recognition helix for DNA binding and modelling suggests that the wings could interact with consecutive minor grooves of the DNA, while the N-termini of the recognition helices would insert into a single major groove (Ni et al. 2010). The most interesting feature of these systems is that the TubZ protein contains a tubulin/FtsZ fold and a flexible C-terminal tail that was not resolved in the structures. Biochemical studies showed that the TubZ C-tail is used to bind TubR (Ni et al. 2010). The TubZ protein assembles into dynamic polymers that exhibit directional polymerization with plus and minus end in a GTP-dependent manner (Chen and Erickson 2008). Subsequent EM structures of TubZ, which showed that it forms double stranded filaments, revealed that its C-terminal tails are indeed solvent exposed (Aylett et al. 2010).

A tram-like mechanism for type III partition was suggested according the combination of latest evidences (“tramping model”, Fig. 8). In this model, the TubR-pBtoxis complex becomes attached to TubZ filaments through the interaction of TubR with the exposed C-terminal regions of TubZ. The hydrolysis of GTP within the TubZ polymer generates treadmilling by polymerization at plus end and depolymerisation at the minus end which should translocate the attached plasmid toward one cell pole (Schumacher 2012).

## 3. Repression of transcription initiation in Bacteria.

As previously introduced, the *segD* locus comprises the  $\omega_2$  transcriptional repressor and its cognate sites upstream the promoter regions of the *cop* ( $P_{copS}$ ),  $\delta$  ( $P_\delta$ ) and  $\omega$  ( $P_\omega$ ) genes (also termed *parS1* to *parS3* sites) that coordinate copy number fluctuation and better-than-random segregation function (de la Hoz et al. 2000) (Fig. 4A and 5). To unravel the mechanism used by

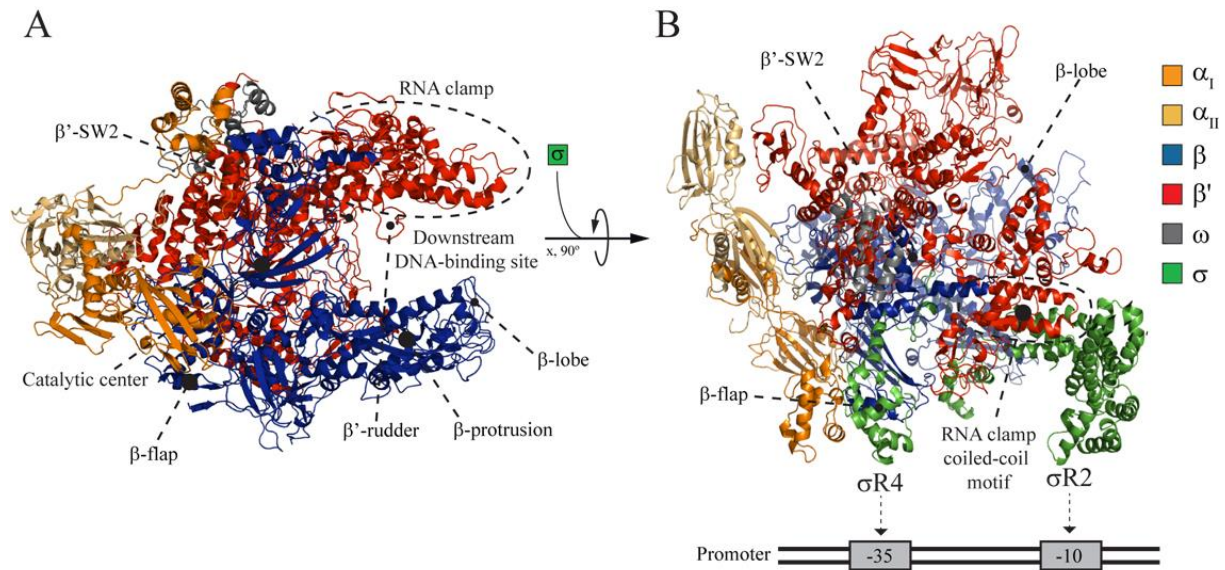
the *segD* locus to regulate the interplay between the different pSM19035–encoded loci we study the repression mechanisms used in bacteria.

Except viruses, all organisms encode for a multi–subunit DNA–dependent RNA polymerase (RNAP). In prokaryotes, this is accomplished by the core RNAP linked to a number of  $\sigma$  factors that specify binding to different promoter elements. In eukaryotes, this process is more complex because of the presence of three distinct RNAP, each responsible for the transcription of a different class of RNAs.

Protein  $\omega_2$  plays a crucial role regulating the transcription of genes required for copy–number–control, accurate segregation and stable maintenance of *inc18* plasmids hosted by Gram–positive bacteria. The  $P_{copS}$ ,  $P_{\delta}$  and  $P_{\omega}$  are specifically transcribed by main *B. subtilis* RNA polymerase holoenzyme containing the primary  $\sigma$  factor present during exponential growth ( $\sigma^A$ , RNAP– $\sigma^A$ ) (Kroos and Yu 2000)..

### 3.1. Bacterial RNAP.

The determination of the crystallography structure of *T. aquaticus* core RNAP revealed the general shape of the enzyme (Zhang et al. 1999). During the past few years, the elucidation of the structure of RNAP from multiple organisms provided enormous insight into how these macromolecular machines interact with DNA and carry out many of the detailed steps in the initiation and elongation of RNA chains (Boeger et al. 2005, Murakami and Darst 2003). It also has revealed that the structure of RNAP, as well as its sequence, is conserved among prokaryotes and between prokaryotes and eukaryotes. Those evidences suggested that the *last universal common ancestor* (LUCA) of the Bacteria, Archaea and Eukarya had an RNAP very similar to the simplest form of contemporary RNAPs found in the Bacteria (Ebright 2000, Werner 2007, Werner 2008). In fact, the crystal structure of *T. aquaticus* RNAP aligns well with a 15Å cryo–EM structure of *E. coli* RNAP (Darst et al. 2002). These data are supporting the idea that the thermophilic and mesophilic RNAPs have similar structures as well as other bacterial RNAP. Therefore, biochemical data derived from work with *E. coli* can be used in conjunction with structural data from *T. aquaticus*. The basic architecture of bacterial RNAP is conserved and active RNAP exists in two active forms. The first is the core enzyme, which is competent for transcription but not for promoter–directed transcript initiation, is composed by 3 essential subunits:  $\alpha_2\beta\beta'\omega$  and two dispensable ones ( $\omega$  and  $\delta$ ) that shares the same names that pSM19035–encoded  $\omega_2$  and  $\delta_2$ , but are unrelated proteins (Fig 9A).



**Figure 9. Important structural and functional features of RNAPs.**

The structure of *T. aquaticus* RNAP core (PDB:1HQM) (A) and *T. thermophiles* holoenzyme (B) (PDB: 1L9U). In this illustration shows the important structural and functional features. *The catalytic center of RNAP*: the catalytic domain that contains the active site Mg ion with the insertion site for the incoming NTPs and the binding sites the RNA 3'-terminus. *RNA β' clamp*: a flexible domain that is predicted to move over the DNA-binding channel during open-complex formation. *The RNAP β' clamp coiled-coil motif*: a conserved domains and an important binding site for R2 of  $\sigma$ . *The β-lobe*: the lobe domain in concert with the β' clamp domain forms a channel that held the downstream DNA. *The β-flap*: the flap interacts with conserved R4 of  $\sigma$ . *The β'-Switch Region 2 (SW2)*: this region interacts with template DNA near the catalytic center. *The β'-rudder*: this domain contributes critically to elongation complex stability. The figure inspired by Werner F. and Grohmann D. (2011) was adjusted and interpreted for this work (Werner and Grohmann 2011, Campbell et al. 2002).

The RNAP  $\alpha$  subunits form dimers ( $\alpha_2$ ) that act as the platform onto which the  $\beta$  and  $\beta'$  subunits bind, and which play a role in transcription activation (Zhang and Darst 1998). The  $\alpha$  subunit consists of two functional domains: a C-terminal domain ( $\alpha$ CTD), and an N-terminal domain ( $\alpha$ NTD) responsible for the dimerization of the  $\alpha$  subunits (Igarashi and Ishihama 1991). The  $\alpha$ CTD and  $\alpha$ NTD are joined by a flexible linker (Jeon et al. 1997). The  $\beta$  and  $\beta'$  subunits creates an overall “crab-claw” shape with two “pincers” surrounding a cleft that contains the RNAP catalytic centre and serves as the binding site for DNA. The cleft is lined with positive residues, whereas the outside surface of RNAP is predominantly negative in charge. Curiously, the  $\beta'$  contains two  $Zn^{2+}$ -binding elements (ZBD and  $Zn^{2+}$  II) in prokaryotic RNAPs, which are not conserved in eukaryotes that have a structural role in the formation of the active polymerase (Zhang et al. 1999). The small  $\omega$  and  $\delta$  accessory subunits have no direct role in transcription, but seem to function as a chaperone (e.g.,  $\omega$ ) to assist the folding of the  $\beta'$  subunit (Fig. 9 A)(Ghosh, Ishihama and Chatterji 2001). The second form is the RNAP holoenzyme that is composed by the core enzymes bound to one of a number of dissociable accessory proteins, termed  $\sigma$  factors (RNAP- $\sigma$ ) (Fig. 9B) (Darst 2001, Murakami, Masuda and Darst 2003).

The crystal structures for holoenzyme from *T. aquaticus* and *T. thermophiles* reveal the interactions between  $\sigma$  and core RNAP (Fig. 9B). These interactions are quite extensive, as had been predicted by biochemical studies (Gruber et al. 2001, Sharp et al. 1999). In holoenzyme,  $\sigma$  is folded into three flexibly linked domains,  $\sigma 2$ ,  $\sigma 3$  and  $\sigma 4$ , containing conserved regions R1.2 – R2.4, R3.0 – R3.1, and R4.1 – R4.2, respectively (Murakami, Masuda and Darst 2002b).  $\sigma R2$  is bound to the  $\beta'$  clamp, with the major contact between  $\sigma R2.2$  and the coiled–coil domain of  $\beta'$ .  $\sigma 3$  is located within the active site channel, contacting primarily the  $\beta$  subunit near the active site.  $\sigma R4$  wraps around the flap tip helix of the  $\beta$  flap domain. The  $\sigma$  factors are also essential to determine promoter specificity by binding directly to the  $-10$  element in the promoter through region  $\sigma 2$  ( $\sigma R2.4$ ) and to the  $-35$  element through region  $\sigma R4$  ( $\sigma R4.2$ ) (Barne et al. 1997, Dombroski et al. 1992). All these interaction permits the transcription to initiate at correct sites (Fig. 9 B) (Burgess et al. 1969).

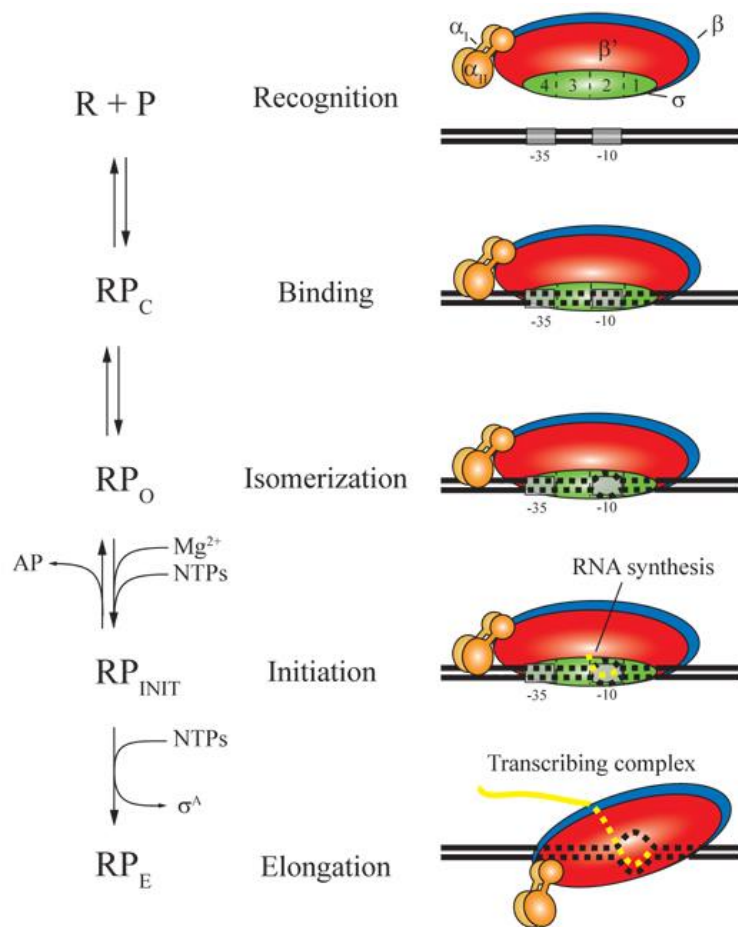
### 3.2. Transcription initiation at bacterial promoter.

Transcription initiation at given promoter ( $P$ ) is comprised by a series of sequential steps (Fig. 10) (Vassylyev et al. 2007a, Lane and Darst 2010, Zhang et al. 2012). There are three main steps in the transcription cycle: initiation, elongation and termination. During initiation, the core bacterial RNAP enzyme, binds to one of the family of  $\sigma$  initiation factors. The resulting holoenzyme is able to binds specifically to the  $-10$  and  $-35$  elements (relative to the  $+1$  start site) of promoter DNA, forming the closed complex (RP<sub>c</sub>) (Burgess et al. 1969, Kovacic 1987) in a process called promoter recognition. RP<sub>c</sub> isomerizes through kinetic intermediates (RP<sub>1</sub> unstable intermediates that are not represented in figure) to the open complex (RP<sub>o</sub>), in which the promoter melting of  $\sim 14$  bp ( $-12$  to  $+2$ ) in the DNA surrounding of the transcription start site is achieved to allow active–site access to the template strand (Saecker et al. 2002). Functions associated with RP<sub>o</sub> formation predominantly reside on the  $\sigma$  ( $\sigma R2.3$ ,  $\sigma R1.1$  and  $\sigma R1.2$ ),  $\beta$  ( $\beta$ -lobe) and  $\beta'$  ( $\beta'$ -rudder and  $\beta'$ Sw-2 regions) subunits (Gruber and Gross 2003, Haugen, Ross and Gourse 2008, Saecker, Record and Dehaseth 2011). In the presence of nucleotides triphosphates (NTPs), the RP<sub>o</sub> is capable of initiating transcription. The  $\sigma R3.2$  and the  $\beta'$ -Sw2 regions play an important role in the initial RNA synthesis (Ebright 2000, Haugen et al. 2008, Saecker et al. 2011). The RNAP– $\sigma$  remains at the promoter in an initial transcription complex (RP<sub>INIT</sub>) that undergoes reiterative rounds of short transcript formation and release, called abortive transcription products (AP), before releasing contacts with the DNA and escaping from the promoter (Vo et al. 2003). Although the role of abortive initiation and promoter escape

remain poorly understood, the efficient extension of abortive products (AP) was suggested to require the  $\sigma$ R3.2 and  $\beta'$  Sw-2 regions among other (Kulbachinskiy and Mustaev 2006, Pupov et al. 2010, Bochkareva and Zenkin 2013). After RNAP leaves the promoter, it forms a transcription elongation complex ( $R_E$ ), the  $\sigma$  subunit dissociates and the transcription is then performed by the core RNAP. The  $R_E$  is processive and extremely stable (Krummel and Chamberlin 1989), transcribing at an average rate of 30 – 100 nt/sec for tens of kb down the DNA template (Fig.10)(Vogel and Jensen 1994). Transcription ends when RNAP reaches an intrinsic termination signal, characterized by an RNA hairpin in the nascent transcript, or is acted upon by the termination factor  $\rho$ , causing the RNA transcript and the DNA to be released and freeing the core RNAP to begin another round of transcription (Reynolds and Chamberlin 1992). Regulatory molecules can modulate all steps in this enzymatic cycle of RNA synthesis; understanding this regulation requires knowledge of the structure of intermediates in the cycle.

### **3.3. Regulation of Transcription initiation.**

Transcription initiation is the first step toward the gene expression. The complexity of its process offers many points of regulation. The binding of a transcription factor to its operator can activate or repress transcription initiation. Some transcription factors function solely as activators or repressors, whereas others can function as either according to the target promoter (Perez-Rueda and Collado-Vides 2000). In general, the activators improve the performance of a promoter by increasing its affinity for RNAP, but they can also stimulate RPo formation and facilitate promoter escape. Three general mechanisms are described for ‘simple’ activation. The “*class I*” of activators that bound to the upstream site and contacts the  $\alpha$ CTD of RNAP and recruiting the latter to promoter region (Ebright 1993). The “*class II*” that binds to a target that is adjacent to the promoter -35 element (at, or near to position -41.5) and contemporary interacting with the domain  $\sigma$ R4 (Dove, Darst and Hochschild 2003). The “*activators by conformation changes*” that generally binds at, or near the promoter elements altering the conformation of the target to enhance the interaction of RNAP holoenzyme with the -10 and the -35 elements (Sheridan, Opel and Hatfield 2001). Contrary, repressor proteins reduce transcription initiation at target promoters. Three general mechanisms are used. By “*steric hindrance*” in which the repressor-binding site overlaps the core promoter elements, prevents the RNAP binding to promoter DNA (Majors 1975). By “*looping*” in which the repressors bind to promoter distal sites and repression will be achieved by DNA looping (Muller, Oehler and Muller-Hill 1996). By “*the modulation of an activator protein*”, when the repressor functions as an anti-activator and blocks the promoter recognition by the RNAP-  $\sigma$  (Shin et al. 2001).



**Figure 10. Summary of the intermediates in the process of initiation of RNA synthesis.**

The RNAP (R) interacts with promoter DNA (P) to form the closed complex ( $RP_C$ ). Dashed lines show the promoter DNA that is bound by the RNAP holoenzyme. The duplex DNA around the transcript start site is unwound (represented by a 'bubble' in the DNA that is bound by the RNAP holoenzyme) to form the open complex ( $RP_O$ ). The initiating complex ( $RP_{INIT}$ ) is formed and synthesis of the DNA–template–directed RNA chain (shown as a dashed yellow line) begins with formation of a phosphodiester bond between the initiating and adjacent phosphodiester nucleoside triphosphates (NTPs). Elongation is the final stage, and the RNA chain length increases, shown as a solid yellow line. The bacterial RNAP are schematically shown by a cartoon: the coloured forms represented the  $\sigma$  factor (green), the  $\alpha_I$  end  $\alpha_{II}$  (light orange and orange respectively), the  $\beta$  (blue) and  $\beta'$  (red) sub–units.

Generally, the gene regulation in prokaryotes is achieved largely by proteins, having predominantly HTH DNA binding motifs that places an  $\alpha$ –helix into the DNA major groove to bind to specific operator DNA sequences (Wintjens and Rooman 1996). This family of transcription factors binds to a palindromic sequence of DNA to repress or activate expression of associated genes (Ptashne 1986). A less frequent superfamily of prokaryote transcription factors containing a RHH domain was described to specifically recognize arrays of inverted or tandem repeats (de la Hoz et al. 2004, Youderian, Bouvier and Susskind 1982, Saint–Girons et al. 1984).

### 3.4. The RHH superfamily of transcription factors.

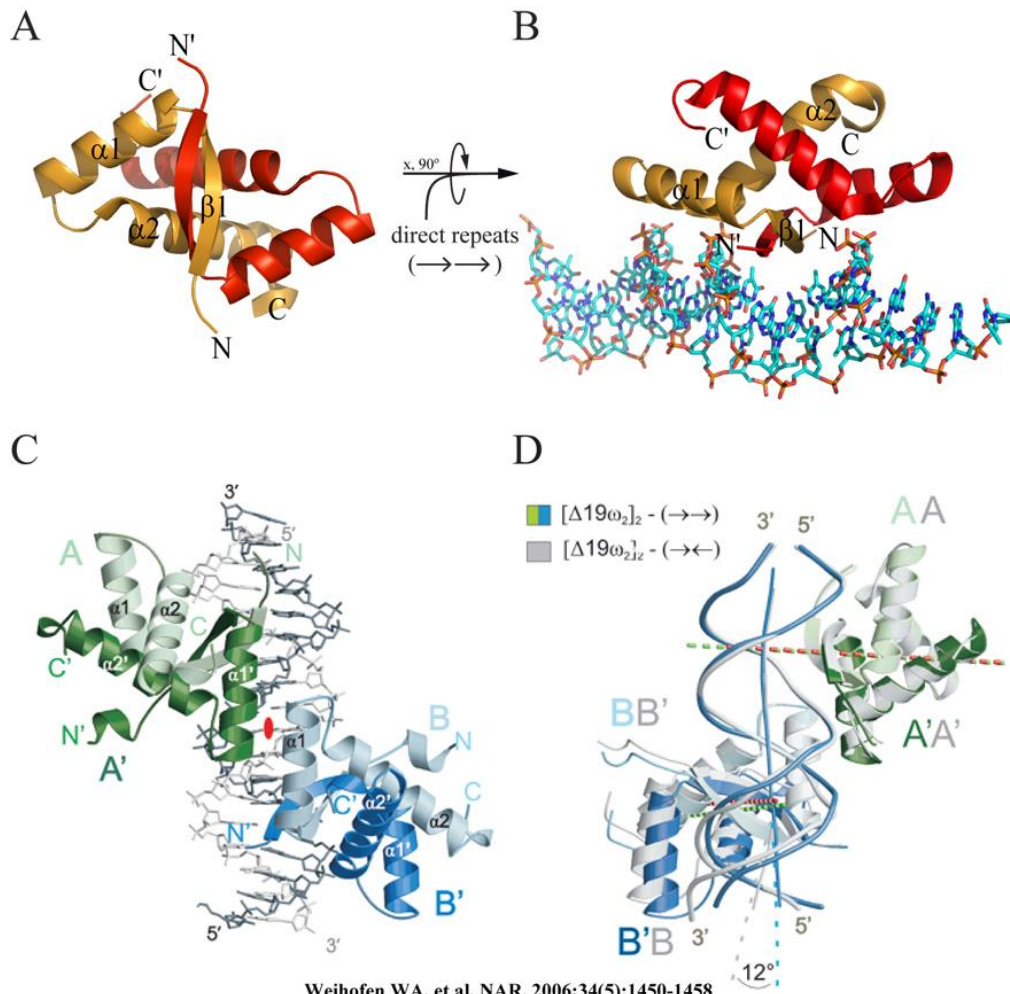
The RHH superfamily uses a conserved three dimensional structural motif to bind to DNA in a sequence–specific manner that was first characterized for *E. coli* MetJ and bacteriophage P22 Arc repressor proteins (Somers and Phillips 1992, Raumann et al. 1994). This functionally diverse protein superfamily regulates the transcription of genes that are involved in several cellular processes. Indeed, other members include proteins involved in the control of plasmid

copy number as pMV158–CopG and pSM19035– $\omega_2$  (Gomis–Ruth et al. 1998b) as well as CBP proteins of type Ib (pSM19035– $\omega_2$  and TP228–ParG)(Golovanov et al. 2003) and Type II (pSK41–ParR) (Vecchiarelli, Schumacher and Funnell 2007) involved in plasmid segregation.

Most members of the RHH superfamily are transcriptional repressors, with some exceptions like *P. aeruginosa* AlgZ and *H. Pylori* NikR, that present positive and negative regulation of their promoters (Ramsey, Baynham and Wozniak 2005, van Vliet et al. 2002, van Vliet, Ernst and Kusters 2004).

The RHH motif can be present within the amino–acid sequence of a protein, either as an isolated RHH motif or as part of larger proteins that have additional domains located on either side of the RHH DNA–binding domain. The functional unit of these proteins is a dimer, in which two RHH motifs are tightly intertwined to form a stable domain (RHH<sub>2</sub>) that has a two–fold symmetry and is capable of binding to DNA. The paired short  $\beta$ –strands that are present at the N terminus of each RHH monomer form an antiparallel  $\beta$ –sheet that fits into the major groove of the target DNA (Fig. 11A and B). The  $\beta$ –strands residues of the RHH superfamily confer the sequence specificity for the target DNA and this is a distinctive feature compared to the ubiquitous HTH superfamily, in which the specificity is achieved by an  $\alpha$ –helix. Moreover, a conserved set of non–specific contacts to the DNA phosphate backbone are established by the homodimer protein–backbone amide nitrogens at the N–terminus of the  $\alpha_2$  helix of the RHH<sub>2</sub> domain, on either side of the major groove. This interaction is electrostatically favourable because the positive dipole at the helix N–terminus is orientated directly towards a negatively charged phosphate of the backbone. These contacts anchor the RHH<sub>2</sub> domain to the DNA and orientate the base–contacting  $\beta$ –sheet correctly for optimal interaction with the DNA bases (Raumann et al. 1994).





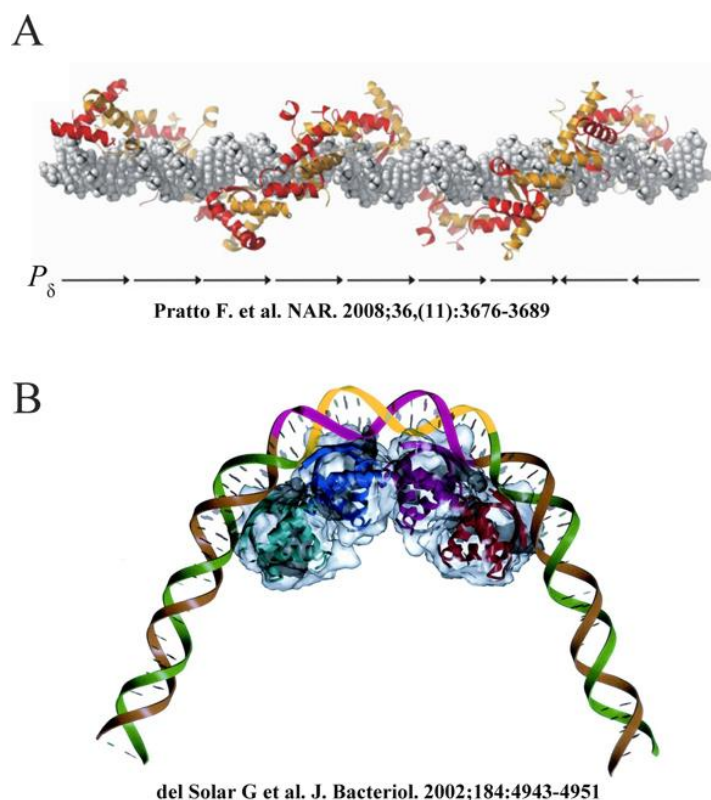
Weihofen WA. et al. NAR. 2006;34(5):1450-1458

**Figure 11. The structure and DNA binding of ribbon-helix-helix  $\omega_2$  protein.**

(A) Three-dimensional structure of  $\omega$  dimer from a bottom view. The N-terminal region of protein is missing. (B) Side view of the  $\omega$  dimer in complex with DNA containing two directed repeats ( $\rightarrow\rightarrow$ ). The antiparallel  $\beta$ -sheets are inverted in the major groove making sequence-specific nucleotide base contacts. (C) The co-crystal structure of  $\omega_2\Delta N19$  in complex with two directed repeats ( $\rightarrow\rightarrow$ ). DNA backbone trace in light grey for top strand and dark grey for bottom strand. (D) Superimposition of the two crystal structures determined for  $\omega_2\Delta N19$  bound to directed ( $\rightarrow\rightarrow$ ) [PDB:2BNW] and inverted ( $\rightarrow\leftarrow$ ) [PDB:2BNZ]. The DNA of directed repeats is nearly straight whereas the one of inverted repeats is slightly deflected of about 12 degree. The two subunits are drawn in orange and red (A) and (B). The  $\omega\Delta N19$  monomers A/A' and B/B' are in light and dark green and blue, respectively (C) and (D) (Weihofen et al. 2006).

All RHH proteins bind DNA as higher-order oligomers and contact multiple sites within operators that are arranged as inverted or tandem repeats (Chivers and Sauer 2000, de la Hoz et al. 2004). The overall DNA binding mode of each individual RHH<sub>2</sub> is similar, but the details of the specific DNA base contacts do not seem to be conserved across the RHH superfamily. Each family member binds to a unique sequence (or sequences) within operators that are usually arranged as inverted or tandem repeats. MetJ can bind to a symmetric operator sequence of 8 bp, by making contacts that follow the two-fold symmetry of the protein dimer (Somers and Phillips 1992), whereas the Arc, CopG and  $\omega_2$  recognize palindromic sub-site sequences of 11 bp, 9 bp

and 7 bp, respectively, and they make asymmetric contacts with their cognate sites (Raumann et al. 1994, Gomis-Ruth et al. 1998a, Weihofen et al. 2006). Additionally,  $\omega_2$  recognizes also a non-palindromic sub-site and therefore there are three possibilities for the orientation of the two adjacent sub-sites: direct ( $\rightarrow\rightarrow$ ), inverted ( $\rightarrow\leftarrow$ ) or divergent repeats ( $\leftarrow\rightarrow$ ) (de la Hoz et al. 2004). These sub-site orientations modulate the affinity of the  $\omega_2$  repressor for an operator. The  $\beta$ -ribbon of each repressor comprises 5 to 9 amino acid residues per each sub-unit in the case of  $\omega_2$ , Arc, CopG and MetJ. These differences, also determine the specificity of RHH proteins for a sequence substrate. In general, RHH proteins use one or more amino acid side chains from each N-terminal  $\beta$ -strand to make direct nucleotide base contacts. Although the identities of these three side chains vary across the family, Lys or Arg in the  $\beta$ -strand typically make the largest number of specific contacts. Currently no “code” exists that directly relates the amino acid identity within the  $\beta$ -strand to a specific DNA sequence (Schreiter and Drennan 2007).



**Figure 12. Models of two different nucleoprotein complexes at the DNA operators.**

(A) Model of nine  $\omega_2$  bound to *parS* DNA based on the crystal structures determined for two dimers of  $\omega_2\Delta N19$  bound to directed ( $\rightarrow\rightarrow$ ) [PDB:2BNW] and inverted ( $\rightarrow\leftarrow$ ) [PDB:2BNZ] repeats complexes (Weihofen et al. 2006) with the DNA shown in space filling (grey/blue) and  $\omega_2$  in ribbon representations (one monomer is orange, the other red). (B) Model of CopG binding to its target DNA. The DNA strands are displayed in green and brown, except the region corresponding to the 13-bp symmetric element, which is labelled in yellow and magenta. The structure of the CopG dimers is indicated by ribbon plots within a transparent Connolly surface. Four CopG dimers bind to four successive DNA helix turns, and, as a result, the target DNA is bent at a total angle of about  $120^\circ$  (del Solar et al. 2002).

When structures of RHH proteins solved alone and bound to DNA are compared, there is essentially no conformational change within the RHH<sub>2</sub> domain after DNA binding. Curiously, in the  $\omega_2$ -DNA structure, the conformation of an  $\omega_2$ -bound DNA fragment is similar to an unbound DNA, which might indicate that binding of  $\omega_2$  to its operator does not induce substantial changes in the DNA conformation (Weihofen et al. 2006, Pratto et al. 2008, Pratto et al. 2009)

(Fig. 11C and D; Fig. 12A). DNA fragments in the  $\omega_2$ -DNA structure are almost linear and this is a big difference if compared with the other available RHH-DNA co-crystal structures in which some degree of bending of the DNA operator is observed (Fig. 12). In fact, the structures of two dimers each of Arc, CopG and MetJ bound to their respective operator sequences all revealed an overall bending of the DNA by 50–60° over its length (Raumann et al. 1994, Gomis-Ruth et al. 1998a, Somers and Phillips 1992) (Fig. 12B). However, the molecular details of the cause of this bend vary.



## *Objectives*



Our aim was to study the active partition system of plasmid pSM19035 through detailed *in vitro* and *in vivo* analysis of its components:  $\delta_2$  and  $\omega_2$  proteins.

To better understand the mechanisms of segregation of plasmid DNA the following objectives are proposed:

- 1 – Characterization of  $\delta_2$  nsDNA binding domain.
- 2 – Characterization of  $\delta_2$  dimerization and oligomerization domains.
- 3 – Characterization of  $\omega_2$ - $\delta_2$  interaction domains.
- 4 – Characterization of early stage of plasmid segregation machinery and their dynamics.

Finally, the molecular mechanism for the direct modulation of RNAP- $\sigma^A$  transcription activity by  $\omega_2$  has been also addressed with following objectives:

- 5 – Analysis of the role in the overall control of pSM19035 played by  $\omega_2$  and  $\delta_2$  proteins.
- 6 – Assessment of potential interaction between  $\omega_2$  and RNAP sub-units.





## *Materials and Methods*



## 1. Materials.

### 1.1. Strains.

The strains used or constructed during this work are detailed in the following tables:

**Table 1. *E. coli* strains.**

STRAIN	GENOTYPE	USE
XL 1 Blue	recA1, endA1, gyrA96, thi-1, hsdR17, supE44, relA1, lac [F' proAB lacI <sup>q</sup> ZΔM15 Tn10(Tet)]	Construction and maintaining of plasmids.
BL21 (DE3)	pLysS B, F- <i>dcm</i> , <i>ompT</i> , <i>hsdS</i> (rB- mB-), <i>gal</i> (DE3) [pLysS Cat] (Yanisch-Perron, Vieira and Messing 1985)	Overproduction of proteins: δ y ω
JM107	F' lac [pro A+proB+] att lambda, dam, dcm, del (lacPro) m15, endA1, gyrA96, hsdR17, lacI <sup>q</sup> , relA1, supE44, thi-1, traD36 (Alonso, Shirahige and Ogasawara 1990)	Construction and maintaining of plasmids.

**Table 2. *B. subtilis* strains.**

STRAIN	GENOTYPE	USE
BG214	<i>amyE</i> , <i>attSPB</i> , <i>metB5</i> , <i>sigB37</i> , <i>trpC2</i> , <i>xin-1</i> (Fujita and Sadaie 1998)	Wild type
NIG2001	<i>trpC2</i> , <i>pheA1</i> , <i>neo<sup>r</sup></i> , <i>rpoC<sub>his6</sub></i> (de la Hoz et al. 2000)	To purify the RNAP-σ <sup>A</sup> multi-subunit enzyme.
BG508	<i>amyE:P<sub>δ</sub>lacZ</i> , <i>attSPB metB5</i> , <i>sigB37</i> , <i>RecA4</i> , <i>trpC2</i> , <i>xin-1</i> (Pratto et al. 2008)	To study the utilization of <i>P<sub>δ</sub>lacZ</i> in presence of ω or ω2.
BG947	<i>amyE:P<sub>Hyperspank</sub>:δ:gfp</i> , <i>attSPB metB5</i> , <i>sigB37</i> , <i>trpC2</i> , <i>xin-1</i> (Ceglowski and Alonso 1994)	To study the cellular localization of δ-gfp fusion protein upon induction of IPTG.
BG1097	<i>amyE:P<sub>Hyperspank</sub>:δD60A:gfp</i> , <i>attSPB</i> , <i>metB5</i> , <i>sigB37</i> , <i>trpC2</i> , <i>xin-1</i> (this work)	To study the cellular localization of δD60A-gfp fusion protein upon induction of IPTG.

### 1.2. Plasmids.

In table 3 are detailed the plasmids used and/or constructed during this work.

**Table 3. Plasmids.**

NAME	DERIVED	RESIST.	DESCRIPTION
pSM19035	–	Em	Low-copy number plasmid that contains duplicated and inverted sequences (see Fig. 1) (Ceglowski and Alonso 1994).
pDB101	pSM19035	Em	Low-copy number mini-derivative of pSM19035 (see Fig. 1) (Ceglowski and Alonso 1994).
pBT233	pDB101	Em	Low-copy number mini-derivative lacking duplicated regions (Fig 1)(de la Hoz et al. 2000).
PHP13		Cm, Em	Shuttle vector for <i>E. coli</i> and <i>B. subtilis</i>

pHP14	pHP13	Cm, Em	Shuttle vector for <i>E. coli</i> and <i>B. subtilis</i> with the MCS in a different orientation
pT712	–	Ap	It contains the phage T7 late promoter $\phi 10$ ( $P_{\phi 10}$ ) (GIBCO–BRL).
pET3a	–	Ap	It contains $P_{\phi 10}$ (NOVAGEN).
pET15b	–	Ap	The pET–15b contains $P_{\phi 10}$ . The vector carries a sequence at the 5'–end coding six contiguous His (His Tag) followed by a thrombin recognition site. (NOVAGEN).
pET21b	–	Ap	The pET–15b contains $P_{\phi 10}$ . The vector carries a sequence at the 5'– and the 3'–end coding six contiguous His (His Tag) (NOVAGEN).
pDR11	–	Sp	Integrative vector for <i>B. subtilis</i> , it has Hyperspank promoter controlled by IPTG (David Rudner Lab).
pGEM–T easy	–	Ap	The high copy number pGEM–T Easy Vectors contains T7 and SP6 RNA polymerase promoters flanking a multiple cloning region (Promega).
pT712– $\omega$	pT712	Ap	Plasmid to overproduce the $\omega$ protein (Pratto et al. 2008).
pT712– $\omega\Delta 19$	pT712	Ap	To overproduce the $\omega\Delta 19$ protein (Pratto et al. 2008)
pT712– $\omega 2$	pT712	Ap	To overproduce the $\omega 2$ protein (this work).
pCB746	pET21b	Ap	To overproduce the $\delta$ –his <sub>6</sub> protein (Pratto et al. 2008).
pCB871	pET15b	Ap	To overproduce the his <sub>6</sub> – $\delta$ protein (this work).
pCB755	pET21b	Ap	Plasmid to overproduce the $\delta D60A$ –his <sub>6</sub> protein (Soberon et al. 2011).
pCB855	pET21b	Ap	Plasmid to overproduce the $\delta D211A$ –his <sub>6</sub> protein (Soberón et al. 2011).
pCB853	pET21b	Ap	Plasmid to overproduce the $\delta K242A$ –his <sub>6</sub> protein (Soberon et al. 2011).
pCB854	pET21b	Ap	Plasmid to overproduce the $\delta K248S$ –his <sub>6</sub> protein (Soberon et al. 2011).
pCB856	pET21b	Ap	Plasmid to overproduce the $\delta K255A$ –his <sub>6</sub> protein (Soberon et al. 2011).
pCB857	pET21b	Ap	To overproduce the $\delta K259A$ K260A–his <sub>6</sub> protein (de la Hoz et al. 2000).
pCB872	pET21b	Ap	To overproduce the $\delta D60A$ D211A–his <sub>6</sub> protein (this work).
pCB869	pET21b	Ap	To overproduce the $\delta R119C$ D189C–his <sub>6</sub> protein (this work)
pCB870	pET21b	Ap	To overproduce the $\delta P152C$ Y155C–his <sub>6</sub> protein (this work).
pCB957	pET21b	Ap	To overproduce the $\delta N\Delta 20$ –his <sub>6</sub> protein (this work).
pCB864	pET21b	Ap	To overproduce the $\delta N\Delta 41$ –his <sub>6</sub> protein (this work).
pCB865	pET21b	Ap	To overproduce the $\delta N\Delta 111$ –his <sub>6</sub> protein (this work).
pCB866	pET21b	Ap	To overproduce the $\delta N\Delta 166$ –his <sub>6</sub> protein (this work).
pCB867	pET21b	Ap	To overproduce the $\delta N\Delta 199$ –his <sub>6</sub> protein (this work).

pCB913	pET15b	Ap	To overproduce the his <sub>6</sub> - $\delta$ C $\Delta$ 255 protein (this work).
pCB914	pET15b	Ap	To overproduce the his <sub>6</sub> - $\delta$ C $\Delta$ 227 protein (this work).
pCB915	pET15b	Ap	To overproduce the his <sub>6</sub> - $\delta$ C $\Delta$ 197 protein (this work).
pCB916	pET15b	Ap	To overproduce the his <sub>6</sub> - $\delta$ C $\Delta$ 164 protein (this work).
pUC57	pUC19	Ap	Contains the promoter sequence of <i>copS</i> (de la Hoz et al. 2000).
pUC30	pUC19	Ap	Contains the <i>orf<math>\omega</math></i> sequence (Ceglowski and Alonso 1994).
pBT291	pT712	Ap	Contains the <i>orf<math>\delta</math></i> y <i>orf<math>\omega</math></i> genes sequences (Pratto et al. 2008).
pCB578	pHP13	Cm, Em	Contains the sequence of $\delta$ promoter and $\delta$ : <i>gfp</i> gene (Pratto et al. 2008).
pCB586	pHP13	Cm, Em	Contains the <i>orf<math>\omega</math></i> (Pratto et al. 2008) (Pratto et al. 2008).
pCB702	pHP14	Cm, Em	Contains the sequence of $\delta$ promoter and $\delta$ : <i>gfp</i> gene and <i>orf<math>\omega</math></i> gene (Pratto et al. 2008)–
pCB703	pHP14	Cm, Em	Contains the $P_{\delta}$ $\delta$ and $P_{\omega}$ $\omega$ $\Delta$ N19 genes (Pratto et al. 2008).
pCB706	pHP14	Cm, Em	Contains the sequences of <i>orf<math>\delta</math></i> and <i>orf<math>\omega</math></i> genes (Pratto et al. 2008).
pCB742	pHP13	Cm, Em	Contains the $P_{\omega}$ $\omega$ $\Delta$ N19(Pratto et al. 2008).
pCB760	pHP13	Cm, Em	Contains $P_{\delta}$ $\delta$ D60A: <i>gfp</i> (Pratto et al. 2008).
pCB761	pHP14	Cm, Em	Contains the sequences of $\delta$ promoter and $\delta$ D60A: <i>gfp</i> gene and <i>orf<math>\omega</math></i> gene (Pratto et al. 2008).
pCB840	pHP14	Cm, Em	Contains the sequences of $P_{\delta}$ $\delta$ D60A: <i>gfp</i> gene and $P_{\omega}$ $\omega$ $\Delta$ N19 gene (Hanahan 1983)
pCB841	pHP14	Cm, Em	Contains the sequences of $P_{\delta}$ $\delta$ : <i>cfp</i> , $P_{\omega}$ $\omega$ : <i>yfp</i> genes (this work).
pCB843	pHP14	Cm, Em	Contains the sequences of $P_{\delta}$ $\delta$ and $P_{\omega}$ $\omega$ : <i>yfp</i> genes (this work).
pCB846	pHP13	Cm, Em	Contains the $P_{\omega}$ : <i>yfp</i> (this work).
pCB847	pHP14	Cm, Em	Contains the sequences of $P_{\delta}$ $\delta$ D60A and $P_{\omega}$ $\omega$ : <i>yfp</i> genes (this work).
pCB860	pHP14	Cm, Em	Contains the sequence of $\delta$ promoter and $\delta$ D211A: <i>gfp</i> gene and <i>orf<math>\omega</math></i> gene (this work).
pCB861	pHP14	Cm, Em	Contains the sequence of $\delta$ promoter and $\delta$ K242A: <i>gfp</i> gene and <i>orf<math>\omega</math></i> gene (this work).
pCB873	pHP14	Cm, Em	Contains the sequence of $\delta$ promoter and $\delta$ K242A: <i>gfp</i> gene (this work).
pCB874	pHP14	Cm, Em	Contains the sequence of $\delta$ promoter and $\delta$ D211A: <i>gfp</i> gene (this work).
pCB879	pHP14	Cm, Em	Contains the sequence of $\delta$ promoter and $\delta$ K248S: <i>gfp</i> gene (this work).
pCB879	pHP14	Cm, Em	Contains the sequence of $\delta$ promoter and $\delta$ K248S: <i>gfp</i> gene and <i>orf<math>\omega</math></i> gene this work).
pCB880	pHP14	Cm, Em	Contains the sequence of $\delta$ promoter and $\delta$ K255A: <i>gfp</i> gene (this work).

pCB880	pHP14	Cm, Em	Contains the sequence of $\delta$ promoter and $\delta K255A:gfp$ gene and $orf\omega$ gene (this work).
pCB881	pHP14	Cm, Em	Contains the sequence of $\delta$ promoter and $\delta D60A D211A:gfp$ gene and $orf\omega$ gene (this work).
pCB882	pHP14	Cm, Em	Contains the sequence of $\delta$ promoter and $\delta K259A K260A:gfp$ gene and $orf\omega$ gene (this work).
pCB897	pHP14	Cm, Em	Contains the sequence of $\delta$ promoter and $\delta:mt$ ( <i>Metallothionein</i> ) gene and $orf\omega$ gene (this work).
pCB898	pHP14	Cm, Em	Contains the sequence of $\delta$ promoter and $\delta D60A:mt$ ( <i>Metallothionein</i> ) gene and $orf\omega$ gene (this work).
pCB900	pHP14	Cm, Em	Contains the sequence of $\delta$ promoter and $\delta K242A:mt$ ( <i>Metallothionein</i> ) gene and $orf\omega$ gene (this work).
pCB901	pHP14	Cm, Em	Contains the sequence of $\delta$ promoter and $\delta:mt$ ( <i>Metallothionein</i> ) gene (this work).
pCB902	pHP14	Cm, Em	Contains the sequence of $\delta$ promoter and $\delta D60A:mt$ ( <i>Metallothionein</i> ) gene (this work).
pCB904	pHP14	Cm, Em	Contains the sequence of $\delta$ promoter and $\delta K242A:mt$ ( <i>Metallothionein</i> ) gene (this work).
pCB917	pHP14	Cm, Em	Derived from pCB702 the plasmid contains the $orf\delta$ and $orf\omega$ genes . The NdeI restriction site was cloned at +1 position of . Del $\delta$ gene. (this work).
pCB921	pHP14	Cm, Em	Contains the sequence of $\delta$ promoter and $\delta D60A/D211A:gfp$ gene (this work).
pCB922	pHP14	Cm, Em	Contains the sequence of $\delta$ promoter and $\delta K259A/K260A:gfp$ gene (this work).
pCB938	pHP14	Cm, Em	Derived from pCB917, it contains the sequence of $\delta$ promoter and $\delta \Delta N20/\Delta C255$ gene and $orf\omega$ gene (this work).
pCB939	pHP14	Cm, Em	Derived from pCB917, it contains the sequence of $\delta$ promoter and $\delta \Delta C255$ gene and $orf\omega$ gene (this work).
pCB940	pHP14	Cm, Em	Derived from pCB917, it contains the sequence of $\delta$ promoter and $\delta \Delta C197$ gene and $orf\omega$ gene (this work).
pCB941	pHP14	Cm, Em	Derived from pCB917, it contains the sequence of $\delta$ promoter and $\delta \Delta C164$ gene and $orf\omega$ gene (this work).
pCB942	pGEM–T easy	Ap	Contains the $\omega 2$ gene cloned under the control of $P_{\omega}$ promoter (this work).
pCB943	pHP14	Cm, Em	Derived from pCB917, it contains the sequence of $\delta$ promoter and $\delta \Delta N20$ gene and $orf\omega$ gene (this work).
pCB955	pHP13	Cm, Em	Contains the sequence of $\omega$ promoter and $\omega 2$ gene (this work).

pCB956	pHP14	Cm, Em	$\omega 2$ , $\delta:gfp$ Contains the sequence of $\delta$ promoter and $\delta:gfp$ , $\omega$ promoter and $\omega 2$ gene (this work).
pT712- $\omega 2$	pT712	Ap	To overproduce the $\omega 2$ protein (this work).

### 1.3. Reagents and Materials.

Chemicals and reagents are listed in table 4. The software and bioinformatic tools employed during the development of this work are listed in table 5.

**Table 4. Reactives and Materials**

MANUFACTURER	PRODUCT
B. Braun Biotech	Labsonic U
Biometra	T3 Thermocycler
BioRad	Micro Bio-Spin columns, Bio-Rad protein assay, Exposure Cassette-K (20x25CM), Personal Molecular Imager (PMI) FX, Power Pac 300, Gel Doc 2000, Molecular Imager ChemiDoc XRS+, Gel Dryer MODEL 583.
Calbiochem	IPTG, Rifampicin, CHAPS.
CRISON	Micro pH 2001
Eppendorf	Thermomixer 5436, Centrifuge 5424, Centrifuge 5810R.
Euroclone	Kit LiteAbiot
Fluka	Methanol, Ethanol, Casein hydrolysate, Spermidine
Forma Scientific	Bio Freezer
GE-Healthcare	G-50 and G-25 Sepharose, Q-Sepharose, SP-sepharose, Superose 6 <sup>TM</sup> , Superdex 75, Sephacryl S-500 HR, anti-rabbit IgG-horseradish peroxidase and anti-mouse IgG, PVDF membrane, HMW Native Marker, Ultrospec 3100 pro. AKTA purifier.
Gilson	P2, P10, P100, P1000
Heidolph	Rotamax 120, MR300, REAX 2000.
ICN	SDS, Ammonium sulphate
Kodak	Storage Phosphor Screen; Cassette con BioMax MS Intensifying Screen.
Konika Minolta	Medical film (18x24CM) y (30x40CM)
MBI Frementas	Restriction enzymes.
Merk	Sodium acetate trihydrate, Boric acid, Hydrochloric acid, Formic acid, Isoamyl alcohol, Coomassie blue, xylocyanol, Bromophenol blue, Chloroform, Magnesium chloride hexahydrate, Dimethyl sulfoxide, Absolute ethanol, Imidazole, Isopropyl alcohol, Glycine, Sodium hydroxide, D/L tryptophan, L-Methionine, Calcium Chloride, PEG-6000, Titriplex (EDTA), Triton-X 100, Urea, 2-nitrophenyl- $\beta$ -galactopyranoside, TLC-PEI cellulose F.
Mettler	Analytical balance AE 240
Microtek	Scan Maker TMA1000XL
Millipore	Filter 0.05 $\mu$ m (VM), 0.45 $\mu$ m (HAWP), 0.22 $\mu$ m (Millex-GS)
MP Biomedicals	Glycerol
New England Biolabs	Restriction enzymes, T4 Polynucleotide Kinase (PNL), T4 DNA ligase
Olympus	Camera Olympus BX61, CCD DP70 colour .
Panreac	Glacial Acetic Acid, Vaseline
Perkin-Elmer	[ $\alpha^{32}$ P]-dATP, [ $\alpha^{32}$ P]-dCTP, [ $\alpha^{32}$ P]-dGTP, [ $\gamma^{32}$ P]-dGTP,

Pierce	Bis (N-hydroxysuccinimide ester) disuccinimidyl suberate (DSS)
Pronadisa	Agarose, Bacteriological agar, yeast extract
Qiagen	Ni-NTA agarose
Roche	Restriction enzymes, FastStart Taq DNA polymerase, pancreatic RNase A, DAPI, Proteinase K.
Serva	Acrylamide, bisacrylamide
Shimadzu	UV-spectrophotometer UV-1800
Sigma	Ampicillin, ethidium bromide, chloramphenicol, glutaraldehyde, Lysozyme, Xylene cyanol, Thiourea, $\beta$ -mercaptoethanol, Polyethylenimine (PEI), Gold (I) chloride.
Spectrum	Dialysis membrane.
Startage	Pfu Turbo DNA polymerase
Thermo Scientific.	NanoDrop ND-1000 Spectrophotometer, Sorvall RC6 Plus, French Press.
UBS	Alkaline phosphatase (SAP), LB, Tris Ultrapure
Vector Laboratories	Vectashield
Whatman	Phosphocellulose

**Table 5. Software and servers.**

SOFTWARE	USE
Adobe Acrobat Pro	Reading, conversion and modification of PDF files.
Adobe Illustrator CS4-CS5	Processing and images' layout
Adobe Photoshop CS4-CS5	Images processing (Ogden and Rosenberg 2007).
Clustal W	Multiple sequence alignment Software (Aiyar 2000).
Chimera	Analysis and visualization of 3D protein structures (Pettersen et al. 2004).
DALI Structural alignment	Protein structure alignment server (Holm and Rosenstrom 2010).
ExPASy Proteomics Databases and Tools	Bioinformatic resource portal: scientific databases and software (Gasteiger E. 2005).
HeliQuest	Graphic representation of the layout and properties of protein $\alpha$ -helices (Gautier et al. 2008).
ImageJ	Software to display, edit, analyse, process images. <b>ObjectJ</b> plugin was used for microscopy image analysis and statistics (Schneider, Rasband and Eliceiri 2012).
I-Tasser	Protein structures and functions prediction server (Roy, Kucukural and Zhang 2010).
Jalview	Bioinformatics software for the analysis and representation of sequence multiple alignments (Waterhouse et al. 2009).
Microsoft Excel 2011	Statistics and graphs.
Microsoft Power Point 2011	Presentations.
Microsoft World 2011	Text editing.
PHD prediction protein	Protein secondary structure prediction server (Rost 1996).
PyMol	Analysis and visualization of 3D protein structures (DeLano 2002).
Quantity One 1D Analysis	DNA and protein quantification.
Serial Cloner 2-1	Molecular biology software to analyse and manipulate DNA, plasmid and Primer sequences
T-coffee	Multiple sequence alignment Software (Taly et al. 2011).



## 1.4. Primers.

Oligonucleotide primers, sequences and melting temperature are listed in table 6.

**Table 6. Oligonucleotides.**

NAME	SEQUENCE	T m
T7 Promoter	5'-taatacgaactcactataggggaattg-3'	62.6
T7 Terminator	5'-gcttagttattgctcagcggg-3'	63.7
Sp6	5'-tatttagtgacactatag-3'	43.4
pHP14 P-delta Fw <sup>a</sup>	5'-ggtttcccagtcacg-3'	61.6
pHP14 omega-end Rev <sup>b</sup>	5'-cacacaggaacagctatgac-3'	59.8
delta-end XhoI-2 Rev	5'-ataagctcgagttcttttcgttttctaattgaa-3'	66.8
P-delta EcoRI Fw	5'-aaagaattcctggagggaag-3'	58.4
P-omega Fw	5'-cacgacgttgtaaacgacgg-3'	67.3
GFP-ATG	5'-gaattgggacaactccag-3'	53.8
CFP-Primer	5'-atagaattcaagttgtcaggtaaatatttccg-3'	67.5
KpnI-Primer	5'-attgtaccaagcttttcccagtcacgac-3'	74.3
OligoA MT Fw	5'-ccgggatccgctagcaggggaattccaccatgggtaaggagaagaactttc-3'	71.4
OligoB MTBH-ST-H3 Rev	5'-aaaaaagcttagcagccggatcctagc-3'	73.6
delta NdeI(Met1) Fw	5'-ggcgtacatagggagaaggaactc-3'	68.3
delta ATG(Met-13) Rev	5'-cataactacgccccattc-3'	57.9
delta STOP-XhoI Rev	5'-aaactcgagtcattcttttcgttttctaattgaataattcgc-3'	75.1
delta 428-449 Up	5'-gcttgctactctcttagcacc-3'	59.9
delta 428-449 Down	5'-ggtgctaagagagtagcaagc-3'	59.9
delta D60A Fw	5'-cgataaggccttacaagc-3'	53.8
delta D60A Rev	5'-gcttgtaaggccttatcg-3'	53.8
delta D211A Fw	5'-gtttgattttatcgttgcgtggccgtatcaactaaataaggaac-3'	79.5
delta D211A Rev	5'-gttccttatttagttgatacggccagcgaacgataaaatcaaac-3'	79.5
delta K242A Fw	5'-ccgttttagaccaggtactactgcattactcgttgataatattttgaaaac-3'	79.0
delta K242A Rev	5'-gtttccaaaatattatcaagcgaagtaatgcagtaagtacctggtctaaaacgg-3'	79.0
delta K248S Fw	5'-cctttatgctctgtaatgccgtttgcagaccaggtacttacttttact-3'	78.1
delta K248S Rev	5'-agtaataaagtaagtacctggtctgcaaacggcattacagagcataaagg-3'	78.1
delta K255A Fw	5'-cagagcatgcaggctatgacaaaaag-3'	70.8
delta K255A Rev	5'-gtcatagcctgcatgctctgtaattgc-3'	70.9
delta K259A/K260A Fw	5'-gctatgacgcagcagtttcatcatgaag-3'	71.8
delta K259A/K260A Rev	5'-ggataaaactgctgcgtcatagcctttatgc-3'	73.3
delta R119C Fw	5'-ctgccaaaattaactgttcatggagc-3'	70.2
delta R119C Rev	5'-cgtccatgaacaagtaattttggcag-3'	70.2
delta D189C Fw	5'-cctatttgattgtttacaagaacaatttaacc-3'	68.2
delta D189C Rev	5'-gggttaaattgttctgtaaacaataatagg-3'	68.2
delta P152C/Y155C Fw	5'-gtaccaactgtgtagcgtttgtacaataatgc-3'	70.8
delta P152C/Y155C Rev	5'-gcattattgtacaacgctacacgttggtacag-3'	72.6
delta D100C Fw	5'-gttcatttgacttgaatttagacttgatccctggc-3'	70.5
delta D100C Rev	5'-caagtctaaattacaagtcaaatgaacaatagaagaagc-3'	68.5
delta L104C Fw	5'-gataatttagactgtatccctggcagctttgattg-3'	70.5
delta L104C Rev	5'-cgtgccagggatacagctaaattatcagtaaatg-3'	71.5
delta N178C Fw	5'-gaagaagttacatgtaacattcaaaactatattcc-3'	65.5
delta N178C Rev	5'-gtttgaaatgttacatgtactttctctctgc-3'	65.5
delta Q181C Fw	5'-caacaacattgttaactatatttctatttgattg-3'	64.5
delta Q181C Rev	5'-ggaaatatagttacaatgtttgtactttc-3'	63.5
delta NdeI-NΔ7 Fw	5'-gagaaggaagaactccatagcttgaagaattaagg-3'	72.1
delta NdeI NΔ20 Fw	5'-cgtttaagcaatcatatggaagcaattg-3'	69.0
delta NdeI NΔ41 Fw	5'-caaaattatcacatattgttctacttg-3'	63.2
delta NdeI NΔ111 Fw	5'-gcagttgatcatatgttactgcc-3'	67.1
delta NdeI NΔ166 Fw	5'-gcgagtgattaccatgatccctttac-3'	67.7

delta NdeI NΔ199 Fw	5'-cctggactacatgatcggtttg-3'	66.1
delta CΔ164-XhoI Rev	5'-aaactcgagtcacactcgcaccagattgc-3'	77.9
delta CΔ197-XhoI Rev	5'-aaactcgagtcacccagggttaaattgtcttg-3'	72.9
delta CΔ227-XhoI Rev	5'-aaactcgagtcattatgtgtctatacagctctccag-3'	73.9
delta CΔ255-XhoI Rev	5'-aaactcgagtcattatgctctgtaatgccgttttag-3'	74.1
pCB702 NdeI-delta Fw	5'-gaatggggcgtacataggagaaggaactcaaatactgaag-3'	79.1
pCB702 NdeI-delta Rev	5'-ccttcccatatgtacccccattctttttgtatagtaattgtatc-3'	75.4
pCB702 BssSI-omeg Fw	5'-atagaaagaagctcgtgattgtggaaatttaggcgcacaaaaagc-3'	81.8
pCB702 BssSI-omeg Rev	5'-cccacaatcacgagcttcttcttcttactcttatttatc-3'	75.9
P-omega HindIII Fw	5'-gcagccaagctttccagtc-3'	69.9
Start omega	5'-gtgagtgattgtggaaatttagc-3'	67.2
Medio omega Fw	5'-gtcgtgctgactgcacc-3'	64.7
Medio omega Rev	5'-ggtgcaagtcagcacgaac-3'	64.7
omega N5C Fw	5'-tttttccatagattgtggatgttaggcgcacaaaaagcaaacg-3'	76.3
omega K10C Fw	5'-tttttccatagattgtggaaatttaggcgcacaaatgtcacaacg-3'	76.3
omega STOP-BamHI Rev	5'-tatcctaggttaaagttgtcaggtaaatttccgtatatatc-3'	72.5
omega 3' K-C-K	5'-aagatcctaacctttacattaccaagttgtcaggtaaatattccg-3'	76.6
delta 3' K-C-K	5'-ataccgggacctttacattaccctcaggtcttttcgtttctaatt-3'	79.3

<sup>a</sup>Forward (Fw), <sup>b</sup>Reverse (Rv)

## 1.5. Media.

In the table 7 are listed the media with their compositions.

**Table 7. Media.**

Type	Composition
Luria-Bertani	- Luria-Bertani liquid Medium (10g/L tryptone, 5.0g/L yeast extract, 5.0g/L NaCl, pH 7.2 at 37°C); - LB solid Medium (10g/L tryptone, 5.0g/L yeast extract, 5.0g/L NaCl, 10g/L Agar, pH 7.2 at 37°C).
GM1	1X S-base, 0.5%, glucose, 0.1% yeast extract, 0.02% casein hydrolysate, 0.8 mM MgSO <sub>4</sub> , 0.025% D/L tryptophan and 0.02% L-Methionine
GM2	GM1 medium supplemented with 3.3 mM MgSO <sub>4</sub> , and 0.5 mM CaCl <sub>2</sub> .
ZY-5052	ZY medium (10g/L tryptone, 5g/L yeast extract), NPS (100mM PO <sub>4</sub> <sup>3-</sup> , 25mM SO <sub>4</sub> <sup>2-</sup> , 50mM NH <sub>4</sub> <sup>+</sup> , 100mM Na <sup>+</sup> , 50mM K <sup>+</sup> ) 50X5052 (0.5% glycerol, 0.05% glucose, 0.2% of alpha-lactose).
MMS7	50mM, MOPS (pH 7.0), 10mM (NH <sub>4</sub> <sup>+</sup> ) <sub>2</sub> SO <sub>4</sub> , 5mM potassium phosphate (pH 7.0), 2mM MgCl <sub>2</sub> , 0.7mM CaCl <sub>2</sub> , 1μM ZnCl <sub>2</sub> , 5μM FeCl <sub>3</sub> , 50μM MnCl <sub>2</sub> , 1% D-glucose, 0.1% sodium glutamate. The medium was further supplemented after autoclave with 0.04 % tryptophan and 0.04 % L-methionine.

## 1.6. Buffers.

In the table 8 are listed the buffers and their compositions. If not indicated otherwise, the salt concentration should be considering 50 mM and glycerol is 0%.

**Table 8. Buffers.**

BUFFER	COMPOSITION
A	50 mM Tris-HCl (pH 7.5)

	10 mM MgCl <sub>2</sub>
<b>B</b>	50 mM Sodium phosphate buffer (pH 7.5) 10 mM MgCl <sub>2</sub>
<b>C</b>	50 mM Potassium phosphate buffer (pH 7.5) 10 mM MgCl <sub>2</sub>
<b>D</b>	50 mM TEA (pH 7.5) 10 mM MgCl <sub>2</sub>
<b>E</b>	50 mM Tris-HCl (pH 8) 5 mM MgCl <sub>2</sub>
<b>F</b>	50 mM Tris-HCl (pH 8) 5 mM MgCl <sub>2</sub> 50 mM KCl.

## 2. Methods

### 2.1. Cells manipulation.

#### 2.1.1. Competent cells production.

##### *a) E. coli.*

Competent cells were obtained as described: exponential growing cells were cultured in LB at 37 °C with shaking until OD<sub>560</sub> 0.4. Cells were harvested by centrifugation, and treated with 0.1 M MgCl<sub>2</sub> and 0.1 M CaCl<sub>2</sub>, which permeabilizes the cells membrane by producing holes. The cells were stored at -80° C in the presence of 15% glycerol until use (Hanahan 1983).

##### *b) B. subtilis.*

Competence naturally occurs under certain growth conditions of nutrient limitation. To make competent cells a colony was inoculated in a liquid culture of GM1, which was incubated for 16 h at 30 °C without agitation. This culture was used to inoculate fresh GM1 medium to OD<sub>560</sub> 0.05 and incubated further at 37 °C with vigorous agitation (250 rpm) until the cells reached the stationary growth phase. Cells were harvested, by centrifugation, after 90 min from point of stationary phase and stored at -80°C with 50% glycerol (Wilson and Bott 1968).

#### 2.1.2. Bacterial Transformation.

##### *a) E. coli.*

*E. coli* transformation was carried out by following the heat shock method (Hanahan 1983). After a 10 min of incubation in ice, the mixture of 200 µl of competent cells and 10–100 ng of plasmid DNA were placed at 42 °C for 1 min (heat shock). The Ca<sup>2+</sup>-induced pores were opened

and double-stranded plasmid enters passively in the cells cytosol. Cells were kept further on ice for 2 min, to restore the membrane. 1 ml of LB medium was added to the reaction, and incubated for 1 h at 37 °C with stirring for cells to allow expression of plasmid-encoded antibiotic resistance gene(s). The cells were plated on LB-agar plate, having selective antibiotics, and incubated 15 h at 37 °C.

**b) *B. subtilis*.**

Cells of *B. subtilis* were transformed by the method of Wilson and Bott 1968. Cells stored at –80 °C were diluted in GM2 medium (1:10), and incubated for 1 to 3 h at 37°C under stirring. Then 200 µl of cells were mixed with 100–200 ng of DNA and incubated for 1 h at 37° C with shaking. Here single-stranded plasmid or chromosomal actively enters in the cell cytosol. Finally the cells were plated on LB-agar with the required antibiotic.

## **2.2. Protein purification.**

### **2.2.1. Protein overproduction.**

All proteins used in this work were overexpressed from BL21 (DE3) strains, except for the RNAP-  $\sigma^A$  multi-subunit enzyme that was produced from *B. subtilis* JH642 strain (Fujita and Sadaie 1998). Protein  $\omega$  and  $\omega\Delta N19$  were cloned into pT712 (GIBCO-BRL). Protein  $\delta$  and its variant were cloned into pET21b and pET15b. In these vectors, target genes are cloned under control of  $\phi 10$  T7 promoter (Studier and Moffatt 1986). The plasmid was transformed in *E. coli* BL21 (DE3) strain that contains a single copy of gene 1 encoding for T7 RNAP integrated as a single copy in the host chromosome under control of the inducible *lacUV5* promoter ( $P_{lacUV5}$ ). The addition of IPTG (0.2 – 1 mM) induces  $P_{lacUV5}$  to transcribe gene 1, which in turn its product (T7 RNAP initiates high-level expression of the target gene in the plasmid. *E. coli* BL21(DE3) (pLysS) cells bearing the selected plasmids were grown to mid-exponential phase ( $OD_{600}= 0.4$ ) at 37 °C before the addition of 1 mM IPTG. Rifampicin (200 µg/ml) was added in culture after 30 min of IPTG induction. Cells grew an additional 2h at 37 °C and were pelleted and stored at –20 °C.

The auto-induction medium ZY-5052 was used to overproduce but also increase the solubility of  $\omega 2$  protein (Studier 2005). Auto-induction is more convenient than IPTG because increases the solubility of proteins due to the slow growth. Once the culture reached the saturation, the expression of protein was auto-induced. The cells were inoculated into ZY rich auto-inducing medium and grown to saturation for 16 h at 30 °C and then the cells were harvested and stored at –20 °C.

### 2.2.2. Protein purification.

The theoretical isoelectric point of all relevant proteins was calculated. This pI is important to predict a strategy of purification according the buffer and the properties of the columns to be used during the purification. If not stated otherwise all purification states were performed at 4 °C.

#### *a) Purification of $\omega$ and $\omega\Delta N19_2$ .*

The  $\omega_2$  (pI=9,51) and  $\omega\Delta N19_2$  (pI=9,01) proteins were purified as previously described (Misselwitz et al. 2001). Cells were resuspended in buffer B (50 mM Sodium phosphate buffer, pH 7.5, 10 mM MgCl<sub>2</sub>, 2 mM DTT, 0.2 mM PMSF, 5% glycerol) containing 100 mM NaCl and lysed with a French press (1,500 psi). The crude extract was centrifuged at 12,000g for 30 min (rotor Sorvall SS-34) and the supernatant was used for further purification steps.

To separate the protein from nucleic acids, polyethyleneimine (PEI) (0.25 %, OD<sub>260</sub> = 120) was added to the supernatant for 2h. The supernatant was centrifuged at 12,000g for 30 min. The proteins contained in the supernatant were precipitated with 50% of ammonium sulphate (AS). The pellet was diluted in Buffer B (0 mM NaCl) up to obtain a solution with that corresponds to 50 mM NaCl ionic strength. The proteins were loaded into a phosphocellulose column (previously activated and equilibrated with buffer B containing 50 mM NaCl). The  $\omega_2$  and  $\omega\Delta N19_2$  proteins retained in the phosphocellulose were washed several times and eluted with 200 mM of NaCl. Once eluted, the salt concentration was diluted up to 100 mM and then loaded in SP-sepharose previously equilibrated with buffer B with 100 mM NaCl. The retained proteins were washed with increasing concentration of Salt and finally eluted free of contaminants with 175 mM of NaCl. To concentrate the elution, the proteins were loaded one more time in a mini-phosphocellulose column and eluted in buffer B containing 300 mM of NaCl. The  $\omega_2$  and  $\omega\Delta N19_2$  proteins were dialyzed in buffer A with 300 mM NaCl and 50% glycerol for 4 h and stored at -20 °C. The protein concentrations were determined by absorption at 280 nm using molar extinction coefficients of 2,980 M<sup>-1</sup> cm<sup>-1</sup> for  $\omega_2$  and  $\omega\Delta N19_2$ .

#### *b) Purification of $\delta_2$ -His<sub>6</sub> and its variants.*

The His-tagged protein  $\delta$  protein and its mutants (pI = 5.34) were overexpressed in *E. coli* BL21 (DE). The mass cells were resuspended and lysed in buffer B containing 1M NaCl and 0.5 mM imidazole. After centrifugation (1800 rpm for 45 min),  $\delta_2$  protein as well as other full length variants were found in the soluble fraction. The supernatant was loaded onto a Ni<sup>2+</sup>-NTA previously equilibrated with buffer B containing 1 M NaCl and 0.5 mM imidazole. The matrix was washed with an imidazole gradient from 2.5 to 50 mM. The fraction containing  $\delta_2$  protein

were diluted up to 50 mM NaCl and loaded onto a Q-Sepharose column. After washing the column the protein was eluted at 200 mM NaCl. The pure protein was dialyzed against buffer A (Tris-HCl pH 7.5, 50 mM, 50 % glycerol, 100 mM NaCl) and stored at  $-20^{\circ}\text{C}$ .

Comparative tests between  $\delta_2$  and  $\delta_2$ -His<sub>6</sub> proteins were carried out in our laboratory. It was demonstrated that both proteins had similar biochemical features in similar range of concentrations.

**c) Purification of  $\delta_2$  truncated variants.**

The purification protocol previously described was ineffective. Truncated variants of  $\delta$  (His<sub>6</sub>- $\delta\text{C}\Delta 255$  [pI=5.24]; His<sub>6</sub>- $\delta\text{C}\Delta 227$  [pI=4.81]; His<sub>6</sub>- $\delta\text{C}\Delta 197$  [pI=4.91] and His<sub>6</sub>- $\delta\text{C}\Delta 164$  [pI=5.88]) were insoluble after lysis and centrifugation, therefore, a new purification protocol implying the use of urea was developed. The truncated proteins were overexpressed by induction with 1 mM IPTG in *E. coli* strain BL21 (DE), conditions which ensured high expression levels. Cells were lysed using a French Press in buffer B containing 1M NaCl and 10% glycerol. The lysate (1800 rpm for 45 min) was centrifuged and the supernatant was discarded. The pellet, containing the truncated  $\delta$  variant was washed three times in buffer B containing 1 M NaCl. After washing step, the pellet was incubated with buffer B containing 1 M NaCl and 4M urea by string for 4 h. In presence of 4M urea, the truncated protein was found in the supernatant fraction. After centrifugation (18000 rpm for 45 min) the supernatant was loaded onto a Ni<sup>2+</sup>-NTA column previously equilibrated with buffer B containing 1 M NaCl and 4M urea. The truncated protein trapped in the matrix was washed with increasing concentrations of imidazole (5 mM, 20 mM, 40 mM, 60 mM) before to be eluted with 100 mM imidazole. The pure protein was then passed through sequential dialysis in buffer A containing 100 mM NaCl with decreasing concentration of urea (from 2M to 0 M) in order to eliminate de urea. The protein was then recollected and stored at  $-20^{\circ}\text{C}$ .

**d) Purification of *B. subtilis* RNAP.**

The RNAP- $\sigma^A$  was purified from *B. subtilis* NIG2001 strain as reported (Fujita and Sadaie 1998). In this strain, the *rpoC-his6* fusion gene, presence as a unique copy in its native locus on the chromosomal, is under the control of the native promoter for *rpoBC* operon, by this way the fully active his-tag RpoC subunit is expressed at physiological levels. The cells of NIG2001 were grown in exponential conditions and were harvested once reached the mid-exponential phase ( $\text{OD}_{560} \approx 0.6$ ). The *B. subtilis* cell extract was resuspended and lysed using a French Press in buffer E containing 0.3 M NaCl, 0.5 mM imidazole and 20 % glycerol. The supernatant containing the RNAP- $\sigma^A$  was separated by centrifugation to further be loaded to Ni<sup>2+</sup>-NTA

column. The matrix was washed with increasing concentration of imidazole up to 20 mM and finally the RNAP- $\sigma^A$  was eluted at 400 mM of imidazole. To concentrate the RNAP- $\sigma^A$ , the elution fraction was diluted up to 50 mM NaCl and loaded onto a Q-Sepharose column. The multi-protein was eluted at 300 mM KCl. The RNAP- $\sigma^A$  was dialyzed against buffer F containing 50 % glycerol and stored at  $-20^\circ\text{C}$ .

### **2.3. DNA manipulation.**

#### **2.3.1. DNA isolation and quantification.**

The plasmid DNA was isolated from *E. coli* cells by the alkaline lysis protocol (Birnboim and Doly 1979). When required the plasmid DNA was purified by a CsCl gradient or by using the DNA purification kit from Qiagen. The DNA concentration was quantified by absorbance at 260 nm using the molar extinction coefficients of  $6,500\text{ M}^{-1}\text{ cm}^{-1}$ , and its purity was determined using a coefficient relating the absorbance at 260 nm and 280 nm of the samples (Sambrook J 1989).

#### **2.3.2. DNA electrophoresis.**

##### ***a) Nucleic acids separation by agarose gel Electrophoresis.***

Agarose gel electrophoresis is a routinely used method for separating and estimating the size of circular or linear DNA molecules (Sambrook J 1989). This method was largely employed in this work to generate substrates for molecular cloning or biochemical assays. The agarose gel was prepared and ran in 1X Tris-acetate-EDTA (TAE) buffer.

##### ***b) Denaturing Gel Electrophoresis for Sequencing (D-PAGE).***

The D-PAGE was prepared as described in the protocol (Slatko and Albright 2001). The accuracy of DNA sequence determination depends largely upon resolution of the sequencing products in denaturing polyacrylamide gels. The DNA sequences were heated 2 min at  $95^\circ\text{C}$  in formamide loading buffer (95% (v/v) formamide 0.09% (w/v) bromophenol blue, 0.09% (w/v) xylene cyanol FF), then placed on ice prior to loading in gel. The gels used for sequencing were 40-cm long, contain 6% or 8% acrylamide and 6M urea and ran at 40W constant power in 1X Tris-borate-EDTA (TBE) buffer.

#### **2.3.3. Radioactive DNA labelling.**

Labelling was performed by fill-in the 3'-end of tailed dsDNA with the large fragment of DNA Pol I (Klenow enzyme). DNA fragments with one or both 3'-ends were incubated with Klenow for 15 min at room temperature in presence of 250  $\mu\text{M}$  de dCTP, dGTP, dTTP and

[ $\alpha^{32}\text{P}$ ] dATP. The remaining unincorporated nucleotides were eliminated by Sephadex G-50 filtration.

#### **2.3.4. Preparation and purification of DNA fragments.**

##### **a) *P<sub>copS</sub>* promoter region (*parS3*):**

To obtain *copS* DNA used in EMSA and footprinting assays, the pUC57 was digested with *Hind*III and *Kpn*I, generating 5'-overhangs on only one strand. The digestion was loaded onto an agarose gel 0.8% and the band corresponding to the *copS* fragment was gel purified and subsequently labelled as described in 2.3.3.

##### **b) *P<sub>o</sub>* (*parS2*):**

To obtain *P<sub>o</sub>* (*parS2*) DNA used in EMSA, the pUC30 was digested with *Hind*III and *Kpn*I, generating 5'-overhangs on one strand or with *Hind*III and *Eco*RI to generate 5'-overhangs on both strands. The digestion was loaded onto an agarose gel 0,8% and the band corresponding to *P<sub>o</sub>* fragment was purified from the gel and subsequently labelled as described in 2.3.3.

#### **2.3.5. Site-specific mutagenesis.**

To perform site-directed mutagenesis the 'megaprimer' protocol was used (Kammann et al. 1989). This method involves two rounds of PCR that utilize two 'flanking' primers and one internal mutagenic primer containing the desired base substitution(s):

- 1- The first two PCRs were performed using the mutagenic internal primers and the corresponding flanking primers. The products of this first round, the 'megaprimer', were purified and used for the second round.
- 2- The two 'megaprimers' and the flanking primers were used for a second PCR. The final PCR product contained the desired mutation in a particular DNA sequence.
- 3- The mutated DNA sequence was gel purified and cloned in a specific plasmid vector.

#### **2.4. *In vitro* assays.**

##### **2.4.1. Non-denaturing and denaturing protein electrophoresis.**

###### **a) *Native electrophoresis (N-PAGE).***

N-PAGE was prepared as describe in protocol to study protein-DNA interaction by EMSA (Garner and Revzin 1981). The 4% or 6% polyacrylamide gel was prepared in 1X TAE buffer. The DNA loading buffer (30% (v/v) glycerol, 0.25% (w/v) bromophenol blue, 0.25% (w/v) xylene cyanol FF) was added to mixture of protein-DNA prior to loading in the N-PAGE gel. The samples migrated under constant voltage of 150V at 4 °C.



***b) Blue Native electrophoresis (BN–PAGE).***

BN–PAGE was prepared and used as described (Wittig, Braun and Schagger 2006). The Coomassie blue G250 was used to eliminate the effect of protein charges on mobility. The blue native loading buffer (200 mM Tris–HCl pH 6.8, 40% glycerol, 0.4% (p/v) Coomassie Brilliant Blue G) was added to 1.5–3µg of protein. Samples containing loading buffer were incubated for 10 minutes at 4 °C prior to loading in the wells of 5% PAGE. The gel ran under constant voltage (75V) in the cold room (4 °C) until the tracking dye reached the bottom of the gel. The gel was stained with Coomassie Blue and the native molecular mass of proteins was determined by HMW native marker (GE healthcare).

***c) Sodium Dodecyl Sulphate–PolyAcrylamide Gel Electrophoresis (SDS–PAGE).***

SDS–PAGE was prepared as described (Sambrook and Russell 2006). The loading buffer (2% SDS, 1% β–mercaptoethanol, 10% glycerol, 50 mM Tris–HCl pH 6.8) was boiled for 2 min, prior to loading in the stacking gel. The gel ran under constant voltage (150V) at room temperature. Several polyacrylamide concentration and gradient gels were employed in this study.

***d) Two–dimensional (2–D) electrophoresis.***

2D–PAGE was used to analyse RNAP– $\sigma^A$ – $\omega_2$  complexes, 2–D electrophoresis technique was used to separate proteins according to two independent properties in two discrete steps (O'Farrell 1975). The first–dimension, isoelectric focusing (IEF), separates proteins according to their isoelectric points (pI); the second–dimension, the SDS–PAGE, separates proteins according to their molecular mass. For 2D–PAGE, 40 µg of RNAP– $\sigma^A$  protein complex were precipitated and resuspended in appropriate buffer for IEF [250 µl 7M Urea, 2M Thiourea, 4% CHAPS, 10mM DTT and 2% ampholytes 3–11NL (GE Healthcare)]. The first–dimension IEF separation was obtained using applying sample to an IPG strip of 7cm covering wide pH range (3–11NL). After IEF, the second–dimension was obtained by placing the strip on the top of the gradient 3–10% SDS–polyacrylamide gel (GE Healthcare) and further electrophoretic separation. According to the use, the 2–D gel was either stained with Blue coomassie or transfer to polyvinylidene fluoride (PVDF) membrane from Millipore (0.45 µm). The 2–D electrophoresis preparation, separation, transfer and further spots identification through peptide mass fingerprinting was carry out by the CNB proteomics facility.

#### **2.4.2. Homo- and hetero-oligomeric interactions between proteins.**

In this studies we used of several coupled techniques to characterize the protein-protein interaction of  $\omega_2$ ,  $\delta_2$  and RNAP- $\sigma^A$  proteins from *B. subtilis*.

##### **a) *Electrophoresis under native condition.***

N-PAGE was used to determine the homo- and hetero- oligomeric states of proteins.

##### **b) *Homo-oligomeric by cross-linking assays.***

Proteins cross-linking was carried out in buffer C (or buffer D) containing 50 mM NaCl by incubation with increasing concentrations of suberic acid-bis(N-hydroxysuccinimide) ester (DSS) (0.1–1 mM) for 10 min at 37 °C. The reactions were stopped with trichloroacetic acid.  $\delta_2$  and  $\omega_2$  proteins precipitates were washed with acetone, dried, dissolved in SDS sample buffer and loaded onto 10% and 15% SDS polyacrylamide gels respectively.

##### **c) *Hetero-dimeric interaction between $\omega_2$ and $\delta_2$ .***

Protein cross-linking was used to study  $\omega_2$ - $\delta_2$  interactions. The cross-linking reactions were performed mixing 3  $\mu$ g of each protein in presence or absence of 1.2  $\mu$ g of pCB30 in buffer C (or D) supplemented with 1 mM ATP and incubated for 15 min at 37 °C in 20  $\mu$ l volume. The cross-linking agent DSS was added, to a final concentration of 500  $\mu$ M, and the reactions were left 10 min more at room temperature. The reactions were stopped by addition of 10 $\mu$ l stop buffer B and separated using a 10–15% SDS-PAGE. The bands obtained were identified by Peptide Mass Fingerprinting MS.

##### **d) *Hetero-dimeric interaction between $\omega_2$ and RNAP- $\sigma^A$ .***

The cross-linking reaction was performed as previously described. A constant amount of RNAP- $\sigma^A$  and  $\omega_2$  (3  $\mu$ g) was diluted in buffer C (or D) containing 50 mM NaCl and 1 mM ATP or 0.25 mM/each of NTPs (ATP, CTP, GTP, UTP). The cross-linking samples were separated using a 4–10% SDS-PAGE and the novel bands were identified by Peptide Mass Fingerprinting MS.

#### **2.4.3. Limited proteolysis assay.**

For proteolytic studies, 20 $\mu$ l of reaction containing  $\delta_2$  (3  $\mu$ M) in buffer A supplemented with 1 mM ATP in presence or absence of 150 $\mu$ M of pCB30 was pre-incubated at 37 °C. The reaction was then subjected to proteolysis by addition of increasing concentration of proteinase K (0.5–2  $\mu$ g/ml) end further incubation for 60 min at room temperature. The reaction was stopped by addition of stop buffer (50 mM Tris-HCl, pH 7.5, 400 mM glycine, 3%  $\beta$ -mercaptoethanol, 2%

SDS, 10% glycerol), before the products were loaded onto a 15% SDS–PAGE gel. The signal was quantified using a PhosphorImager.

#### **2.4.4. Peptide mass fingerprinting MS.**

To identify the proteins peptide mass fingerprinting analysis was used. The MALDI–TOF–TOF measurements of spotted peptide solutions were carried out on a Proteome–Analyser 4700 (Applied Biosystems, Foster City, USA) as described previously (Lioy et al. 2006) by Proteomics Facility of CNB–CSIC.

#### **2.4.5. Western blotting analysis.**

Cellular crude extract and/or purified proteins were separated by SDS–PAGE and electrotransferred to PVDF membrane using either wet or semi–dry methods in Tris–Glycine buffer (25mM Tris–HCl, 128mM Glycine, 0.1% SDS, 10% methanol, pH 8.5). The membrane was blocked with 5% skim milk and probed 2h at room temperature with the primary antibody [1:5000 dilutions was used for rabbit polyclonal anti- $\omega_2$  and mouse polyclonal anti- $\delta_2$ ; 1:2000 dilutions for anti–RNAP core enzyme ( $\alpha$ – $\alpha$ – $\beta$ – $\beta'$ ), anti- $\alpha$  and anti- $\sigma^A$ ]. After this incubation, the membrane was washed three times in TBS Tween 0.05% and probed for 1 h at room temperature with the appropriate dilution of horseradish peroxidase (HRP)–conjugated secondary antibody. The labelled proteins were detected using ECL (LiteAbiot) and autoradiography film (Konica Minolta).

#### **2.4.6. Far western blotting analysis.**

To study protein–protein interaction the FWB method was employed (Wu, Li and Chen 2007). The FWB technique is quite similar to Western blotting. In a Western blot, an antibody is used to detect the corresponding antigen on a membrane. In a classical FWB analysis, a labelled or antibody–detectable “bait” protein is used to probe and detect the target “prey” protein on the membrane. In this work, the samples containing the prey proteins were separated by SDS–PAGE (**a**) or native PAGE (**b**) and then transferred to a membrane.

(**a**) The proteins were separated by SDS–PAGE and transferred to PVDF membrane using buffer supplemented with SDS up to 0.1%. After transfer, the membrane was submitted to overnight incubation at 4 °C in renaturing solution (TBS Tween 0.05%, 10% glycerol and 5 mM  $\beta$ –mercaptoethanol). In this step, the SDS is removed to allow protein renaturation in the membrane. The membrane was washed 2 h at room temperature with phosphate buffered saline (PBS) 1X and subsequently blocked for 2 h at room temperature in PBS 1X and 5% skim milk.

The membrane was incubated 16 h at 4 °C with a solution (TBS 0.05% and 5% skimmed milk) containing 2 µg/ml of the second protein (bait). The membrane was washed 5 times in TBS 0.05% and further incubated with rabbit polyclonal antibodies against the bait to detect the protein–protein interaction as previously described for Western Blotting protocols.

(b) The proteins were separated by N–PAGE and wet transferred in Tris–Glycine buffer without to PVDF membranes (Wu et al. 2007). The membrane was washed 5 min in 8% acetic acid, 5 min in pure water before continuing the protocol as previously described with the blocking, incubation with bait and antibodies and film exposure.

#### **2.4.7. Protein and DNA interactions.**

##### **a) EMSA.**

For EMSA, gel–purified 423–bp [ $\alpha^{32}\text{P}$ ]– $P_{\omega}$  DNA (0.1 nM) was incubated in buffer A containing 50 mM NaCl for 15 min at 37 °C with different amounts of  $\omega_2$ ,  $\delta_2$  or RNAP– $\sigma^A$  or a constant amount of one and variable amount of the second or third protein in the in a 20 µl final volume, and immediately loaded onto the gel (de la Hoz et al. 2000, de la Hoz et al. 2004, Hellman and Fried 2007, Garner and Revzin 1981). The samples were separated on a 6% N–PAGE. Gels were run with 1X TAE at 150V at room temperature and dried prior to autoradiography. To obtain apparent dissociation constant ( $K_{\text{Dapp}}$ ) values from EMSA experiments were used. The relative concentration of free DNA and protein–DNA complexes were densitometrically determined under non–saturating conditions from differently exposed autoradiographs of EMSA gels. Protein concentrations that transfer 50% of the free–labelled DNA into complexes are approximately equal to the  $K_{\text{Dapp}}$  under conditions where the DNA concentration is much lower than the  $K_{\text{Dapp}}$ .

##### **b) Filter binding.**

The rate of dissociation of  $\omega_2$  and  $\delta_2$  or both proteins from *parS* DNA complexes was measured by using alkali–treated filters (millipore, type HAWP 0.45 µm) as previously described (Alonso et al. 1993). The standard reaction (20 µl) contained the 423–bp [ $\alpha^{32}\text{P}$ ]– $P_{\omega}$  (*parS*) DNA (1 nM) and different amounts of  $\omega_2$  and or  $\delta_2$  (in the presence or absence of cold DNA) in buffer A containing 50 mM NaCl. The reaction was incubated for 15 min at 37 °C and then diluted in ice–cold buffer A (1 ml) and filtered through 0.5M KOH–treated filters. Filters were dried and the amount of radioactivity retained on the filter was determined by scintillation counting. The DNA retained on the filter was corrected for the retention of radiolabelled DNA in the absence of proteins. The specific activity of the labelled DNA was measured as 10% TCA precipitable material. All reactions were performed in duplicate.

### c) *DNase I footprinting.*

For footprinting experiments, the reaction conditions were as for EMSA. The 423-bp [ $\alpha^{32}\text{P}$ ]-*HindIII-KpnI P<sub>ω</sub> (parS)* DNA (1 nM) was incubated with  $\omega_2$ ,  $\delta_2$  and RNAP- $\sigma^A$  or a combination of all proteins under the same conditions as the EMSA experiments previous addition of DNase I (de la Hoz et al. 2000, de la Hoz et al. 2004), The proteins added, and their concentrations, are specified in the figure legends. . The reactions were incubated 5 min at 37 °C and stopped by adding 25 mM EDTA. The DNA were precipitated with ethanol and resuspended with 10  $\mu\text{l}$  of formamide buffer [80% (v/v) formamide, 0.1 % (v/v) bromophenol and 0,1% (v/v) xilencianol]. The samples were analysed by 6% D-PAGE and dried prior to autoradiography. As size control markers, ladders obtained with the chemical sequencing reaction Potassium permanganate footprinting.

KMnO<sub>4</sub> footprinting was performed as previously described (Monsalve et al. 1996). The 423-bp [ $\alpha^{32}\text{P}$ ]-*HindIII-KpnI P<sub>ω</sub> (parS)* DNA (1 nM) was used as substrate for potassium permanganate footprinting. The reactions were performed in 25  $\mu\text{l}$  a solution containing 50 mM Tris-HCl (pH7.5), 10 mM MgCl<sub>2</sub>, in presence of RNAP- $\sigma^A$  and/or  $\omega_2$  and with or without the initiating NTPs (1 $\mu\text{M}$  of ATP and GTP). The reactions were incubated at 37 °C with the first proteins, 5 min after the second proteins was then added and the reaction were incubated 5 min more at 37 °C. The samples were then treated with KMnO<sub>4</sub> (4 mM) for 30 seconds at 37 °C and the reactions were stopped by addition of 5 $\mu\text{l}$  of a solution containing 1M  $\beta$ -mercaptoethanol and 1.5 M sodium acetate. The DNA was gel filtrated by a Sephadex G-50 spin column and the DNA was cleaved by incubation with 1M piperidine at 90 °C (Maxam and Gilbert 1980). Reactions were precipitated and resuspended first in TE buffer (10 mM Tris HCl, 1 mM EDTA, pH 8.0). The formamide loading buffer was added to samples, and the reaction was resolved on an 8% D-PAGE and the gel autoradiographed.

### 2.4.8. Transcription run-off experiment.

The promoter region of  $\omega$  gene, the 423-bp [ $\alpha^{32}\text{P}$ ]-*P<sub>ω</sub>* DNA (0.4 nM) was obtained by enzymatic digestion (*EcoRI* and *HindIII*) from pCB30. The 423-bp DNA fragment was used as a template for *in vitro* transcription run off assays. The reaction mixtures was incubated different amounts of  $\omega_2$ ,  $\delta_2$  or both in buffer E (50 mM Tris-HCl (pH 8), 6 mM MgOAc, 5 mM DTT) contained, UTP, CTP, GTP, ATP (0.5 mM each plus 1:10,000 [ $\alpha^{32}\text{P}$ ]-UTP 3000 Ci/mmol) and 20 U of RNasin (Promega) in 20  $\mu\text{l}$  of a solution. After 15 min of incubation at 37 °C, 30 nM *B. subtilis* RNAP- $\sigma^A$  was added to reactions and incubated 5 min more at 37 °C. The reactions were

stopped with 1  $\mu$ l of 0.5 M EDTA and 10  $\mu$ l of formamide buffer. The RNAs were analysed by 8% D-PAGE, and the gel autoradiographed. Chemical sequencing reactions of purines were run in parallel to determine the sizes of the cDNAs obtained.

#### **2.4.9. ATPase assay.**

##### **a) *Thin layer chromatography (TLC).***

The ATPase activity of  $\delta_2$  (or its variants) was determined by thin layer chromatography (TLC) (Carrasco et al. 2005). Standard tests was performed in buffer C containing 50 mM NaCl and 1 mM ATP (with a 1:100 000 ratio of labelled [ $\gamma$ - $^{32}$ P]ATP/ cold ATP) in presence or absence of *parS* DNA were assembled on ice. A constant amount of  $\delta_2$ , *parS* DNA and increasing concentrations of  $\omega_2$  were added and the samples incubated for 30 to 180 min at 37 °C. Aliquots were taken at several times the reactions were stopped with 25 mM EDTA. ATPase activity was measured by thin layer chromatography using 200 mM potassium phosphate as eluent. The reaction products were captured by PhosphorImager analysis (Molecular Dynamics) and quantified by Quantity One 1-D Analysis Software.

##### **b) *NADH-coupled ATPase assay.***

The ATP hydrolysis activity of  $\delta_2$  protein and its stimulation by  $\omega$  and *parS* DNA was also observed via a coupled spectrophotometric enzyme assay (Morrical, Lee et al. 1986, Hobbs, Sakai et al. 2007). Absorbance measurements were taken with a Shimadzu CPS-240A dual-beam spectrophotometer equipped with a temperature controller and 6-position cell chamber. The cell path length and band pass were 1 cm and 2 nm, respectively. The regeneration of ATP from ADP and phosphoenolpyruvate driven by the oxidation of NADH can be followed by a decrease in absorbance at 340 nm. Rates of ssDNA-dependent RecA-mediated ATP hydrolysis and the lag times were measured in buffer A containing 50 mM NaCl, 50 $\mu$ g/ml BSA, 5% glycerol and 5 mM ATP for variable time at 37 °C in a 100  $\mu$ l reaction mixture. An ATP regeneration system (0.5 mM phosphoenolpyruvate, 10 units/ml pyruvate kinase) and a coupling system (0.25 mM NADH, 10 units/ml lactate dehydrogenase, 3 mM potassium glutamate) were also included. The orders of addition of 25  $\mu$ M pCB30 DNA, the proteins and their concentrations were indicated in the text. The amount of ADP accumulated was calculated as describe (Arenson, Tsodikov and Cox 1999).

#### 2.4.10. Electron Microscopy.

To visualize protein–DNA complexes, transmission electron microscopy (TEM) technique was used. The formations of  $\omega_2$ -*parS*,  $\delta_2$ -*parS* or  $\delta_2$ - $\omega_2$ -*parS* complexes for electron microscopy were performed in 10  $\mu$ l reaction in buffer D (50 mM TEA pH 7.5, 50 mM NaCl, 10 mM MgCl<sub>2</sub>). Circular or linear pCB30 DNA (100 ng) and 60 nM of  $\omega_2$  or 75 nM up to 600 nM of  $\delta_2$  were incubated 15 min at 37 °C. The complexes were fixed with glutaraldehyde at 0.2% final concentration for 10 min and the cross–linking reaction was stopped by 200  $\mu$ l of 50 mM Tris–HCl pH 7.0 buffer. The DNA–protein complexes were separated from unbound proteins or glutaraldehyde by gel filtration and were visualized by EM after negative staining with 1% uranyl acetate (Pratto et al. 2008). A fraction of the sample was deposited on a freshly cleaved mica surface and the sample processed as previously described (Spiess 1988). EM observations were performed with a Philips EM400T, and the images were processed with *ImageJ* software.

#### 2.5. *In vivo* assays.

Most of this work was performed in *B. subtilis*, a model system of gram–positive bacteria of the Firmicutes phylum, because of its amenability to genetic manipulation. All the systems studied derived from the broad–host–range Firmicutes pSM19035 and the system tested in *B. subtilis* might function in the same manner for *Streptococci*.

##### 2.5.1. Plasmid stability.

The number of plasmid copies per cells was estimated as previously described (Ceglowski et al. 1993). The plasmid containing the antibiotic resistance to chloramphenicol and target genes was transformed into *B. subtilis* cells. The plasmid–containing cell was grown in LB at 30 °C during 16 h (~ 15 generations). The culture was diluted in pre–worm fresh LB to OD<sub>560</sub> ~ 0.05 and incubated 8 h at 30 °C (~ 8 generations). This cycle was repeated up to 100 generations. Samples every 20 generations were plated on LB. The numbers of plasmid–containing cells were determined by replica plating onto chloramphenicol–containing plates. The frequency of plasmid loss (L) was calculated as  $L = 1 - (P)^{1/g}$ , where P is the number of cells bearing plasmids after growth for g generation. The relative loss rate was expressed as percentage and calculated as  $L = (L_N - L_X) / (L_N - L_P) \times 100$ , where L<sub>N</sub> is the loss rate per cell generation of negative control (empty vector), L<sub>X</sub> is the empirical loss rate of  $\delta_2$  and  $\omega_2$  variant and L<sub>P</sub> is loss rate per cell generation of positive control (vector–bearing  $\delta$  and  $\omega$  genes).

### 2.5.2. $\beta$ -Galactosidase assays.

Aliquots of 100  $\mu$ l of *B. subtilis* cells grown to  $OD_{600} = 0.6$  were pelleted and resuspended in 1ml Z buffer (0.1M sodium phosphate buffer pH 7.0, 10 mM KCl, 1 mM  $MgSO_4$ , 50 mM  $\beta$ -mercaptoethanol) containing 0.4 mg/ml lysozyme. After 5 min incubation at 37 °C, Triton X-100 (final concentration 0.08%) was added, mixed, and the lysates clarified by 5 min centrifugation at  $12,000 \times g$ .  $\beta$ -Galactosidase was assayed in the cell lysates as described (Miller 1972). At zero time, the assay was initiated by adding 200  $\mu$ l of 4 mg/ml ONPG (o-nitrophenyl- $\beta$ -galactopyranoside). The sample was incubated at room temperature for the appropriate length of time until the solution turned yellow. The reaction was terminated by the addition of 0.5 ml of 1 M  $Na_2CO_3$ . Then, the absorbance data for  $A_{420}$ ,  $A_{550}$ , and  $A_{600}$  were measured and the  $\beta$ -galactosidase specific activities in Miller units was calculated as follow:

$$\underline{\beta\text{-galactosidase units}} = 1,000 * \frac{A_{420} (1.75 * A_{550})}{t_{(\text{min})} * V_{(\text{ml})} * OD_{600}}$$

where: **t** is the time (in min) of incubation; **V** is the volume of cells used; **A<sub>420</sub>** & **A<sub>550</sub>** are the absorbance which measures the yellow colour present due to ONPG cleavage (420nm) and the scatter from cell debris (550nm) respectively; **OD<sub>600</sub>** reflects cell density in the cell suspension.

### 2.5.3. Fluorescence Microscopy.

*B. subtilis* cells bearing the indicated plasmid or expression cassette were grown overnight in MMS7 with the corresponding antibiotic marker at 30 °C. The cultures (1.5 ml) were diluted in fresh medium to  $OD_{560} \sim 0.05$  and incubated until  $OD_{560} \sim 0.4$ . When indicated IPTG (10  $\mu$ M final concentration) to induce synthesis of  $\delta$ :GFP<sub>2</sub> or  $\delta$ D60A:GFP<sub>2</sub>. For nucleoid visualization, the sample (1.5 ml) was incubated with DAPI (final concentration 5  $\mu$ g/ml) on ice and darkness for 10 min before slide preparation (Pratto et al. 2008). The cells were harvested, and the pellet (50  $\mu$ l) resuspended in pre-worm MMS7 medium, an aliquot was placed on a polylysine-coated glass slide and cover with a coverslip, and incubated at 32°C as previously described (Sengupta, Laughlin and Niven 2010). Images were acquired using a Nikon Eclipse E-1000 fluorescence microscope equipped with a Nikon C-CU Universal condenser, a Smrock GFP-3035 bright-line zero band-pass filter cube, and a Hamamatsu Orca-ER c4742-95 charge-couple device (CCD) camera. Pictures were taken at 20 s interval during 10 min, and analysed with the Image Pro Plus 6.1 software using macrodirected cell recognition and measurement of the focus number and position as described (Sengupta et al. 2010).



## ***Results***

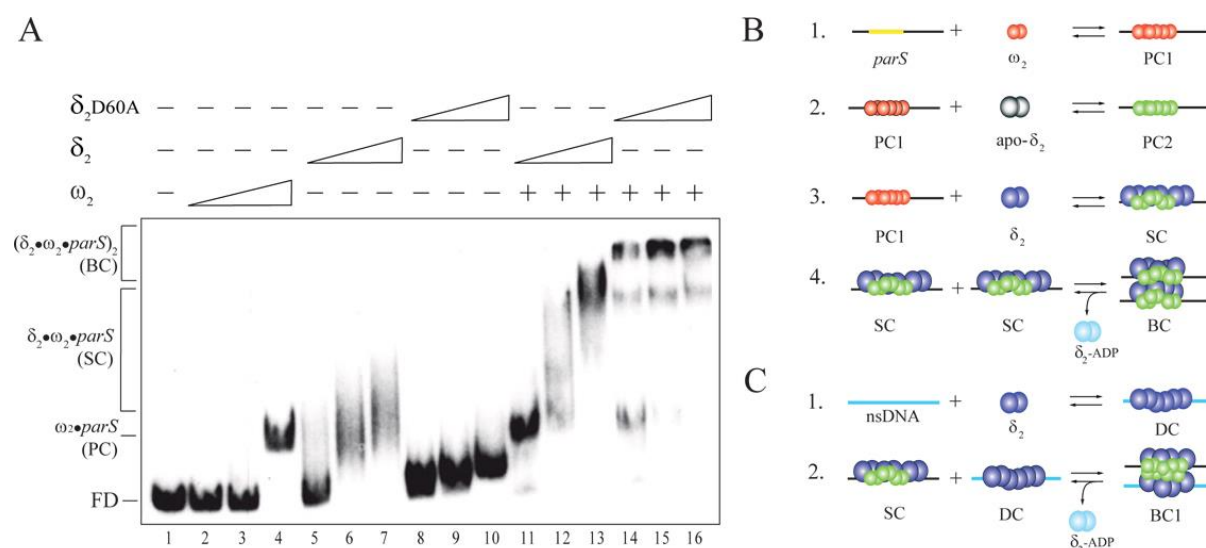


## 1. Chapter I: The pSM19035 plasmid partition system.

### 1.1. Molecular characterization of pSM19035 partition system.

#### 1.1.1. $\omega_2$ protein forms a discrete complex on *parS* DNA.

Protein  $\omega_2$  binds with high affinity and specificity to the different *parS* sites ( $P_{cop}$ ,  $P_\omega$  and  $P_\delta$ ) (de la Hoz et al. 2004). Here,  $\omega_2$  protein was purified and its affinity for the *parS2* DNA ( $P_\omega$ ) was confirmed by EMSA leading to formation of partition complex 1 (PC1, Fig. 13). The binding ability of  $\omega_2$  was confirmed to show positive cooperativity and we found that the half-life of a  $\omega_2$ -*parS2* complex is  $\sim 3$  min (Fig. 13A and Fig. 16). The apparent equilibrium constant ( $K_{Dapp}$ ) of  $\omega_2$ -*parS2* DNA was calculated to be  $\sim 6 \pm 1$  nM. Similar results were observed with the variant  $\omega_2\Delta N19$  that only have the ribbon-helix-helix domain ( $K_{Dapp} \sim 8 \pm 1$  nM) and both proteins  $\omega_2$ ,  $\omega_2\Delta N19$  also presented very low affinity binding for nsDNA ( $K_{Dapp} > 1 \mu M$ ) (data not shown).



**Figure 13. Complexes formed by  $\omega_2$  and  $\delta_2$  binding to *parS* DNA.**

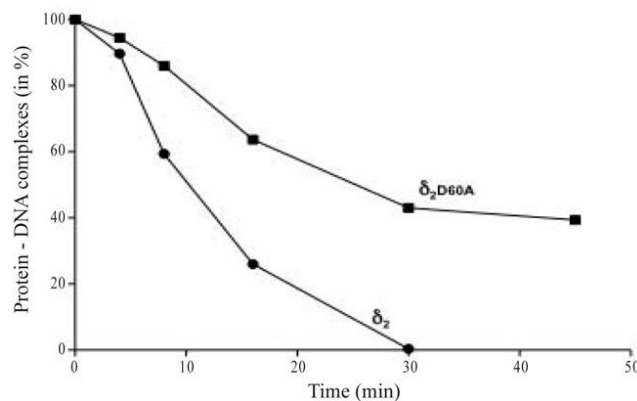
(A) *parS* DNA (0.1 nM) was incubated with increasing amounts of  $\omega_2$  (1.5, 3 and 6 nM),  $\delta_2$  (140, 280 and 560 nM),  $\delta_2D60A$  (35, 70 and 140 nM) or a constant amount of  $\omega_2$  (1.5 nM, indicated by plus) and increasing concentrations of  $\delta_2$  or  $\delta_2D60A$  for 15 min at 37°C in buffer A containing 1 mM ATP. (B)  $\omega_2$  bound to *parS* DNA (yellow box and black line) led to a short-living partition complex 1 (PC1) (1); the interaction of  $\omega_2$  at PC1 with  $\delta_2$  (out of scale), even in the apo form, led to a long-living partition complex 2 (PC2) (2);  $\delta_2$  bound to PC1 led to segrosome complex (SC) formation (3); and the interaction of two SCs led to bridging complex (BC) formation (4). (C) Protein  $\delta_2$  bound to nsDNA (light blue lane) led to dynamic complex (DC) formation (1); and the interaction of SC with DC led to bridging complex 2 (BC1) formation (2).

#### 1.1.2. Protein $\delta_2$ forms diffuse complex on DNA.

The ability of  $\delta_2$  protein to bind DNA was tested by EMSAs assays. We observed that in presence of 1 mM ATP and 10 mM  $Mg^{2+}$ ,  $\delta_2$  bound cooperatively with high affinity to nsDNA ( $K_{Dapp} \sim 150 \pm 10$  nM), forming a diffuse complex (DC,  $\delta_2$ -nsDNA) (Fig. 13, lanes 6–7).

Moreover, when ATP was omitted in the reaction any kind of complexes was observed in the experiments (data not shown). This widespread migration observed only in presence of ATP indicated a high degree of dynamism in the formation of  $\delta_2$ -DNA complexes.

The role played of ATP in  $\delta_2$  DNA binding was taken into account and two variants, the  $\delta_2$ K36A and  $\delta_2$ D60A that have mutated important residues for the ATP binding and hydrolysis, were analysed. These proteins presented two divergent behaviour:  $\delta_2$ K36A was defective in nsDNA binding in the presence of ATP, whereas the  $\delta_2$ D60A variant bound nsDNA with even 3-fold apparent higher affinity than  $\delta_2$  leading to formation of less diffuse complexes (Fig. 13, lanes 8 to 10,  $K_{Dapp}$   $40 \pm 6$  nM). To explain the differences on the  $K_{Dapp}$  between  $\delta_2$  and  $\delta_2$ D60A, the half-life of the preformed  $\delta_2$ -*parS* DNA or  $\delta_2$ D60A-*parS* DNA complexes was measured by filter binding assays, in the presence of ATP 1mM and 50-fold excess of cold *parS* DNA as competitor. As shown in Fig. 14, the time-dependent decrease of the retained nsDNA was used to calculate the half-life of protein-nsDNA complexes. The half-life of  $\delta_2$ -DNA was  $\sim 10$  min. The half-life for the  $\delta_2$ D60A-nsDNA complex was  $\sim 3$ -fold longer ( $\sim 28$  min) when compared with protein, indicating that ParA phenotype deficient in ATP hydrolysis lead to formation of  $\delta_2$ D60A-DNA complexes that are long-living. Altogether, the results suggested that  $\delta_2$  nucleation to nsDNA requires ATP binding and its release from nsDNA appear facilitated by ATP hydrolysis.



**Figure 14. The half-life of  $\delta_2$ -DNA and  $\delta_2$ D60A-nsDNA complexes.**

The 423-bp [ $\alpha^{32}$ P]-*parS* DNA (0.1 nM) was incubated with  $\delta_2$  (150 nM) or  $\delta_2$  D60A (40 nM) for 15 min at 37°C in buffer A containing 50 mM NaCl and 1 mM ATP. The reaction mixture was then diluted 20-times with buffer A containing 1 mM ATP. Then a 50-fold excess of cold *parS* DNA was added to the preformed protein-DNA complexes. At different times an aliquot (20  $\mu$ l) was removed, mixed with ice-cold buffer A containing 50 mM NaCl and 1 mM ATP (500  $\mu$ l) to stop the reaction and filtered through nitrocellulose filters in a filter holder. The filters were dried and the amount of radioactivity bound to the filter was determined by scintillation counting. The value obtained for the DNA retained by the protein was corrected for retention in the absence of the protein ( $< 2\%$  of total input) and was considered as 100%. The specific activity of the input DNA was measured as TCA precipitable material. All reactions were performed in duplicate and the experiment performed at least three times.

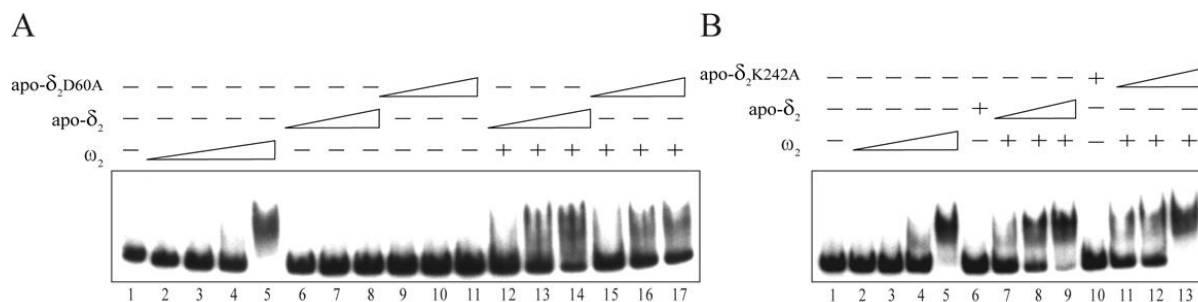
### 1.1.3. Proteins $\omega_2$ and $\delta_2$ bind *parS* DNA forming segresome and bridging complexes.

At limiting  $\omega_2$  concentration ( $< K_{Dapp}$ ; e.g. 1.5 nM) formation of partition complex (PC1,  $\omega_2$ -*parS*) were not observed (Fig. 13, lane 2). To determine whether  $\delta_2$  contribute to PCs formation EMSA studies were performed mixing both proteins in the reaction. As revealed in figure 13B, lanes 13 and 14, the presence of limiting  $\delta_2$  (e.g. 75 nM) or  $\delta_2D60A$  (e.g. 37 nM) concentrations, PCs were formed even at low  $\omega_2$  concentration. Under this conditions the  $\omega_2$  binding to *parS* DNA was increased more than 4-fold by the presence of  $\delta_2$ . Moreover, sub-saturating ( $\sim K_{Dapp}$ , e.g. 150 nM) or saturating  $\delta_2$  (e.g. 300 nM) concentrations increased ternary complex formation leading to the accumulation of slow mobility complex termed segresome (SC,  $\delta_2$ - $\omega_2$ -*parS*) and bridging complexes (BC, *parS*- $\omega_2$ - $\delta_2$ - $\omega_2$ -*parS*) (Fig. 13B, lanes 11, 12 and 13). Higher order complexes were also observed with  $\delta_2D60A$  variant: *parS* pairing (BC, *parS*- $\omega_2$ - $\delta_2$ - $\omega_2$ -*parS*) and/or alternatively *parS*-nsDNA pairing (BC1, *parS*- $\omega_2$ - $\delta_2$ -nsDNA) (Fig. 13A, lanes 14–16). The comparison between the BCs of  $\delta_2$  or  $\delta_2D60A$  revealed as  $\delta_2D60A$  accumulated bands that migrated slower than SC (BC; Fig. 13B, lanes 14–16). The results revealed that  $\delta_2$  and  $\omega_2$  formed ternary (SC) and quaternary (BC) intermediates on *parS* DNA.

### 1.1.4. The interaction of $\omega_2$ with $\delta_2$ markedly increases partition complex formation.

To further investigate if the increase of PC enhanced by  $\delta_2$  was ATP dependent, EMSA studies were also performed in absence of ATP. Limiting concentration of apo- $\delta_2$  or apo- $\delta_2D60A$  ( $>1500$  nM) failed to bind *parS* DNA (Fig. 15A, lanes 6–11). Limiting apo- $\delta_2$  or apo- $\delta_2D60A$  concentrations increased at least 6- to 8-fold  $\omega_2$ -*parS* DNA complexes formation when 0.75 nM  $\omega_2$  was present in the reaction (Fig. 15A, lanes 13–14 and 16–17). If ATP was added, the increased affinity is reciprocal, with  $\omega_2$  that strongly stimulate  $\delta_2$ -*parS* complex formation. To verify the former hypothesis,  $\delta_2$  was replaced by  $\delta_2K242A$ , a mutant that is deficient in the nsDNA binding (see results, paragraph 1.1.2.).

In the presence of limiting  $\omega_2$  concentrations ( $\sim 6$ -fold lower than  $K_{Dapp}$ ), addition of apo- $\delta_2K242A$  (or  $\delta_2K242A$  at  $\sim 100$ -fold lower than  $K_{Dapp}$ ) facilitated  $\omega_2$  binding to *parS* DNA (Fig. 15B, lanes 11–13). Similar results were observed when  $\delta_2K36A$  was used (data not shown). We observed  $\omega_2$  and  $\delta_2$  interaction increases the  $\omega_2$   $K_{Dapp}$  by at least  $\sim 6$ -fold, this effect occurred independently to ATP and/or DNA binding state of  $\delta_2$  protein. The results indicated that the on- or the off-rate of  $\omega_2$ -*parS* DNA complexes equilibrium was modified by  $\delta_2$  presence.

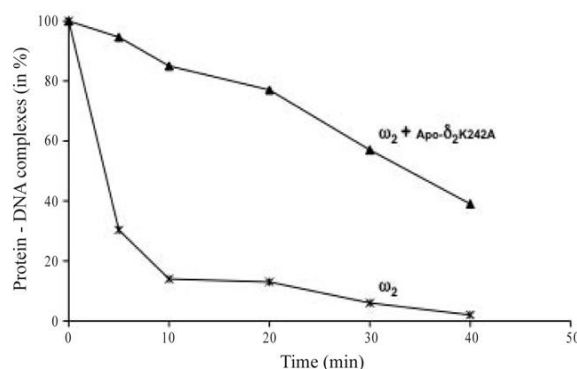


**Figure 15. apo- $\delta_2$  facilitates  $\omega_2$ -*parS* DNA complex formation.**

(A) The 423-bp [ $\alpha^{32}$ P]-*HindIII*-*KpnI* *parS* DNA (0.1 nM) was incubated with increasing concentrations of  $\omega_2$  (0.75–6 nM), apo- $\delta_2$  or apo- $\delta_2$ D60A (25, 50 and 100 nM), or in the presence of  $\omega_2$  (0.75 nM, indicated by plus) and increasing amounts of apo- $\delta_2$  or apo- $\delta_2$ D60A for 15 min at 37° C in buffer A. (B) *parS* DNA was incubated with increasing concentrations of  $\omega_2$  (0.75–6 nM) or in the presence of a fixed amount of apo- $\delta_2$  or apo- $\delta_2$ K242A (100 nM), or  $\omega_2$  (0.75 nM, indicated by plus) and increasing amounts of apo- $\delta_2$  or apo- $\delta_2$ K242A (25, 50 and 100 nM) for 15 min at 37° C in buffer A.

### 1.1.5. Interaction of $\omega_2$ with $\delta_2$ discriminates between short-living and long-living partition complexes.

To address whether  $\delta_2$  either increase the on-rate or decrease the off-rate of the reaction, the dissociation rate of the  $\omega_2$ -*parS* was measured in the presence or the absence of  $\delta_2$ K242A. The *parS* DNA was incubated with 6 nM  $\omega_2$  (half-saturating concentrations) or with or without 100 nM apo- $\delta_2$  K242A. The half-life of the  $\omega_2$ -*parS* complex observed in the experiments was short lived (~ 3 min), but in the presence of apo- $\delta_2$ K242A increased > 10 fold to ~ 34 min (Fig. 16). Both the  $\delta_2$  variant either the lack of ATP employed in the mixture reactions ensured how such increase in the half-life was independent of ParA nsDNA binding effect.



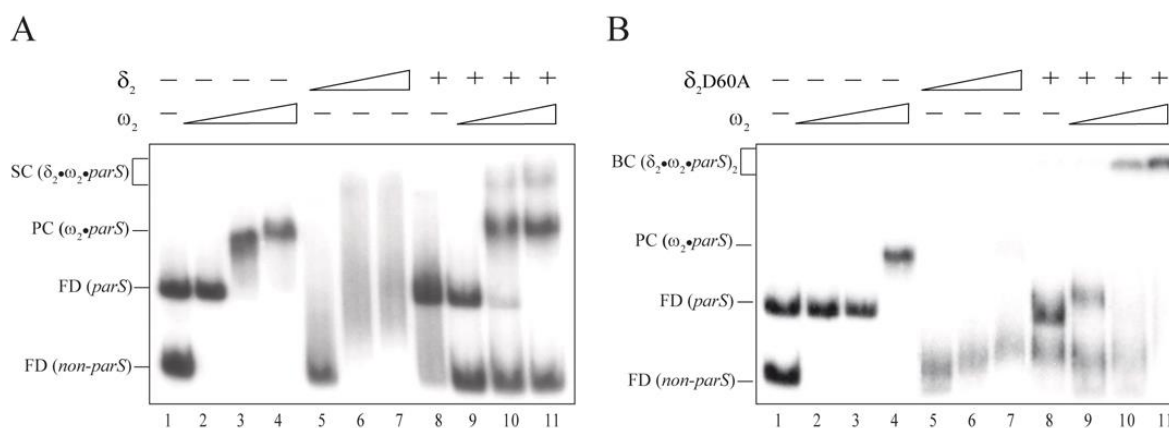
**Figure 16.  $\delta_2$ - $\omega_2$  interaction enhances the half-life of the PC.**

The 423-bp [ $\alpha^{32}$ P]-*parS* DNA (0.1 nM) was incubated with  $\omega_2$  (6 nM) or  $\omega_2$  (6 nM) and  $\delta_2$ K242A (100 nM) for 15 min at 37°C in buffer A containing 1 mM ATP. The reaction mixture was then diluted 20-times with buffer A containing 1 mM ATP and a 50-fold excess of cold *parS* DNA was added to the preformed protein-DNA complexes. At different times a sample was mixed with ice-cold buffer A containing 1 mM ATP (500  $\mu$ l) to stop the reaction and filtered through nitrocellulose filters in a filter holder. The filters were dried and the amount of radioactivity bound to the filter was determined by scintillation counting. The value obtained for the DNA retained by the protein was corrected for retention in the absence of the protein (< 2 % of total input) and was considered as 100%. The specific activity of the input DNA was measured as TCA precipitable material. All reactions were performed in duplicate and the experiment performed at least three times.

Our results suggested that the addition of apo- $\delta_2$ K242A decreased the dissociation rate of the PC, implying that  $\omega_2$ - $\delta_2$  interaction produced structural changes that lead to formation of a stable partition complex (PC2,  $\omega_2$ -*parS* DNA).

### 1.1.6. Protein $\omega_2$ -bound to *parS* DNA promotes $\delta_2$ re-localization.

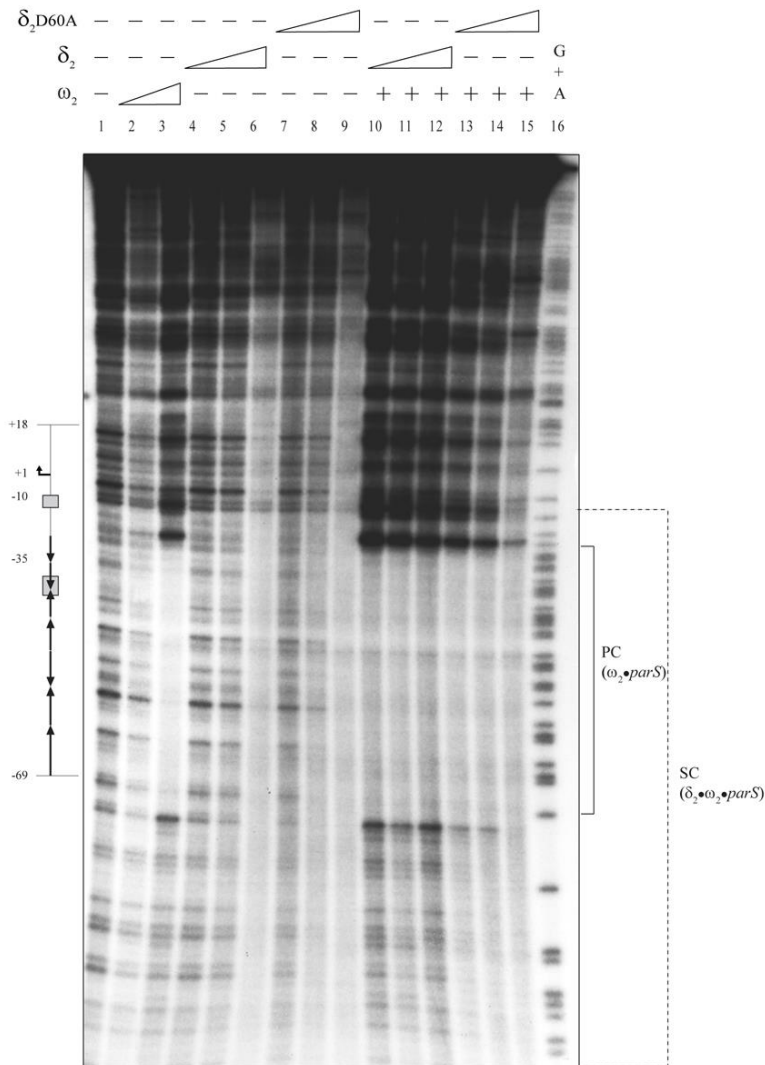
To re-evaluate the hypothesis that  $\delta_2$  interacts with  $\omega_2$  and facilitates the interaction with *parS* DNA and to test if  $\omega_2$  promotes redistribution of  $\delta_2$  towards the PC, EMSA experiments were performed with *parS* and nsDNAs. Protein  $\delta_2$  or  $\delta_2$ D60A was pre-bound to nsDNA (Fig. 17A and 17B, lanes 5–7), and then preformed  $\omega_2$ -*parS* DNA was added to the reaction mixture. Protein  $\delta_2$  or  $\delta_2$ D60A pre-bound to nsDNA interacted poorly with *parS* DNA when  $\omega_2$  was omitted to reaction (Fig. 17A and 17B, lane 8). At limiting  $\omega_2$  concentrations,  $\delta_2$  was dislodged from nsDNA when compared to the absence of  $\omega_2$  (Fig. 17A, lanes 8–9). At sub-saturating  $\omega_2$  concentrations, the PC and SC were accumulated (Fig. 17A, lanes 10–11). Our results shown that  $\omega_2$  bound to *parS* DNA promotes the re-localization of  $\delta_2$  towards *parS* DNA forming a SC, as judged by the accumulation of free nsDNA, and the slow moving SCs (Fig. 17A, lanes 10–11). However, when  $\delta_2$  was replaced by  $\delta_2$ D60A the accumulation of free nsDNA was decreased when compared to the situation (Fig. 17B, lanes 9–11), suggesting that dislodging might require ATP hydrolysis. Under this condition, the accumulation of BCs was observed.



**Figure 17. Protein  $\omega_2$  promotes  $\delta_2$  redistribution.**

(A) The 183-bp [ $\alpha^{32}$ P]-*Bam*HI-*Hind*III nsDNA (0.1 nM) was incubated with increasing concentrations of  $\delta_2$  (120, 240 and 480 nM, lanes 5–7) or the 423-bp [ $\alpha^{32}$ P]-*parS* DNA (0.1 nM) with increasing concentrations of  $\omega_2$  (3–12 nM, lanes 2–4). nsDNA was pre-incubated with  $\delta_2$  (120 nM) and then *parS* DNA and increasing concentrations of  $\omega_2$  (3–12 nM) were added. (B) nsDNA was incubated with increasing concentrations of  $\delta_2$ D60A (37, 75 and 150 nM, lanes 5–7) or *parS* DNA with increasing concentrations of  $\omega_2$  (3–12 nM, lanes 2–4). nsDNA was pre-incubated with  $\delta_2$ D60A (75 nM) for 5 min, and then *parS* DNA and increasing concentrations of  $\omega_2$  (3–12 nM) were added and the reaction incubated for 15 min at 37°C in buffer A containing 1 mM ATP. The absence of a component is indicated by minus, and the presence of a fixed amount by a plus or variable concentration by a triangle, respectively.

The  $\delta_2$  and  $\delta_2$ D60A proteins bound to DNA molecules led to BC formation that seems different on a quality level. The BC observed for  $\delta_2$  should be composed by two or more SCs paired ( $parS-\omega_2-\delta_2-\omega_2-parS$  DNA) due to rapid release of nsDNA. While the BCs formed by  $\delta_2$ D60A could be either composed by two or more SCs ( $parS-\omega_2-\delta_2$ D60A- $\omega_2-parS$ ) or SC and DCs ( $parS-\omega_2-\delta_2$ D60A-nsDNA) (Figure 17A, lanes 10–11 and Figure 17B, lanes 10–11).



**Figure 18. DNase I footprinting shows that  $\omega_2$  redistributes  $\delta_2$  to form a SC.**

*parS* DNA was incubated with  $\delta_2$  (150, 300 and 600 nM),  $\delta_2$ D60A (35, 75 and 150 nM) or  $\omega_2$  (7.5 or 15 nM) or a fix concentration of  $\omega_2$  (15 nM) and increasing concentrations of  $\delta_2$  or  $\delta_2$ D60A for 15 min at 30°C, in buffer A containing 1 mM ATP. Then DNaseI was added. In lane 16 the size standard G + A was loaded. The DNA region protected from DNase I digestion by  $\omega_2$ ,  $\delta_2$  or both are denoted.

To evaluate whether  $\omega_2$  promotes re-localization of  $\delta_2$ , also enzymatic footprinting experiments were performed. The *parS* sequences were specifically protected from DNase I cleavage by the binding of  $\omega_2$  (Fig. 18, lanes 3). Similar results were observed for  $\omega_2\Delta N19$  (data not shown). At concentrations below their  $K_{Dapp}$ , only restricted regions of *parS* DNA were bound by  $\delta_2$  or  $\delta_2$ D60A in a sequence-independent manner (Fig. 18, lanes 4 and 7). At saturating protein concentrations,  $\delta_2$  or  $\delta_2$ D60A bound onto *parS* DNA and protected extended regions, from DNase I attack, in a concentration-dependent manner (Fig. 18, lanes 6 and 9). When sub-saturating  $\omega_2$  concentrations were added to pre-formed DCs ( $\delta_2-parS$  DNA complexes) the  $\omega_2$



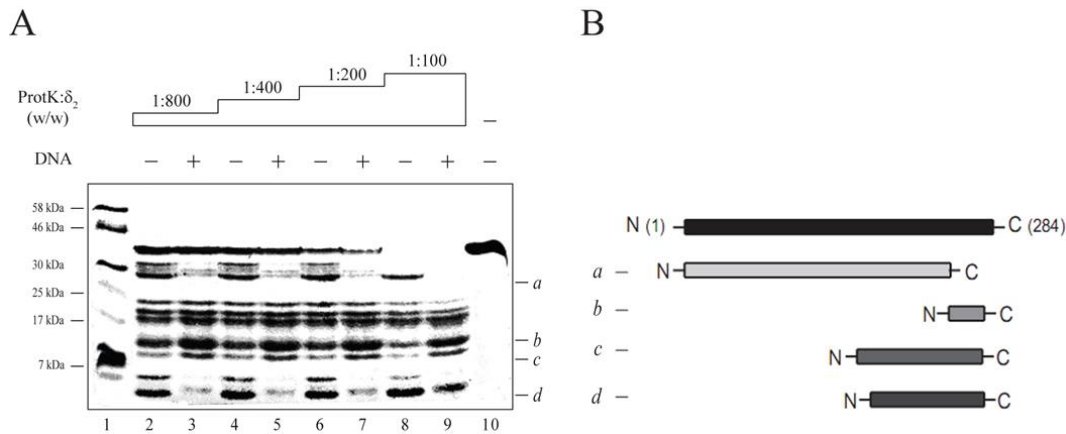
cognate site became protected from DNase I attack, even in the presence of saturating  $\delta_2$  concentrations (Fig. 18, lanes 10–12). However,  $\delta_2$  bound to *parS* DNA was poorly re-localized by  $\omega_2\Delta N19$  (data not shown).

When sub-saturating  $\omega_2$  concentrations were added to pre-formed  $\delta_2$ D60A-*parS* complexes the  $\omega_2$  cognate site was protected from DNase I but still *nsDNA* sequences adjacent to *parS* site were also observed to be protected by  $\delta_2$ D60A (Fig. 18, lanes 13–15). Protein  $\omega_2$  bound to *parS* DNA partially redistributed  $\delta_2$ D60A next to it (Fig. 18, lanes 9 vs. 15). This results demonstrated that  $\omega_2$  bound to *parS* DNA redistributes  $\delta_2$  to adjacent regions, to form a SC but also that the N-terminal 18 amino acid residues of  $\omega_2$  is involved in specific contacts with  $\delta_2$ .

### 1.1.7. Characterization of DNA binding domain of $\delta_2$ .

#### 1.1.7.1. $\delta_2$ undergoes a conformational change upon interaction to DNA.

To define functional  $\delta_2$  regions involved in *nsDNA* binding limited proteolysis was performed. Preliminary analysis of  $\delta$  sequence and its potential cleavage sites were predicted for proteinase K, trypsin and others enzymes using PeptideCutter. Proteinase K (ProtK) and trypsin (Tryp) recognized around 164 and 34 possible cleaving sites along the entire  $\delta$  sequences respectively and they were employed for proteolysis assays. In the presence of 1 mM ATP, 3  $\mu$ g of  $\delta_2$  was pre-incubating with 2  $\mu$ g of pCB30 or with a mock reaction lacking pCB30. Next, different concentrations of proteinase K were added to reaction mixture and incubated for 1h at room temperature. As observed, the full length  $\delta$  (MM ~ 34 kDa) was gradually digested by increasing the ProtK: $\delta_2$  ratios. In the presence of *nsDNA* ProtK generated specific polypeptide  $\delta_2$  fragments that were different when compared with the absence of *nsDNA* (Fig. 19A). The full length  $\delta_2$  was totally proteolyzed in presence of 1:100 of ProtK: $\delta$  ratio (w/w) (Fig. 19A, lanes 8 and 9). Comparing the pattern generated, two polypeptide fragments of ~29 kDa and ~5 kDa (Fig. 19A, lane 8, band “a” and “b”) were majoritarian when DNA was omitted, meanwhile other two bands of ~15 kDa and ~12 kDa (Fig. 19A, lane 9, bands “c” and “d”) were more abundant in presence of DNA. Similar results were obtained using Trypsin protease instead of proteinase K (data not shown).



**Figure 19. The  $\delta_2$  DNA binding domain maps to its C-terminus.**

(A) Partial proteolysis assays. Protein  $\delta_2$  (4 mg) was pre-incubated (+) or not (-) with the 423-bp *parS* DNA for 15 min at 37°C, in buffer A containing 1 mM ATP. Increasing concentrations of ProtK were added and the mixtures were analysed on a 15% SDS-PAGE. In lane 1 the molecular weight marker and in lane 10 untreated  $\delta_2$  were present. The relevant proteolysis bands were marked (*a* to *d*). (B) Identification of relevant polypeptides. The polypeptides were isolated (bands *a* to *d*), subjected to partial proteolysis and mass spectrometry and the corresponding regions are drawn.

**Table 9. List of peptides matched to  $\delta_2$ .**

Band	MM (kDa)	$\delta$ identified peptides	Sequence coverage (%)
<i>a</i>	≈ 29	1–31, 38–67, 71–116, 119–138.	44.0%
<i>b</i>	≈ 15	216–239, 260–284.	15.8%
<i>c</i>	≈ 13	216–239, 242–255, 260–284	20.0%
<i>d</i>	≈ 5	216–239, 242–248, 260–284	17.6%

To identify the regions of the protein protected upon the interaction to DNA, the gel purified “*a*” to “*d*” bands were subjected to limited tryptic digestion, and the polypeptides analysed by MALDI-ToF-ToF. The results and identified residues of  $\delta$  are resumed (Table 9 and represented in Fig. 19B). It is worth noticing that the 139–216 region of  $\delta$  lacks trypsin cognate sites, implying a loss of information. Altogether, the data shown that 68 residues from the C-terminal domain (residues 216–284) of  $\delta_2$  becomes less sensitive to protease upon DNA binding and suggest the involvement of that region in the nsDNA binding.

#### 1.1.7.2. Identification of $\delta_2$ residues involved in the binding to DNA.

In general, the major feature of proteins that interact with nsDNA is that they contain surfaces or structures that carry positively charged residue. These residues interact with the negatively charged phosphate backbone of DNA chain. The crystal structure of  $\delta_2$  did not reveal any know DNA-binding motif as well as others small ParA ATPases. To get a hint of a specific region and residues involved in the nsDNA binding, structural alignment of the crystallized  $\delta_2$  was performed using DALI and Phyre2 servers (see Fig. 7). The structural alignment analysis

revealed a high degree of conservation of tertiary folding with others ParA homologues as well as others proteins like MinD, MipZ, NifH and BchL (Table 10). At sequence level,  $\delta_2$  protein showed only 23.8%, 19.7% and 17.5% of sequence identity with *T. thermophilus* Soj, *E. coli* ParF and P1 ParA respectively but the structural superposition of  $\delta$  monomer achieved good root-mean-square deviation (RMSD) values as 2.1 Å with *T. thermophilus* Soj, 2.9 Å with P1 ParA and 3.0 Å *E. coli* ParF (Fig. 20A, 20B and 20C) (Leonard et al. 2005a, Dunham et al. 2009, Hu, Gogol and Lutkenhaus 2002). It revealed that there are charged residues, but they are poorly conserved among ParA ATPases (Fig. 7).

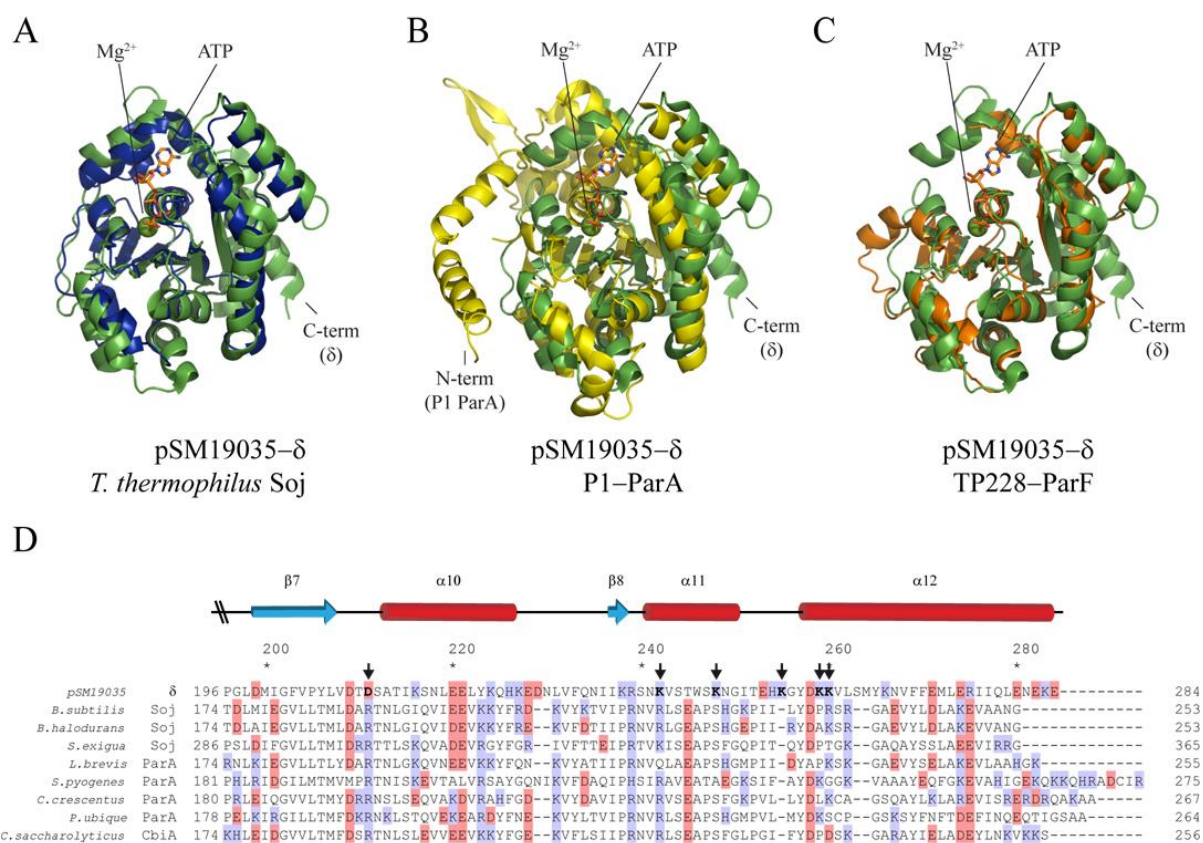
**Table 10. Structural alignment of  $\delta_2$  protein.**

<b>ParA-like protein</b>	<b>PDB</b>	<b><sup>a</sup>RMSD (Å)</b>	<b>aa</b>	<b>Id. (%)</b>	<b><sup>b</sup>Local Id. (%) (aa <math>\delta</math>:aa protein)</b>	<b><sup>c</sup>Local Sim. (%) (aa <math>\delta</math>:aa protein)</b>
pSM19035 $\delta_2$	2OZE	0.0	284	100	100%	100%
<i>T. thermophilus</i> Soj	2BEJ	2.1	322	23.8	25.8% in 264 aa (15–276:1–246)	58.0% in 264 aa (15–276:1–246)
cp32–3 ParA	3K9H	2.2	369	22.0	30.6% in 268 aa (16–276:1–246)	63.4% in 268 aa (16–276:1–246)
P1 ParA	3EZ6	2.9	398	17.5	23.8% in 189 aa (20–190:106–294)	59.3% in 189 aa (20–190:106–294)
TP228 ParF	4DZZ	3.0	206	19.8	43.8% in 32 aa (139–170:74–105)	78.1% in 32 aa (139–170:74–105)
<i>C. tepidum</i> ParA	3EA0	3.0	265	19.7	28.5% in 123 aa (31–147:13–125)	57.0% in 123 aa (31–147:13–125)
<i>Synechocystis</i> Sp. ParA	3CWQ	3.2	209	21.9	23.4% in 137 aa (23–153:1–135)	52.6% in 137 aa (23–153:1–135)
P7 ParA	3EZ9	3.4	403	18.9	24.8% in 238 aa (18–230:108–344)	58.0% in 238 aa (18–230:108–344)
<b>MinD family</b>	<b>PDB</b>	<b>RMSD (Å)</b>	<b>aa</b>	<b>Id. (%)</b>	<b>Local Id (%)</b>	<b>Local Sim (%)</b>
<i>P. furiosus</i> MinD	1G3R	2.5	237	19.9	22.5% in 178 aa (31–204:11–169)	56.7% in 178 aa (31–204:11–169)
<i>E. coli</i> MinD	3Q9L	2.5	260	19.6	23.9% in 184 aa (22–201:2–174)	53.3% in 184 aa (22–201:2–174)
<i>C. Vibrioides</i> MipZ	2XJ9	3.0	278	17.0	22.3% in 148 aa (23–170:6–133)	50% in 148 aa (23–170:6–133)
<b>Other Proteins</b>	<b>PDB</b>	<b>RMSD (Å)</b>	<b>aa</b>	<b>Id. (%)</b>	<b>Local Id (%)</b>	<b>Local Sim (%)</b>
<i>A. vinelandii</i> NifH	2AFK	3.2	289	13.0	28.6% in 49 aa (27–73:96–141)	44.9% in 49 aa (27–73:96–141)
<i>R. Sphaeroides</i> BchL	3END	3.3	297	14.0	32.9% in 79 aa (9–83:39–112)	54.4% in 79 aa (9–83:39–112)

<sup>a</sup>RMSD (root-mean-square deviation) is the measure of the average distance between the atoms (usually the backbone atoms) of superimposed proteins. <sup>b</sup>Local Id (identity) represents the best local alignment between overlapping aminoacids. The value was calculated by PRSS/PRFX Sequence Shuffling. <sup>c</sup>Local Sim (similarity) represents the similarity between residues of the best local alignment.

A careful analysis of the alignments of *T. thermophilus* Soj, P1 ParA or *E. coli* SopA sequence-independent DNA binding residues and the sequence of PSI-BLAST and surface-exposed charged residues of  $\delta_2$  suggested a potential role for residues K242, K248, K255 and K259 K260 in DNA binding (Fig. 20D). Another residue, the D211 of  $\delta$ , was used as a control because it appeared curiously aligned with residues of opposite charge (Fig. 20D).

To determine whether the charged residues identified by *in silico* analysis were involved in the association of  $\delta_2$  to DNA. Site-directed mutagenesis were planned, the residues D211, K242 and K259 K260 were replaced by alanine, and the K248 by serine. The PCR products were cloned in pET21 vector and mutated genes were used to overexpress and purify as done with the protein.

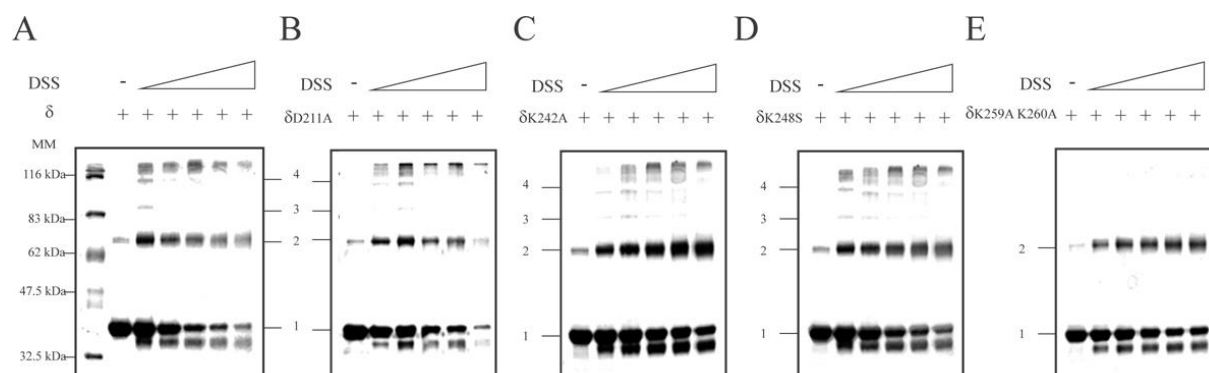


**Figure 20. The conserved  $\delta$  C-terminal domain.**

Superimposition of full-length monomer structures of  $\delta$  (PDB: 2OZE, green) and *T. thermophilus* Soj (A, PDB: 2BEK, blue), P1 ParA (B, PDB: 3EZ9, yellow) and TP228 ParF (C, PDB: 3K9H, orange) were displayed using PyMOL. (D) Above the secondary structure of C-terminus of  $\delta_2$  is represented, the red cylinders and cyan arrows indicated the  $\alpha$ -helix and the  $\beta$ -sheet motif respectively. Below, the corresponding alignment of C-terminal domains of  $\delta_2$  ParA homologues is shown with conserved acidic and basic residues are highlighted in red and blue color respectively. The black arrows indicated the D211, K242, K248, K255, K259 and K260 residues of  $\delta_2$  that were substituted.

### 1.1.7.3. Oligomeric state and ATPase activity of the $\delta$ mutants.

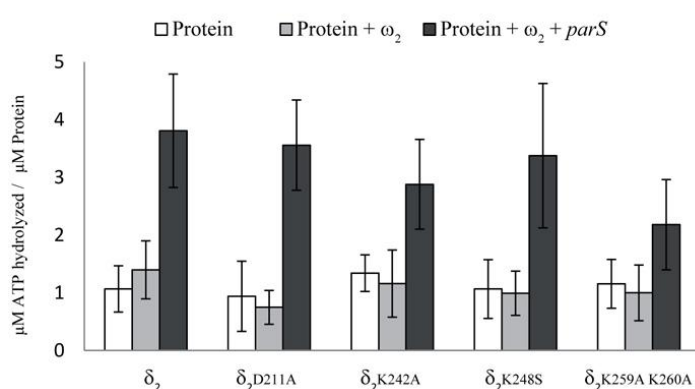
The small pSM19035- $\delta_2$  is a dimer in solution, even in its apo-form (Pratto et al. 2008). Therefore, to check whether the purified proteins  $\delta$ D211A,  $\delta$ K242A,  $\delta$ K248S and  $\delta$ K259A K260A maintain that ability, the mutants were treated with increasing concentration of disuccinimidyl-suberate (DSS), a homobifunctional amine-specific protein crosslinking reagent with a spacer arm of 11.4 Å, and the reaction mixture was separated by SDS-PAGE (Fig. 21A–21E).



**Figure 21. The oligomeric state of  $\delta$  mutants.**

An equal amount (3  $\mu$ g) of proteins  $\delta$  (A),  $\delta$ D211A (B),  $\delta$ K242A (C),  $\delta$ K248S (D) and  $\delta$ K259A K260A (E) were pre-incubated at 37 °C in buffer B and further incubated 10 min more with increasing concentrations of DSS (0.01–0.5nM), then the products of reactions were loaded on a 15 % SDS-PAGE.

Except  $\delta$  K259A K260A, not only bands to respective monomers but also dimers and other products of high molecular mass were observed in presence of DSS. The oligomers formation of double mutant  $\delta$  K259A K260A was affected. The results shown how these mutations did not affect the region involved in protein dimerization, but for  $\delta_2$  K259A K260A it might impair the dimer-dimer interaction.



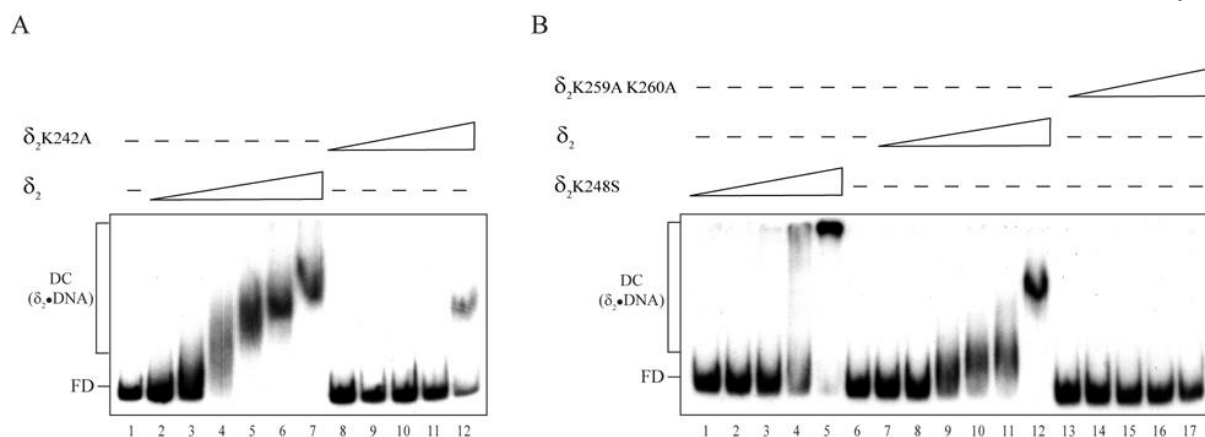
**Figure 22. Stimulation of the ATPase activity of  $\delta_2$  variants by  $\omega_2$  and *parS* DNA.**

ATPase activity of the 0.5  $\mu$ M  $\delta_2$  protein and its variants ( $\delta_2$ D211A,  $\delta_2$ K242A,  $\delta_2$ K248S and  $\delta_2$ K259A K260A) alone (white bars), in presence of only 125 nM  $\omega_2$  protein (light grey bars), or in presence of both 125 nM  $\omega_2$  protein and 0.25 nM of *parS* DNA (dark grey bars).

In order to confirm if the mutants were functionally active, their abilities to hydrolyse ATP were then examined by TLC. The ATPase activity of  $\delta_2$  or its mutant variants was low after 180

min of incubation (Fig. 22). When  $1.5\mu\text{M}$   $\omega_2$  and  $25\text{nM}$  *parS* DNA were added to the reaction mixture, an increase of  $\sim 3$ -fold in the rate of ATP hydrolysis was observed for  $\delta_2$ ,  $\delta_2\text{D211A}$ ,  $\delta_2\text{K248S}$ , whereas it was around  $\sim 2$ -fold for  $\delta_2\text{K242A}$  and  $\delta_2\text{K259A K260A}$  (Fig. 22). The results confirmed that  $\omega_2$  maintained the ability to increase the ATP rate of  $\delta_2$  mutants. Altogether suggested that the mutants are still active, maintaining unchanged their capacity to form dimer in solution, bind ATP and interact with  $\omega$ .

#### 1.1.7.4. The $\delta_2\text{K242A}$ , $\delta_2\text{K248S}$ , and $\delta_2\text{K250A K260}$ variants bind DNA with low affinity.



**Figure 23.  $\delta_2$  variants with decreased binding to *parS* DNA.**

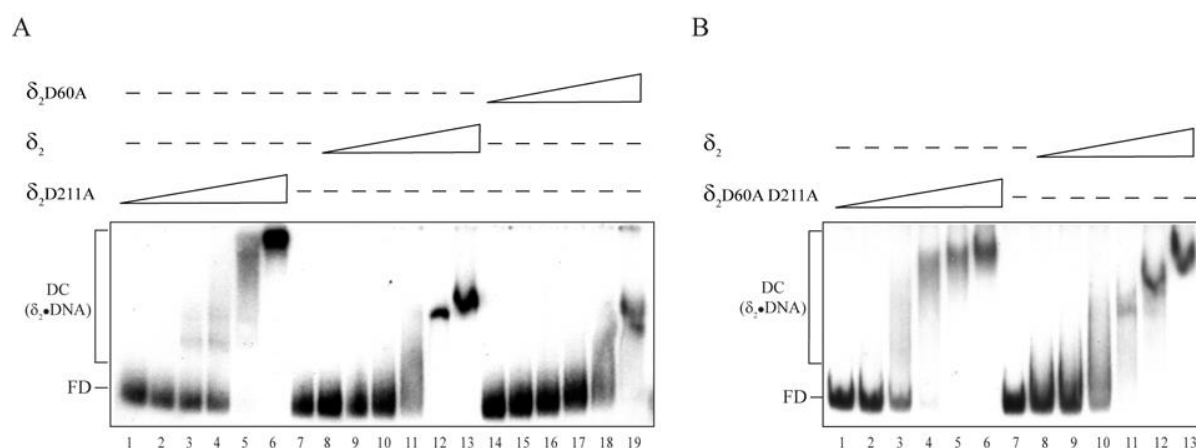
(A) The 423-bp [ $\alpha^{32}\text{P}$ ]-*parS* DNA (0.1 nM) was incubated with increasing amounts of  $\delta_2$  (0.035 to  $1.2\mu\text{M}$ ) or  $\delta_2\text{K242A}$  (0.3 to  $4.8\mu\text{M}$ ) for 15 min at  $37^\circ\text{C}$ , in buffer A containing 1 mM ATP. (B) 0.1 nM *parS* DNA was incubated with increasing amounts of  $\delta_2$  (0.035 to  $1.2\mu\text{M}$ ),  $\delta_2\text{K248S}$  (150 to  $2.4\mu\text{M}$ ) or  $\delta_2\text{K259A K260A}$  (0.3 to  $4.8\mu\text{M}$ ) for 15 min at  $37^\circ\text{C}$ , in buffer A supplemented with 1 mM ATP.

To test the effects of semi-conservative residues substitutions located at the C-terminus on DNA binding, the  $\delta_2\text{K242A}$ ,  $\delta_2\text{K248S}$  and  $\delta_2\text{K250A K260}$  proteins were tested by EMSA with *parS* DNA *in vitro*. In the apo form,  $\delta_2$  failed to bind to DNA in nM range ( $K_{\text{Dapp}} > 2\mu\text{M}$ ). Similar results were obtained when the proteins were in the ADP-bound form. Protein  $\delta_2$  bound cooperatively both to *parS* and nsDNA with similar affinity ( $K_{\text{Dapp}} 150 \pm 10\text{ nM}$ ). Protein  $\delta_2$  bound DNA forms dynamic complexes that leading to very slow mobility complexes at  $1.2\mu\text{M}$  of protein (Fig. 23A, lines 3–7 and Fig. 23B, lines 9–12). In presence of ATP,  $\delta_2\text{K242A}$  (Fig. 23A, lane 12) or  $\delta_2\text{K248S}$  (Fig. 23B, lanes 4–5) bound nsDNA with low affinity (in the  $\mu\text{M}$  ranges), leading to formation of one discrete complex at high protein concentration. Protein–nsDNA complex formation was marginal when  $\delta_2$  was replaced by  $\delta_2\text{K250A K260A}$  (Fig. 23B, lanes 13–17). The  $\delta_2\text{K242A}$  mutant bound DNA with  $\sim 30$ -fold ( $K_{\text{Dapp}} > 3\mu\text{M}$ ) and the  $\delta_2\text{K248S}$  with  $\sim 15$ -fold ( $K_{\text{Dapp}} > 2\mu\text{M}$ ) lower affinity relative to  $\delta_2$ . Similar results were also obtained by filter binding (see Table 11). All the results obtained up to the time were suggesting that these

mutants were properly folded therefore the DNA binding defect presented by  $\delta_2$  K242A,  $\delta_2$ K248S or  $\delta_2$ K250A K260A seem to be a genuine effect due to residues substitution.

#### 1.1.7.5. Proteins $\delta_2$ D60A, and $\delta_2$ D60A D211A bind DNA with higher affinity.

As observed in the PSI-BLAST alignment (Fig. 20D) the aspartate at position 211 of  $\delta_2$  was aligned with positively charged arginine of other ParA proteins. That arginine was highly conserved among ParA proteins but not in  $\delta_2$ . In order to find out how a negatively charged residue could affect the *ns*DNA binding the Asp 211 of  $\delta_2$  was mutated to Ala. The effect of this substitution was checked by EMSA assays. Contrary to what observed by Lys to Ala or Ser mutations, the  $\delta_2$ D211A mutant showed a ~6-fold and ~3-fold enhanced affinity for *ns*DNA in presence of ATP relative to  $\delta_2$  and  $\delta_2$ D60A respectively (Fig. 24 A and Table 11). The band shifts were qualitatively different from those formed by  $\delta_2$ ; the interaction of  $\delta_2$ D211A with *ns*DNA, at very low protein concentrations, was leading to formation of discrete bands rather than diffuse bands (Fig. 24A, lanes 3–6). However, when ATP was omitted, no significant differences were observed in comparison with protein (data not shown) and  $K_{Dapp}$  of reaction was  $>1.5 \mu\text{M}$ . A double mutant  $\delta_2$ D60A D211A was also generated, the double mutant bound with very high efficiency *parS* DNA forming diffuse complexes and its  $K_{Dapp}$  was found to be ~6 nM, 25-fold higher than  $\delta_2$ . (Fig. 24B, lanes 3–6). This double mutant was designed and built intentionally to increase the stability of  $\delta_2$ -DNA complex. and to be further used in structure resolutions of the DC or SC complexes.



**Figure 24.  $\delta_2$  variants with increased binding to *parS* DNA.**

(A) The 423-bp [ $\alpha^{32}\text{P}$ ]-*parS* DNA (0.1 nM) was incubated with increasing amounts of  $\delta_2$  (0.035 to 1.2  $\mu\text{M}$ ),  $\delta_2$ D211A (2.4 to 75nM) and  $\delta_2$ D60A (2.4 to 75nM) for 15 min at 37°C, in 1mM ATP buffer A. (B) 0.1 nM *parS* DNA was incubated with increasing amount of  $\delta_2$  (0.035 to 1.2  $\mu\text{M}$ ) and  $\delta_2$ D60A D211A (1.1 to 37.5  $\mu\text{M}$ ) for 15 min at 37°C, in buffer A.

To investigate the causes of its increase in the  $K_{Dapp}$ , the half-life of  $\delta_2$ D211A–DNA complexes was determined again by filter binding and it was  $\sim 32$  min. The half-life of  $\delta_2$ D211A·DNA and  $\delta_2$ D60A·DNA complexes were comparable, but the ATP binding and hydrolysis of the  $\delta_2$ D211A was not impaired. It seems likely that  $\delta_2$  and  $\delta_2$ D60A bind DNA with similar affinities, but the lacking of ATP hydrolysis of  $\delta_2$ D60A is responsible of a decrease of off-rate constant. In contrast the off-rate of  $\delta_2$ D211A should be similar to the  $\delta_2$  due to comparable ATPase activity and lack of DNA binding in the apo-form, whereby the on-rate seemed to be increase in that mutant. Altogether the results suggest how the ATP binding and the C-terminal arrangement are relevant in the nsDNA binding, but their contribution in the formation and stability of complex is substantially different.

**Table 11. Relative binding of  $\delta_2$  or  $\delta_2$  variants to DNA.**

Protein	Adenine Nucleotide cofactor	EMSA $K_{Dapp}$ (nM)	FILTER BINDING $K_{Dapp}$ (nM)
$\delta_2$	ATP	$\sim 150$	$\sim 130$
$\delta_2$ D60A	ATP	$\sim 75$	$\sim 45$
$\delta_2$ D211A	ATP	$\sim 25$	$\sim 20$
$\delta_2$ K242A	ATP	$\sim 3000$	$\sim 1000$
$\delta_2$ D60A D211A	ATP	$\sim 6$	$\sim 6$
$\delta_2$ K248S	ATP	$\sim 1500$	$\sim 700$
$\delta_2$ K259A K260A	ATP	ND	$>2000$
$\delta_2$	ADP	$>2000$	ND
$\delta_2$ D60A	ADP	$>2000$	ND
$\delta_2$ D211A	ADP	$>2000$	ND
$\delta_2$ D60A D211A	ADP	$>2000$	ND
$\delta_2$ K242A	ADP	$>3000$	ND
$\delta_2$ K248S	ADP	$>2000$	ND
$\delta_2$ K259A K260A	ADP	$>3000$	ND

#### 1.1.7.6. Protein $\omega_2$ bound to *parS* promotes $\delta_2$ K242A and $\delta_2$ D211A recruitment and plasmid pairing.

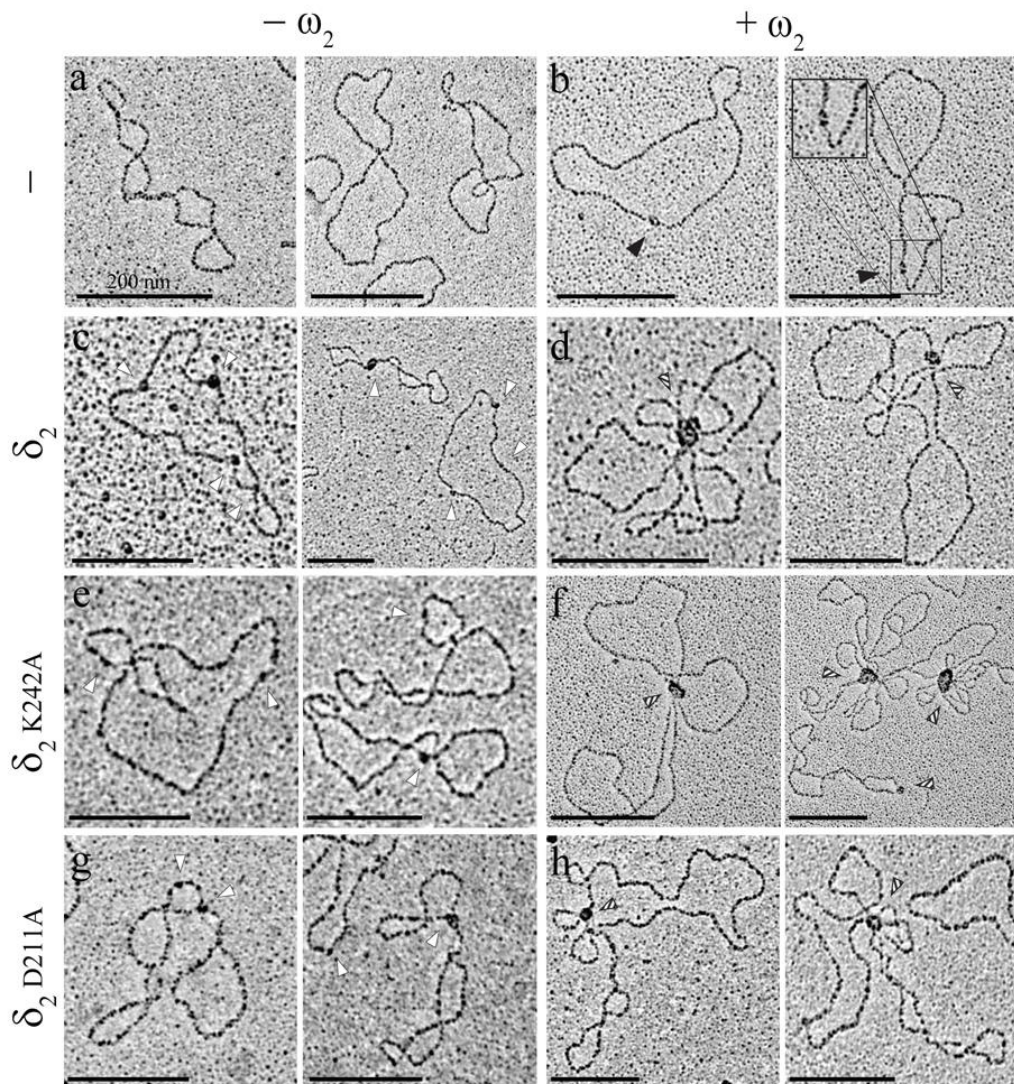
The presence of  $\delta_2$ , stimulates the formation of ternary complex  $\omega_2$ –*parS*– $\delta_2$ , and the interaction of two SC lead to plasmid pairing (or BC). When the phenotype of  $\delta_2$ K242A was tested in vivo, no obvious defect was observed (see results, paragraph 1.2.2.). Since the  $\delta_2$ K242A variant oligomerizes and hydrolyses ATP in a comparable manner with  $\delta_2$ , it was assumed that the  $\delta_2$ K242A variant might show a high off rate when complexed to nsDNA. To characterize whether  $\delta_2$ K242A variant binds nsDNA with normal rates with a different method, the protein–DNA complex  $\delta_2$ ,  $\delta_2$ D211A or  $\delta_2$ K242A formation and plasmid pairing were measured and their results compared by EM analysis.. Under this experimental condition,  $\omega_2$  (60 nM) alone



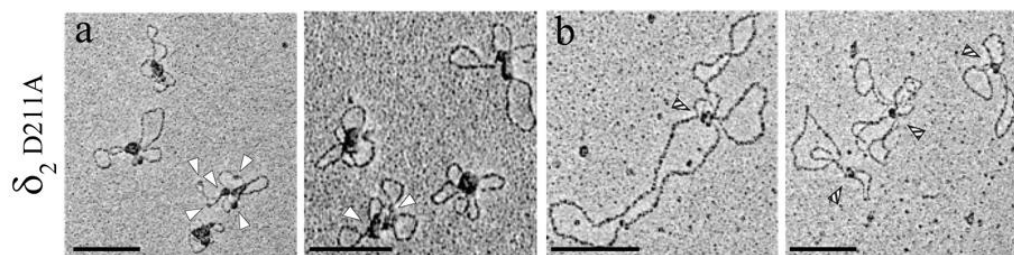
were able to form discrete complexes in ~80% of the DNA molecules (Fig. 25A, “b”) but it failed to promote significant amount of plasmid paired complexes (~1%, n=456) contained two *parS* DNA molecules that were paired by  $\omega_2$  (Table 12). Protein  $\omega_2$  does not spread significantly beyond its *parS* site, with 7–10  $\omega_2$ /DNA molecules that are displaced relative to their neighbours by 7–bp so as to assemble as a left-handed helix that wraps around *parS* DNA. In presence of both proteins, at molar ratios of  $\omega_2$ : $\delta_2$  (1:2.5), protein clusters larger than  $\omega_2$  or  $\delta_2$  alone were observed in ~70% of DNA molecules, suggesting that SC complexes were formed. In ~20% of the *parS*–protein complexes (n = 362) plasmid pairing was observed (Fig. 25A, “d”). When the  $\delta_2$ K242A mutant was incubated with plasmid DNA at a concentration that could not form a complex with nsDNA, as measured by EMSA, binary protein–DNA complexes were formed in ~38% (n=531) (Fig. 25A, “e”), indicating that DNA binding ability of  $\delta_2$ K242A was not prevented. When plasmid DNA containing *parS* sites (1 nM) was incubated with  $\omega_2$  and  $\delta_2$  K242A at 1:10 ratios, the presence of both proteins increased to ~80% the formation of proteins–DNA complex. The  $\delta_2$ K242A was facilitating the formation of intermolecular bridge (plasmid pairing) in ~39% (n=326) of the *parS* DNA molecules (Fig. 25A, “f”). When the molar ratio was reduced to 1:5 protein clusters were observed in ~62% of the DNA molecules, and ~18% of the *parS* DNA molecules were paired with DNA molecules (n=586) (Table 12).

By other hands, the high efficiency of  $\delta_2$ D211A in DNA binding was also confirmed by EM analysis. In presence of 75 nM of  $\delta_2$ D211A, nucleoproteins complexes were observed in ~75% (n=118) (Fig. 25A, “g”). The type and the volume of the complex were undistinguishable from those formed by 150 nM of  $\delta_2$ . When  $\delta_2$ D211A (75 nM), was incubated with  $\omega_2$  (60 nM), the ternary complex were observed in ~60% of DNA molecules promoting plasmid pairing in ~12% of DNA molecules (Fig. 25A, “h”; Table 12). A double amount (150 nM) of  $\delta_2$  D211A generated a type of complexes qualitatively different from those observed previously (with  $\delta_2$  and  $\delta_2$  K242A). The  $\delta_2$  D211A mutant was found to be associated with many discrete regions of the nsDNA molecules (~99%, n=423) forming a large cluster or multiples point of nucleation in a same plasmid (Fig. 25B, “a”).

A



B



**Figure 25. EM visualization of protein–DNA complexes.**

(A) pCB30 DNA (*parS2*) (*a*) was incubated with (+) or not (–)  $\omega_2$  (60nM) (*b, d, f, h*) and  $\delta_2$  (150nM) (*c, d*),  $\delta_2$ K242A (600nM) (*e, f*) or  $\delta_2$ D211A (75nM) (*g, h*) in the presence of 1 mM ATP and the complexes formed were visualized by electron microscopy. (B)  $\delta_2$ D211A (150nM) (*a, b*) was incubated with pCB30 DNA alone (*a*) or with  $\omega_2$  (60nM) (*b*). PCs are indicated by black triangles, DC complexes by white triangles and SC or BC by triangles with black and white stripes. Scale bars in black indicate 200 nm.

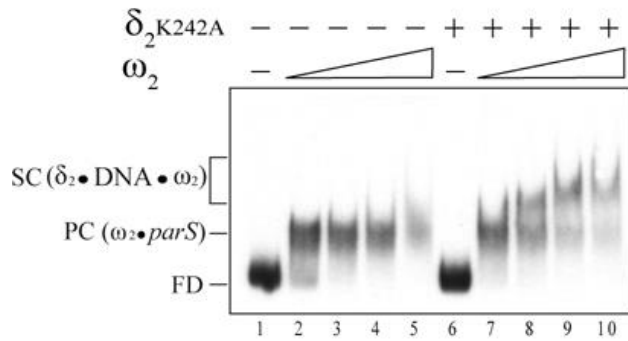
When  $\omega_2$  was added to reaction at the molar ratio of 1:2.5 the large binary complex of  $\delta_2$ D211A–nsDNA were totally disassembled forming ternary complex in ~74% of DNA molecules and promoting intermolecular bridge in ~17% of the *parS* DNA molecules (n=473) (Fig. 25B, “b”). For  $\delta_2$ D211A, the interaction with  $\omega_2$  prevails over nsDNA binding and lead to SC and BC formation. These results showed that  $\delta_2$ D211A and  $\delta_2$ K242A possessed different DNA binding proprieties.  $\delta_2$ K242A DNA binding is not prevented but only less efficient compared with  $\delta_2$  and  $\delta_2$ D211A.

**Table 12. EM data.**

$\delta$ variants (nM)		$\omega_2$ (nM)	Clusters/DNA molecule (%)	Pairing (%)	n
–		60	41.5	0.9	456
$\delta_2$	150	–	80.6	3.9	525
	150	60	69.6	22.6	362
	300	–	89.0	4.4	363
	300	60	ND	ND	ND
$\delta_2$ D211A	75	–	74.6	3.1	218
	75	60	60.2	12.3	201
	150	–	99.0	8.0	423
	150	60	74.2	16.7	473
$\delta_2$ K242A	300	–	ND	ND	ND
	300	60	61.6	18.1	586
	600	–	37.8	3.0	531
	600	60	81.0	39.1	326

#### 1.1.7.7. Protein $\omega_2$ stimulates $\delta_2$ K242A binding to DNA.

In previous section was reported that  $\delta_2$  increased the binding affinity of  $\omega_2$  for *parS* DNA and vice versa. We can predict that  $\omega_2$  might decrease the off rate of  $\delta_2$ K242A–nsDNA complexes. To confirm if the presence of  $\omega_2$  increase the stability of  $\delta_2$ K242A for nsDNA, EMSA experiments were performed in the presence of increasing  $\omega_2$  concentrations. In the absence of  $\delta_2$  K242A, the  $\omega_2$ –*parS* complexes facilitated the formation of a discrete mobility complex that was attributed to PC1 ( $\omega_2$ –*parS* DNA complexes) (Fig. 26, lanes 2–5). In the presence of  $\delta_2$  K242A, the formation of a slow mobility ternary complex was observed (Fig, 26, lanes 8–9), suggesting that  $\omega_2$  stimulated the  $\delta_2$  K242A DNA binding, and both proteins had a positive effect in the half–life of PC2 and  $\delta_2$ K242A–nsDNA.

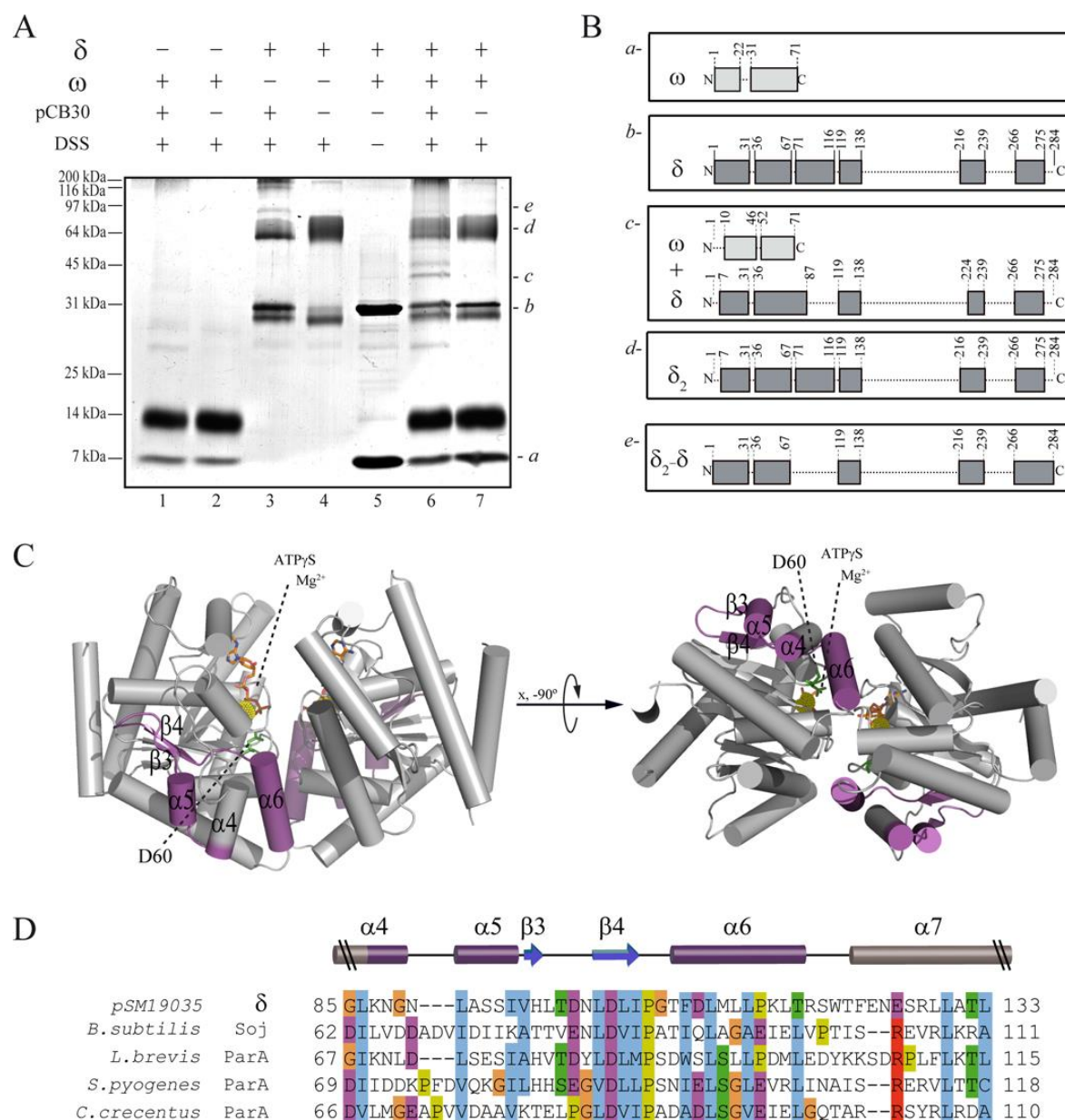


**Figure 26. Protein  $\omega_2$  facilitates the loading of  $\delta_2$ K242A onto *parS* DNA.** The 423-bp [ $\alpha^{32}$ P]-*HindIII*-*KpnI* DNA (0.1 nM) was incubated with increasing concentrations of  $\omega_2$  (6 to 48 nM) with or without the addition that a constant amount of  $\delta_2$ K242A (300 nM) in buffer C containing 1 mM ATP.

### 1.1.8. $\delta_2$ - $\omega_2$ interacting domains.

#### 1.1.8.1. Mapping $\delta_2$ - $\omega_2$ protein interacting domains.

Protein  $\delta_2$ , even in the apo form, increased ~6-fold the binding affinity of  $\omega_2$  for *parS* DNA (see paragraph 1.1.1.4.). Similar results were observed when  $\delta_2$  was replaced with functional variants as  $\delta_2$ D60A or  $\delta_2$ K242A. To confirm the interaction between  $\delta_2$  and  $\omega_2$ , cross-linking experiments, with DSS, were used for protein-protein interaction. Proteins  $\omega_2$  and  $\delta_2$  were able to form homo- and heterodimers, and the presence of *parS* DNA slightly stimulates protein oligomer formation (Fig. 27A, lane 1 and 3). When both proteins were pre-incubated and then cross-linked in absence of DNA, the resulting pattern seemed like a sum of the two independent reactions (Fig. 27A, lane 7). Interesting, two newly bands of ~43 and ~50 kDa appeared when  $\omega_2$  and  $\delta_2$  were cross-linked in presence of plasmid DNA containing a *parS* site (Fig. 27A, lane 6, band “c”). The molecular masses of the two bands are in agreement with that which would result from the interaction of one monomer of  $\delta$  and a monomer or dimer of  $\omega$  respectively. Western blotting analysis confirmed that those novel bands were recognized by polyclonal antibody anti- $\omega$  and anti- $\delta$  (data not shown). To identify the region on  $\delta_2$  involved in the interaction with  $\omega_2$ , the bands corresponding to monomers of  $\omega$  and  $\delta$  (Fig. 27A, lane 5, band “a” and “b” respectively), to  $\omega$ - $\delta$  heterodimer (lane 6, band “c”) and  $\delta_2$  dimers (lane 3, band “d”) were gel purified and subjected to partial proteolysis followed by Peptide mass fingerprinting MS analysis. In our indirect analysis, the peptides not involved in protein-protein interaction should be detected, whereas the DSS covalent bound peptides  $\omega$ - $\omega$ ,  $\omega$ - $\delta$  or  $\delta$ - $\delta$  should be not correlated with an expected peptide by the software used. This analysis is qualitative, and the no detection of a given peptide could be due to direct protein-protein cross-link or simply to limitations of MALDI-TOF-TOF technique (Fig. 27B).



**Figure 27. A central domain of  $\delta_2$  interacts with the  $\omega_2$  and with itself.**

(A) Specific interaction between  $\delta_2$  and  $\omega_2$ , at 2:1  $\omega_2$ : $\delta_2$  ratios, in the presence of *parS* DNA using DSS. The resulting products were resolved by 10–15% SDS-PAGE. The bands “a” and “b” (lane 5), “c” (lane 6), “d” and “e” (lane 3) were gel purified for MALDI-TOF-TOF identification. (B) Matched peptide sequences. In light or dark grey boxes are represented the identified (of  $\omega$  and/or  $\delta$ ) and in dotted lines the missing regions, respectively. (C) The relevant region involved in the putative interaction with  $\omega$  or with itself are highlighted in the crystal structure in purple ( $\alpha 4$ – $\alpha 5$ – $\beta 3$ – $\beta 4$ – $\alpha 6$ ), the ATP $\gamma$ S·Mg $^{2+}$  in orange and yellow, and the position of residue D60 in green (PDB 2OZE, displayed using PyMOL). (D) Sequence and secondary structure alignment of 85–133  $\delta$  regions. The residues are coloured according the Clustal X Default Colouring Scheme (Jalview).

The DNA binding domain (22–31) of  $\omega_2$  was not observed when the band “a” was analysed (peptide coverage ~89%). When band “b” (sequence coverage ~57%) and “d” (sequence coverage ~54%) were analysed 6 and 7 discrete regions of  $\delta$  were not observed: the 1–7 residues peptides that are present in band “b” but absent in band “d” could contribute to  $\delta$ – $\delta$  interaction or simply missing due to unknown reason. The remaining 6 regions were equally missing

between both samples, and potentially could be involved in  $\delta$ - $\delta$  or/and  $\omega$ - $\delta$  interactions. The results indicated that the band “c” was composed by polypeptides of both proteins, one monomer of  $\omega$  and one of  $\delta$  cross-linked (the sequence coverage was  $\sim 77\%$  for  $\omega$  and  $\sim 42\%$  for  $\delta$ ). The  $\omega$  peptides missing in the analysis of band “c” were at positions 1–10 and 47–52. By the other side, the comparison of  $\delta$  spectra highlighted two differences in the spectrum of the band “c” (Fig. 27B, data not shown). The 68–71 residues peptide were detected whereas the 87–119 residues was clearly not observed. As shown from the  $\delta$  structure (Fig. 27C, the 87–119 residues are highlighted in purple), the  $\omega$ - $\delta$  interacting region is close to the ATP binding or hydrolysis domains (Walker A’ [51–61]). The region presented some conserved hydrophobic (light blue) and negative (purple) residue that could be involved in the interaction with the N-terminus of  $\omega$  (Fig. 27D).

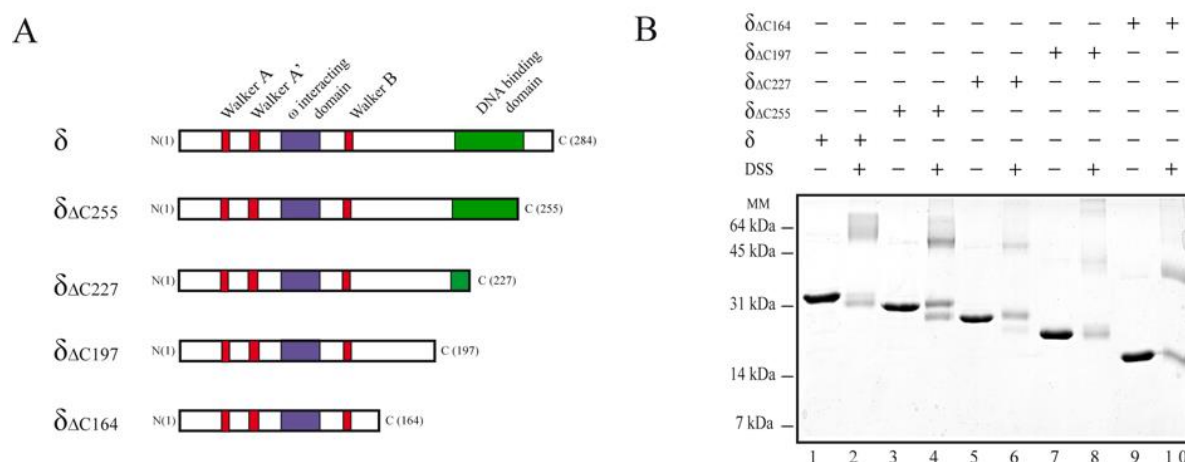
Two other regions were not present in such interaction (Fig. 27B). The first one encompassing the 139–224 intervals, that was 8 peptides larger than the critical region 139–216 lacking of trypsin sites, and it could be also involved in  $\omega$ - $\delta$  interaction. The second region (239–266) which contained several trypsin sites can be confused with the noise because the length of produced peptides does not reach the threshold for detection. Summarizing, the  $\omega$  N-terminus was confirmed to be necessary, especially the first 10 residues which seem to play an essential role in the interaction with  $\delta_2$ . The regions on  $\delta$  involved in the interaction with  $\omega$  are more complicated to define but our results highlighted three regions (87–119, 216–224) of  $\delta_2$  potentially involved in such interaction. The results are also suggesting that the DNA could somehow stimulate the interaction between  $\omega_2$  and  $\delta_2$ .

#### **1.1.8.2. The central region of $\delta$ is involved in $\delta_2$ - $\delta_2$ interaction.**

To identify the regions on  $\delta_2$  involved in self-interaction, the newly covalently bound protein  $\sim 65$  kDa (Fig. 27A, band “e”) that corresponded to  $\delta_2$ - $\delta$ , were compared with bands “b” and “d”. In the band “e”, one discrete region (residues 68–119) was not observed (Fig. 27B, band “e”). When the 68–119 interval was mapped in  $\delta_2$ , it revealed an exposed surface distant from the DNA binding domain, but overlapping with the  $\omega$ - $\delta$  interacting domain (87–119 interval). Two similar regions, also observed in the band “d”, were not present in  $\delta_2$ - $\delta$  interaction. The first one encompassing the 139–216 and the second, the 239–266 region. The  $\delta_2$ - $\delta$  interacting region is close to the ATP binding or hydrolysis domains (Walker A’ [residues 51–61] and walker B [142–147]) (Fig. 27).

### 1.1.8.3. C-terminal domain of $\delta$ is not involved in homodimer formation.

The  $\delta$  C-terminus is essential in nsDNA binding, previous findings were also including this region as possible candidate in the  $\omega_2$ - $\delta_2$  interaction. To map the regions of  $\delta_2$  involved in the interaction with  $\omega_2$ , deletions from the 3'-end of the gene, DNA sequencing and subsequent protein were performed. We performed C-terminal deletions that included residues from 164 to 284 (Fig. 28A).



**Figure 28. The  $\delta$  DNA binding domain is not essential for homodimer formation.**

(A) Illustration showing the  $\delta_2$  C-terminal deletions. In white is represented the unidentified regions, in red are highlighted the Walker A, A' and B, in purple the  $\omega$ - $\delta$  interacting domain (residues 87–119) and in green the DNA binding domain (residues 211–260). The position of the last residue present is indicated. (B) Proteins  $\delta$ ,  $\delta_{\Delta C255}$ ,  $\delta_{\Delta C227}$ ,  $\delta_{\Delta C197}$  and  $\delta_{\Delta C164}$  (3  $\mu$ g) formed dimer in solution when incubated in buffer B with the crosslinking reagent DSS (0.5 mM), and the samples were loaded on a 15 % SDS-PAGE.

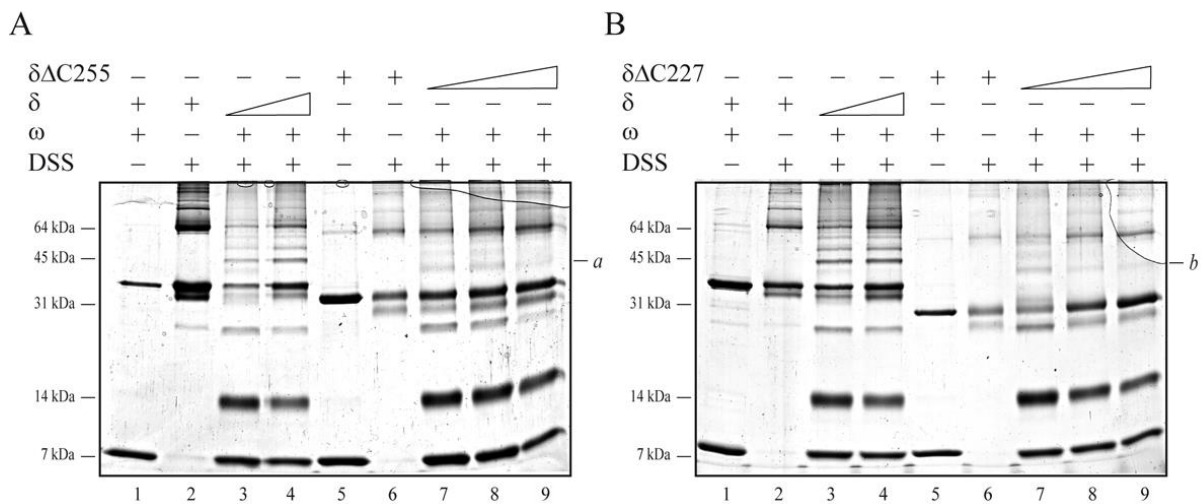
The entire sequence and four sequential deletions from the 3' end of  $\delta$  gene were amplified and cloned in expression vector carrying an N-terminal His-tag sequence. The  $\delta$  proteins were purified using the same protocol of the one carrying the C-terminal tag. All activities measured were comparable when the  $\delta$  variant having a His-tag at the C-terminus that behaves a  $\delta$  protein (data not shown). In contrast, the  $\delta_{\Delta C255}$ ,  $\delta_{\Delta C227}$ ,  $\delta_{\Delta C197}$  and  $\delta_{\Delta C164}$  C-terminal deletions were partially insoluble compared with  $\delta$ . The purification protocol was modified and C-terminal deletions were isolated under denaturing condition and finally refolded.

To test if the structure of deletion proteins were properly re-established, we explored their dimerization properties.  $\delta_2\Delta C255$ ,  $\delta_2\Delta C227$ ,  $\delta_2\Delta C197$  and  $\delta_2\Delta C164$  proteins, analysed by DSS cross-linking, were able to form homodimer, as well as higher oligomer (Fig. 28B). This results indicated that all deletion proteins reached the right conformation to promote oligomer formation.

#### 1.1.8.4. C-terminal domain of $\delta$ does not interact with $\omega_2$ protein.

To study the effect of  $\delta_2$  C-terminal domain, the DNA binding, the ATPase activity and the interaction with  $\omega_2$  of  $\delta_2$  deletion were taken into account. Proteins  $\delta_2\Delta C255$ ,  $\delta_2\Delta C227$ ,  $\delta_2\Delta C197$  and  $\delta_2\Delta C164$  variants were defective in DNA binding (Fig. 30A and 30 B, lanes 8 and 12) even at high protein concentration ( $>2\mu\text{M}$ ) when analysed by EMSA. ).

Except  $\delta_2\Delta C255$ , the  $\delta_2$  C-terminal deletions ( $\delta_2\Delta C227$ ,  $\delta_2\Delta C197$ ,  $\delta_2\Delta C164$ ) were unable to hydrolyse ATP. The  $\delta_2\Delta C255$  bound and hydrolysed ATP with low efficiency and just above the background levels, but addition of  $\omega_2$ -bound to *parS* DNA stimulated the  $\delta_2\Delta C255$  ATPase (by  $< \sim 1.5$ -fold) to some extent (data not shown).



**Figure 29. The  $\delta_2\Delta C255$  and  $\delta_2\Delta C227$  form heterodimers in presence of  $\omega_2$ .**

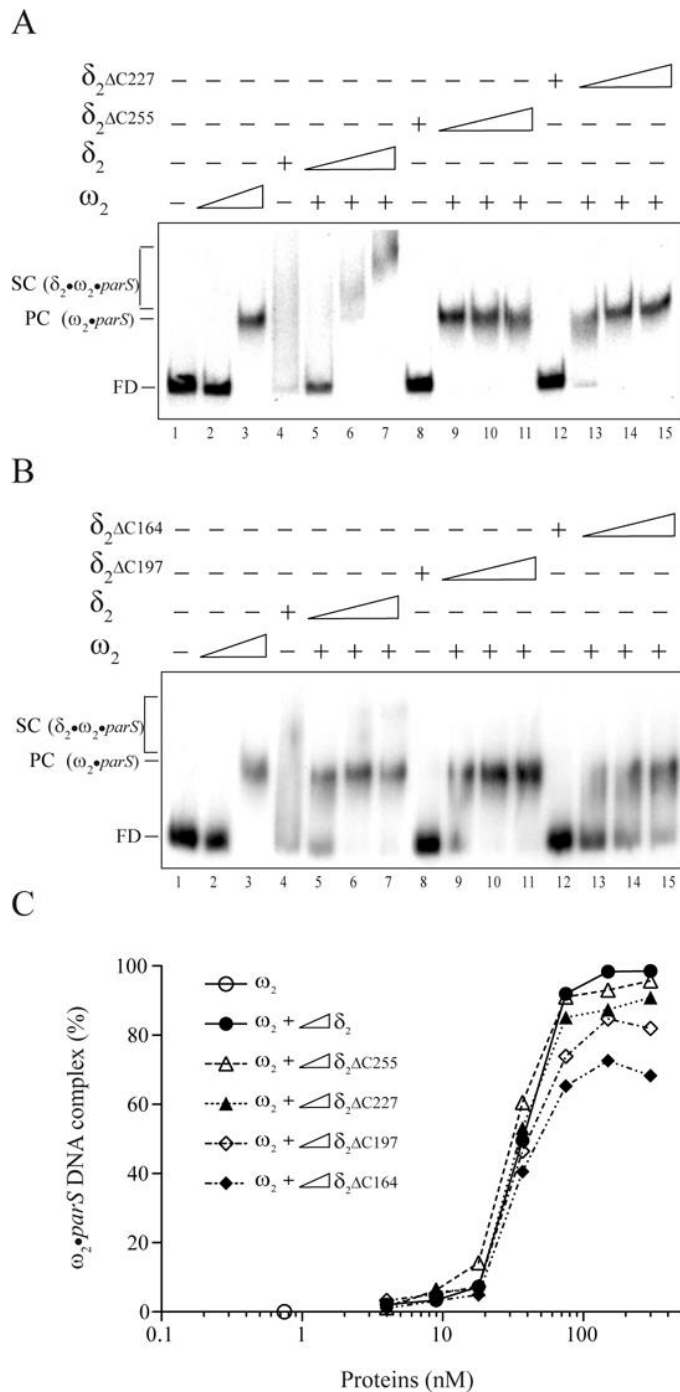
(A) Protein  $\omega_2$  (3  $\mu\text{g}$ ) and  $\delta_2$  (3–6  $\mu\text{g}$ , lanes 2–3) or  $\delta_2\Delta C255$  (3–9  $\mu\text{g}$ , lanes 7–9) were incubated in buffer B at 37°C for 10 min in presence of ATP (1 mM) and *parS* DNA. The reactions were then cross-linked with DSS (0.5 mM). The resulting products were resolved by 10–15% SDS-PAGE. The band “a” (lanes 7–9) corresponds to specific protein  $\omega$ - $\delta\Delta C255$  interaction. (B) Specific protein-protein interaction between  $\omega_2$  (3  $\mu\text{g}$ ) and  $\delta_2$  (3–6  $\mu\text{g}$ , lanes 2–3) or  $\delta_2\Delta C227$  (3–9  $\mu\text{g}$ , lanes 7–9, band “b”) were fixed with DSS (0.5 mM). The band “b” (lanes 7–9) highlighted the  $\omega$ - $\delta\Delta C227$  interaction.

A possibility is that the  $\delta_2\Delta C227$ ,  $\delta_2\Delta C197$  and  $\delta_2\Delta C164$  variants neither bind nor hydrolyse ATP. To test this hypothesis, the  $\delta_2$  C-terminal deletions were incubated with ATP and [ $\alpha^{32}\text{P}$ ]-ATP, treated with UV light, to facilitate the nucleotide cross-linking, proteins resolved on SDS-PAGE and the gel was stained with Coomassie Brilliant Blue or autoradiographed.  $\delta_2$  and its C-terminal deletion variants became radiolabelled, suggesting that the C-terminal deletions bind ATP (data not shown).

Interesting, when  $\delta_2\Delta C255$  and  $\delta_2\Delta C227$  were incubated with  $\omega_2$ -*parS* DNA and DSS, two novel weak bands of ~36 kDa and ~33 kDa were observed suggesting that  $\delta_2\Delta C255$  and  $\delta_2\Delta C227$  still interacted with  $\omega_2$  (Fig. 29A, lanes 7–9, band “a” and 29B, lanes 7–9, band “b”). Contrarily,



when the  $\delta_2\Delta C197$  or  $\delta_2\Delta C227$  were used in the cross-linking, any novel  $\delta\cdot\omega$  band was observed (data not shown).



**Figure 30. The  $\delta$  DNA binding domain is not essential for interaction with  $\omega_2$ .**

(A) The 423-bp [ $\alpha^{32}P$ ]-HindIII-KpnI *parS* DNA (0.1 nM) was incubated with different amounts of  $\omega_2$  (0.75 and 6 nM),  $\delta_2$ ,  $\delta_2\Delta C255$  or  $\delta_2\Delta C227$  (160 nM), or a fixed amount of  $\omega_2$  (0.75 nM) and increasing concentrations of  $\delta_2$ ,  $\delta_2\Delta C255$  or  $\delta_2\Delta C227$  (40 to 160 nM) for 15 min at 37 °C, in buffer C containing 1 mM ATP. (B) The 423-bp [ $\alpha^{32}P$ ]-*parS* DNA was incubated with different amounts of  $\omega_2$  (0.75 and 6 nM),  $\delta_2$ ,  $\delta_2\Delta C197$  or  $\delta_2\Delta C164$  (160 nM), or a fixed amount of  $\omega_2$  (0.75 nM) and increasing concentrations of  $\delta_2$ ,  $\delta_2\Delta C197$  or  $\delta_2\Delta C164$  (40 to 160 nM). The free DNA (FD) and the formed complexes are indicated. (C) The plot of  $\omega_2\cdot parS$  DNA complex formed in the presence of  $\omega_2$  (0.75 nM) and increasing concentration of C-terminal  $\delta_2$  variants. Values are the average of more of three independent experiments.

To effectively prove if the C-terminal domain is essential  $\omega_2$ - $\delta_2$  interaction, we took advantage of  $\omega_2$ -*parS* (or PC's) formation by EMSA. When limiting concentration  $\omega_2$  (< 3nM) were incubated with *parS* DNA no protein-DNA complexes were observed; however the addition of a  $\delta_2\Delta C255$ ,  $\delta_2\Delta C227$ ,  $\delta_2\Delta C197$  or  $\delta_2\Delta C164$  variant was able to promote the formation of  $\omega_2$ -*parS* complexes (Fig. 30A and 30B, lanes 9–11 and 13–15). As extrapolated

## Chapter I

from the Figure 30C, the  $K_{Dapp}$  of PC formation of C-terminal variants was comparable (~ 40 nM), suggesting that all  $\delta_2$  deletion variants interact with  $\omega_2$  with similar efficiency and promotes its structural transition.

Although all proteins still maintained the ability to stimulate the PC formation, the stability of the  $\omega_2$ -*parS* complex is directly proportional with the length of  $\delta_2$ . It seems that the deletion of large domains produced less stable proteins in solution, resulting in a reduction of the maximum effect of PC formation. Altogether the results suggested that the first 164 residues on  $\delta_2$  are involved in specific interaction with  $\omega_2$ , and furthermore that the DNA binding features are not essential in the interaction with  $\omega_2$ .

## 1.2. Cytological characterization of pSM19035 par system.

### 1.2.1. Quantification of $\omega_2$ and $\delta_2$ molecules per cell.

To study the dynamic localization and to understand how  $\omega_2$  and  $\delta_2$ -mediated plasmid stability three different systems were used for *in vivo* analysis. They were based in the middle copy number pHP14 (7 copies  $\pm$  2/ cell). In the first system,  $\omega$  (or its variants  $\omega:yfp$  or  $\omega\Delta N19$ ) and  $\delta$  (or its variants  $\delta:gfp$ ,  $\delta D60A:gfp$ , etc.) genes were cloned with their own promoters ( $P_\omega$  or  $parS1$  and  $P_\delta$  or  $parS2$ ), the expression levels of genes were regulated by  $\omega_2$  protein (or  $\omega:YFP_2$  or  $\omega_2\Delta N19$ ), and they were assumed to be at physiological levels (or absence of a fitness cost). In the second system, expression of  $\delta$  (or its variants  $\delta:gfp$ ,  $\delta D60A:gfp$ , etc.) constitutively expressed from the  $\delta$  promoter ( $parS2$ ), in the absence of  $\omega_2$ , and it should indicate the maximum level reached by  $\delta$  proteins in the cells. In the third system, the  $\delta:gfp$  or  $\delta D60A:gfp$  gene was under the control of the LacI repressor, and its expression was inducible by IPTG addition, and the  $\omega_2$  or  $\omega_2\Delta N19$  repressors, ectopically expressed by plasmid integration, only controlled their own expression (Pratto et al. 2008, Pratto et al. 2009).

The presence of  $\omega_2$  or  $\delta_2$  did not alter the plasmid copy number (7 copies  $\pm$  2/ cell). The amount of  $\omega_2$  or protein  $\delta_2$  present in various cells bearing plasmid was determined in a semi-quantitative immune-blotting analysis. Serial dilutions of purified  $\omega_2$  or  $\delta_2$  were used as a standard for comparison against cell extracts made from a known quantity of bacterial cells. The results are reported in Table 13.

**Table 13. Determination of  $\omega_2$  and  $\delta_2$  molecules per cell.**

Strain	Plasmid	System	Relevant Genotype	IPTG ( $\mu$ M)	$\omega_2$		$\delta_2$	
					Mol./cell	$\mu$ M	Mol./cell	$\mu$ M
BG214	pCB586	I	<i>parS1</i> , $\omega$	–	~ 1.350	1.9	–	–
BG214	pCB702	I	<i>parS2</i> , $\delta:gfp$ , <i>parS1</i> , $\omega$	–	~ 1.250	1.8	~ 1.400	~ 2.0
BG214	pCB578	II	<i>parS2</i> , $\delta:gfp$	–	–	–	~ 6.500	~ 9
BG947	–	III	<i>lacZ</i> , $\delta:gfp$	10	–	–	~ 12.500	~ 18

Cells carrying a plasmid-borne  $\delta$  and  $\omega$  or  $\omega\Delta N19$  genes, averaged 1,400  $\delta_2$  molecules (or ~ 2  $\mu$ M, assuming a cell volume of 1.2 femtoliter) and ~ 1,300  $\omega_2$  or  $\omega\Delta N19$  molecules (~ 1.8  $\mu$ M) per cell. Similar results were observed with cells carried a plasmid-borne  $\delta:gfp$  and  $\omega$  or  $\omega\Delta N19$  genes. However, in the absence of  $\omega_2$  (or  $\omega_2\Delta N19$ ) transcriptional repressor constitutive number of  $\delta_2$  or  $\delta:GFP_2$  molecules averaged ~ 6,500 molecules per cell, its expression increased >7 fold if compared with *parABS* system. In the second system, the amount of the cellular copy number of  $\delta:GFP_2$  upon addition of 10  $\mu$ M IPTG averaged ~12,000 molecules per cell. This result

showed that at almost physiological level both  $\omega_2$  and  $\delta_2$  protein showed the lowest expression and are present at equimolar ratio in the cells.


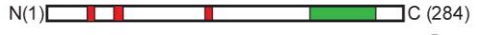
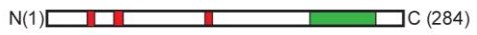


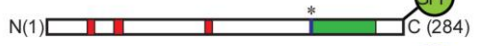
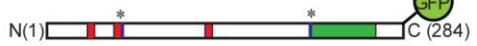
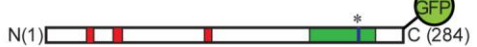



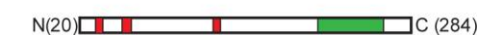

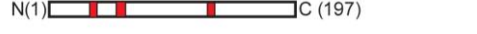
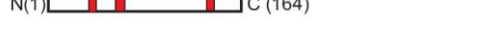

### 1.2.2. The $\delta_2$ DNA binding domain and its role in the plasmid stability.

To analyse the influence of  $\delta_2$  DNA binding domain in plasmid stability and  $\delta_2$  localization,  $\omega$  and *parS* sequences together with different mutations of  $\delta$  (D60A, D211A, K242A, K248S, K255A and K259A K260A) fused at the 3'-end with the *gfp* gene were cloned into pHP14 control vector that lacked an active partition system (*par*<sup>-</sup>). In those plasmids,  $\omega$  and  $\delta$  genes were under the regulation of their own promoters and the expression of both were controlled by  $\omega_2$ . This system has a great advantage in plasmid partitioning because it assumed to ensure physiological levels of proteins. The absence of one of the three components,  $\omega_2$ ,  $\delta_2$  (or  $\delta$ :GFP<sub>2</sub>) and *parS* sites, render the cells impaired in plasmid partitioning (Table 14).

Plasmid stability was not affected by the GFP C-terminal fusion as observed in *par* systems containing  $\delta_2$  or  $\delta$ :GFP<sub>2</sub>. Conversely, the  $\delta_2$ D60A, which binds but it does not hydrolyse ATP, was unable to stabilize the randomly segregated plasmid (<1%). An increase in the  $\delta_2$  binding affinity for nsDNA (~ 25-fold), as in the  $\delta_2$ D60A D211A double mutant, was not sufficient to stabilize plasmid segregation (<1%). Mutants variant that bound nsDNA with high ( $\delta_2$ D211A) or low ( $\delta_2$ K248S) affinity *in vitro* showed a similar stability than the wild type system, >91% of the cells have increased plasmid stability (Tab. 14).

The other mutant ( $\delta_2$  K242A,  $\delta_2$ K255A, and  $\delta_2$ K259A K260A), when expressed together with wild type  $\omega_2$ , were unable to fully stabilize plasmid segregation (41% to 61%) (Tab. 14). The  $\delta_2$ K259A K260A mutant that was defecting in nsDNA binding and in dimer-of-dimer formation *in vitro*, presented only partially affected maintenance. Since the plasmid stability of  $\delta_2$ K242A,  $\delta_2$ K255A, and  $\delta_2$ K259A K260A variants were only reduced 2-fold *in vivo* we asked whether  $\delta_2$  binding to nsDNA required for plasmid partition. To test this question we have constructed a  $\delta$ K242A:GFP<sub>2</sub> as well as other  $\delta$ K248S:GFP<sub>2</sub>,  $\delta$ K255A:GFP<sub>2</sub> and  $\delta$ K259A K260A:GFP<sub>2</sub> and finally addressed protein localization. All of these proteins, in absence of  $\omega_2$ , formed clouds of fluorescence on the nucleoid (data not shown), suggesting that the protein binds nsDNA *in vivo*. Furthermore, when a methodology that allowed us to test the transient protein-protein interaction as EM determination, it was observed that  $\delta_2$ K242A interacts with nsDNA with only 2- to 4-fold less affinity than wild type protein (Fig. 25A, "e"). Our results indicated that the  $\delta_2$  K242A,  $\delta_2$ K255A, and  $\delta_2$ K259A K260A variants bind nsDNA both *in vivo* and *in vitro*, but the protein-nsDNA complexes show a high off-rate when measured by EMSA.

Table 14. Effect of the pSM19035 Par system on plasmid stability.

Par Genes		$\delta$ genotype	Stability
<i>parB</i> -like	<i>parA</i> -like		
none	$\delta$		<1%
$\omega$	none	—	<1%
$\omega$	$\delta$		100%
$\omega:yfp$	$\delta$		<1%
$\omega$	$\delta:gfp^a$		99.6%
$\omega$	$\delta D60A:gfp^a$		<1%
$\omega$	$\delta D211A:gfp^a$		97.2%
$\omega$	$\delta D60A D211A:gfp^a$		<1%
$\omega$	$\delta K242A:gfp^a$		42.2%
$\omega$	$\delta K248S:gfp^a$		90.1%
$\omega$	$\delta K255A:gfp^a$		60.4%
$\omega$	$\delta K259A K260A:gfp^a$		55.8%
$\omega$	$\delta \Delta N20^b$		67.8%
$\omega$	$\delta \Delta C255^b$		29.4%
$\omega$	$\delta \Delta C197^b$		2.9%
$\omega$	$\delta \Delta C164^b$		1.5%
$\omega$	$\delta \Delta N20 C255^b$		<1%

*B. subtilis* cells bearing the *Par*<sup>-</sup> vector (~ 7 copies per cell) or derivatives bearing the whole pSM19035 *par* locus or part of it were grown in antibiotic-free LB medium at 30 °C, and the frequency of plasmid loss during exponential growth was measured until at least 100 generations. <sup>a</sup>The influence of  $\omega$  and  $\delta$ -*gfp* genes and its variants and their role in plasmid stability. <sup>b</sup>The effect of  $\omega$  and  $\delta$  truncated genes in plasmid stability.

The influence of  $\delta$  truncated genes and their role in plasmid stability were also study (Tab. 14). To avoid any type of interference in protein folding, the  $\delta$  genes were not fused to *gfp*: three different 3'-end ( $\delta \Delta C255$ ,  $\delta \Delta C197$  and  $\delta \Delta C164$ ), a 5'-end ( $\delta \Delta N20$ ) and a 5'/3'-end ( $\delta \Delta N20 C255$ ) truncated  $\delta$  sequences were separately cloned downstream of the  $\delta$  promoter region ( $P_\delta$ ) and inserted in pCB586.

As observed in Table 14, only  $\delta\Delta N20$  (~68%) and  $\delta\Delta C255$  (~30%) still had positive effects in plasmid maintenance whereas the other deletion variants were unable to stabilize the plasmid (<3%). These results revealed how the C-terminus of  $\delta$  (DNA binding domain) played an essential role in plasmid maintenance *in vivo*. Plasmid stabilization was only partially affected by punctual mutation but it was completely impaired by deletion of DNA binding domain. More complicated to understand was the role in plasmid stability of the N-terminus of  $\delta$ .

### 1.2.3. Protein $\delta_2$ facilitates plasmid pairing.

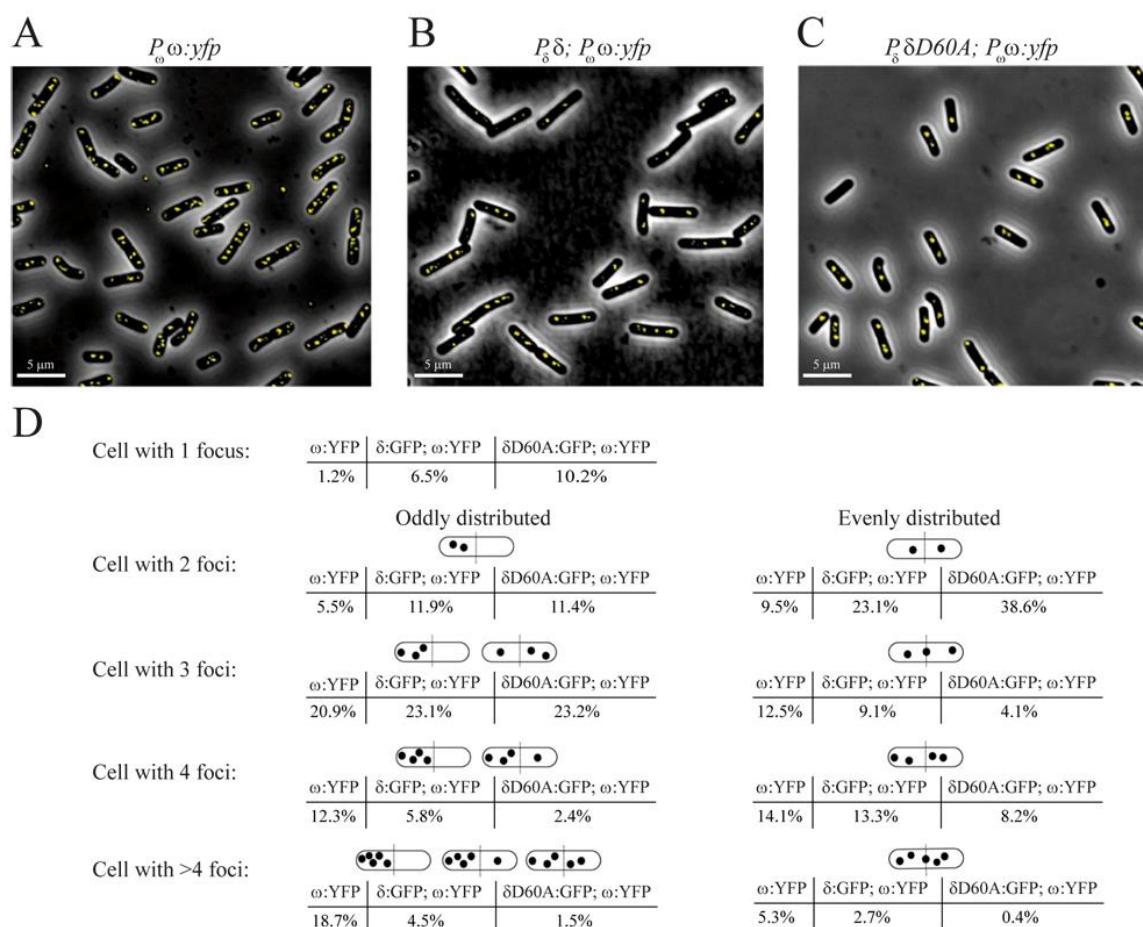
Plasmid-borne  $P_{\omega}$   $\omega:yfp$  (pCB846),  $P_{\omega}$   $\omega:yfp$  and  $P_{\delta}$   $\delta$  (pCB843) or  $P_{\omega}$   $\omega:yfp$  and  $P_{\delta}$   $\delta D60A$  (pCB847) had no significant changed plasmid copy number (~ 8 copies/ cell), or their relative protein concentrations (~1,400  $\delta_2$ , or  $\delta_2 D60A$  and ~ 1,300  $\omega:YFP_2$  molecules/cell) (Table 13). In plasmid-borne  $P_{\omega}$   $\omega:yfp$ , fluorescent  $\omega:YFP_2$  formed discrete foci that were broadly distributed without showing any specific pattern (Fig. 31A and 31D). One to eight  $\omega:YFP_2$  foci per cell were observed, suggesting that the newly replicated plasmids remain “bound” and the fluorescence of  $\omega:YFP_2$  co-localized with plasmid-borne *parS* site (Fig. 31A). The fluorescence of  $\omega:YFP_2$  correlates with the one of LacI:GFP bound to plasmid-borne array of *lacO* operators *in vivo* (data not shown). A correlation of the plasmid copies with the number of  $\omega:YFP_2$  foci revealed that only ~ 50% of the cells contained 4 or more foci cell (Fig. 31D). Since plasmid copy number was not significantly altered during the experimental time, we have to assume that there were ~ 1.3 plasmid copies/focus. This data suggested that stochastic co-localization or pairing of some plasmid is observed with low efficiency in presence of  $\omega_2$  *in vivo*.

In the presence of  $\delta_2$ , a reduction in the number of  $\omega:YFP_2$  fluorescent foci per cell and a significant re-localization of foci was observed (Fig. 31B and 31D). The data confirmed that  $\omega:YFP_2$  interacts with  $\delta_2$  *in vivo*. A quantification of cell containing foci, from > 2,000 cells, revealed that in the presence of  $\delta_2$ , there were 3 or less  $\omega:YFP_2$  foci per cell in ~ 72 %, suggesting that each  $\omega:YFP_2$  foci might have an average of ~ 2.8 plasmid copies (Fig. 31D). There was a preferential plasmid re-localization and capture toward cell quarters in bilobed cells, and at mid cell in cells with one nucleoid.

When  $\delta_2$  was replaced by the  $\delta_2 D60A$ , there were 3 or less  $\omega:YFP_2$  foci per cell in ~88 % of total cells (Fig. 31D) and an average of 3.3 plasmid/foci. The foci tend to co-localize with the nucleoids at cells quarters (Fig. 31C).

Altogether these data demonstrated that when only  $\omega:YFP_2$  is present, the plasmids are randomly distributed and the plasmid pairing is restricted inside the cells. The concomitant

presence of  $\delta_2$  or  $\delta_2D60A$  and  $\omega$ :YFP<sub>2</sub> enhanced plasmid pairing by a directly increase of plasmid/foci of around 2.1– or ~2.5– fold respectively and changed the localization of plasmids in the cells.

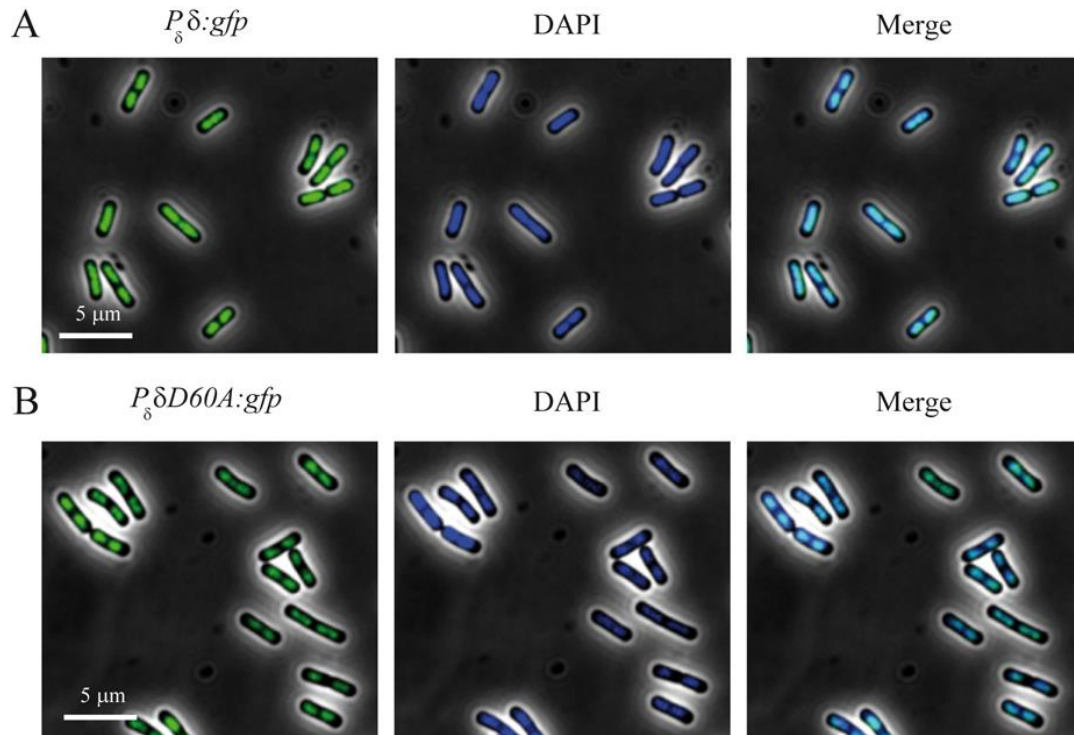


**Figure 31. Subcellular position of  $\omega$ :YFP<sub>2</sub> foci in presence or absence of  $\delta_2$  or  $\delta_2D60A$ .**

Cells bearing plasmid borne  $P_{\omega} \omega:yfp$  (pCB846) (A),  $P_{\omega} \omega:yfp$  and  $P_{\delta} \delta$  (pCB843) (B) or  $P_{\omega} \omega:yfp$  and  $P_{\delta} \delta D60A$  genes (pCB847) (C) were grown in MMS7 at 30 °C. (D) The percentages of cells having  $\omega$ :YFP<sub>2</sub> foci disposed around the cell center are shown. The relative positions of the foci (1 to more than 4 foci) of 2000 cells are shown schematically.

#### 1.2.4. Protein $\omega_2$ bound to *parS* stimulates $\delta_2$ disassembles from the nucleoid.

To determine the type of complexes formed by  $\delta$ :GFP<sub>2</sub> or  $\delta D60A$ :GFP<sub>2</sub> in the presence or the absence of  $\omega$  or  $\omega \Delta N19$  genes, plasmid-borne  $P_{\delta} \delta:gfp$  (pCB578);  $P_{\delta} \delta D60A:gfp$  (pCB760);  $P_{\delta} \delta:gfp P_{\omega} \omega$  (pCB702),  $P_{\delta} \delta D60A:gfp P_{\omega} \omega:yfp$  (pCB761) or  $P_{\delta} \delta D60A:gfp P_{\omega} \omega \Delta N19$  (pCB846) were analysed.



**Figure 32. Subcellular localization of  $\delta$ :GFP<sub>2</sub> or  $\delta D60A$ :GFP<sub>2</sub>.**

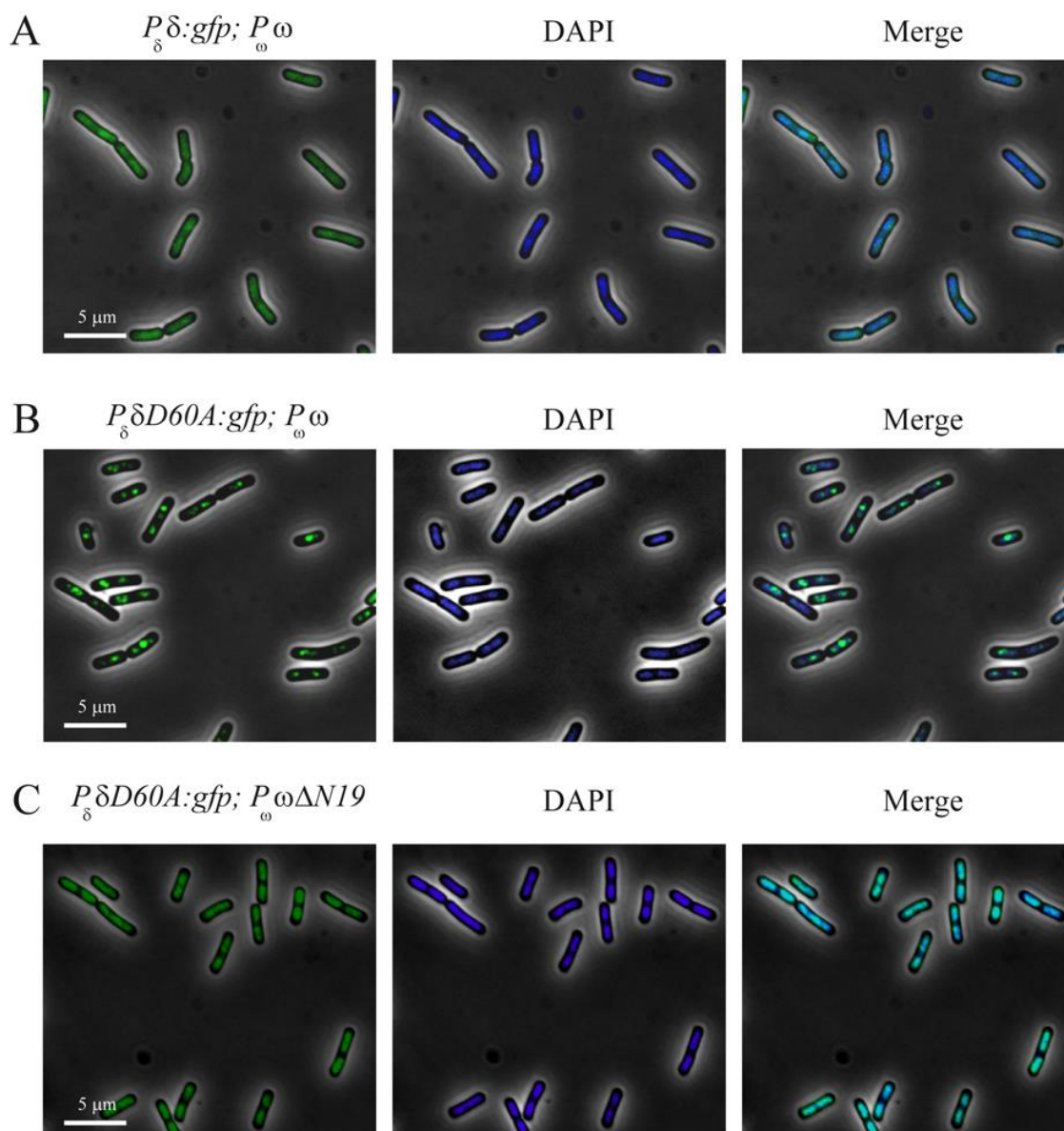
Cells bearing plasmid borne  $P_{\delta} \delta:gfpl$  (pCB578) (A) or  $P_{\delta} \delta D60A:gfpl$  gene (pCB760) (B) were grown in MMS7 at 30 °C. Images of cells with fluorescence from  $\delta$ :GFP<sub>2</sub> or  $\delta D60A$ :GFP<sub>2</sub>, images of the same cells stained with DAPI to show DNA and the merge of both images are shown. Scale bar is 5 μm.

Protein  $\delta$ :GFP<sub>2</sub> or  $\delta D60A$ :GFP<sub>2</sub>, at constitutive levels (in absence of  $\omega$  repression, system II, ~ 12,000 molecules/cell, see results, paragraph 1.2.1.), are regularly distributed over the nucleoid, rather than forming DNA-independent threads or oscillate between the poles (Fig. 32A and 32B). The  $\delta$ :GFP<sub>2</sub> fluorescence showed a slow dynamic instability (or disassembly rate), because low-density areas of fluorescence were observed (Fig. 32A). Curiously, similar results were observed when  $\delta$ :GFP<sub>2</sub> was replaced by  $\delta D60A$ :GFP<sub>2</sub> that binds but it cannot hydrolyse ATP (Fig. 32B).

In the presence of both  $\omega_2$  and  $\delta$ :GFP<sub>2</sub>, at or near physiological concentrations (system I, ~ 1300 molecules/cell each), the  $\delta$ :GFP<sub>2</sub> fluorescence seemed to be irregularly distributed (Fig. 33A). The cloud of  $\delta$ :GFP<sub>2</sub> fluorescence overlapped with DAPI stained DNA and it showed a dynamics behaviour with areas lacking fluorescence when compared to the absence of  $\omega_2$  (Fig. 33A).

To gain insight whether the loss of  $\delta$ :GFP<sub>2</sub> cloudiness (or dissociation from the nucleoid) requires ATP hydrolysis the behaviour of  $\delta D60A$ :GFP<sub>2</sub> was studied. In the presence of  $\omega_2$ ,  $\delta D60A$ :GFP<sub>2</sub>, lost the regular distribution of the fluorescence, and accumulated discrete foci or patched regions on the nucleoid were observed (Fig. 33B).





**Figure 33. Subcellular localization of  $\delta$ :GFP<sub>2</sub> or  $\delta$ D60A:GFP<sub>2</sub> foci in presence of  $\omega_2$  or  $\omega_2\Delta N19$ .**

(A),  $P_\delta \delta D60A:gf$  and  $P_\omega \omega$  (pCB761) (B), or  $P_\delta \delta D60A:gf$  and  $P_\omega \omega\Delta N19$  genes (pCB840) (C) were grown in MMS7 at 30 °C. Images of cells with fluorescence from  $\delta$ :GFP<sub>2</sub> or  $\delta$ D60A:GFP<sub>2</sub>, images of the same cells stained with DAPI to show DNA and the merge of both images are shown. Scale bar is 5  $\mu$ m.

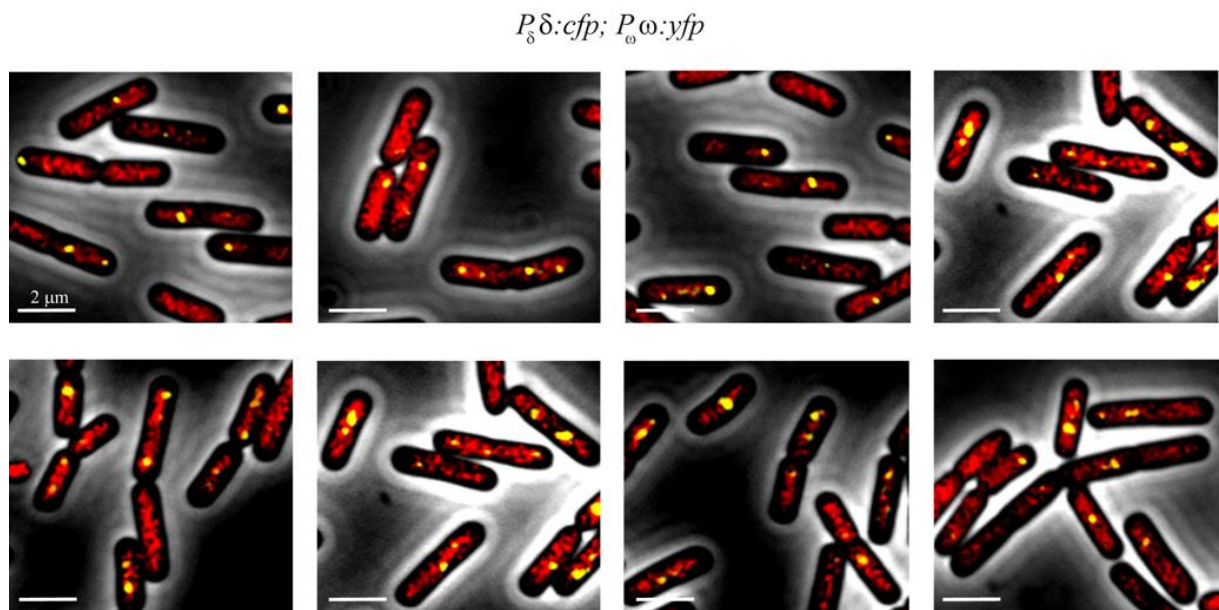
The  $\delta$ D60A:GFP<sub>2</sub>, upon interaction with the  $\omega_2$ -*parS* complex, lead to more to stable plasmid–nucleoid and/or plasmids pairing formation (BC and BC1). As previously observed for plasmid–borne *omega:yfp* and *deltaD60A* genes (Fig. 31C), the *parS*- $\omega_2$ - $\delta_2$ D60A complexes observed in the discrete patched regions should present many discrete plasmids paired to the nucleoid. When  $\omega_2$  was replaced by  $\omega_2\Delta N19$ , the  $\delta$ D60:GFP<sub>2</sub> lost the discrete foci localization to show again the nucleoid clouding (Fig. 33C).

These data suggested that GFP<sub>2</sub> or  $\delta$ D60A:GFP<sub>2</sub> slowly disassembly from the nucleoid in the absence of  $\omega_2$  and /or ATP hydrolysis. The interaction of  $\omega_2$  (bound to *parS*) facilitates the

disassembly and relocation of both  $\delta$ :GFP<sub>2</sub> or  $\delta$ D60A:GFP<sub>2</sub> proteins from the nucleoid, but the disassembly of the BC (foci or patched regions form by  $\delta$ D60A:GFP<sub>2</sub>) is observed in presence of  $\delta_2$  proteins that have genuine ATP hydrolysis.

### 1.2.5. Nucleoid bound $\delta$ :CFP<sub>2</sub> capture and tethers plasmid copies.

To test whether plasmid–nucleoid pairing occurs *in vivo* and if the interaction of  $\delta_2$  with  $\omega_2$  led to diffusion of the fluorescent region a plasmid–borne  $P_\delta \delta:cfp$  and  $P_\omega \omega:yfp$  genes have been used. In the presence of  $\omega$ :YFP<sub>2</sub> and  $\delta$ :CFP<sub>2</sub> (~1,300 molecules/cell each),  $\delta$ :CFP<sub>2</sub> formed a regular cloud of fluorescence on the nucleoid, and  $\omega$ :YFP<sub>2</sub> formed 1 to 3 discrete foci per nucleoid in ~75% of total cells, rather than located elsewhere (<1% of total cells) indicating plasmid–pairing occurred (Fig. 34). Areas lacking the cloud of  $\delta$ :CFP<sub>2</sub> fluorescence (~20% of total cells) also lacked the  $\omega$ :YFP<sub>2</sub> focus. Those complexes, do not show a high rate of  $\delta$ :CFP<sub>2</sub> disassembly. It seems that  $\omega$ :YFP<sub>2</sub> failed to stimulate the  $\delta$ :CFP<sub>2</sub> ATPase activity although any type of foci or patched regions were observed for  $\delta$ :CFP<sub>2</sub>. The results suggested that  $\delta$ :CFP<sub>2</sub> upon interacting with  $\omega$ :YFP<sub>2</sub> captures and tethers plasmids to the nucleoid (plasmid–nucleoid pairing) (Fig. 34).



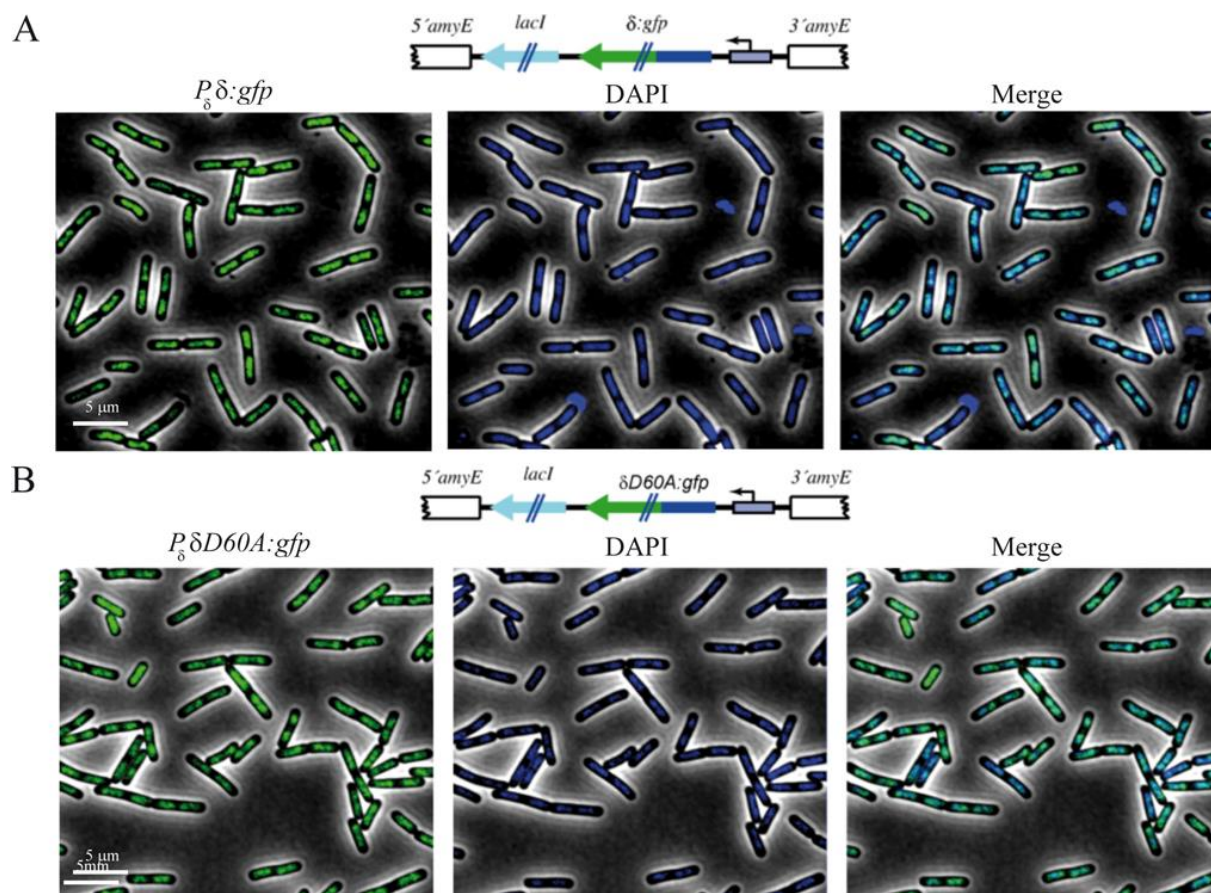
**Figure 34. Subcellular localization of  $\delta$ :CFP<sub>2</sub> and  $\omega$ :YFP<sub>2</sub>.**

The relative distributions of cells bearing–plasmid borne  $P_\omega \omega:yfp$  and  $P_\delta \delta:cfp$  genes were grown in MMS7 at 30 °C. Images of cells with fluorescence from  $\delta$ :CFP<sub>2</sub> (in red) and  $\omega$ :YFP<sub>2</sub> (in yellow) are shown. Scale bar is 5  $\mu$ m.

### 1.2.6. The $\omega_2$ –*parS* complexes facilitate $\delta_2$ redistribution over the nucleoid.

To determine the type of structures that  $\delta$ :GFP<sub>2</sub> or  $\delta$ D60A:GFP<sub>2</sub> could form inside the cells the concentrations of both fusion protein was artificially increased by expressing the  $\delta:gfp$  or

$\delta D60A:gfp$  gene, integrated as unique copy in the *amyE* locus, from an IPTG-inducible promoter. Upon IPTG addition, the  $\delta:GFP_2$  or  $\delta D60A:GFP_2$  expression, which was uncoupled from the  $\omega_2$  expression, increased. The number of  $\delta:GFP_2$  or  $\delta D60A:GFP_2$  molecules/cell, upon addition of 10  $\mu M$  IPTG, averaged  $\sim 6,500$  (see results, paragraph 1.2.1.), without any negative effect on plasmid stability (Pratto et al. 2008).

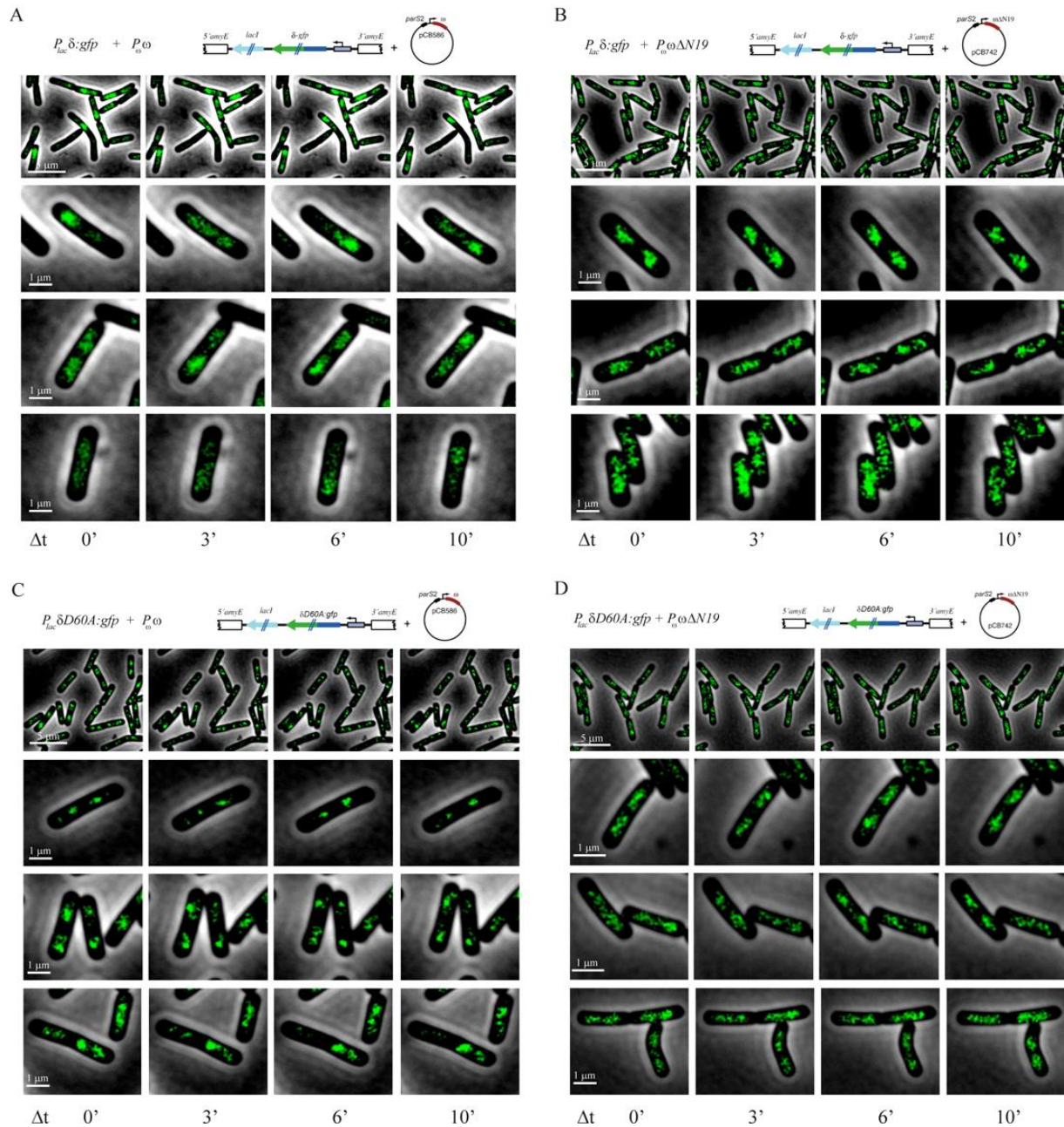


**Figure 35. Localization of induced  $\delta:GFP_2$  or  $\delta D60A:GFP_2$ .**

Illustration showing the structure of the  $P_{lac} \delta:gfp$  (A) or  $P_{lac} \delta D60A:GFP$  (B) expression cassettes integrated in the host-chromosome. Cells bearing-chromosomal borne  $P_{lac} \delta:gfp$  (BG947) or  $P_{lac} \delta D60A:gfp$  gene (BG1097) expressed from an IPTG-inducible promoter were grown in MMS7 at 30 °C. Images of cells with fluorescence from  $\delta:GFP_2$  or  $\delta D60A:GFP_2$ , images of the same cells stained with DAPI to show DNA and the merge of both images are shown. Scale bar is 5  $\mu m$ .

In the absence of  $\omega_2$ ,  $\delta:GFP_2$  or  $\delta D60A:GFP_2$  formed dynamic clouds of fluorescence distributed over the nucleoid, equally to what observed in the system II. Structures that resembled single or “double filament” in the presence or absence of nsDNA were rare  $< 3\%$  (Fig. 35A and 35B) (Ringgaard et al. 2009). The dynamics of  $\delta:GFP_2$  or  $\delta D60A:GFP_2$  fluorescence lead to discrete areas lacking fluorescence inside the nucleoid in both case (Fig. 35A and 35B). However, when  $\delta:GFP_2$  was replaced by  $\delta D60A:GFP_2$  the cloud of fluorescence was less

dynamic, suggesting that the small differences between both proteins could be addressed to the less ATP hydrolysis of  $\delta$ D60A:GFP<sub>2</sub> and its long living protein–DNA complex.



**Figure 36. Localization of induced  $\delta$ :GFP<sub>2</sub> or  $\delta$ D60A:GFP<sub>2</sub> in the presence of  $\omega_2$  or  $\omega_2\Delta N19$ .**

The  $P_{lac} \delta:gfp$  (A and B) or  $P_{lac} \delta D60A:gfp$  (C and D) gene integrated into the *B. subtilis* chromosome, and plasmid-borne  $P_{\omega}$  ( $pCB586$ ) or  $P_{\omega\Delta N19}$  gene ( $pCB742$ ). Images of cells with fluorescence from  $\delta$ :GFP<sub>2</sub> or  $\delta$ D60A:GFP<sub>2</sub> of the same cells are shown for a viable time. Scale bar is 5  $\mu$ m.

In the presence of physiological  $\omega_2$  and increased  $\delta$ :GFP<sub>2</sub> concentrations, time-lapse microscopy revealed that the  $\delta$ :GFP<sub>2</sub> formation of DNA-independent threads were rare, <1% ( $n= 200$ ) (Fig. 36A and 36B).

The  $\delta$ :GFP<sub>2</sub> fluorescence was apparently more dynamic than when both proteins were present at physiological levels (see Fig. 33A vs. 36A). A decrease in the level of  $\delta$ :GFP<sub>2</sub> fluorescence at a given location was taken as an indirect measure of  $\delta$ :GFP<sub>2</sub> disassembly from the nucleoid, rather than no assembly because in the absence of  $\omega_2$  the fluorescence was regularly distributed over the nucleoid. It is likely that the interaction of  $\delta$ :GFP<sub>2</sub>–bound to the nucleoid with the  $\omega_2$ –*parS* complex stimulate the  $\delta$ :GFP<sub>2</sub> ATPase and facilitate  $\delta$ :GFP<sub>2</sub> disassembly from the nucleoid (Fig. 36A).

To gain insight in the fate of the fluorescence individual cells were analysed. As revealed in Figure 35A, the 5–fold excess of  $\delta$ :GFP<sub>2</sub> fully distributed over nucleoid but in the presence of physiological  $\omega_2$  concentrations, the nucleoid lost fluorescence and then recovered it in a time dependent fashion, although the extent of the  $\delta$ :GFP<sub>2</sub> cloud was variable (Fig. 36A), suggesting that  $\delta$ :GFP<sub>2</sub>–ADP free in solution is rejuvenated to  $\delta$ :GFP<sub>2</sub> with subsequent reassembly on new regions of the nucleoid, because discrete foci in the cytosol were not detected. As expected  $\omega_2\Delta N19$  failed to facilitate the dynamic  $\delta$ :GFP<sub>2</sub> assembly–disassembly (Fig. 36B). In the presence of  $\omega_2$ ,  $\delta D60A$ :GFP<sub>2</sub>–mediated clouding was less dynamic with the formation of discrete foci or patched regions on the same nucleoid (Fig. 36C). This pattern was comparable to the one observed in Figure 33B. To explain the discrete fluorescent foci observed it was assumed that  $\omega_2$ –*parS* upon interaction  $\delta D60$ :GFP<sub>2</sub> failed to promote efficiently BC1 disassembly. When  $\omega_2$  was replaced by  $\omega_2\Delta N19$  the disassembly and subsequent reassembly of  $\delta$ :GFP<sub>2</sub> or  $\delta D60$ :GFP<sub>2</sub> was less dynamic. Interesting, the  $\delta D60$ :GFP<sub>2</sub> were forming a cloud of fluorescence on the nucleoid (Fig. 36D), indicating that the foci or patched regions were induced by the presence of  $\omega_2$ .



## 2. Chapter II: Protein $\omega_2$ regulates plasmid copy number, faithful partition and the toxin–antitoxin system.

### 2.1. Molecular characterization of $\omega_2$ transcriptional regulation.

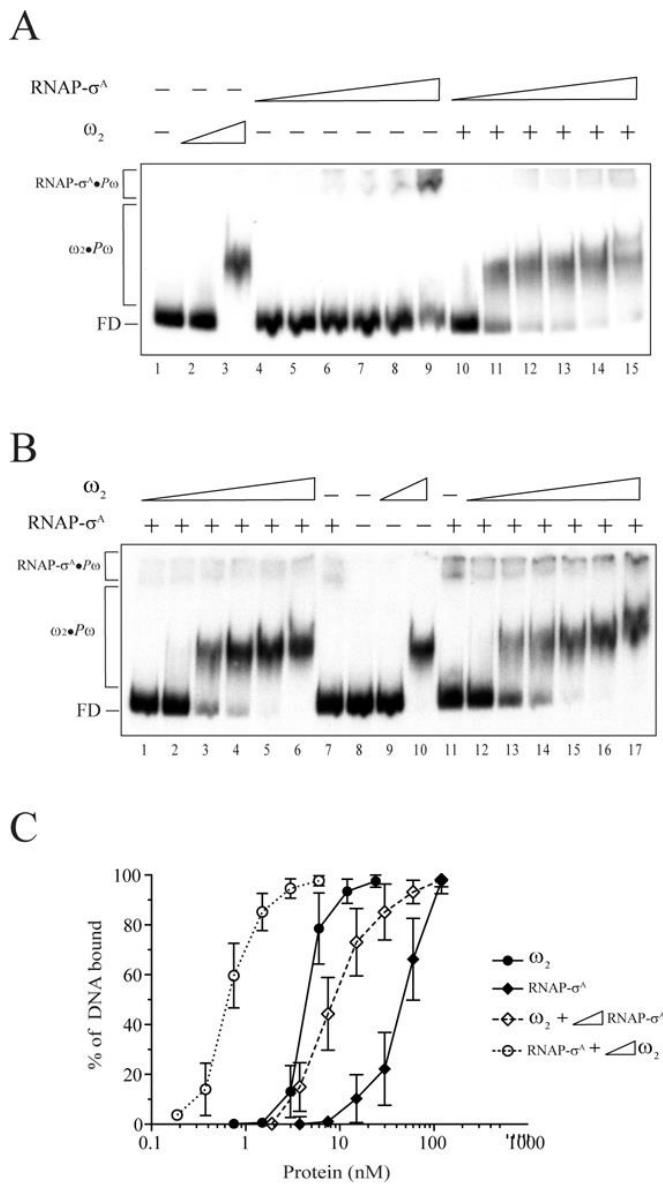
In *B. subtilis*, the ratio between a pSM19035 variant and the *oriC* (origin of chromosomal replication) is approximately 2:1, suggesting two plasmid copies per cell. The smallest possible increase of plasmid copy number, from 2 to 4, corresponds to a dramatic 100% change in concentration during cell proliferation. Thus, the feedback control of low copy plasmids is notoriously difficult, and easily leads to random oscillations. Furthermore, slight variations in the feedback control scheme result in markedly different efficiencies of noise suppression. The  $\omega_2$  transcriptional repressor and its cognate sites upstream the promoter regions of the *cop* ( $P_{copS}$ ),  $\delta$  ( $P_\delta$ ) and  $\omega$  ( $P_\omega$ ) genes. These promoter regions termed until now *parS1 to parS3* and *parS1' to parS3'* sites, because they laid between the  $-21$  to  $-83$  (being  $+1$  the transcription start site) (Fig. 1). Protein  $\omega_2$  provides a sophisticated degree of interplay and a regulated co–ordination of plasmid copy number fluctuation and stable inheritance (Fig. 3 and Fig.4). The interplay between the expression of these genes products stabilizes the plasmid faithful segregation by  $\sim 10$ –fold (de la Hoz et al. 2000), and contribute to minimize the metabolic burden that the plasmid might impose on the host cell.

#### 2.1.1. RNAP– $\sigma^A$ facilitates $\omega_2$ – $P_\omega$ DNA interaction.

As previously described  $\omega_2$  binds with high affinity and co–operativity to its cognate site embedded in the promoter region of the  $\omega$  gene ( $P_\omega$ ) and with an apparent binding constant ( $K_{Dapp}$ ) of  $\sim 6$  nM (results, paragraph 1.1.1). The  $\omega_2$  and RNAP– $\sigma^A$  binding sites overlap in the  $P_\omega$ ,  $P_\delta$  and  $P_{copS}$ . As revealed in (Fig. 1 and 4A),  $P_\omega$  DNA contains a series of seven 7–bp repeats at position  $-21$  to  $-69$  (relative to the start site,  $+1$ ). The RNAP– $\sigma^A$  binding region is at position  $-47$  to  $+18$ . According these data, we can infer that the region ranging  $-69$  and  $-21$  should be strictly involved in the promoter regulation, this region included the  $-35$  specific sequence that is recognize by the  $\sigma^A$  transcription factor.

To discover the mechanism of  $\omega_2$ –mediated regulation of  $P_\omega$  utilization, we first investigated whether  $\omega_2$  influences the RNAP– $\sigma^A$  recruitment to the promoter region. The interaction of  $\omega_2$  and RNAP– $\sigma^A$  with the  $P_\omega$  DNA was assayed by EMSA. Protein  $\omega_2$  bound with high affinity and co–operativity to  $P_\omega$  DNA ( $K_{Dapp}$  of  $6 \pm 1$  nM) (Fig. 37A, lanes 2–3 and 37C, lanes 9–10). No apparent binding was observed in the presence of limiting  $\omega_2$  concentrations (e.g., 0.75 nM)

(Fig. 37A, lane 2). RNAP- $\sigma^A$  specifically bound  $P_\omega$  DNA with a  $K_{Dapp}$  of  $29 \pm 9$  nM (Fig. 37A, lanes 2–9, Fig.37C). We first investigated the influence of RNAP- $\sigma^A$  in the recruitment of  $\omega_2$  to the promoter region at 0.75 nM of  $\omega_2$  (8-fold below  $K_{Dapp}$ ) and increasing RNAP- $\sigma^A$  concentrations (1.9 to 60 nM). Both elements were incubated together with  $P_\omega$  DNA (Fig. 37A, lanes 11–15). As observed, the presence of limiting RNAP- $\sigma^A$  concentrations (3.7 nM) increased the formation of  $\omega_2$ - $P_\omega$  DNA complexes at least 4-fold, actually more than 75% of the  $P_\omega$  DNA was forming a  $\omega_2$ - $P_\omega$  DNA complex (Fig. 37A, lane 11) suggesting that  $\omega_2$  might interact with RNAP- $\sigma^A$  prior to binding to  $P_\omega$  DNA, and by an allosteric transition the  $\omega_2$ -RNAP- $\sigma^A$  complex shows increase binding affinity of  $\omega_2$  for  $P_\omega$  DNA.



**Figure 37. Cooperative binding of  $\omega_2$  and RNAP- $\sigma^A$  to  $P_\omega$  DNA.**

(A) The 423-bp [ $\alpha^{32}P$ ]-HindIII-KpnI  $P_\omega$  DNA (0.2 nM) was incubated with increasing  $\omega_2$  (0.75 and 6 nM, lanes 2–3), RNAP- $\sigma^A$  (1.9 to 60 nM, lanes 4–9), or a fix concentration of  $\omega_2$  (0.75 nM, lanes 10–15) and increasing concentrations of RNAP- $\sigma^A$  (1.9, 3.7, 15, 30 and 60 nM, lanes 10–15) in buffer A for 15 min at 37°C. (B) The  $P_\omega$  DNA (0.2 nM) was incubated with increasing  $\omega_2$  (0.75 and 6 nM, lanes 9 and 10) or a fix concentration of RNAP- $\sigma^A$  (7.5 nM, lanes 1–7 or 15 nM, lanes 11–17) and increasing  $\omega_2$  concentrations (0.19, 0.37, 0.75, 1.5, 3 and 6 nM, lanes 1–6 and 12–17) in buffer A for 15 min at 37°C. (C) The binding to  $P_\omega$  DNA of  $\omega_2$  (filled circles) or the RNAP- $\sigma^A$  (filled rhombus) and the combination of the two proteins, a fix amount of  $\omega_2$  (0.75 nM) and increasing RNAP- $\sigma^A$  concentrations (empty rhombus) or a fix RNAP- $\sigma^A$  (15 nM) and increasing  $\omega_2$  concentrations (empty circles) are represented in the plot with their relative protein concentration on the x-axis. The signals present in the protein-DNA complex and in the free DNA (FD) were determined by densitometry. Values are the average of more of three independent experiments.

Since the effect of cooperative binding of  $\omega_2$  may not be distinguished from  $\omega_2$ -RNAP- $\sigma^A$  interaction before binding to  $P_\omega$  DNA, and to further disclose whether  $\omega_2$  increased RNAP- $\sigma^A$



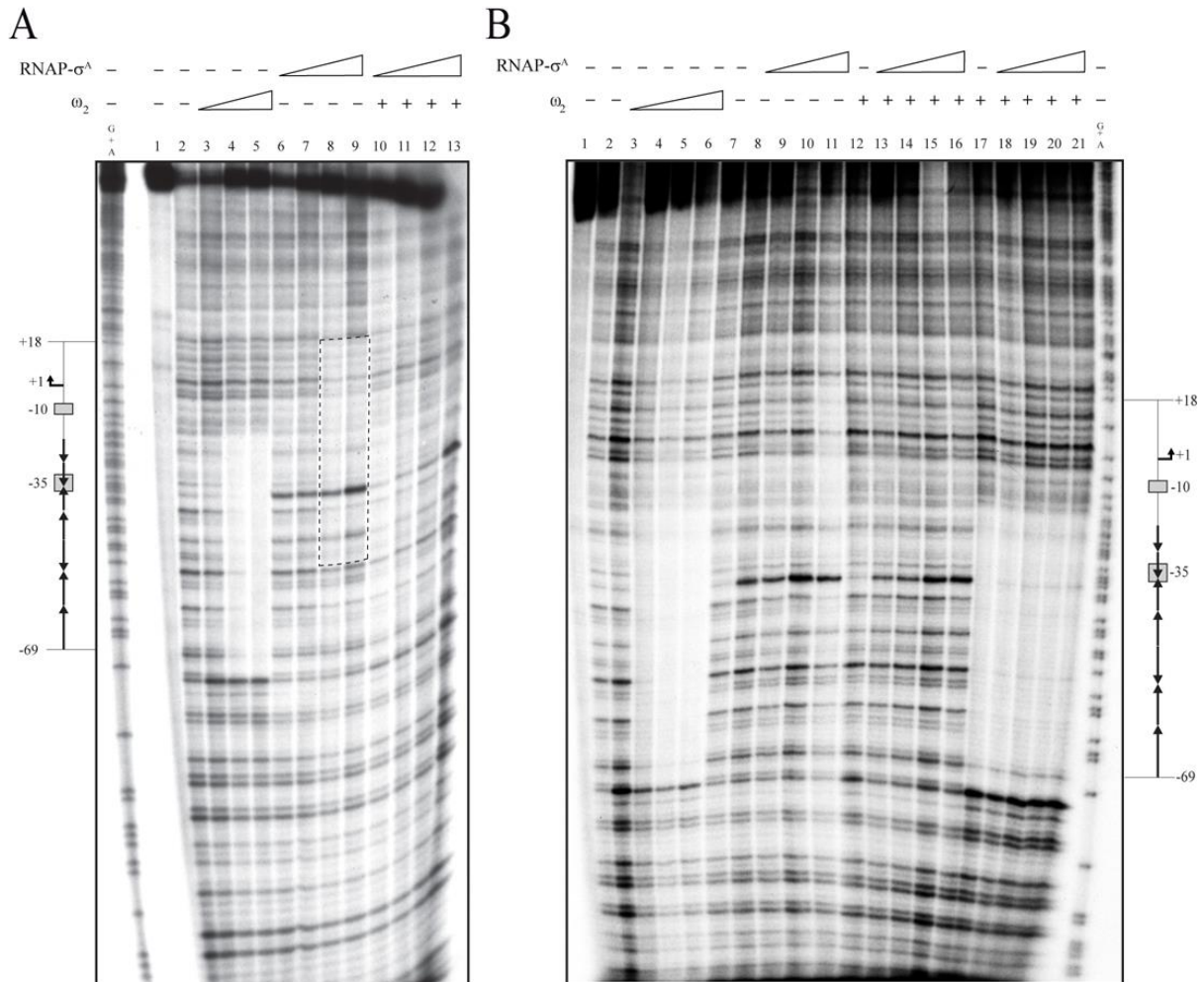
binding to  $P_{\omega}$  DNA, a constant amount of limiting RNAP- $\sigma^A$  (7.5 or 15 nM) and increasing  $\omega_2$  concentrations were incubated with  $P_{\omega}$  DNA, and EMSA studies were performed. The addition of limiting RNAP- $\sigma^A$  (7.5 nM, 4-fold below  $K_{Dapp}$ ) concentrations increased  $\omega_2$ - $P_{\omega}$  DNA complexes formation by at least 6-fold, with a new  $K_{Dapp}$  of  $0.9 \pm 0.2$  nM (Fig. 37B, lanes 2–6) confirming a cooperative binding mechanism, so that the addition of a 15 nM of RNAP- $\sigma^A$  increased  $\omega_2$ - $P_{\omega}$  DNA complexes formation by at least 10-fold, with a  $K_{Dapp}$  of  $0.4 \pm 0.2$  nM (Fig. 37B, lanes 12–17 and chart in Fig. 37C). The addition of  $\omega_2$  also increased RNAP- $\sigma^A$ - $P_{\omega}$  DNA complexes formation by at least 3-fold, with a  $K_{Dapp}$  of  $9.5 \pm 3.4$  nM (Fig. 37B, lanes 12–17, and Fig. 37C). These results are not compatible with a steric hindrance hypothesis of  $\omega_2$ -mediated transcriptional repression of  $P_{\omega}$  utilization. The experiments suggested that the  $\omega_2$  and RNAP- $\sigma^A$  interact leading to stable  $\omega_2$ - $P_{\omega}$  DNA complexes, but we cannot be sure that both proteins co-exist on the same the  $P_{\omega}$  region. If we consider the molar ratio at equilibrium condition were  $\sim 4$   $\omega_2$  and  $\sim 45$  RNAP- $\sigma^A$  molecules per  $P_{\omega}$  DNA segment, it seems that there are not sufficient  $\omega_2$  to occupy all the heptads presented in the total  $P_{\omega}$  DNA of the reaction.

### 2.1.2. RNAP- $\sigma^A$ and $\omega_2$ can co-exist at $P_{\omega}$ DNA region.

To test whether  $\omega_2$  and RNAP- $\sigma^A$  co-exist in the same DNA segment limiting  $\omega_2$  (4-fold lower than  $K_{Dapp}$ ) and sub-stoichiometric or stoichiometry RNAP- $\sigma^A$  concentrations were incubated with  $P_{\omega}$  DNA and the complex incubated with DNase I. As previously shown that  $\omega_2$  bound onto its operator site protected a contiguous region from DNase I attack (see results, paragraph 1.1.6.). As expected,  $\omega_2$  bound onto its operator site protected a contiguous region (–22 to –75 referred to the +1 initiation site) from DNase I attack (Fig. 38A, lanes 4–5), and RNAP- $\sigma^A$  made an extensive contact with the upstream region (positions +18 to –47) with a clear hypersensitive site at position –37 (Fig. 38A, lanes 6–9) when the reaction was performed in buffer A with 1 mM ATP.

When a constant amount of  $\omega_2$  and RNAP- $\sigma^A$  were incubated with  $P_{\omega}$  DNA a weak protection site from DNase I attack, extended from position –65 to –6, was observed (Fig. 38A, lanes 10–11). When the RNAP- $\sigma^A$ : $\omega_2$  ratios increased the specific hypersensitive site RNAP- $\sigma^A$  reappeared (Fig. 38A, lanes 13) suggesting that  $\omega_2$  shows a partial occupancy. At stoichiometric concentrations  $\omega_2$  does not occlude the binding of RNAP- $\sigma^A$ . leading to RNAP- $\sigma^A$  close complex (PR<sub>C</sub>). Since,  $\omega_2$  binds with slightly higher affinity and co-operativity to two contiguous heptads in the  $\rightarrow\leftarrow$  than in the  $\rightarrow\rightarrow$  orientation (de la Hoz et al. 2004, Weihofen et

al. 2006), we favour the hypothesis that the  $\rightarrow\leftarrow$ -heptads, which overlaps with the  $-35$  element and its neighbours, will be bound by  $\omega_2$  and the  $\omega_2 \cdot \text{RNAP}-\sigma^A$  interaction might occur at the pre-recruitment state.



**Figure 38. Protein  $\omega_2$  modulate RNAP- $\sigma^A$  to  $P_\omega$  DNA.**

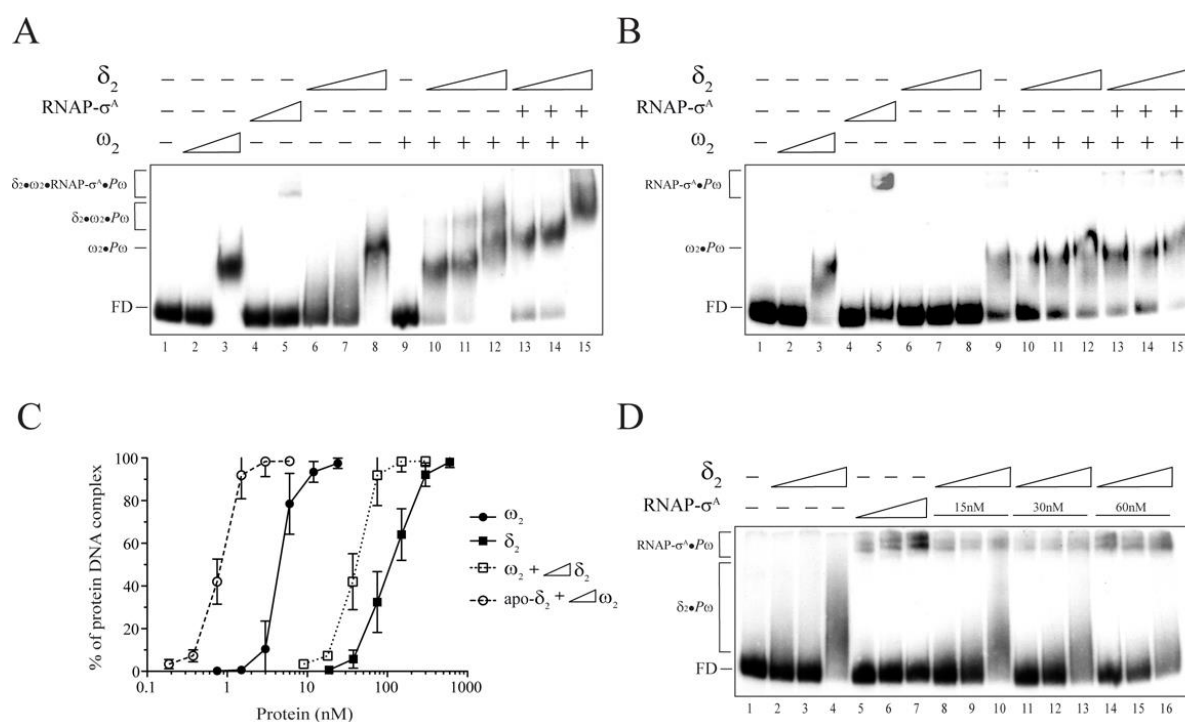
(A) [ $\alpha^{32}\text{P}$ ]- $P_\omega$  (1 nM) was incubated in buffer A supplemented with 1mM ATP with increasing  $\omega_2$  (7.5, 15 and 30 nM) or RNAP- $\sigma^A$  (3.7, 7.5, 15 and 30 nM) or a fix amount of  $\omega_2$  (7.5 nM) and then increasing RNAP- $\sigma^A$  concentrations (3.7, 7.5, 15 and 30 nM). After DNase I treatment the complexes analysed by dPAGE. Schematic representation of the operator site-promoter  $P_\omega$  region; the +1 site is denoted. The broken line (lanes 8–10) highlighted the extended footprint of RNAP- $\sigma^A$ . (B) The [ $\alpha^{32}\text{P}$ ]- $P_\omega$  (1 nM) was incubated with increasing  $\omega_2$  (7.5, 15, 30 and 60 nM, lanes 3–6) or RNAP- $\sigma^A$  (3.7, 7.5, 15 and 30 nM, lanes 8–11) or a fix amount of  $\omega_2$  (7.5 nM, lanes 12–16; 60nM lanes 17–21) and then increasing RNAP- $\sigma^A$  concentrations (3.7, 7.5, 15 and 30 nM, lanes 13–16 and 18–21). Schematic representation of the operator site-promoter  $P_\omega$  region; the +1 site is denoted. The broken line (lanes 6–9) highlighted the extended footprint of RNAP- $\sigma^A$

In the presence of saturating  $\omega_2$  concentrations only protection of a contiguous region from DNase I attack typical of the protein alone was observed (Fig. 38B, lanes 18–21), suggesting that  $\omega_2$  can displace RNAP- $\sigma^A$  from  $P_\omega$  DNA. The latter seems to be the mechanism by which  $\omega_2$  repress the transcription. The same general conclusions can be extended to the other  $\omega_2$

cognate sites (see Fig. 5) in the presence of saturating concentrations of both proteins (see de la Hoz et al. 2000)

### 2.1.3. RNAP- $\sigma^A$ does not affect cooperative DNA binding of $\delta_2$ and $\omega_2$ .

We have shown that  $\omega_2$  has two activities: it repress transcription upon binding to  $P_\omega$  DNA, and, in concert with the  $\delta_2$  motor that decreases the off rate of the  $\omega_2$ - $P_\omega$  complexes (see Fig. 15 and 16), leads to plasmid pairing and faithful segregation (see results, paragraph 1.1.). It is likely that the presence of  $\delta_2$  might contribute to  $P_\omega$  utilization.



**Figure 39. Cooperative binding of  $\omega_2$  and RNAP- $\sigma^A$  to  $P_\omega$  DNA.**

The 423-bp [ $\alpha^{32}\text{P}$ ]-*HindIII-KpnI*  $P_\omega$  DNA (0.2 nM) was incubated in buffer A containing 1 mM ATP (A) or lacking it (B) for 15 min at 37° C. The reaction were performed with increasing  $\omega_2$  (0.75 and 6 nM), RNAP- $\sigma^A$  (7.5 and 30 nM),  $\delta_2$  (37, 75 and 150 nM), a fix concentration of  $\omega_2$  (0.75 nM) and increasing concentrations of  $\delta_2$  (37, 75 and 150 nM) or a fix concentration of  $\omega_2$  (0.75 nM) and RNAP- $\sigma^A$  (7.5 nM) and increasing concentrations of  $\delta_2$  (37, 75 and 150 nM) (C) The binding to  $P_\omega$  DNA of  $\omega_2$  (filled circles) or  $\delta_2$  (filled square) and the combination of two proteins, a fix amount of  $\omega_2$  (0.75 nM) and increasing  $\delta_2$  concentrations (empty square) or a fix  $\delta_2$  (37 nM) and increasing  $\omega_2$  concentrations (empty rhombus) are represented in the plot with their relative protein concentration on the x-axis. The signals present in the protein-DNA complex and in the free DNA (FD) were determined by densitometry. Values are the average of more of three independent experiments. (D) Binding of  $\delta_2$  and RNAP- $\sigma^A$  to  $P_\omega$  DNA. The 423-bp [ $\alpha^{32}\text{P}$ ]-*HindIII-KpnI*  $P_\omega$  DNA (0.2 nM) was incubated with increasing  $\delta_2$  (37, 75 and 150 nM), RNAP- $\sigma^A$  (7.5, 15 and 30 nM), or a fix concentration of RNAP- $\sigma^A$  (15, 30 or 60 nM) and increasing  $\delta_2$  concentrations (37, 75, 150, 3 nM) in buffer A containing 1 mM ATP for 15 min at 37° C.

To test whether the interaction between  $\delta_2$  and  $\omega_2$  affect the interaction of the latter with RNAP- $\sigma^A$  EMSA experiments were performed in the presence (Fig. 39A) and the absence (Fig. 39B) of ATP. As previously reported,  $\omega_2$ , RNAP- $\sigma^A$  and  $\delta_2$  bound  $P_\omega$  DNA with  $K_{\text{Dapp}} \sim 6$ ,  $\sim 30$

and >2000 nM, respectively, in the absence of a nucleotide cofactor, but in the presence of ATP,  $\delta_2$  binds DNA with a  $K_{Dapp} \sim 150$  nM and it increased  $\omega_2$  binding to  $P_\omega$  DNA at least 6-fold. On the other side,  $\omega_2$  increased  $\delta_2$  binding to  $P_\omega$  DNA by 3-fold (Fig. 39A, lanes 10–12) leading to PC, SC and BC complex formation (see results, paragraph 1.1.1.; Fig. 39B and 39C).

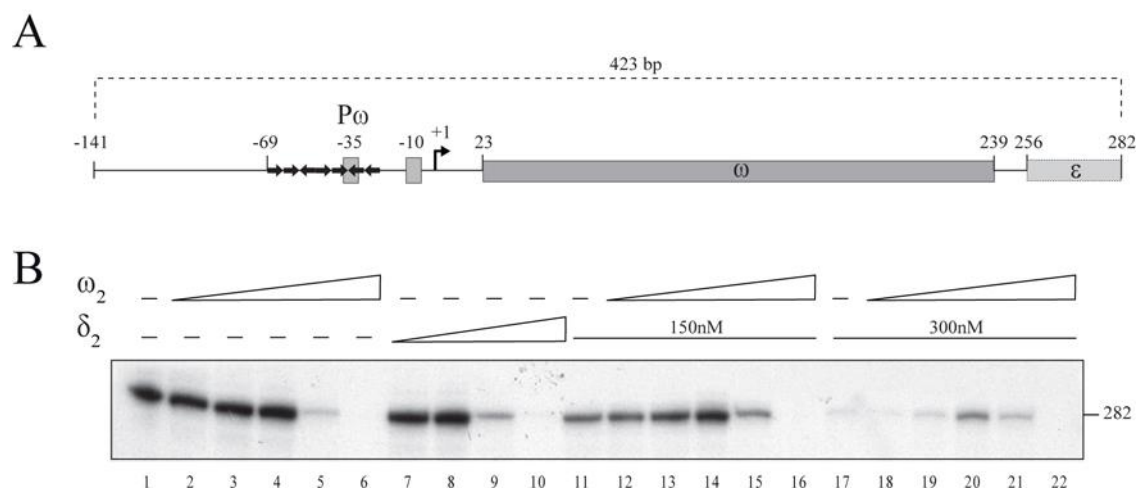
To test whether the interaction of  $\omega_2$  with  $\delta_2$  or RNAP- $\sigma^A$  are mutually exclusive, a constant and limiting amount of  $\omega_2$  (0.75 nM) and RNAP- $\sigma^A$  (7.5 nM) were incubated with increasing  $\delta_2$  concentrations (Fig. 39A, lanes 13–15). Addition of limiting RNAP- $\sigma^A$  concentrations revealed the formation of a quaternary complex that showed a slower mobility than the ternary  $\delta_2$ - $\omega_2$ - $P_\omega$  DNA complexes (Fig. 39A, lane 15). As previously reported, in absence of ATP,  $\delta_2$ -apo interacts with very low affinity to nsDNA (Fig. 39B, lanes 6–8), but markedly stimulated,  $\omega_2$ - $P_\omega$  DNA complex formation (Fig. 39B, lanes 10–12 and Figure 39C). Interestingly, when limiting RNAP- $\sigma^A$  concentration (7.5 nM) were added to the reaction mixture, the quaternary complex was not observed, suggesting that  $\delta_2$  contribute to the appearance of slow mobility complexes (Fig. 39A, lanes 13–15 vs. 39B, lanes 13–15).

To confirm whether  $\delta_2$  affects the interaction of RNAP- $\sigma^A$  with  $P_\omega$  DNA, sub-stoichiometric to stoichiometric amounts of RNAP- $\sigma^A$  and increasing  $\delta_2$  concentrations were incubated with  $P_\omega$  DNA and the complex formed analysed by EMSA (Fig. 39D). Protein  $\delta_2$  neither increased the affinity of RNAP- $\sigma^A$  for  $P_\omega$  DNA nor RNAP- $\sigma^A$  increased the affinity of  $\delta_2$  for  $P_\omega$  DNA (Fig. 39D, lanes 8–16). Our results suggested that the  $\delta_2$  binding to  $P_\omega$  DNA exclude the RNAP- $\sigma^A$  binding to the same substrate and *vice versa*.

#### 2.1.4. Protein $\omega_2$ affects $P_\omega$ utilization.

To gain insight of the mechanism by which  $\omega_2$  regulates promoter utilization, we performed transcription run-off experiments by RNAP- $\sigma^A$  (20 nM) in the absence or the presence of increasing  $\omega_2$  and  $\delta_2$  concentrations. The run-off transcripts were produced *in vitro* by RNAP- $\sigma^A$  in the presence of the four nucleotides (one radiolabelled) using a linear DNA substrate containing  $P_\omega$  DNA (2 nM) (Fig. 40A). RNAP- $\sigma^A$  “run” to the end of the fragment made a labelled mRNA of a discrete length that was monitored and quantified (Fig. 41B). An mRNA species of 282-nt in length was detected for  $P_\omega$  DNA (Fig. 40B, lane 1). Addition of 15  $\omega_2$  molecules per DNA molecule strongly inhibited  $P_\omega$ , and 30  $\omega_2$  / DNA blocked mRNA synthesis from  $P_\omega$  DNA (Fig. 40B, lanes 5 and 6). Concentrations of  $\omega_2$  equal to or higher than those required to repress  $P_\omega$  utilization did not affect the expression of an unrelated promoter ( $P_{cro}$  of

phage A2, data not shown) excluding that a contaminant RNase or any other nonspecific effect could be responsible for the lack of RNA synthesis at saturating  $\omega_2$  concentrations. Quantification of the transcripts in the presence of limiting  $\omega_2$  concentrations (3.5 to 7.5 nM) (Fig. 40B, lanes 2–4) suggested that  $\omega_2$  might increase mRNA synthesis from  $P_\omega$  at least 2–fold.



**Figure 40. RNAP- $\sigma^A$  transcription run-off experiments.**

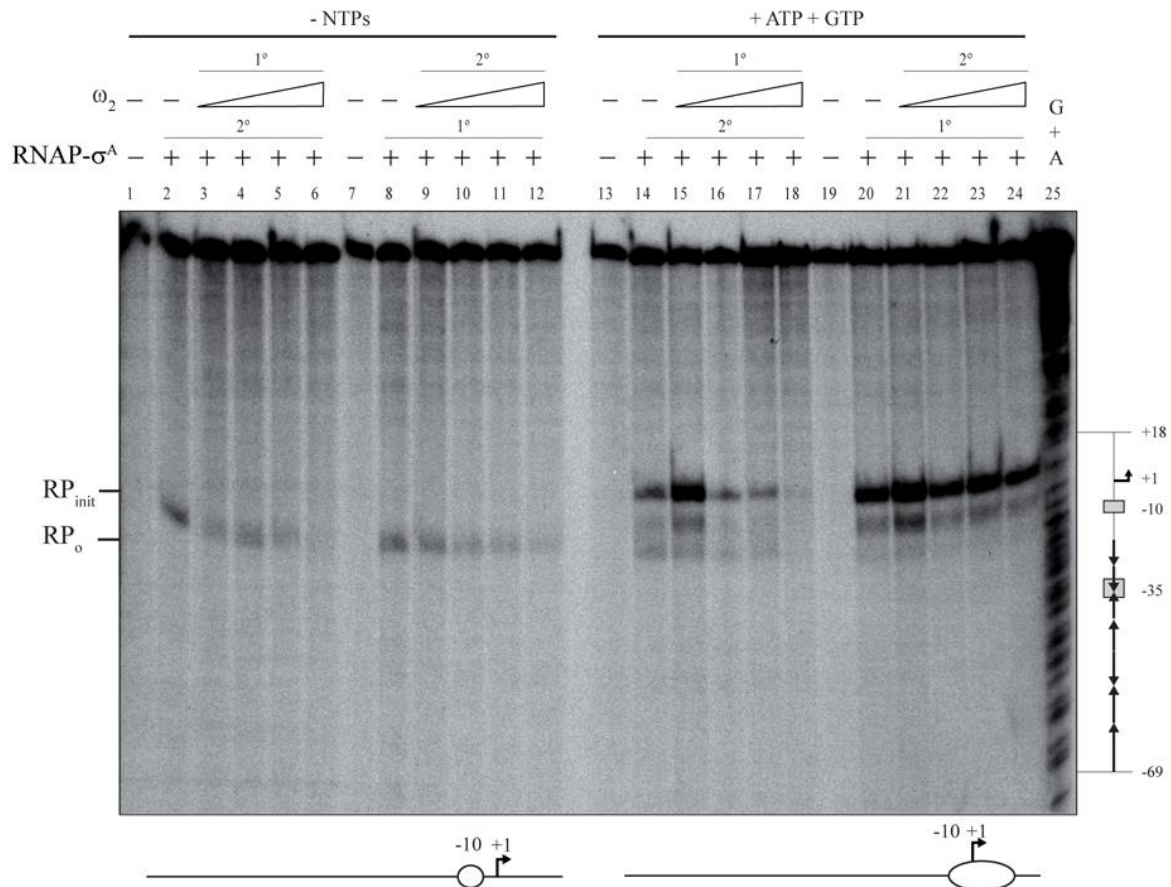
(A) The 423-bp *HindIII-KpnI P $\omega$*  DNA is schematically represented. The heptads are represented by arrows and their relative orientations ( $\rightarrow$  or  $\leftarrow$ ) are shown. The -35, -10 elements (boxed), the transcription start sites (filled bend arrow), the  $\omega$  and part of the  $\epsilon$  gene are indicated. (B), The 423-bp [ $\alpha^{32}P$ ]-*HindIII-KpnI P $\omega$*  DNA (2 nM) was incubated with RNAP- $\sigma^A$  (20 nM) in the absence or presence of increasing concentrations of  $\omega_2$  (3.7, 7.5, 15, 30 and 60 nM) or in the presence of a fix  $\delta_2$  (150 or 300 nM) concentration, and increasing concentrations of  $\omega_2$  subjected to *in vitro* transcription.

To test whether the binding of  $\delta_2$  to nsDNA or the interaction of  $\omega_2$  with  $\delta_2$  affected  $P_\omega$  utilization, transcription run-off experiments were performed in presence of increasing  $\delta_2$  concentrations. Interesting, sub-saturating and stoichiometric  $\delta_2$  concentrations inhibited and blocked  $P_\omega$  utilization, respectively (Fig. 40B, lanes 9 and 10). It is likely that  $\delta_2$  could form bed structures that halt RNAP- $\sigma^A$  progression. However, in the presence of a fix amount of  $\delta_2$  (150 or 300 nM) and increasing  $\omega_2$ , the addition of 7.5  $\omega_2$  molecules per DNA molecule significantly stimulated  $P_\omega$  utilization (Fig. 40B, lanes 13–14 and 20), to be further inhibited when higher  $\omega_2$  concentrations were reached (Fig. 40B, lanes 15–16 and 21–22).

### 2.1.5. Protein $\omega_2$ inhibits RNAP- $\sigma^A$ transition from close to open complex.

In the previous section we have shown that  $\omega_2$  stimulates RNAP- $\sigma^A$  close complex (RPC) formation. To uncover the mechanism of  $\omega_2$ -mediated repression of  $P_\omega$  we investigated open complex (RPO) formation and abortive initiation (RP<sub>INIT</sub>) assays under variable  $\omega_2$  concentrations by KMnO<sub>4</sub> footprinting in the absence or presence of GTP and ATP. The addition of these two NTPs promoted abortive mRNA products through the synthesis of short

oligonucleotides. From  $P_{\omega}$  mRNA molecules 9-nt in length containing only A and G residues by RNAP- $\sigma^A$  were observed. It is believed that the  $\sigma^A$  factor is released under this conditions.

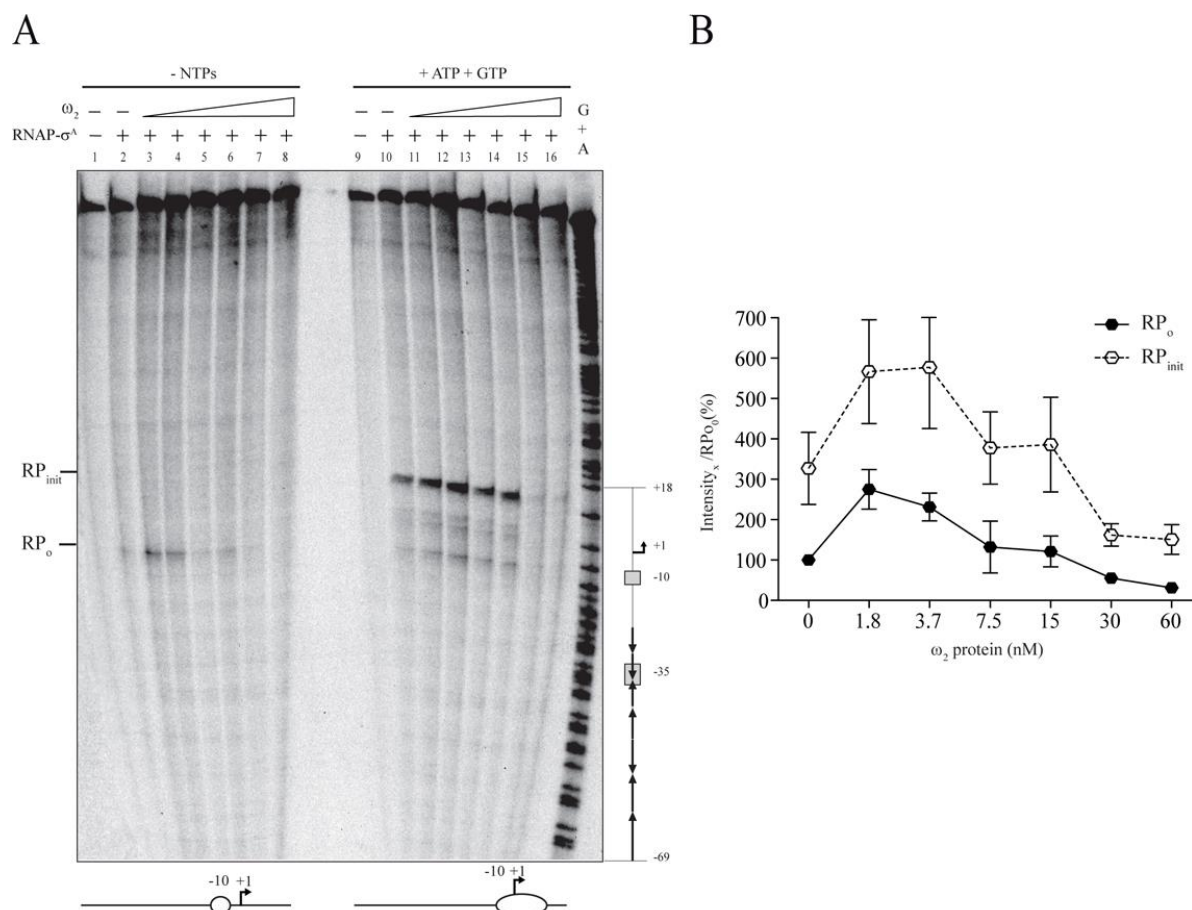


**Figure 41. Effect of  $\omega_2$  on the formation of a RNAP- $\sigma^A$ -promoter  $RP_0/RP_{INIT}$  at  $P_{\omega}$ .**

The 423-bp HindIII-KpnI  $P_{\omega}$  DNA (1 nM) was incubated with RNAP- $\sigma^A$  (7.5 nM) in the absence or presence of increasing concentrations of  $\omega_2$  (3.7, 7.5, 15, 30 and 60 nM) and/or the initiating nucleotides (0.1 mM of GTP and ATP) and DNA melting (open complex) was probed by  $KMnO_4$  footprinting. The positions hypersensitive to  $KMnO_4$  are marked ( $RP_0$  and  $RP_{INIT}$ ) and depicted at the bottom; the coordinates are indicated relative to the transcription start point. Chemical sequencing reactions for purines (G + A) are shown, the relevant regions of  $P_{\omega}$  depicted.

In the absence of nucleotide precursors, the analysis of the preferential  $KMnO_4$  attack to non-base-paired thymine and their position on  $P_{\omega}$  DNA revealed that RNAP- $\sigma^A$  (7.5 nM) promoted spontaneous DNA opening centred at position -10 (-11T, -10T) on the template strand or the formation of a  $RP_0$  complex (Fig. 41, lanes 2 and 8). However, no oxidized thymines after 30 sec  $KMnO_4$  exposure, on the template strand, were detected in the absence of RNAP- $\sigma^A$  (Fig. 41, lanes 1 and 7). Then, the  $P_{\omega}$  DNA was first pre-incubated with variable  $\omega_2$  concentrations (Fig. 41, lanes 3-6) or a fix amount of RNAP- $\sigma^A$  (7.5 nM) (Fig. 41, lanes 9-12) for 5 min, and then  $\omega_2$  was added. When 3.7 to 15 nM of  $\omega_2$  were added prior 7.5 nM of RNAP- $\sigma^A$  in absence of NTPs, the amount of  $KMnO_4$  promoted cleavage product slightly decreased under sub-saturating  $\omega_2$  concentration (Fig. 41, lanes 3-4). In the presence of stoichiometric or saturating

$\omega_2$  concentrations the cleavage products were not detected indicating that such concentrations of  $\omega_2$  inhibited  $RP_O$  formation (Fig. 41, lanes 5–6). When  $\omega_2$  was added to the pre-formed  $RP_O$ ,  $KMnO_4$ -mediated cleavage was only decreased indicating that  $\omega_2$  regulation at  $P_\omega$  DNA occurs before  $RP_{INIT}$  complex formation (Fig. 41, lanes 9–12).



**Figure 42. The regulatory effect of  $\omega_2$  on  $RNAP-\sigma^A$ -promoter  $RP_O$  at  $P_\omega$ .**

(A) The 423-bp *HindIII-KpnI*  $P_\omega$  DNA (1 nM) was incubated with increasing concentrations of  $\omega_2$  (1.8, 3.7, 7.5, 15, 30 and 60 nM) and then with a fix amount of  $RNAP-\sigma^A$  (3.7 nM) in the absence (lanes 1–8) or presence (lanes 9–16) of the initiating nucleotides (0.1mM of GTP and ATP) and DNA melting (open complex) was probed by  $KMnO_4$  footprinting. The positions hypersensitive to  $KMnO_4$  are marked ( $RP_O$  and  $RP_{INIT}$ ) and depicted at the bottom; the coordinates are indicated relative to the transcription start point. Chemical sequencing reactions for purines (G +A) are shown, the relevant regions of  $P_\omega$  depicted. (B), The signals present in the hypersensitive sites  $RP_O$  (filled circles) and  $RP_{INIT}$  (empty circles) produced according increasing concentrations of  $\omega_2$  and fix amount of  $RNAP-\sigma^A$  (3.7 nM) were determined by densitometry and their relative intensity plotted.

In the presence of nucleotide precursors (ATP and GTP),  $RNAP-\sigma^A$  (7.5 nM) promoted abortive initiation ( $RP_{INIT}$ ), and the  $KMnO_4$  attack revealed the formation of an extended single-stranded bubble, with cleavage at position  $-10T$ ,  $-6T$ ,  $-5T$  and  $+7T$  (Fig. 41, lanes 14 and 22). When  $\omega_2$  and  $RNAP-\sigma^A$  were omitted no cleavage was observed (Fig. 41, lanes 13 and 19). Pre-incubation of  $P_\omega$  DNA with sub-saturating  $\omega_2$  concentrations resulted in a increase in cleavage, and at saturating  $\omega_2$  concentrations led to a strong decrease in  $KMnO_4$  cleavage after  $RNAP-\sigma^A$  addition (Fig. 41, lanes 15–18; Fig. 43A, lanes 11–16). When  $RP_O$  was performed, by incubation

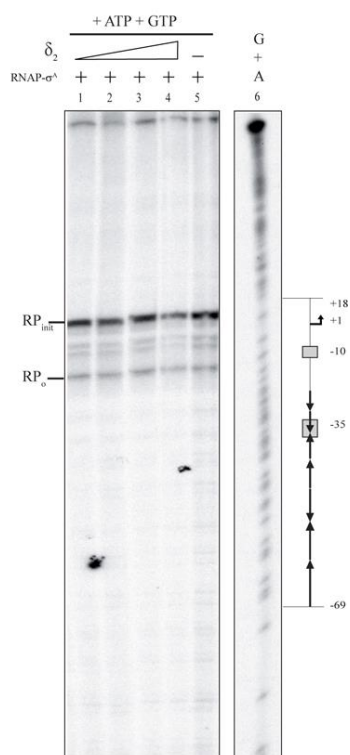
of  $P_{\omega}$  DNA with RNAP- $\sigma^A$ , the KMnO<sub>4</sub> cleavage pattern was moderately affected by addition of  $\omega_2$  (Fig. 41, lanes 21–24). These data showed that  $\omega_2$  at stoichiometric concentrations (1 to 2  $\omega_2$  /heptad) inhibits RP<sub>O</sub> formation, but also reaffirmed that limiting  $\omega_2$  concentrations facilitate RNAP- $\sigma^A$ · $P_{\omega}$  DNA complex formation as observed by *in vitro* transcription (Fig. 40B, lanes 2–4). Our results suggested that the  $\omega_2$  might act between the unstable RP<sub>I</sub> and the RP<sub>O</sub> steps because it had no apparent effect when added to pre-formed RP<sub>O</sub>.

In order to quantify the increase of RNAP- $\sigma^A$ - $P_{\omega}$  DNA complex formation promoted by limiting  $\omega_2$  concentration, the sensitivity of KMnO<sub>4</sub> footprinting was raised reducing the spontaneous RP<sub>O</sub> formation promoted by RNAP- $\sigma^A$ . When  $P_{\omega}$  DNA was pre-incubated with increasing  $\omega_2$  concentration and then limiting RNAP- $\sigma^A$  (3.7 nM) was added,  $\omega_2$  facilitated both RP<sub>O</sub> (Fig. 42A, lanes 3–4) or RP<sub>INIT</sub> (Fig. 42A, lanes 11–14) in absence or presence of nucleotide precursors, respectively. The RP<sub>O</sub> and RP<sub>INIT</sub> radiographed signals were quantified by densitometry and related to the signal produced by limiting RNAP- $\sigma^A$  (3.7 nM) (Fig. 42B). As revealed, the addition limiting  $\omega_2$  (3.7 nM) increased RP<sub>O</sub> and RP<sub>INIT</sub> complexes formation by at least 2-fold if compared with the lack of it. The data altogether revealed that, in presence of limiting RNAP- $\sigma^A$  concentration, a partial occupancy of promoter by  $\omega_2$  stimulates the RP<sub>O</sub> formation while the full occupancy prevents the RP<sub>O</sub> formation. Our results highlighted the dual control of RP<sub>O</sub> formation by global  $\omega_2$ .

### 2.1.6. Protein $\delta_2$ does not inhibits RNAP- $\sigma^A$ transition from RP<sub>C</sub> to RP<sub>INIT</sub> complex.

To test whether  $\delta_2$ -mediated inhibition of  $P_{\omega}$  utilization followed a similar or a different mechanism, KMnO<sub>4</sub> experiments in the presence of increasing  $\delta_2$  concentrations, RNAP- $\sigma^A$  and ATP and GTP were performed. Pre-incubation of  $P_{\omega}$  DNA with sub-stoichiometric to stoichiometric  $\delta_2$  concentrations, and then addition of RNAP- $\sigma^A$  did not affect the KMnO<sub>4</sub> cleavage pattern when compared to the absence of  $\delta_2$  (Fig. 43, lanes 1–4 vs. 5), suggesting that  $\delta_2$  decrease  $P_{\omega}$  utilization (Fig. 40, lanes 9 and 10) not just by impeding the RP<sub>INIT</sub> step, but perhaps through gene silencing (halting RNAP- $\sigma^A$  progression) as proposed for other partition systems to whom  $\delta_2$  and  $\omega_2$  belong (Rodionov et al. 1999, Lynch and Wang 1995).





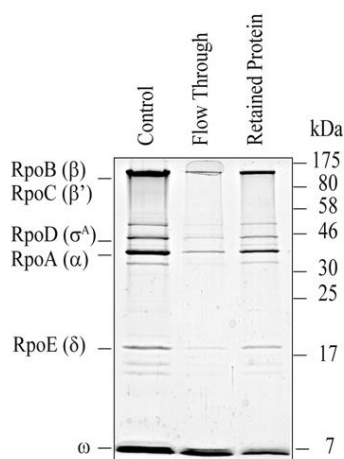
**Figure 43. RNAP- $\sigma^A$ -promoter  $RP_{\omega}$  at  $P_{\omega}$  is not affected by  $\delta_2$ .**

The 423-bp *HindIII-KpnI*  $P_{\omega}$  DNA (1 nM) was incubated with a fix amount of RNAP- $\sigma^A$  (7.5 nM) in the absence (lane 5) or presence of increasing  $\delta_2$  concentrations (75, 150, 300 and 600 nM) in the presence of the initiating nucleotides (0.1 mM/each of GTP and ATP) and DNA melting (open complex) was probed by  $KMnO_4$  footprinting. The positions hypersensitive to  $KMnO_4$  are marked ( $RP_{\omega}$  and  $RP_{INT}$ ); the coordinates are indicated relative to the transcription start point. Chemical sequencing reactions for purines (G+A) are shown, the relevant regions of  $P_{\omega}$  depicted.

## 2.1.7. Mapping $\omega_2$ -RNAP- $\sigma^A$ domains.

### 2.1.7.1. Protein $\omega_2$ interacts with RNAP- $\sigma^A$ .

To gain insights in the mechanism of cooperative interaction between  $\omega_2$  and RNAP- $\sigma^A$  or if such interaction occurs via  $P_{\omega}$  DNA different approaches have been used. The cooperative binding of  $\omega_2$  and RNAP- $\sigma^A$  to  $P_{\omega}$  DNA (Fig. 37A and 38B), and the proximity of their corresponding binding sites (Fig. 4A) suggest that both proteins might interact with each other. To disclose the molecular basis of RNAP- $\sigma^A$  recruitment onto  $P_{\omega}$  DNA by  $\omega_2$ , we looked for specific protein-protein interactions. In the first step, the association of RNAP- $\sigma^A$  and  $\omega_2$  was performed taking advantage that RNAP- $\sigma^A$  contains a histidine tag at the C-terminal end of  $\beta'$  subunit (Anthony et al. 2000). In the presence of His-tagged RNAP- $\sigma^A$ ,  $\omega_2$  binding to  $Ni^{2+}$  agarose significantly increased, even in the absence of  $P_{\omega}$  DNA, and after elution both RNAP- $\sigma^A$   $\omega_2$  were co-eluted from the matrix in the presence of 400 mM imidazole (Fig. 44). Limiting cross-linking experiments were performed in the presence of increasing RNAP- $\sigma^A$ , and revealed using anti- $\omega_2$  polyclonal antibodies suggested that  $\omega_2$  might interact with the  $\sigma$  (42.9 kDa) and  $\beta$  (133.6 kDa) and/or  $\beta'$  (134.2 kDa) subunits. Both  $\beta$  and  $\beta'$  proteins showed similar molecular masses (see Table 14), hence another approach should be used for protein discrimination.



**Figure 44. RNAP- $\sigma^A$  retains  $\omega_2$ .**

His-tagged RNAP- $\sigma^A$  (1.5  $\mu$ g) mixed with  $\omega_2$  were loaded onto a 50  $\mu$ l Ni<sup>2+</sup> micro-column at room temperature, in buffer A supplemented with 5mM Imidazole. After extensive washing, the retained proteins were eluted with 50  $\mu$ l buffer A containing 1 M NaCl and 0.4 M imidazole, separated by SDS-PAGE, and stained with Coomassie blue.

To confirm the interactions between  $\omega_2$  and RNAP- $\sigma^A$ , and to define which subunit of RNAP- $\sigma^A$  was responsible for its association with  $\omega_2$  far-western blotting experiments were performed. RNAP- $\sigma^A$ ,  $\omega_2$  and BSA, as control, were co-incubated and then separated by SDS-PAGE. The molecular mass of the potential interacting partner was markedly different (Table 15), ranging from the small  $\delta$  (20.3 kDa) to the large  $\beta'$  (134.2 kDa) subunit under SDS-PAGE, hence the proteins were separated under conditions in which  $\omega$  (7.9 kDa) was run with the front. The separated proteins were transferred onto membrane, the prey re-natured and the membrane blocked. Then, the membrane was incubated with the bait, and the protein-protein interaction detected with polyclonal antibodies. When  $\omega_2$  was used as a bait, an interaction with itself (not shown) and with the  $\beta$  or the  $\beta'$  subunit of RNAP- $\sigma^A$  was observed (Fig. 45A, Ab anti- $\omega_2$  condition). No signal was observed with the other subunits of whole RNAP- $\sigma^A$  (Fig. 45A, Ab anti- $\omega_2$  condition).

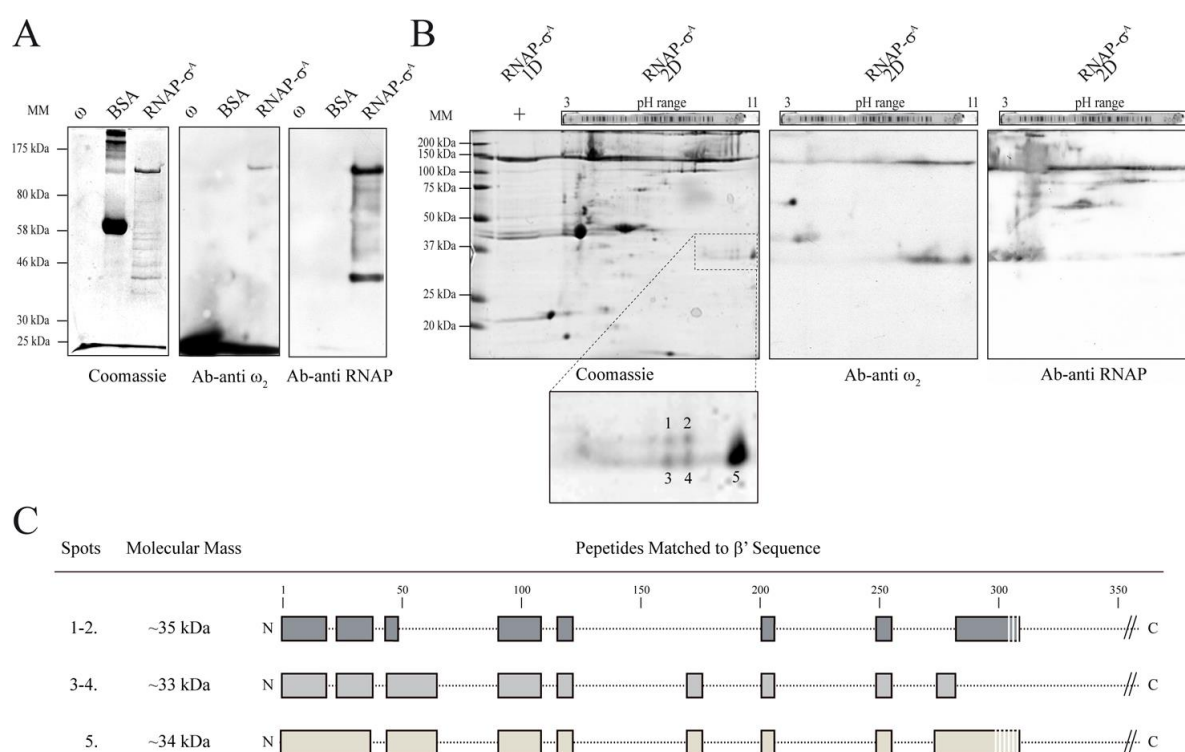
**Table 15. *B. subtilis* RNA polymerase sub-units.**

Sub-unit	amino acids	Da	pI
RpoA ( $\alpha$ )	314	34,818	4.79
RpoB ( $\beta$ )	1193	133,686	4.92
RpoC ( $\beta'$ )	1199	134,252	8.79
RpoD ( $\sigma^A$ )	371	42,948	4.80
RpoE ( $\delta$ )	173	20,398	3.85

### 2.1.7.2. The $\beta'$ subunit of RNAP- $\sigma^A$ interacts with $\omega_2$ .

Protein  $\omega_2$  might interact with the  $\beta$  or the  $\beta'$  subunit of RNAP- $\sigma^A$  (Fig. 45A). To discriminate with which RNAP- $\sigma^A$  subunits  $\omega_2$  interacts, and to re-evaluate whether  $\omega_2$  interacts with the  $\sigma$

subunit, we took advantage of the fact that except  $\beta'$  (pI 8.8), the *B. subtilis* subunits of RNAP- $\sigma^A$  have an acidic pI ( $\alpha$  [pI 4.7],  $\beta$  [pI 4.9],  $\sigma$  [pI 4.8] and  $\delta$  [pI 3.8]) (see Table 15). Under two-dimensional separation we were able to distinguish  $\beta$  from  $\beta'$  sub-units not only through their pI but also because  $\beta'$  migrated slightly below  $\beta$  sub-unit in 2D-PAGE (see coomassie, Fig. 44B). In the absence of  $P_{\omega}$  DNA, the prey proteins were then transferred onto a membrane, the preys were re-natured, the membrane blocked with skim milk, and the membranes incubated with  $\omega_2$  as bait.



**Figure 45. Far western blotting of  $\omega_2$ , RNAP- $\sigma^A$ .**

(A) Protein  $\omega_2$  (1  $\mu$ g) RNAP- $\sigma^A$  (1  $\mu$ g) and BSA (5  $\mu$ g) were separated by SDS-PAGE and stained (denoted as Coomassie). The proteins were transferred onto nitrocellulose membranes, re-natured and then detected with antibody against  $\omega_2$  (AB-anti $\omega_2$ ) or RNAP- $\sigma^A$  (AB-anti RNAP- $\sigma^A$ ). (B) RNAP- $\sigma^A$  (1  $\mu$ g) separated by SDS-PAGE and then focused in a pH 3–11 gradient, and stained (Coomassie). The proteins were transferred onto nitrocellulose membranes, re-natured and then detected with antibody against  $\omega_2$  (AB-anti  $\omega_2$ ) or RNAP- $\sigma^A$  (AB-anti RNAP- $\sigma^A$ ). The basic polypeptide ~34 kDa were gel purified and partially proteolysed as described in Materials and methods. (C) Identification of relevant polypeptides. The polypeptides subjected to partial proteolysis and mass spectrometry and the identified regions are indicated. The sequence coverage of the indicated polypeptide was > 40%.

As observed by FWB, protein  $\omega_2$  was interacting with proteins in the basic region of the gel (Fig. 45B, Ab anti- $\omega_2$  condition). These regions were corresponding to  $\beta'$  with molecular mass of ~134 kDa and to unexpected spots with lower molecular masses of ~34 kDa (Fig. 45B). These polypeptides (termed 1–2, 3–4 and 5) were gel purified, and subjected to limiting

proteolysis. Limiting trypsin proteolysis of the gel purified 1–2, 3–4 and 5 polypeptide bands in concert with mass spectrometry analysis allowed us to identify them as the N-terminal domain of the  $\beta'$  subunit of RNAP- $\sigma^A$  (Fig. 45C). Polypeptides ranging 1 to 316 aa of the  $\beta'$  N-terminal domain were encountered in all the spots analysed, indicating that they contained specific domains recognize by  $\omega_2$ . Within this region discrete domains were mapped, and the contribution of the  $\beta'$ -ZDB, the  $\beta'$ -pincer (including the  $\beta'$ -Lid,  $\beta'$ -coiled coil and  $\beta'$ -rudder) and the  $\beta'$ -Sw2 regions on  $RP_C$  and  $RP_O$  formation were proposed (Murakami et al. 2002a, Murakami et al. 2002b, Vassylyev et al. 2002, Vassylyev et al. 2007a) (Fig. 8). These results underline that the  $\beta'$  specifically interact with  $\omega_2$ , suggesting the implication of the specific regions located in the  $\beta'$  N-terminus.

## 2.2. Characterization of $\omega_2$ transcriptional regulation.

The *inc18* family members that encoded for *ermB* also codes for a  $\omega$ -variant,  $\omega_2$  gene (e.g., pIP501, pAM $\beta$ 1, pRE25) whose product (79 residues long) shares 83% identity when compared with  $\omega_2$  (71 residues long) (Fig. 4B). Some of those plasmids that lack  $\omega_2$ , show traces of the 3'-end of the gene.

### 2.2.1. Protein $\omega_2$ is a functional transcription repressor.

The global  $\omega_2$  and  $\omega_2$  regulators belong to the family of proteins with a RHH<sub>2</sub> fold (Fig. 11). Monomeric  $\omega$  shared 98% identity in the first 55 residues with  $\omega_2$ , but the degree of identity dropped to 18% in the remaining 16 residues (Fig.4B). With the aim of addressing whether  $\omega_2$  interacts with  $P_\omega$  *in vivo*, the  $P_\omega \omega_2$  sequence was fused to the 5' non-coding region of a promoter-less *lacZ* gene, integrated as single copies into the *amyE* locus of the *B. subtilis* chromosome and different combinations of plasmid-borne genes were then provided *in trans*.

Cells bearing plasmid-borne  $\omega$ ,  $\omega\Delta N19$  or  $\omega_2$  genes were grown and the  $\beta$ -galactosidase assayed from the lysates. The analysed strains revealed that transcription from the  $P_\delta:lacZ$  gene is repressed by the  $\omega_2$  and  $\omega_2\Delta N19$ . As shown in Table 16,  $\omega_2$  expressed in trans was able to repress  $P_\delta:lacZ$  with less than 2-fold efficiency than wild type  $\omega_2$ . This results suggested that  $\omega_2$  gene expressed a functional protein capable of inhibiting mRNA synthesis from  $P_\delta$  promoter *in vivo*.

**Table 16. The  $\beta$ -galactosidase activity of  $P_\delta$ .**

---

$\beta$ -galactosidase activity\*

---

Gene in trans	$P_\delta$
Vector	2317 ± 22
$\omega$	32 ± 12
$\omega\Delta N19$	44 ± 15
$\omega2$	55 ± 14
$\omega K52A$	46 ± 09
$\omega E53A$	41 ± 08
$\omega D56A$	411 ± 42
$\omega R64A$	80 ± 09
$\omega R70A$	46 ± 11

\* The  $\beta$  galactosidase activity is expressed in Miller units. Values are means of at least four separate experiments

### 2.2.2. Protein $\omega2$ is functionally active in plasmid partition.

To further investigate whether  $\omega2$  were also functional in concert with  $\delta2$  stabilizing the plasmid, the  $\omega2$  gene was fused downstream the  $P_\omega$  promoter and cloned into pHP14 vector containing  $P_\delta$  and  $\delta:gfp$  sequences. As previously described, the absence of one of the three components,  $\omega2$ ,  $\delta2$  and/or  $parS$  DNA impaired the plasmid segregation. The partition system composed by  $\omega2$  and  $\delta:GFP2$  fully stabilized the plasmid along 100 generation (Table 17). These results suggested that  $\omega2$  can fully replace to  $\omega$  and it interacts with  $\delta2$  protein through its N-terminus working actively in plasmid partition *in vivo*.

**Table 17. Plasmid stability ( $\omega2$ ).**

$par$ genotype	Stability
–	< 1%
$\omega$	< 1%
$\omega2$	< 1%
–	$\delta$
$\omega$	$\delta:gfp$
$\omega2$	$\delta:gfp$

### 2.3. Characterization of $\omega2$ $\alpha1$ – $\alpha2$ domains for the repression of $P_\omega$ utilization.

From the dispensability of the unstructured N-terminal domain (residues 1–19,  $\omega2\Delta N19$ , condition) and the C-terminal domain (71–79), the buried  $\beta$ -sheet domain in the major groove of DNA (28–32), and the sequence divergence in the predicted coiled (65–72) and  $\alpha2'$  (73–78)

domains; the  $\alpha 1$  (34–46) and perhaps the proximal part of the  $\alpha 2$  domain (51–56) can be involved in the interaction with RNAP- $\sigma^A$  (Fig. 4B). In this region the dimer–dimer and the monomer–monomer interface were mapped in the conserved ( $\alpha 1$ ) region, that is stabilized by the conserved region of the  $\alpha 2$  domain and hydrophobic side–changes between both  $\alpha$ –helices (Murayama et al. 2001a, Weihofen et al. 2006). The electrostatic properties of this conserved regions for the interaction with the  $\beta'$  subunit of RNAP- $\sigma^A$  were investigated. The accessible charged residues in the conserved domain were replaced by alanine (K52A, E53A, D56A, R64A and K70A). With the aim of mapping the  $\omega_2$  domain involved in the interaction with RNAP- $\sigma^A$ , the  $P_\omega$  DNA and the  $\omega_2$  mutant variants were introduced in a strain bearing the  $P_\delta:lacZ$  gene integrated into the *amyE locus* of the *B. subtilis* chromosome and the level of  $\beta$  galactosidase expression measured. As revealed in Table 16, *in vivo* utilization of  $P_\delta$  promoter were reduced more than 28–fold in the presence of plasmid–borne  $\omega$  gene or its variants ( $\omega K52A$ ,  $\omega E53A$ ,  $\omega R64A$  and  $\omega K70A$ ), whereas in presence of the  $\omega D56A$  variant the reduction of the promoter utilization was only 5–fold reduced. By Western blot analysis, we could rule out the potential low expression of the  $\omega$  gene variants (data not shown). These preliminary results suggest that the D56 residues might be involved in the interaction with RNAP- $\sigma^A$ . or alternatively might simply effect the appropriate folding of protein variant.

## *Discussion*





Low-copy number plasmids have developed a number of strategies to ensure their stable maintenance in bacterial populations: (i) multimer resolution system to maximize random assortment, (ii) active toxin-antitoxin system to inhibit cell proliferation of plasmid-free cells, and (iii) faithful plasmid partition. The replication and copy number control systems of plasmid are two mechanisms strictly interdependent. Whereas plasmid replication system delivers sufficient number of plasmid copies, its copy number control mechanism provides the safety measure to minimize the metabolic cost on the host and to avoid copy number fluctuations. DNA replication errors might lead to replication fork stalling. The homologous recombination machinery re-establishes the replication fork but it might generate dimers if the recombination intermediates are not properly resolved. The multimer resolution system maximizes the number of plasmid monomers accessible for segregation, therefore is regarded as “passive” stabilization system that supports the random segregation of plasmids to daughter cells. Usually there are two “active” stabilization systems that ensure better than random segregation: partition (Par) and toxin-antitoxin (TA) systems. In the plasmids of the *inc18* group, to which pSM19035 belongs, all functions that contribute to stably spread in bacteria of the Firmicute phylum are interlinked by the global  $\omega_2$  regulator. Protein  $\omega_2$  is able to: i) corrects downward fluctuations in plasmid copy number by repressing CopS. As a result, the synthesis of the *repS* gene products increased to initiate plasmid replication; ii) control the synthesis of the toxin-antitoxin module that blocks the appearance of plasmid-free segregants; and iii) regulate the expression of the type Ib proteins  $\delta_2$  (ParA) and itself (ParB) and actively participate in concert with  $\delta_2$  to ensure faithful segregation (de la Hoz et al. 2000, Lioy et al. 2012, Pratto et al. 2008).

ParA proteins of type I uses *non-specific* chromosomal DNA binding to partitioning their plasmids and this feature could be (or one of) the reason for their evolutionary success. Moreover, the larger group of ParA/MinD superfamily that provides positional information for spatial organization to which the ParA of type I belongs continues to expand. Orphan ParA proteins are required for segregating cytoplasmic protein clusters and the polar localization of chemotaxis proteins (ParA in *V. cholera* and PpfA *R. Sphaeroides*) (Ringgaard et al. 2011, Roberts et al. 2012), conjugative transfer machinery (VirC1 in *A. tumefaciens*) (Atmakuri et al. 2007), type IV pili (TadZ/CpaE in *A. actinomycetemcomitans*) (Perez-Cheeks et al. 2012) and cellulose synthesis (YjhQ/BcsQ in *E. coli*) (Le Quere and Ghigo 2009). All these reasons make the study of partition system of pSM19035 also very interesting as a model system.

In this work, several results are presented that provided insights into the molecular mechanisms by which symmetric  $\omega_2$  regulates the transcription, and the action mode of the type I par system composed by  $\delta_2$  and  $\omega_2$ .

## 1. The active partition systems of pSM19035.

The pSM19035 plasmid of *inc18* family is one of the best-studied plasmids that can replicate in a broader range of bacteria of the Firmicutes phylum. Although the crystal structures of  $\delta_2$  and  $\omega_2$  proteins of pSM19035 are being solved (Murayama et al., 2001, Pratto et al., 2008) the knowledge about the molecular mechanisms of pSM19035 partition is still incomplete. The ParA–ParB interactions and their dynamics are continuously studying. With the aim to increase our understanding of faithful plasmid segregation, several detailed biochemical analysis were performed in this studies.

### 1.1. The role of $\delta_2$ C-terminal region is essential for pSM19035 segregation.

The large ParA proteins contain a site-specific and a nsDNA binding domains. The small ParA proteins lack the N-terminal site responsible for specific DNA binding and but still present the nsDNA binding domain. The large P1–ParA and the small pSM19035– $\delta_2$  are dimers in solution (Pratto 2008, Dunham 2009), whereas the small ParAs from host-origin (e.g., Soj) and TP228–ParF are monomers in solution, but the can switch from monomer to dimer upon binding to ATP molecule (Leonard, 2005; Schumacher 2012). It was shown that plasmid-encoded ParAs (e.g., F–SopA, P1–ParA, pSM19035– $\delta_2$ ) or chromosomal-encoded small ParAs ATPases (e.g., Soj), in the ATP bound form, bind nsDNA through its C-terminus region (Hester and Lutkenhaus 2007, Dunham et al. 2009, Castaing, Bouet and Lane 2008). However, the small plasmid-encoded ParA ATPase (TP228–ParF) interacts with itself through the C-terminus to form bundles (Schumacher 2012).

In the presence of ATP, ParA proteins bind to nsDNA leading to formation of discrete blobs on single DNA molecules or a cloud of fluorescence on the nucleoid (this work) (Pratto et al. 2009, Soberon et al. 2011, Hwang et al. 2013, Vecchiarelli et al. 2013). Previous reports, revealed that ATP-bound  $\delta_2$  binds to nsDNA, forming a short dynamic complex (DC), having a blob shape containing up to  $5 \pm 1$   $\delta_2$ /nsDNA molecule (Pratto et al. 2008, Pratto et al. 2009), rather than nucleoprotein filaments on nsDNA. Likewise, free  $\delta_2$  in solution is present in several multimer states that can be distinguished by a native gel (data not shown) and forms discrete blob shaped structures containing 2–6  $\delta$  molecules, rather than long bundles in the absence of nsDNA.

The ATP bound state triggers the  $\delta_2$  conformational changes that lead to competence for nsDNA. Two residues of  $\delta_2$ , the K36 and D60 that are located in walker A and A' respectively,

were described to be essential for the ATP binding and hydrolysis (Pratto et al. 2009). The  $\delta_2$ K36A mutant is unable to bind ATP, and  $\delta_2$ D60A binds but does not hydrolyse ATP (Pratto et al. 2008). In absence of ATP, these proteins failed to bind to nsDNA ( $K_{Dapp} > 1500$  nM) (Pratto et al. 2009). In presence of ATP,  $\delta_2$ D60A bound with 3-fold higher affinity to nsDNA and the  $\delta_2$ D60A–nsDNA complexes were long-living compared to  $\delta$ -nsDNA complexes (Fig. 14). The ATP binding, but not hydrolysis, is essential for  $\delta$  binding to nsDNA, both *in vitro* and *in vivo*. It is likely that different propriety in ATP hydrolysis can explain the difference in their  $K_{Dapp}$ :  $\delta_2$ D60A should have the same on-rate but a decrease off-rate compared to  $\delta$ . ATP binding and hydrolysis is closely linked to  $\delta_2$ -nsDNA complex assembly and disassembly. However, the  $\delta_2$  nsDNA binding domain and its role in plasmid stability were not previously described. Our results obtained by limited proteolysis experiments revealed that several regions of  $\delta_2$  become protected upon DNA binding. This region maps in the C-terminus of the protein (see Fig. 19 and Fig. 46A–II). These findings suggest that ATP and nsDNA binding have local consequences and induce conformational changes in the protein and the basic amino acids at the C-terminal region contact the DNA phosphate backbone. The residues required for nsDNA interaction in  $\delta_2$ , Soj, P1–ParA or SopA, which map in the C-terminal domain, are not conserved (Hester and Lutkenhaus 2007, Castaing et al. 2008, Fig. 4).

To evaluate the relevance of the DNA binding features, a set of acid/basic residues at the C-terminus of  $\delta_2$  were mutated and thoroughly tested *in vivo* and *in vitro*. A single point mutations of exposed negative residues D211→A that somehow could be responsible in the control of  $\delta_2$ -nsDNA complex formation, resulted in a  $\delta_2$ D211A protein with increased nsDNA cooperative binding, but the ATP hydrolysis and the plasmid pairing in response to  $\omega_2$  remains substantially unchanged compared with  $\delta_2$  both *in vivo* and *in vitro*. It is likely this substitution was only increasing the on-rate of  $\delta_2$ D211A–nsDNA complexes without altering the off-rate of protein–DNA complexes. Interesting we observed that the basic single or double point mutations of positive residues K242→A, K248→S and K259→A/K260→A, abrogate or reduce drastically nsDNA binding, without affecting protein dimerization and ATP binding and hydrolysis of the Walker domain *in vitro*. An equivalent mutation in chromosomal Soj (e.g., ATP–Soj<sub>2</sub>R218A), however, only marginally (2- to 2.5-fold) reduced the nsDNA binding affinity relative to ATP–Soj<sub>2</sub>, whereas the ATP–Soj<sub>2</sub>R218E variant shows no binding to DNA (Hester and Lutkenhaus 2007). Type Ia ParA ATPases, as P1–ParA<sub>2</sub> or F–SopA<sub>2</sub>, when bound to ATP, mediate segregation by interacting with *parS*-bound ParB (Funnell 2005, Ebersbach and Gerdes 2005, Leonard, Moller–Jensen and Lowe 2005b, Hayes and Barilla 2006). P1–ParA<sub>2</sub> or F–SopA<sub>2</sub> also contains, at the C-terminus, a basic region that comes into contact with nsDNA in a sequence

independent manner (Castaing et al. 2008, Dunham et al. 2009). This basic region of P1–ParA is equivalent to the nsDNA binding motif of  $\delta_2$  ( $\delta_2$ K259A K260A). Indeed, the P1–ParA<sub>2</sub>K375A R378A double mutation, in the ADP bound form, essentially abrogated DNA binding (Dunham et al. 2009).

All the results obtained in this work were suggesting that our mutants were properly folded (wt-like ATPase activity), therefore the DNA binding defect presented by  $\delta_2$ K242A,  $\delta_2$ K248S or  $\delta_2$ K250A K260A seemed to be a genuine effect due to residues substitution. Unexpected, plasmid stability of *par*<sup>-</sup> systems expressing physiological concentrations of  $\omega_2$  and  $\delta$ K242A:GFP<sub>2</sub>,  $\delta$ K255A:GFP<sub>2</sub> or  $\delta$ K259AK260A:GFP<sub>2</sub> variants (~1.9  $\mu$ M/each) revealed that the  $\delta_2$  mutant variants only reduced plasmid stability by factor 2 *in vivo*. Moreover, all  $\delta_2$  fluorescent variants formed clouds of fluorescence in an area corresponding to nucleoid as  $\delta$ :GFP<sub>2</sub> when their expression were uncoupled from the  $\omega_2$  control *in vivo* (data not shown). These apparent paradox was explained by EM analyses of  $\delta_2$ K242A variant without considering the non-trivial differences in molecules concentrations and environmental condition between the *in vitro* and *in vivo* experiments. In fact, protein  $\delta_2$ K242A alone at (300 nM) bound plasmid DNA forming a small cluster onto nsDNA similar to those formed by  $\delta_2$  (150 nM) and its ability to generate plasmid pairing in presence of  $\omega_2$  was 2.5-fold reduced. Furthermore, it was demonstrated by EMSA assays that  $\omega_2$  increases the stability of a  $\delta_2$ K242A–DNA complex, perhaps by decreasing the off-rate of  $\delta_2$ K242A binding to DNA. These results suggested that the  $\delta_2$ K242A–nsDNA complex could be formed, but the high off-rate of the binding reaction *in vitro* did not allow us to visualize the protein–DNA complex when EMSA was used. This is consistent with the *in vivo* observation that the  $\delta_2$ K242A binding defect to nsDNA slightly impaired plasmid segregation.

The essential role of  $\delta_2$  nsDNA binding region was highlighted by C-terminal deletion of the protein. In fact,  $\delta_2\Delta$ C255,  $\delta_2\Delta$ C227,  $\delta_2\Delta$ C197 and  $\delta_2\Delta$ C164 failed to form stable complexes with nsDNA, but they still were able to form dimer and high order of oligomers in solution and interact with  $\omega_2$  producing PC formation *in vitro*. Except  $\delta_2\Delta$ C255, the  $\delta_2$  C-terminal deletions ( $\delta_2\Delta$ C227,  $\delta_2\Delta$ C197,  $\delta_2\Delta$ C164) were unable to hydrolyse ATP although all deletion were detected to bind ATP by UV-cross-linking experiments (data not shown). *In vivo*, the plasmids sharing partition systems composed by  $\delta\Delta$ C197 or  $\delta\Delta$ C164 genes which lack of large C-terminal regions, the active segregation that was abolished, while  $\delta\Delta$ C255, whose product lacks the last 29 residues (or  $\alpha$ 12), was only partially reduced (~ 3-fold).

These study elucidate how the domains needed for ATP binding,  $\delta$ - $\delta$  and  $\delta_2$ - $\omega_2$  interactions, are included in the first 164 residues of  $\delta$ . The region ranging the residues 211–260 (including the relevant  $\alpha_9$ ,  $\beta_7$ ,  $\alpha_{10}$ ,  $\beta_8$ ,  $\alpha_{11}$  and  $\alpha_{12}$  joined by coiled segments) are strictly involved in the interaction with DNA phosphate backbone. Collectively, our findings are supported that the C-terminal moiety of  $\delta_2$  (164–284) is essential for nsDNA binding, and essential step in plasmid faithful partitioning (Fig. 46A–I, –II, –III and –IV).

### 1.2. Protein $\omega_2$ interacts with the central domain of $\delta_2$ .

The type of interactions between ParA and ParB seem to be conserved among the ParA/MinD ATPase family. Several studies on ParB-like proteins as P1-ParB, TP228-ParG, pSM19035- $\omega_2$  and *E.coli* MinE, are in agree in indicating the N-terminus as the domain responsible for the interaction ParA-ParB interaction (Vecchiarelli and Funnell 2013, Barilla, Carmelo and Hayes 2007, Ma, King and Rothfield 2003). Deletion of the first 19 unstructured residues of  $\omega_2$  are essential for its interaction with  $\delta_2$ , and thereby are deficient in stability (Pratto et al. 2008). All the ParB/MinE N-terminal regions have a high degree of structural disorder, but it has been suggested that under certain conditions an  $\alpha$ -helical structure can be formed (Ma et al. 2003, Park et al. 2011). Our structural predictions of flexible N-terminal region of  $\omega_2$  propose basically  $\alpha$ -helical structures for small  $\omega^{1-13}$  peptides that present a clear hydrophobic surface by the VGAGA residues of N-terminus, but larger sequence prediction resulted in an increase the level of disorder, indicating that several conformational state of  $\omega_2$  could co-exist in solution (Fig. 46A–I, appendix, paragraph 2.1.).

Lutkenhaus and co-workers have deeply characterized the interaction between MinD and MinE and recently they proposed “*the Tarzan of the jungle*” model based on raising the possibility that MinE represent different conformational states and MinD-dependent conformational changes in MinE that convert it from a latent to an active form. MinE protein acts as a counterpart of MinD displacing MinC and activating the ATP catalytic activity of MinD. Two structures of intact MinE proteins were solved, and their folding differ significantly. In fact, the *E. coli* MinE<sup>31-88</sup> dimer, lacking the anti-MinCD interacting domain, presented a four-stranded antiparallel  $\beta$  sheet (King et al. 2000), whereas the structure of intact *H. pylori* or *N. gonorrhoeae* MinE was also dimeric, but with six-stranded antiparallel  $\beta$  sheet (Kang et al. 2010, Ghasriani et al. 2010). The additional  $\beta$  strands ( $\beta_1$ ) containing part of the anti-MinCD domain are at the dimer interface sandwiched between the  $\beta$  strands found in the structure of the truncated *E. coli* protein. Recently, crystallization of MinD-MinE<sup>12-31</sup> complexes revealed how the 13–26

of the MinE peptide, which included most of the residues that correspond to the  $\beta$ 1 strand of MinE, were visible in the structure as an  $\alpha$  helix present on each side of the MinD dimer interface (Park et al. 2011). In analogous way, as reported in this work by *in vitro* assays,  $\omega_2$  needs to be necessary bound to *parS*-DNA to interact with  $\delta_2$ , stimulating the ATP hydrolysis and relocalization of the motor protein. It is likely that the  $\omega_2$  free in solution have an inappropriate N-terminus conformational state for  $\delta_2$  interaction, and further binding to *parS* centromeric regions alters the structure of  $\omega_2$ , an essential pre-requisite that should provide the proper N-terminus folding leading to a competence state for  $\delta_2$  interaction.

The binding site(s) for the ParB-like  $\omega_2$  on the ParA-like  $\delta_2$  begin their characterization for the first time with this work. As revealed by  $\omega_2$ - $\delta_2$  crosslink assays in presence of *parS* DNA, we found that the central region of  $\delta_2$  (88-119 and 139-224 regions were not detected) possibly interacts with the N-terminal region of  $\omega_2$  leading to ternary ( $\omega_2$ -*parS*- $\delta_2$ , SC) or quaternary (*parS*- $\omega_2$ - $\delta_2$ -nsDNA, BC or BC1) complexes (Fig. 46A). This is consistent with the *in vivo* characterization of the binding sites for MinE/MinC on MinD and the co-crystal of MinD-MinE (Wu et al. 2011, Park et al. 2011). Accordingly, two symmetrical binding sites for  $\omega_2$  will be present in a  $\delta_2$  dimer and its ATPase could be activated by  $\omega_2$  binding to one side (asymmetrical binding) or required to both sides of an  $\delta_2$  dimer (symmetrical binding). Recent studies suggested that asymmetric binding of MinE to MinD was sufficient to stimulate ATP hydrolysis, and the release of MinD from the membrane (Park et al. 2012). In the case of  $\delta_2$ , is worth keeping in mind that the 139-216 region lacks of specific trypsin protease sites, and the resulting fragment reached the upper mass limit of MALDI-TOF-TOF. The glutamyl endopeptidase and chymotrypsin have 23 and 25 cleavage sites in  $\delta$ , respectively. To predict to recognize specific sites inside the large fragment 139-224,  $\delta$  was cleaved with the glutamyl endopeptidase and chymotrypsin peptidases with the purpose of increasing our understanding. Unfortunately, the extraction of peptides from gel excision by these proteases was less efficient than trypsin.

The C-terminal amino acid of F-SopA is essential for interaction with F-SopB (Kim and Shim 1999, Ravin, Rech and Lane 2003). Since  $\delta$  C-terminal variants still binds  $\omega$ , it lead us to focus our attention at the first 164 residues. The putative  $\delta$ - $\omega$  interaction region maps between residues 88 to 119 of  $\delta$ . This region is close to the Asp60, an important residue of the walker A' domain involved in the coordination of the water molecule for the nucleophilic attack of the  $\gamma$ -phosphate of ATP. This putative region also presented conserved hydrophobic and negative residues that might be reflected by hydrophobic and positive residues located at the N-terminus of  $\omega_2$ . Thereby, we proposed that the central region of  $\delta$ , which is surface exposed and distant

from the DNA binding domain, is the main domain ( $\alpha 4$ ,  $\alpha 5$ ,  $\beta 3$ ,  $\beta 4$  and  $\alpha 6$ ) involved in the interaction with  $\omega_2$ .

It is worth to point out that while the functional characterization of  $\omega_2$ - $\delta_2$  interacting domain was carried out during this study, the chromosomal-encoded *Pseudomonas aeruginosa* ParA–ParB interacting domain was mapped within the 67 to 85 interval (equivalent to residues 89–105 of  $\delta_2$ ) by yeast two hybrids and immunoprecipitation assays (Bartosik et al. 2014). This findings are also in agreements with the results presented here. It is likely that independently of the type of complex formed by the ParB–like proteins on *parS* DNA (spreading over many kilobases by bridging and looping on nsDNA {Lynch, 1995 #862;Rodionov, 1999 #813;Murray, 2006 #863;Graham, 2014 #983} or just binding to the *parS* site, the ParB–ParA interaction and the mechanism used for activation of the ParA ATPase activity might be universally conserved.

### 1.3. Molecular model explaining the pSM19035 plasmid partition system.

Biochemical and cellular analysis reported in this study have provided insights over the multi–steps process involved in type Ib partitioning systems. The dynamics of interaction among  $\delta_2$  motor,  $\omega_2$  CBP, *parS* and chromosomal DNA were deeply examined in this work leading us to formulate more detailed model of ParAB plasmid segregation *in vivo* (Fig. 46 and Fig. 47).

#### 1.3.1. Formation of partition and dynamic complexes (PC1 and DC).

The first step of the partition reaction involves the  $\omega_2$  binding to *parS* site DNA (Fig. 46A–I, and 46B). Plasmid replication occurs mostly at nucleoid–free regions at the cell poles and occasionally moves out of the poles (Wang et al. 2004). The interaction of newly replicated plasmids bearing *parS* sites with  $\omega_2$  lead to PC formation and plasmid clustering (~ 1.3 plasmid copies/focus). The  $\omega$ :YFP<sub>2</sub> foci were broadly distributed without showing any specific pattern *in vivo*. Previously it was shown by surface plasmon resonance that the  $\omega_2$ –*parS* complex is short–living (~ 50 s) (Welfle et al. 2005, Weihofen et al. 2006). From our *in vitro* data we inferred that these cluster intermediates should be transient and discrete. In fact, in the absence of  $\delta_2$ , the  $\omega_2$ –*parS* complexes (PC1) are short living. *In vitro*,  $\omega_2$  mediates plasmid pairing only in ~1% of total protein–DNA complexes when analysed by EM or AFM (Pratto et al. 2009, Soberon et al. 2011). It is worth noticing that unlike  $\omega_2$ –*parS* DNA, pB171–ParB binds to the centromere and forms discrete PCs and large higher order complexes consisting of several DNA fragments joined by ParB at centromere site (BC complex or plasmid pairing) in the absence of pB171–ParA (Ringgaard, Lowe and Gerdes 2007).

*In vitro*, the *parS* DNA region on linear and circular DNA were not significantly distorted by  $\omega_2$  binding, consistent with the prediction based on crystal structures of  $\omega_2$  bound to *parS* sites (Pratto et al. 2008, Pratto et al. 2009). Like  $\omega_2$ , the SopB–DNA structures revealed that SopB did not bend or unwind DNA upon binding (Schumacher, Piro and Xu 2010). Whereas, the centromere region of P1 or P7 plasmids contains a central binding site for the *E. coli* protein IHF (integration host factor) that is an architectural protein that bends DNA by  $\sim 180^\circ$  (Surtees and Funnell 2001). Although different type of conformation of PC could exist upon CBP binding, it appears that the protein–centromere interaction leads to the formation of PC or higher–order structures that are important in the capture and activation of the motor protein for plasmid segregation.

The motor protein  $\delta$ :GFP<sub>2</sub> alone is regularly distributed over the nucleoid forming cloud of fluorescence, indicating that  $\delta_2$  bind chromosome nsDNA. The  $\delta_2$ –nsDNA presented slow dynamic instability even in absence of ATP hydrolysis as the case of  $\delta$ D60A:GFP<sub>2</sub>, effectively the slow  $\delta$ :GFP<sub>2</sub> dissociation followed by random motion and re–association was observed *in vivo*. protein  $\delta_2$ –bound to ATP undergoes a functional transition and become proficient to bind nsDNA, but under this condition P150 should occupy the space of the catalytic water molecule (Pratto et al. 2008) (Fig. 46B). The ATP catalytic activity of  $\delta_2$  by itself or in presence of nsDNA is weak. In fact, the ATP binding, but not hydrolysis, is essential for  $\delta_2$  to form transient and discrete blobs on nsDNA (DC, with a footprint of  $\sim 30$  bp/  $\delta_2$  and  $\sim 5$   $\delta_2$  /blob) both *in vitro* and *in vivo*. Similarly, it seems that also  $\delta_2$  free in solution forms discrete blob shaped structures, rather than long bundles (Pratto et al. 2009) (Fig. 47). We hypothesized that the  $\delta_2$  aggregation structure observed in absence of DNA might be for storage purpose.

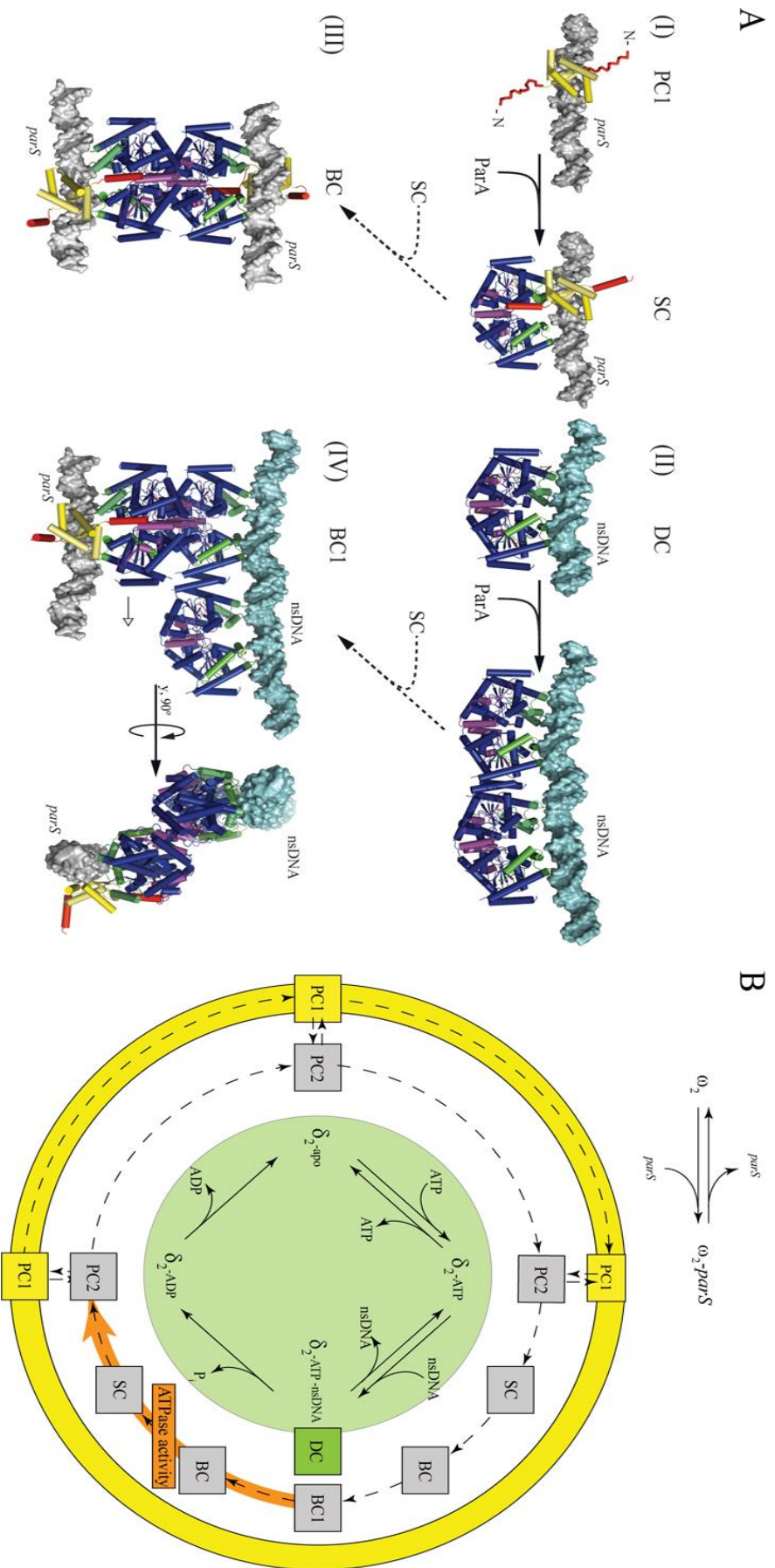
### **1.3.2. Dynamics of PC, SC and BC formation and disassembly.**

The  $\delta_2$  protein positively controls the dynamic activities of  $\omega_2$  on *parS* DNA, and  $\omega_2$  positively controls the dynamic activities of  $\delta_2$  on nsDNA. The transient  $\omega_2$ –*parS* complex (PC1) upon interaction with  $\delta_2$ , even in the apo form, undergoes a functional transition that markedly stabilizes complex leading to the accumulation of the long–lived PC2 intermediate (this work). Since the addition of apo– $\delta_2$ K242A decreased the dissociation rate of the PC, it suggests the evidence that apo– $\delta_2$  or apo– $\delta_2$ K242A transiently interacted with the unstructured N–terminal domain of  $\omega_2$ , facilitating domain folding and/or a more extended  $\omega_2$  structural changes, leading to  $\omega_2^*$  state. It is likely that upon a transient  $\omega_2$ – $\delta_2$  interaction there are two PC states, a transient (PC1,  $\omega_2$ –*parS* DNA) and a stable (PC2,  $\omega_2^*$ –*parS* DNA) one. We proposed that in  $\omega_2^*$  the unfolded end–terminal domain undergoes a structural transition and became folded (Fig. 46).



This newly folded N-terminal region might be capable of interacting with  $\delta_2$ . At stoichiometric concentrations,  $\omega_2$  bound to *parS* DNA promotes dislodging of  $\delta_2$  (or  $\delta_2$ K242A) from nsDNA (this step should be responsible for transient BC1 formation), and re-location towards PC2 leading to SC and then BC formation upon stimulating the  $\delta_2$  binding to nsDNA *in vitro*. It was previously observed by EM and AFM that  $\delta_2$ , stimulates the formation of ternary complex  $\omega_2$ -*parS*- $\delta_2$ , and the interaction of two SC lead to plasmid pairing (or BC) (Pratto et al. 2009).

It is likely that  $\delta_2$ -bound to ATP alone or assembled in DC with nsDNA became proficient to PC1 interaction leading to PC2, SC and/or BCs segregation complex formation (Fig. 46A and 46B). Our data are consistent with the fact that both  $\omega_2$  and  $\delta_2$  undergo functional transitions upon interaction among themselves: i) interaction of  $\omega_2$  with  $\delta_2$  enhances  $\omega_2$ -*parS* complex formation ~8-fold, and the half-life of the formed complex; and ii) interaction of  $\omega_2$  with  $\delta_2$  enhances binding to nsDNA (~4-fold), and the re-localization of  $\delta_2$  towards the  $\omega_2$ -*parS* complex (Pratto et al. 2008, Pratto et al. 2009, Soberon et al. 2011). It seems clear that different  $\omega_2$ : $\delta_2$  ratios and the presence of *parS* DNA play a key role in the regulation of the different stages during plasmid segregation. At high  $\omega_2$ : $\delta_2$  molar ratios ( $\omega_2 > \delta_2$ ), the interaction of *parS*- $\omega_2$  complexes with  $\delta_2$ , at the nucleoid, relocated the plasmid copies from a broad distribution towards the high concentration of  $\delta_2$ -bound to the nucleoid, suggesting plasmid-nucleoid pairing, but also plasmid pairing with ~3.3 plasmid copies/focus *in vivo* (Fig. 47). The tethering of plasmids copies towards  $\delta_2$ -nsDNA complexes, at the nucleoid, should alter the relative stoichiometry of both proteins ( $\omega_2 < \delta_2$ ). At the same time, at about stoichiometric  $\omega_2$ : $\delta_2$  ratios ( $\omega_2 \approx \delta_2$ ),  $\omega_2$  will start to stimulate the  $\delta_2$  ATPase activity (maximal rate at ~1.5:1  $\omega_2$ : $\delta_2$  ratios). The enhanced ATP catalysis at equimolar ratio of both proteins, also suggest that the activation of ATP hydrolysis by  $\omega_2$  should be asymmetric as reported for MinD-MinE (Park et al. 2012).

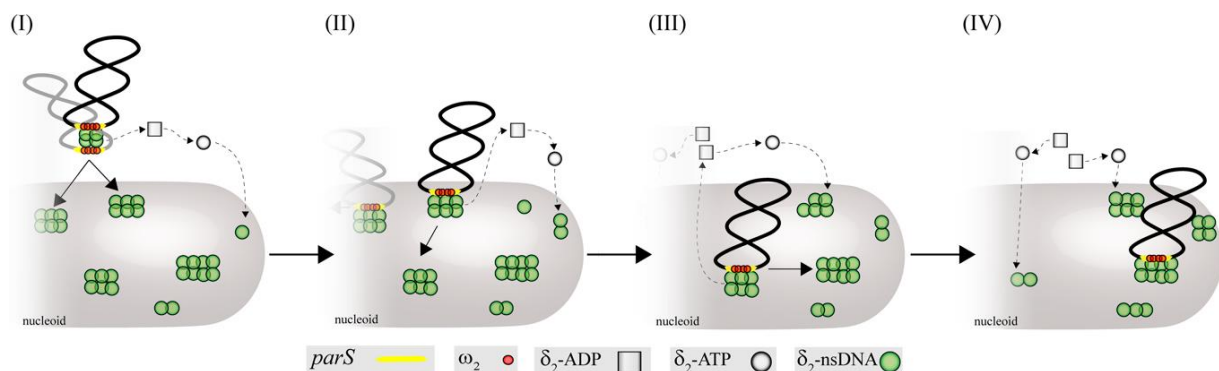


**Figure 46. Dynamics and models of pSM19035 plasmid partition complexes.**

(A) The models of PC1 up to SC (I), DC (II), plasmid–nucleoid pairing (IV) or plasmid–nucleoid pairing (IV) are represented by cartoons. (I) PC1 consisting on  $\omega_2$  (in yellow and red) bound to *parS* DNA (in grey) and a  $\delta_2$  (in blue, green, blue and purple) interacting with  $\omega_2$ –bound to *parS* leading to PC2 and SC. The interaction of  $\delta_2$  with flexible N–terminal region of  $\omega_2$  (messy line in red) will lead to  $\alpha$ –helix formation (red cylinder). The part of  $\delta_2$  required for nsDNA binding (in green) and  $\omega$  interaction (in purple) are highlighted. (II) One (on the left) or two (on the right) contiguous of  $\delta_2$  proteins bound to nsDNA (in cyan) forming DC. This type of polymerization will requires N– or C–terminal interaction. (III) The hypothetical models of plasmid pairing (BC) or plasmid–nucleoid pairing (BC1) imply that two SC or one SC with DC are interacting through the  $\delta_2$ · $\delta_2$  in brown. The models were constructed and manually modified using PyMOL with  $\delta_2$ ·ATP· $\gamma$ S· $\text{Mg}^{2+}$  template. (B) Dynamics of  $\delta_2$  and  $\omega_2$  specific interactions. Protein  $\omega_2$  is in equilibrium between *parS* bound and unbound states. The  $\omega_2$  binding to *parS* site leads to active  $\omega_2$ –*parS* short–living partition complex (PC1, rectangles and ring areas coloured in yellow). The cycle graph of  $\delta_2$  states is included in the green circle area. Different active or inactive forms of the  $\delta_2$  depend on the nucleotide and DNA binding as shown in the light grey area in the middle of  $\omega_2$  and  $\delta_2$  singles forms. Dashed arrows emphasize the preferred direction of transition states. The orange arrow underlines the stimulation of ATP hydrolysis.

The resulting  $\delta_2$ -ADP state will lose affinity for the nucleoid and disassembly of the paired molecules. It is likely that the  $\delta_2$  transition from ATP to ADP -bound state triggers a chain of events that would lead to BCs disassembly toward the initial PC1 complex (BC $\rightarrow$ SC $\rightarrow$ PC2 $\rightarrow$ PC1) (Fig. 46B). Although our results failed to detect  $\delta_2$ -ADP or  $\delta_2$  free in the cytosol, we assumed that discrete  $\delta$ :GFP<sub>2</sub>-ADP or  $\delta$ :GFP<sub>2</sub> molecules, free in solution, are not sufficient to provide a clear fluorescent signal even in the presence of a large excess of  $\delta_2$ . The  $\delta_2$ -ADP will exchange the nucleotide with ATP to rejuvenate toward a nsDNA competent state.

The disassembly of  $\delta_2$  from plasmid-nucleoid paired complex decreases the  $\omega_2$ : $\delta_2$  ( $\omega_2 > \delta_2$ ) ratios that in turn decreased  $\omega_2$ -mediated hydrolysis of ATP and  $\delta_2$  re-assembles in a different region after nucleotide (Fig. 47). The dynamics of  $\delta$ D60A:GFP<sub>2</sub> fluorescence, which leads to discrete foci and patched structures, as well as to areas lacking fluorescence occur in the absence of ATP hydrolysis. Similar results were suggested for the F-SopA ATPase that can show an oscillate pattern in the absence of ATP hydrolysis (Ah-Seng et al. 2013). These results indicated that  $\delta_2$ D60A facilitates plasmid pairing through its re-localization towards PC2 but also demonstrate its inability to disassemble the paired complexes that results in a partition defect. These findings highlighted that plasmid tethering disassembly is crucial and this step needs an ATP-dependent reaction.



**Figure 47. Schematic representation of cellular plasmid partition.**

$\omega_2$  (red circles) can be bound to a *parS* sites (yellow stripe) (PC1).  $\delta_2$  exists in two forms: the ATP -bound form free in the cytosol or bound to the nucleoid (DC) (grey and green circles respectively) and the ADP -bound form (grey squares). The interaction between  $\omega_2$ -plasmid complexes and  $\delta_2$ -ATP bounded lead to plasmid pairing (BC), the interaction and the continually changing local stoichiometry stimulates the  $\delta_2$  ATP hydrolysis and its conversion in the diffusible that will promote plasmid pairing disassembly (I). Once the separated plasmids are free to move towards the nearest high concentration of  $\delta_2$  on the nucleoid (BC1). The ATP hydrolysis will generate a diffusion gradient of  $\delta_2$  on the nucleoid that will move away the plasmids at the early stage of partitioning (II). The movement of single plasmid continues toward local high concentration of  $\delta_2$  (III and IV). For simplicity only one *parS* site for each plasmid and only one plasmid molecule are paired on the nucleoid. It worth to notice that more than one plasmid could be paired on nucleoid.

Following the disassembly, the regenerated individual  $\omega_2$ -*parS* complexes (PC2) should ratchet along the newly formed cloud of  $\delta_2$ -nsDNA (DC) that could be seen as a transportation of plasmid molecules to a distant location on the nucleoid following an oscillating wave of  $\delta_2$  binding and release from the nucleoid (Fig. 47). By this cyclic process, the  $\omega_2$ -*parS* complexes actively move towards the newly separated nucleoids, and positioned them, so at cell division into each daughter cell should receive at least one plasmid copy.

## 2. The global $\omega_2$ regulator.

The mechanism by which  $\omega_2$  binds co-operatively to their cognate sites (composed by two or more consecutive heptads repeats) promoting the formation of short-living complex (PC1) and repressing the promoter utilization were widely investigated through structural and biochemical studies *in vivo* and *in vitro* (Fig. 48A) (de la Hoz et al. 2000, de la Hoz et al. 2004, Weihofen et al. 2006, Pratto et al. 2008, Soberon et al. 2011). Nevertheless, the mechanisms by which the  $\omega_2$  transcriptional regulator controls copy number fluctuation and faithful plasmid segregation plasmid were poorly characterized.

Protein  $\omega_2$  negatively regulates the expression CopS (see Fig. 4). CopS (also termed CopF, CopR, etc.) is a transcriptional repressor, which in concert with the antisense RNA (RNAIII), control plasmid replication by regulation the level of RepS (Brantl and Wagner 1997). Once  $\omega_2$  binds the upstream  $P_{copS}$  region it is able to inhibit *copS* gene expression that corrects any downward fluctuations (de la Hoz et al. 2000, Bingle and Thomas 2001, del Solar et al. 1996). The half-life of the CopR· $P_{II}$  and  $\omega_2$ · $P_{copS}$  DNA complexes is short ( $t_{1/2}$  70 and 30 s) is 20 to 40-fold, respectively, lower than that of the RNAP· $P_{II}$  and  $\omega_2$ · $P_{copS}$  complexes (de la Hoz et al. 2004, Licht, Freede and Brantl 2011), suggesting that *repS* repression requires a constant synthesis of the CopS protein and a down regulation of the *copS* gene leads to an increase in the initiation factor with subsequent increment in plasmid copy number. Thus,  $\omega_2$ -mediated down regulation of CopS de-represses transcription of the *rep* mRNA and indirectly decreases transcription of the antisense RNAIII (de la Hoz et al. 2000, Welfle et al. 2005, Weihofen et al. 2006). Indeed, repression of CopS synthesis by  $\omega_2$  correlates with an increase in plasmid copy number and indirectly ensures stable plasmid maintenance. It is likely that the interplay of RNAIII, Cop and  $\omega_2$  are part of a negative-feedback control system of the minimal replicon of Inc18 plasmids (Brantl and Behnke 1992b, Brantl and Wagner 1994, Brantl and Wagner 1997, Le Chatelier, Ehrlich and Janniere 1994).

In this work, we report the analysis of how the symmetric  $\omega_2$  transcriptional regulator binds to its cognate site to activate transcription at sub-stoichiometric amounts, and then represses it at stoichiometric amounts without occluding RNAP- $\sigma^A$  accessibility to the promoter region. The data suggests that transcriptional activation takes place before repression (Fig. 41 and Fig. 42). The  $\omega_2$  global transcriptional regulator activates transcription initiation by stimulating  $RP_C$  formation and the subsequent isomerization to  $RP_O$  due to a direct contact of the RNAP- $\sigma^A$  with  $\omega_2$ , and to inhibit mRNA synthesis from  $P_\omega$  by blocking  $RP_O$  formation (see the model in Fig. 48B, 48C and 48D). The transcription activation activity of  $\omega_2$  seems to further stimulate by the addition of limiting  $\delta_2$  concentrations (Fig. 40B). The repression activity is observed in the presence of full occupancy of the  $\omega_2$  operator site. At stoichiometric concentrations  $\omega_2$  represses mRNA synthesis of the regulated promoters (Fig. 48B vs. 48D). The regulation of Firmicutes RNAP- $\sigma^A$  by  $\omega_2$  (or  $\omega_22$ ) defines an as yet uncharacterized mechanism by which bacterial transcription is regulated.

### 2.1. The dual behaviour of the $\omega_2$ regulator.

Sequence analyses predict that there are over 2000 proteins containing RHH domains found in bacteria and its bacteriophages (phages), but less than 1% these proteins have been studied with structural or biochemical techniques (Schreiter and Drennan 2007). The majority of dimeric RHH ( $RHH_2$ ) proteins are transcriptional repressors, but four of them (namely a P22-Arc variant, AmrZ [AlgZ], NikR and  $\omega_2$ ) work as both activators and repressors at different promoters (Schreiter and Drennan 2007). Unlike  $\omega_2$ , P22-Arc, AmrZ and NikR can bind with different affinity to different promoters in concert with other putative regulators or different metal stoichiometry, and they can function as repressors when bind to a set of promoters and as activators when bind to another set of promoters (Smith and Sauer 1996, Schreiter et al. 2003, Pryor et al. 2012). However, the strategies employed by P22-Arc, AmrZ and NikR proteins to work as transcriptional activator and/or repressor are still poorly understood.

As reported,  $\omega_2$  bound with high affinity and co-operativity to its cognate site embedded in the promoter region of the  $\omega$  gene ( $P_\omega$ ) and with an apparent binding constant ( $K_{Dapp}$ ) of  $\sim 6$  nM. As derived from the co-crystal structure (PDB: 2BNZ, 2BNW and 2CAX),  $\omega_2$  binding to its operator site narrowed the minor groove and making it insensitive to DNase I attack (protection model, Fig. 48A) (de la Hoz et al. 2004, Weihofen et al. 2006). *B. subtilis* RNAP- $\sigma^A$  was also demonstrated to specifically bind  $P_\omega$  DNA with  $K_{Dapp}$  of  $\sim 25$  nM, making an extensive contact with the upstream region with a clear hyper-sensitive site at position  $-37$  (Fig. 48C) (de la Hoz

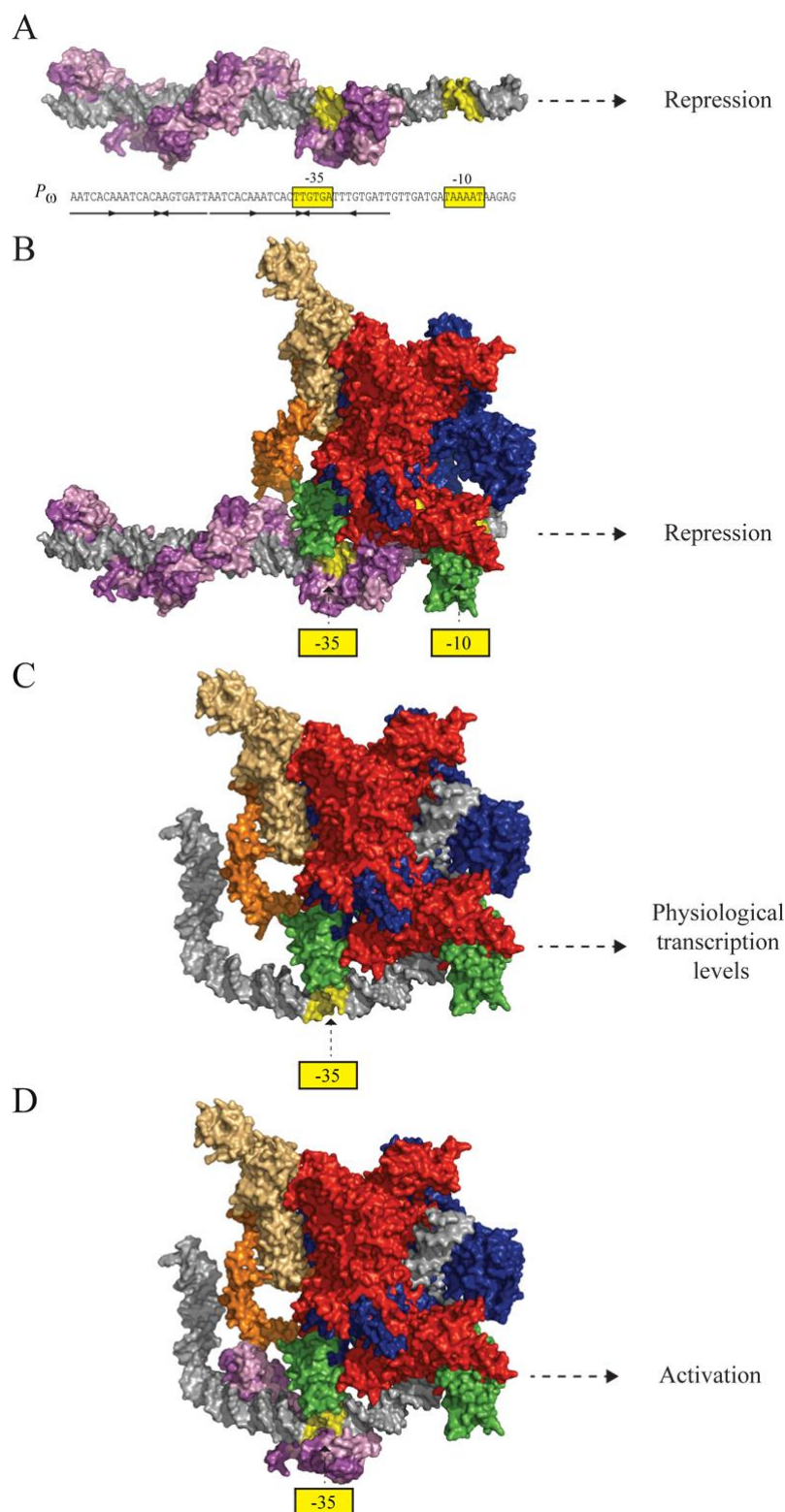
et al. 2000, de la Hoz et al. 2004). The  $\omega_2$  and RNAP- $\sigma^A$  binding sites overlap in the  $P_\omega$ ,  $P_\delta$  and  $P_{\text{copS}}$ . As revealed in (Fig. 1 and 4A),  $P_\omega$  DNA contains a series of seven 7-bp repeats at position -21 to -69 (relative to the start site, +1). The RNAP- $\sigma^A$  binding region is at position -47 to +18 (de la Hoz et al. 2000, de la Hoz et al. 2004). According the published data, we can infer that the region ranging -69 and -21 should be strictly involved in the promoter regulation, this region included the -35 specific sequence that is recognize by the  $\sigma^A$  transcription factor.

Our data revealed a synergism between the  $\omega_2$  and RNAP- $\sigma^A$  for binding and thereby it was a first evidence that both protein interact and suggested they can co-exist at  $P_\omega$ , region. EMSA experiment performed in presence of ATP affirmed that  $\delta_2$ ,  $\omega_2$  and RNAP- $\sigma^A$  can co-exists altogether at promoter regions leading to formation of slow mobility complexes, suggesting a possible role of  $\delta_2$ . We found that  $\delta_2$  per se affected the  $P_\omega$  utilization in run-off experiments. Since the run-off experiment must be done in presence of ATP, we believe that  $\delta_2$  alone will bind to the DNA sequence probably halting the progression of RNAP- $\sigma^A$ . Supporting this hypothesis, we did not detect synergistic effect for  $\delta_2$  and RNAP- $\sigma^A$ , neither through specific interaction neither through inhibition of RNAP- $\sigma^A$  transition from  $\text{RP}_C$  to  $\text{RP}_{\text{INIT}}$  complexes.

The most significant result indicated that the  $\omega_2$  is currently the only characterized RHH<sub>2</sub> proteins that can activate and repress the utilization of the same promoter, at least in a simplified *in vitro* system, on the basis of operator occupancy (Fig. 48). In fact, limiting  $\omega_2$  concentrations facilitate  $\text{RP}_C$  formation and increase the rate of isomerization from  $\text{RP}_C$  to  $\text{RP}_O$  complexes (transcription activation, Fig. 42A and Fig. 42B). Stoichiometric and/or saturating  $\omega_2$  concentrations inhibit  $\text{RP}_O$  formation, and any subsequent steps (e.g.,  $\text{RP}_{\text{INIT}}$ ) (transcriptional repression) (Fig. 48A, 48D). An important role in  $P_\omega$  utilization and transition to  $\text{RP}_O$  to  $\text{RP}_{\text{INIT}}$  is also played by existence of RNAP- $\sigma^A$ - $P_\omega$  DNA preformed complexes. In fact, when stoichiometric  $\omega_2$  concentrations were added after RNAP- $\sigma^A$ ,  $\omega_2$  has a moderate effect in counteracting  $\text{RP}_O$  complexes (Fig. 41), indicating that the regulation mechanisms of  $\omega_2$  might occurs between the  $\text{RP}_I$  and the  $\text{RP}_O$  steps.

Altogether our data are suggesting that regulation of RNAP- $\sigma^A$  transcription by the broad-host-range  $\omega_2$  regulator define an uncharacterized mechanism by which Firmicutes transcription is regulated. We favour the hypothesis that the interaction of  $\omega_2$  with its cognate sub-saturated site and with RNAP- $\sigma^A$  could position it to a location favourable for efficient  $\text{RP}_O$  formation (activation), and increasing  $\omega_2$  concentrations induce a nearly straight DNA conformation and

the interaction with RNAP- $\sigma^A$  could reposition to a location unfavourable for efficient RP<sub>O</sub> formation.



**Figure 48 Three-dimensional model of  $\omega_2$  and RNAP- $\sigma^A$  bound to  $P_o$  DNA.**

(A) Structural model of  $\omega_2$ -bound to  $P_o$  DNA derived from the 3D co-structure of minimal operator site and  $\omega_2\Delta N19$  (1IRQ PDB). Pink/purple  $\omega_2$  forms as left-handed protein-matrix winding around the nearly straight operator DNA. The DNA in space filling is denoted in grey with the -35 and -10 elements in yellow. (B) Cartoon depicted the RNAP- $\sigma^A$ -bound to  $P_o$  DNA and saturating  $\omega_2$  concentrations bound to its cognate site and docked to RNAP- $\sigma^A$ . Structural model of RNAP- $\sigma^A$  was derived from the structure of *T. aquaticus* (PDB: 1L9U) and  $P_o$  DNA from (PDB: 1IRQ). The -35, -10 elements in the promoter DNA are coloured in yellow. (C) The RNAP- $\sigma^A$  is depicted in cartoon representation based on the X-ray crystal structure of the homologous *T. thermophilus* complex with DNA (PDB: 4G7H) and the model of the RP<sub>O</sub> previously proposed (Vassilyev et al. 2002, Vassilyev et al. 2007b, Murakami et al. 2002a) was used as a starting point to create the images. The -35 element is coloured in yellow. (D) Cartoon depicted the RNAP- $\sigma^A$ -bound to  $P_o$  DNA in the presence of limiting  $\omega_2$  concentrations. Brown and light brown  $\alpha_2$ ; blue,  $\beta$ ; red,  $\beta'$  and green,  $\sigma$ . The modelled structures were prepared with PyMol.

Since,  $\omega_2$  binds with slightly higher affinity and co-operativity to two contiguous heptads in the  $\rightarrow\leftarrow$  than in the  $\rightarrow\rightarrow$  orientation (de la Hoz et al. 2000), we thought that the  $\rightarrow\leftarrow$ -heptads, which overlaps with the  $-35$  element and its neighbours, will be bound by  $\omega_2$  and the  $\omega_2$ -RNAP- $\sigma^A$  interaction might occur at the pre-recruitment state. Thereby we hypothesize that in the presence of limiting concentrations,  $\omega_2$  bound to one of its primary binding sub-sites at the  $-35$  element will interact with the  $\beta'$  subunit of RNAP- $\sigma^A$  leading to formation of the ternary ( $\omega_2$ - $P_\omega$ -RNAP- $\sigma^A$ ) complex. However, this ternary complex might promote a DNA distortion that might increase the local concentration of both proteins. These ternary complex facilitates the rate of isomerization from  $RP_C$  to  $RP_O$ , and increases mRNA synthesis from  $P_\omega$  (Fig. 48C and 48D). In the presence of stoichiometric  $\omega_2$  concentrations (full operator occupancy),  $\omega_2$  assembles as a left-handed protein helix wrapping around the nearly straight  $P_\omega$  DNA and facilitates RNAP- $\sigma^A$  accessibility to  $P_\omega$  DNA ( $RP_C$  formation) (Fig. 48A and 48B). In the presence of saturating  $\omega_2$  concentrations  $RP_C$  cannot isomerize to  $RP_O$ .

It is likely that the  $\omega_2$  activator acts as an anchor for RNAP- $\sigma^A$  to  $P_\omega$  DNA, and the increase affinity of  $\omega_2$  on the DNA increases the subsequent RNAP- $\sigma^A$  isomerization leading to transcription activation. Although more studies are need to prove the involvement of  $\delta_2$  in the stimulation of promoter utilization, it seems that limiting  $\delta_2$  concentrations, which increases the half-life of the  $\omega_2$ - $P_\omega$  DNA complex could further increases  $P_\omega$  utilization.

We can image several possibilities to explain this specific transcriptional repression: i) the interaction of left-handed  $\omega_2$  with RNAP- $\sigma^A$  could reposition the RNAP holoenzyme to a location unfavourable for efficient  $RP_O$  to occur; ii) the interaction of left-handed  $\omega_2$  with RNAP- $\sigma^A$  could “lock” it in a conformation unfavourable for  $RP_O$  formation; and iii) the interaction of left-handed  $\omega_2$  with RNAP- $\sigma^A$  could antagonise interactions between the  $\beta'$  N-terminal domain and DNA that might be an essential step for  $RP_O$  formation and stability. We have ruled out steric hindrance. Since (a)  $RP_C$  formation was stimulated by the  $\omega_2$ -RNAP- $\sigma^A$  interaction, but the subsequent isomerization through an unstable intermediate ( $RP_I$ ) to render the stable  $RP_O$  is inhibited, and (b)  $\omega_2$  can establish interactions with its operator site when RNAP- $\sigma^A$  is already bound to  $P_\omega$  DNA, but  $\omega_2$  fails to inhibit the pre-formed  $RP_O$ , we favour options (i) or (ii). Our findings delineate the basic molecular mechanism for the direct modulation of RNAP- $\sigma^A$  transcription activity by  $\omega_2$  alone or in concert with  $\delta_2$ . They also provide an essential framework for understanding  $\omega_2$  *in vivo* role in controlling plasmid copy number and stability systems.



## 2.2. Interplay between the regulator and $\beta'$ subunits of RNAP- $\sigma$ .

The majority of the transcription regulators (activators or repressors) bind to  $\sigma$ ,  $\alpha$ -CTD or  $\beta$  subunit of RNAP- $\sigma$  to regulate transcription (Rhodius and Busby 1998, Hochschild and Dove 1998, Benoff et al. 2002, Browning and Busby 2004).

The work presented here establishes that  $\omega_2$ , as a global regulator, represents an additional exception to the major prokaryotic transcription regulation paradigm. Protein  $\omega_2$  binds to the RNAP  $\beta'$  N-terminal domain, positioning  $\omega_2$  to sense the unique DNA conformation presented at the upstream edge of the transcription bubble in  $RP_0$  (see Fig. 48C and 48D). From the molecular masses of the polypeptides 1–2, 3–4 and to 5 (Fig. 45C) that interacts with  $\omega_2$  as a bait, and the localization of their variable C-terminus the mapping of the  $\beta'$ -rudder and  $\beta'$ -Sw2 regions might be uncertain. We have assumed that part of the  $\beta'$ -rudder region is localized in these polypeptides with observed molecular masses from 33 to 35 kDa (Fig. 45C), although the estimated mass for a protein containing the full  $\beta'$ -rudder and the  $\beta'$ -Sw2 region should be 36.2 kDa and 39.2 kDa, respectively. It is unlike, therefore, the presence of the  $\beta'$ -Sw2 and an intact  $\beta'$ -rudder. This target in the  $\beta'$  N-terminal region contains the A and B (also termed b1, b2 and b3) regions (residues 1 to 316 derived from *B. subtilis*  $\beta'$  subunit). The  $\beta'$  N-terminal end includes the ZDB (residues 53–81), the  $\beta'$ -clamp (215–220), and the pincer. The pincer includes the  $\beta'$ -coiled coil domain (254–299), the major binding site for the  $\sigma$  subunit, and two loops ( $\beta'$ -lid [240–252] and ( $\beta'$ -rudder [296–316]) (Fig. 8) (see Murakami et al. 2002a, Vassilyev et al. 2002, Vassilyev et al. 2007a, Zhang et al. 2012). Few other regulatory protein interacts with the  $\beta'$  subunit RNAP. Most of them are primarily from proteobacterial phages. Phage Xp10 p7 factor interacts with the first 10 residues of the N-terminal region of the  $\beta'$  subunit RNAP (Yuzenkova, Zenkin and Severinov 2008); Mu C protein with part of region F (b7) (Swapna et al. 2011); T7 Gp2 with the jaw (b9–b10) domain and also with  $\sigma$  1.1 domain (James et al. 2012, Bae et al. 2013); and N4 SSB interacts with part of region H (b11) at C-terminal end (Miller et al. 1997). These regulators neither share a specific target domain nor a common mode of action among them. They contact either the  $\beta'$  subunits of RNAP- $\sigma$  upon DNA binding, as Mu C (Swapna et al. 2011); in solution and the interaction is stabilized upon DNA binding, as  $\omega_2$ , or in solution by proteins that do not bind DNA, as N4 SSB, T7 Gp2 and Xp10 p7 (Miller et al. 1997, Camara et al. 2010, Yuzenkova et al. 2008). Furthermore, they show a different mode of action: N4 SSB and Mu C protein specifically acts as transcription activators (Miller et al. 1997, Swapna et al. 2011),  $\omega_2$  shows a dual activity, and T7 Gp2 and Xp10 p7 work as a transcriptional

repressor (James et al. 2012, Yuzenkova et al. 2008). Notably Xp10 p7 also were described to prevent transcription termination (Yuzenkova et al. 2008).

T7 Gp2 (James et al. 2012, Bae et al. 2013), Xp10 p7 (Yuzenkova et al. 2008), and  $\omega_2$  acts at the early stages of RNAP- $\sigma$  isomerization, whereas N4 SSB or Mu C exerts its affect at latter stages (Miller et al. 1997, Swapna et al. 2011). These regulators that act at early stages, which pursue a different mode of action, have no effect on pre-formed RNAP- $\sigma$ - $P$  DNA complexes. The biggest difference between T7 gp2 and Xp10 p7 with  $\omega_2$  is the ability of the latter to activate transcription initiation upon DNA binding (Fig. 48D). Indeed, T7 Gp2 binds to the  $\beta'$ -jaw and  $\sigma$  R1-1 regions and repress transcription without binding to DNA (Bae et al. 2013). T7 Gp2 inhibits RP<sub>O</sub> formation when added prior *E. coli* RNAP- $\sigma^{70}$ , but it has no effect on preformed RP<sub>O</sub> complexes as reported for  $\omega_2$  (Camara et al. 2010).

On the other side, the positioning of  $\omega_2$  and the  $\beta'$  mobile module RNAP- $\sigma^A$  with respect to  $P_{\omega}$  DNA, allowed us to hypothesize that the  $\omega_2$  central region (residues 34 to 56), which includes the  $\alpha 1$  domain, the  $\alpha 1$ - $\alpha 2$  loop or the conserved N-terminal part of the  $\alpha 2$  domain, might be involved in the interaction interact with the  $\beta'$  N-terminal end (residues 1-316) (see appendix, paragraph 2.2.). In this region the dimer-dimer and the monomer-monomer interface were mapped in the conserved ( $\alpha 1$ ) region, that is stabilized by the conserved region of the  $\alpha 2$  domain and hydrophobic side-changes between both  $\alpha$ -helices (Murayama et al. 2001b, Weihofen et al. 2006). The electrostatic properties and this conserved regions suggested that it should face charged residues in the  $\beta'$  subunit of RNAP- $\sigma^A$ . We tested by single point mutation to alanine the most relevant charged residues in  $\alpha 1$ - $\alpha 2$  domain *in vivo*. In fact, we observed that the repression of  $P_{\delta};lacZ$  was only slight reduced for the  $\omega_2$ D56A variant, suggesting a potential role in the interaction with RNAP- $\sigma^A$ . The D56 residues might also essential for correct folding of  $\omega_2$  protein or protein-DNA interaction. Unfortunately our data do not help us to draw any further conclusion, studies to map the residues on  $\omega_2$  that establish the interaction with the  $\beta'$  N-terminus are needed.

Our findings uncover a novel regulatory mechanism and support the view that the  $\beta'$  N-terminal domain is a target site for the  $\omega_2$  regulatory protein. We present a first model, which explains  $\omega_2$ -mediated transcriptional regulation, but despite the substantial progress in delineating new insight about the basic molecular mechanism for the direct modulation of RNAP- $\sigma^A$  transcription activity by  $\omega_2$ , many questions remains to be solved.

## ***Conclusions***



- 1- The C-terminal region of  $\delta_2$  interact with nsDNA. This region is neither essential for  $\delta_2$ - $\omega_2$  or  $\delta_2$ - $\delta_2$  interaction nor ATP binding, but is necessary for ATP hydrolysis.
- 2- The interaction of  $\omega_2$ -bound to *parS* with  $\delta_2$  facilitates structural transition in both proteins and at stoichiometry ratios the ATPase activity is also stimulated.
- 3- The end-terminal region of  $\omega_2$  interacts with the central region of  $\delta_2$ . The central region of  $\delta_2$  is also required for  $\delta_2$ - $\delta_2$  interaction. The  $\omega_2$ - $\delta_2$  and  $\delta_2$ - $\delta_2$  interacting domains are juxtaposed but distinct from each other
- 4- There are different types of *parS*- $\omega_2$ - $\delta_2$ -nsDNA quaternary complex and its formation require ATP binding, but not hydrolysis. At sub-stoichiometric concentrations the quaternary complex lead to plasmid pairing, but stoichiometric concentrations stimulates ATP hydrolysis and disassembly of the quaternary complex. In the ADP-bound form  $\delta_2$  rejuvenate to the ATP-bound form with subsequent reformation of blobs structures on nsDNA.
- 5- Protein  $\omega$ :YFP<sub>2</sub> binds to plasmid-borne *parS* and forms discrete foci, and  $\delta$ :GFP<sub>2</sub> binds to nsDNA and forms clouds of fluorescence on the nucleoid. The interaction of  $\omega$ :YFP<sub>2</sub> bound to *parS* with  $\delta$ :GFP<sub>2</sub> facilitates plasmid capture and tethering towards the nucleoid.
- 6- The continuous cycle of  $\omega$ :YFP<sub>2</sub>- $\delta$ :GFP<sub>2</sub> interaction, the hydrolysis of ATP, the disassembly of the paired complex and the subsequent disassembly facilitate plasmid segregation.
- 7- The  $\omega_2$  cognate *parS* site maps upstream of the promoter (*P*) of *copS*,  $\delta$  and  $\omega$  genes. *parS*-bound  $\omega_2$  show two outcomes: at sub-stoichiometric ratios activate, and at stoichiometric ratios repress transcription.
- 8- Protein  $\omega_2$  cooperatively interacts with  $P_\omega$  DNA,  $\delta_2$  and RNAP- $\sigma^A$ . Such protein-DNA and protein-protein interaction are necessary and sufficient for transcriptional activation and repression.
- 9- Protein  $\omega_2$  facilitates RP<sub>C</sub> formation, but preclude isomerization to RP<sub>O</sub> formation.
- 10- Protein  $\omega_2$ -bound to  $P_\omega$  DNA interacts with the N-terminal region of the  $\beta'$  subunit of RNAP- $\sigma^A$ . This is the first report describing such interaction.



## *Acknowledgements*

±





I would like to sincerely thank Prof. *Juan C. Alonso* for his guidance, understanding, and his advice during my studies and researches. I am very grateful to him for giving me the opportunity to learn so many things. This experience was an opportunity to develop my skills and grown from professional as well as human points of view.

I am very thankful to Prof. *Silvia Ayora*, for her valuable suggestions, assistance and for agreeing to be the mentor of my thesis.

I also thank *Virginina Liroy* & *Nora E. Soberón* for the teaching and help they provided to me at the beginning of this doctoral thesis. Their work was fundamental for the better understanding of pSM19035 partition system. In particular, *Vicky* carried out most of the cytological analysis, whereas *Nora* purified several proteins and she has been essential in many biochemical outcomes reported in this thesis. *Mariagela Tabone* helped me with her experiments to complement the preliminary results on the characterization of  $\omega_2$   $\alpha 1$ - $\alpha 2$  domains *in vivo*.

A special thanks to *Begoña Carrasco* (the “guru” of the Lab.). She provided valuable suggestions for protein purifications but also realized the transcription run-off experiment present in this work.

I would thank Dr. *Rudy Lurz* and *Beatrix Fauler* at Berlin Max Plank Institute for Molecular Genetics for providing me technical assistance and support for Electron Microscopy experiments during my stay in Berlin.

Special thanks to the Comunidad de Madrid for its fellowship (CPI/0266/2008) that allowed me to live great experiences in Spain.

I am grateful to *Paolo Natale* for his support and advices that helped me to complete this experience positively.



## *Appendixes*



## 1. List of Publications.

### Published:

- N. E. Soberón, V. S. Lioy, F. Pratto, **A. Volante** & J.C. Alonso.  
*Molecular anatomy of the Streptococcus pyogenes pSM19035 partition and segrosome complexes.*  
Nucleic Acids Res 2011, 39, 2624–37.
- **A. Volante**, N.E. Soberón, S. Ayora and J.C. Alonso.  
*The interplay between different stability systems contributes to faithful segregation: Streptococcus pyogenes pSM19035 as a model,* Microbiol Spectrum. Aug 2014.

### Submitted:

- V.S. Lioy, **A. Volante**, N.E. Soberón, R. Lurz, S. Ayora and J. C. Alonso.  
*Dissection of the dynamic ParAB plasmid partition machinery in Firmicutes.* Environ. Microbiol.
- **A. Volante** and J. C. Alonso.  
*Functional interactions of ParA and ParB during plasmid partitioning in Firmicutes.* Nucleic Acids Res.

### In preparation:

- **A. Volante**, B. Carrasco, M. Tabone, S. Ayora and J. C. Alonso.  
*Dual control of open complex formation by global  $\omega_2$  regulator upon interacting with the  $\beta'$  N-terminal domain of RNA polymerase.*

## 2. Playing with bioinformatics.

### 2.1. *In silico* analysis of $\omega_2$ and $\delta_2$ proteins.

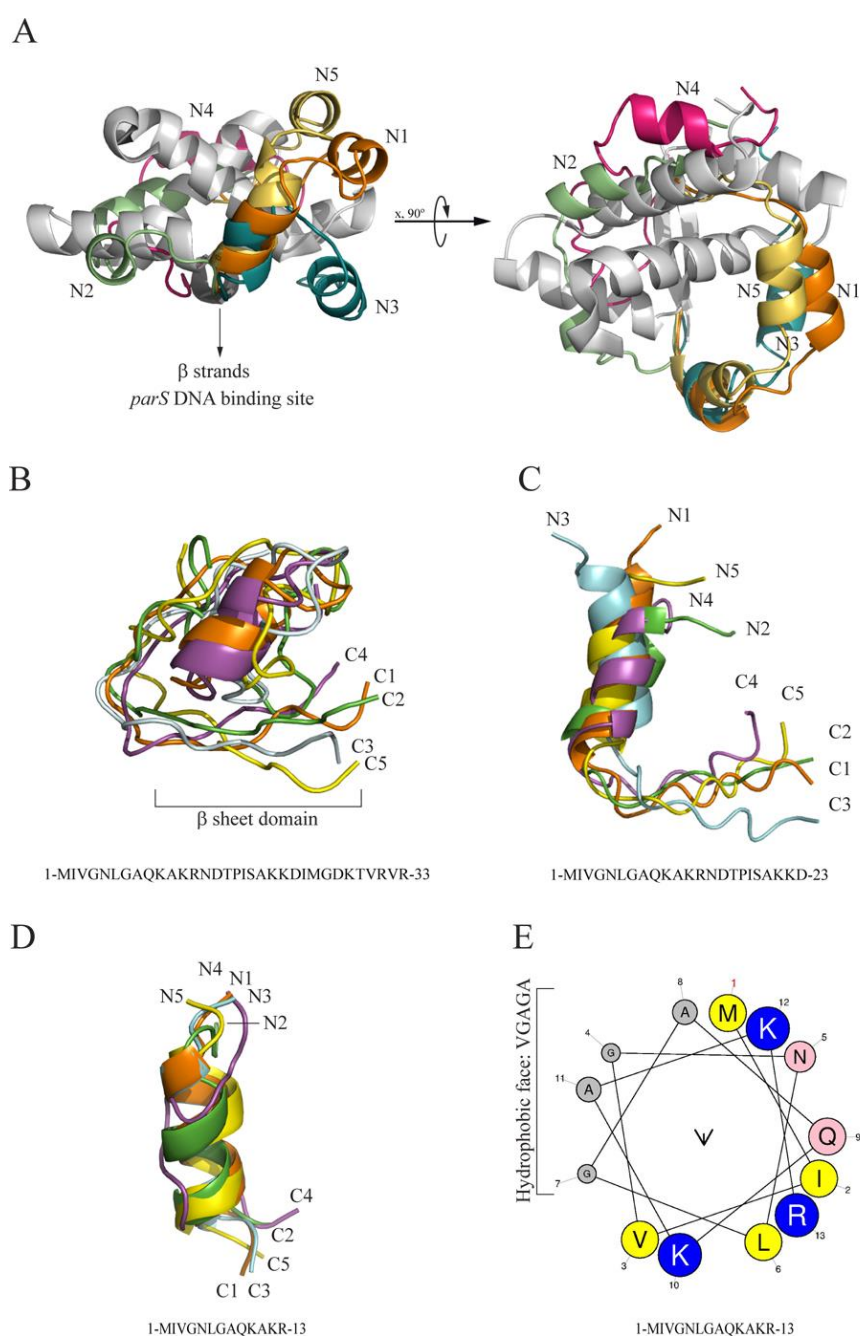
The N-terminal region of  $\omega_2$  plays an essential role in plasmid segregation by mediating the interaction with  $\delta_2$ . Unfortunately, the structure of the first 19 residues of protein is not resolved in the crystal structure. With the intention to investigate the possibility of how the N-terminal region can be structured and positioned around the RHH<sub>2</sub> central domains, the structure of full-length  $\omega$  was predicted by I-TASSER platform (Roy et al. 2010). Up to five full-length atomic models of  $\omega$  monomers were obtained and superimposed to the crystal of  $\omega\Delta N19$ . As expected, the regions containing the RHH domains overlapped completely with the crystals. The N-terminal tails of full-length models formed 1 or 2  $\alpha$ -helix structures and their position assumed different conformations respect to the RHH domain of the protein (Fig. 49A).

These predictions are not totally reliable because they do not take into account that the functional unit of  $\omega$  protein is a dimer, in fact if the models are superimposed over one monomer of the  $\omega\Delta N19$  dimer, the N-termini are colliding with the C-terminus of second monomer of  $\omega\Delta N19$  (Fig. 49A). To overcome this inconvenience and to see whether the length could influence the structures of the N-terminus, three different polypeptides of 33, 23 and 13 residues in length were submitted to I-TASSER (Fig. 49B, 49C and 49D). The larger portion (1–33aa) was chosen because it contained at the C-terminus the residues forming the  $\beta$ -strand (27–32) that could possibly be attached and modelled into the  $\omega$  crystal. As observed, the resulting structure revealed N-terminal regions very disordered that seemed to falling back on the  $\beta$ -strands (Fig. 49B). Even in this case, a reliable model cannot be predicted. However, the prediction of shorter amino acids sequences suggested how the region encompassing the residues 3 to 11 might form  $\alpha$ -helix structures (Fig. 49C and 49D). We follow the hint that the first 13 residues could form an  $\alpha$ -helix structure and we use HELIQUEST to calculate from the first 13 amino acid residues of  $\omega$  its physicochemical properties (Gautier et al. 2008). As observed in Figure 49E, an N-terminus  $\alpha$ -Helix will lead the formation of a hydrophobic surface composed by VGAGA residues of the chain.

This observation might be considered as a working hypothesis for further mechanistic studies about the  $\omega_2$ - $\delta_2$  interaction, because the  $\alpha$ -Helical coiled coils are usually versatile protein domains, supporting a wide range of biological functions.

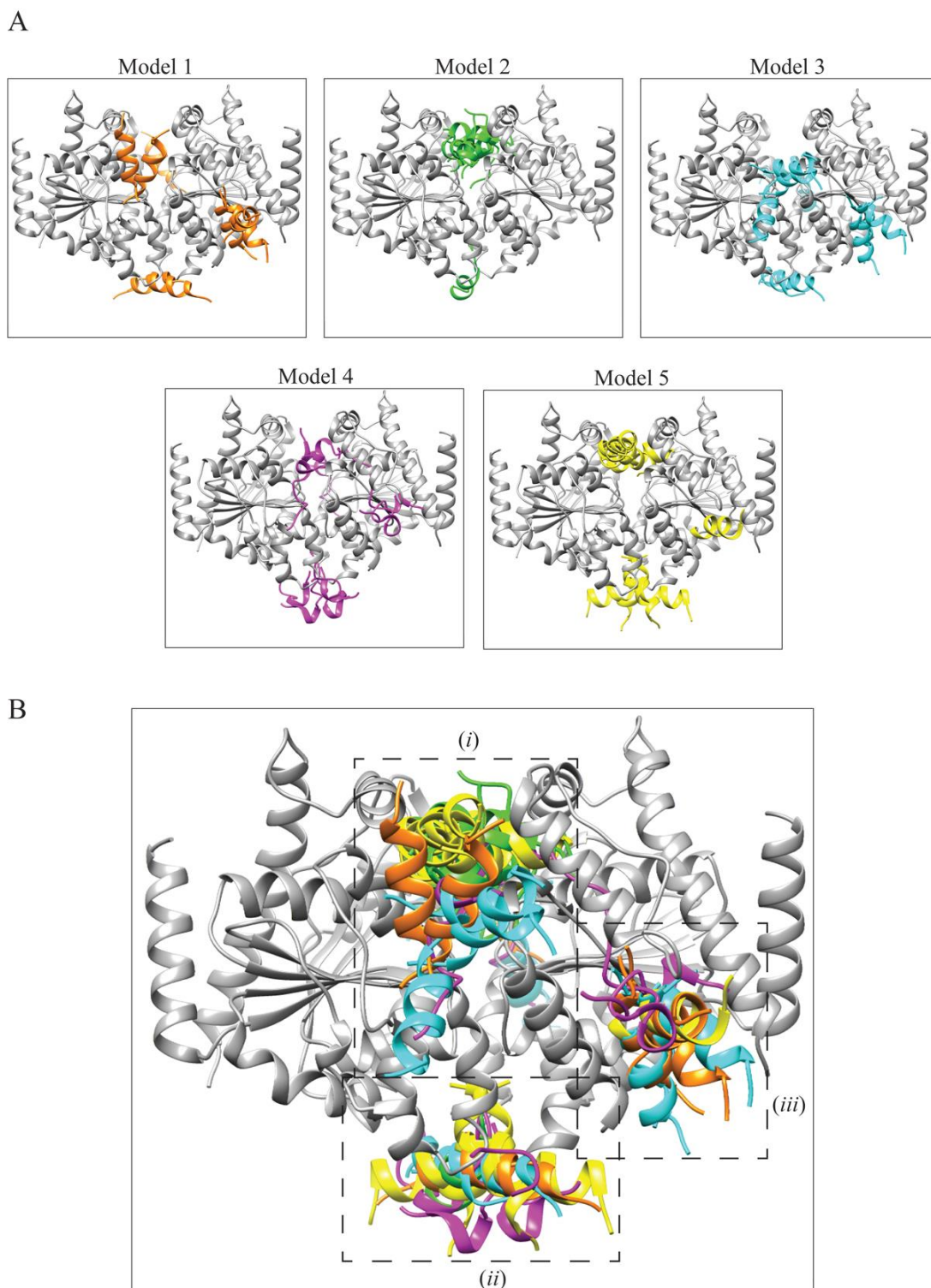
We further investigate whether a hypothetical  $\alpha$ -helix at the N-terminus could interact with the structure of  $\delta_2$  dimer. The N-terminal models obtained in Figure 49D were independently used for searching the best rigid protein-protein docking (Tovchigrechko and Vakser 2006). In this *in silico* analysis, the  $\delta_2$  was considered as “receptor” and the  $\omega$  N-terminus models as

“ligand” proteins. Up to 10 spatial configurations were obtained for each set of “ligand” (Fig. 50A). The resulting simulations revealed three main regions of  $\delta_2$  potentially involved in the interaction with the putative N-terminal of  $\omega_2$ : (i) the tip of the U-shaped  $\delta$  dimer ( $\alpha_3$ ,  $\alpha_6$ ,  $\alpha_{10}$  and  $\alpha_{11}$  that are near or in between the nsDNA domain), (ii) the bottom of U-shaped structure ( $\alpha_6$ ,  $\alpha_7$ ), and (iii) the lateral domain of  $\delta$  monomer ( $\alpha_9$ ,  $\alpha_{12}$ ) (Fig. 50B). Interesting, two of these big regions are situated in the  $\delta$  dimer interface and this hypothetical models are partially in agreement with the results presented in this work.



**Figure 49. Structure predictions of  $\omega$  N-terminal domain.**

(A) The full-length prediction of  $\omega$  protein. The five models of N-terminus are coloured in orange, green, cyan, magenta and yellow. The functional core of RHH<sub>2</sub> is coloured in grey. The five independent I-TASSER models of 1–33aa (B), 1–23aa (C) and 1–13aa (D) residues are represented and superimposed. (E) The visualization of hypothetical  $\alpha$ -Helix structure (1–13aa). The non-polar (yellow), the hydrophobic (grey), the polar (pink) and positively charged (blue) residues are schematically represented.



**Figure 50. The predictive docking between  $\delta_2$  and the  $\omega$  1–13aa N-terminus.**

(A) Single results of  $\omega$ – $\delta_2$  docking are shown for each N-terminus models of  $\omega$ . The  $\delta_2$  “receptor” structure is in grey whereas the “ligand” models are coloured by orange, green, cyan, magenta and yellow. (B) The summary of all docking and the three principal region of  $\delta_2$  affected by the simulations.

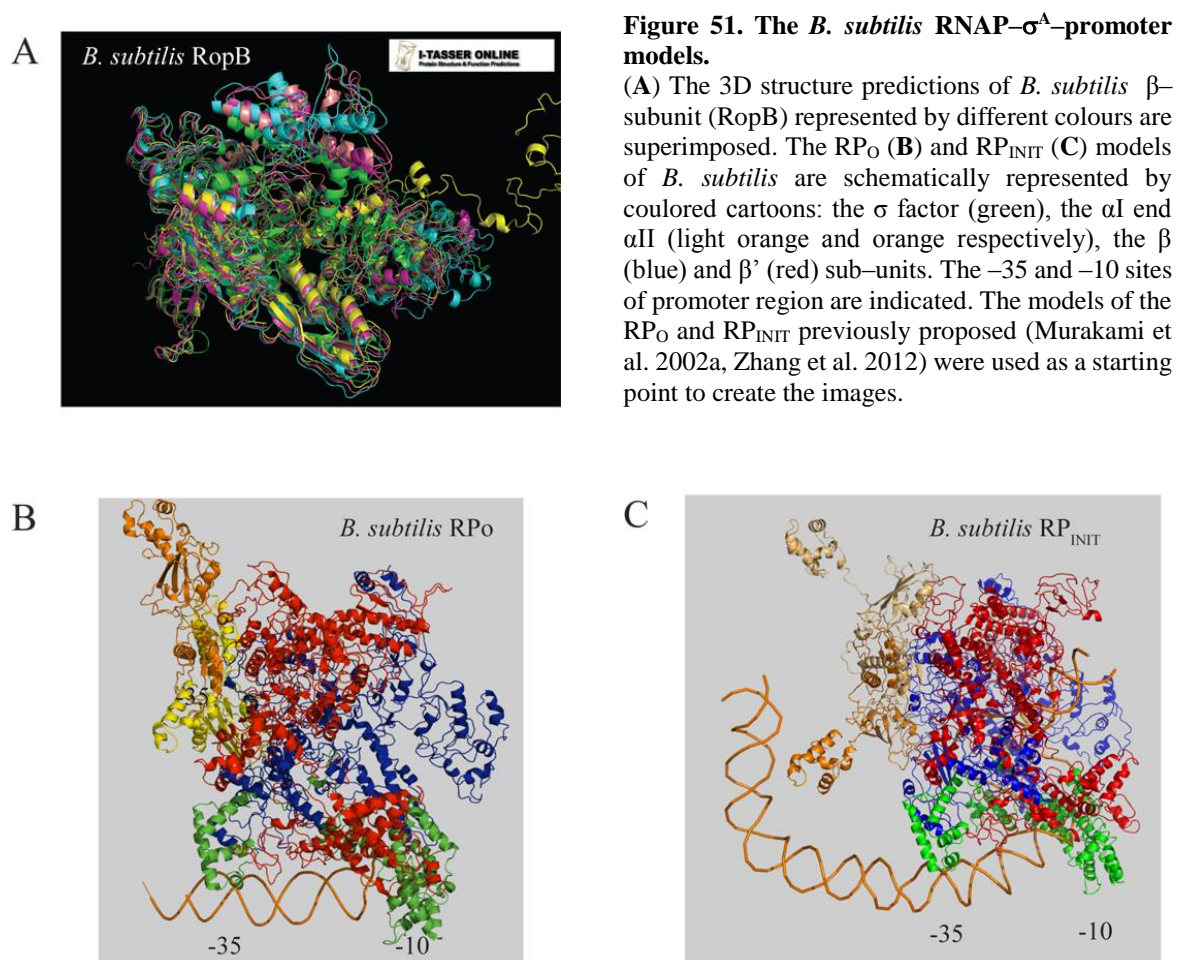
Aware of the limitations of rigid docking, finer simulation of the  $\omega_2$ – $\delta_2$  interaction should be continued using “flexible docking”. This method models the geometry changes of the interacting partners that may occur when a protein–protein complex is formed. Further factors as protein–



DNA complexes could be taken into account to generate action models. Although the hypothesis present in Figure 50 may be far from reality, they provided hints of molecular interactions or mechanisms that need to be empirically proved. This is an example of how bioinformatics tools can provide ideas for experimental work.

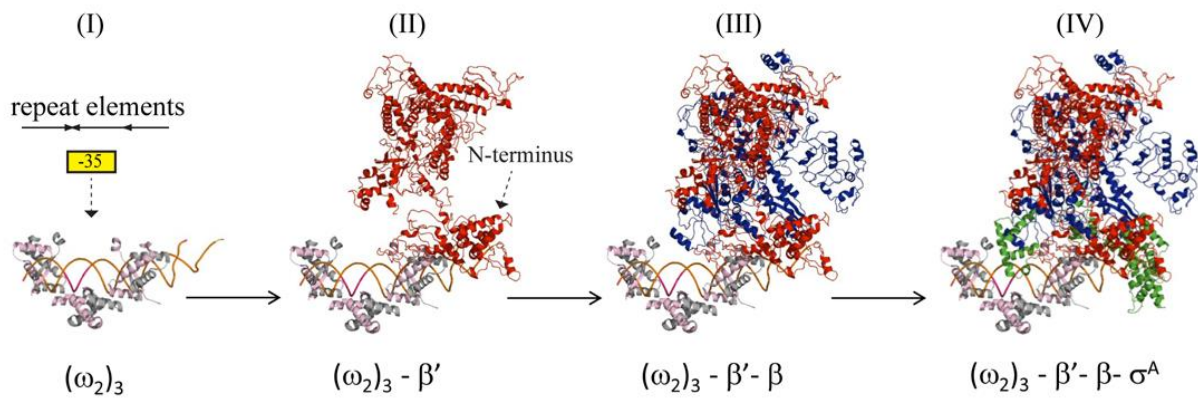
## 2.2. *B. subtilis* RNA polymerase: 3D structure prediction.

To date, the crystal structure of the *B. subtilis* RNAP is not available in the RCSB Protein Data Bank. However the basic architecture of bacterial RNAP is conserved as well as a high degree of structural similarity between the prokaryotic and eukaryotic RNAPs (Ebright 2000). For further information, see the crystals of the bacterial *T. aquaticus* RNAP core (Zhang et al. 1999), the yeast *S. cerevisiae* RNAP (polymerase II, Pol II) (Cramer, Bushnell and Kornberg 2001), and the Pol II ternary elongation complex with a 9–base pair (bp) DNA–RNA hybrid (Gnatt et al. 2001).

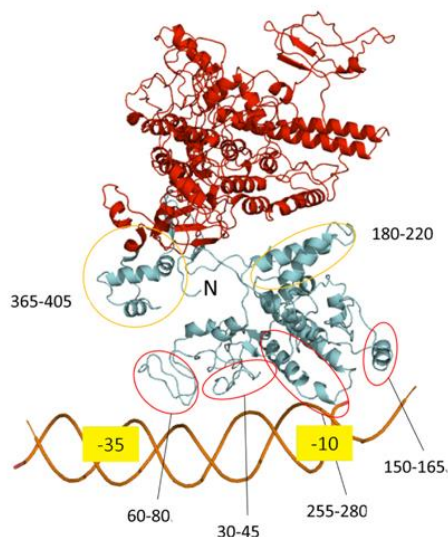


Based on these evidence and with the aim of produce a reliable model of *B. subtilis* RNAP holoenzyme bound to the promoter region, the protein structure of each RNAP subunit was independently predicted from the amino acids sequence using I-TASSER (Roy et al. 2010). For each subunit (RpoA, RpoB, RpoC, RpoD) up to five full-length atomic models were obtained. The five predicted structures were independently analysed (Fig. 51A) and superimposed one at the time with the *T. aquaticus* (Murakami et al. 2002a) (PDB: 1L9U) or the *T. thermophilus* RNAP–promoter co–crystals (Zhang et al. 2012) (PDB: 4G7H) to generate the *B. subtilis* RP<sub>C</sub> and RP<sub>INIT</sub> structural models, respectively (Fig. 51B and 51C). Importantly, the DNA promoter region of –35 and –10 sites and the relative positioning of the RNAP holoenzyme were resolved in the crystals. The *B. subtilis* RP<sub>C</sub> and RP<sub>INIT</sub> models obtained by this method overlaps quite closely to the starting crystals and finally they can be used for further analysis.

A



B



**Figure 52. The model of  $\omega_2$  and RNAP- $\sigma^A$  at  $P_\omega$  DNA.**

(A) The spatial occupancy model of  $\omega_2$ -RNAP- $\sigma^A$ - $P_\omega$ . The RNAP sub-units of *B. subtilis* are schematically represented by colored cartoons: the  $\sigma$  factor (green), the  $\beta$  (blue) and  $\beta'$  (red) sub-units. The –35 and –10 sites of promoter region are indicated by yellow boxes. Pink and grey colours represent the  $\omega_2$  dimers. (B) The  $\beta'$  sub-unit is represented isolated from the other RNAP sub-units bound to promoter. The N-terminal region is coloured in cyan. The neighbouring regions to the promoter and their respective residues are highlighted by red circles. The distal regions by orange circles.

With the aim to investigate whether the spatial arrangement can support the coexistence of both  $\omega_2$  and RNAP elements bounded at the promoter region, the hypothetical *B. subtilis* RNAP

structure and the co-crystals of  $\omega_2$  bound to inverted and to directed DNA repeats (PDB: 2BNZ and 2BNW respectively) were used to build this model.

The -35 was identified as starting point for modelling: (i) the last three heptad repeats of *parS1* ( $P_\delta$ ) and *parS2* ( $P_\omega$ ) sites are surrounding the -35 element of the promoter region (see Fig. 5) and (ii) the -35 sequence of  $P_\omega$  was also present in the sequence of both co-crystals.

A plausible reconstruction of last heptads has been reached by alignment of the -35 element of  $\omega_2$ -*parS* repeats (Fig. 52A, I). Afterwards, one sub-unit at a time was added sequentially to build a 3D model (Fig. 52A, II, III and IV). As observed in figure 52A, any clear steric hindrance is highlight by this model. In fact,  $\omega_2$  and RNAP appears to be recruited in a manner as to allow both elements to be simultaneously bound at the promoter regions in according with our experimental data. In addition, a detailed analysis on the isolated  $\beta'$  sub-unit bound to promoter region suggest important residues situated at the N-terminus of the proteins (Fig. 52B, in cyan) might establish contacts with  $\omega_2$  the bound to last repeats (see Fig. 47B, Fig. 52A, IV and 52B).

### 3. Resumen en Castellano.

#### 3.1. Introducción.

Los plásmidos son elementos genéticos extracromosomales no esenciales para la supervivencia del hospedador pero que frecuentemente le confieren ventajas selectiva como resistencia a antibióticos, la presencia de vías metabólicas útiles en ciertas condiciones ambientales, etc. Los plásmidos replican de manera autónoma y controlada, pueden transmitirse por sí mismos o ser movilizados por ellos mismos o por otro replicón. Se pueden dividir en dos grandes grupos: (a) de pequeño tamaño y alto número de copias, (b) de gran tamaño y bajo número de copias. Generalmente en los plásmidos del primer grupo, por el alto número de moléculas a distribuir, estocasticamente cada célula hija recibe al menos una copia del plásmido. Los plásmidos del segundo grupo requieren sistemas específicos para mantenerse en la célula. Por lo tanto el primer factor que influye en la estabilidad segregacional de un plásmido es el control del número de copia.

Para coexistir establemente con su hospedador, los plásmidos deben controlar su replicación de tal manera que se mantenga un número determinado de copias por célula. Otros sistemas activos que contribuyen a la estabilidad de los plásmidos son los sistemas de la resolución de multímeros, la partición activa de plásmidos o los sistemas de inhibición del crecimiento post-segregacional de las células que no hayan recibido al menos una copia del plásmido.

El plásmido pSM19035 de bajo número de copias resulta 10.000 veces más estable que lo esperado si el mecanismo de segregación fuera al azar. Este plásmido ha desarrollado diferentes sistemas que aseguran su estabilidad segregacional. Algunos de ellos participan activamente a la estabilidad y residen en regiones discretas (*segA*, *segB1*, *segB2*, *segC* y *segD*) del pSM19035 son responsables de la estabilidad segregacional, funcionando independientemente del replicón. La región *segA* está involucrada en la resolución de los multímeros que se forman tras la replicación del plásmido maximizando la segregación al azar. La región *segB1* es un operón formado por los genes  $\omega$ ,  $\varepsilon$  y  $\zeta$ . Aquí, el complejo  $\varepsilon\zeta$  es inactivo, pero para mantenerse como tal se requiere una continua síntesis de la antitoxina  $\varepsilon_2$ . La función principal de estabilización del plásmido se debe a que si no hay una continua síntesis del sistema toxina-antitoxina (TA), y después de degradarse  $\varepsilon_2$ , la toxina  $\zeta$  inhibe la proliferación de aquellas células que hayan perdido las copias del plásmido. La región *segB2* codifica por el sistema de partición compuesto por dos o más regiones centroméricas (*parS*) y dos proteínas homodiméricas,  $\delta_2$  (ParA) and  $\omega_2$  (ParB). Mientras el *segD* es un sistema que contribuye a coordinar el control del número de copias del plásmido como también los sistemas activos de segregación.

### 3.2. Objetivos.

El objetivo que se planteó al inicio de este trabajo fue el estudio del sistema de partición activa del plásmido pSM19035 y el análisis detallado de sus componentes, las proteínas  $\delta_2$  y  $\omega_2$ . Para comprender mejor los mecanismos de segregación del DNA plasmídico se propusieron los siguientes objetivos:

- 1 – Caracterización de los dominios de unión a ADN y de dimerización y oligomerización de la proteína  $\delta_2$ .
- 2 – Caracterización los dominios de interacción entre  $\omega_2$ - $\delta_2$ .
- 3 – Caracterización de los mecanismos moleculares de la modulación de la transcripción por parte de  $\omega_2$
- 5 – Influencia de las proteínas  $\omega_2$  y  $\delta_2$  en el control de la transcripción.
- 6 – Evaluación de posibles interacciones entre  $\omega_2$  y RNAP.

### 3.3. Resultados y Discusión.

La proteína  $\omega_2$  se une específicamente a los sitios *parS* formando un complejo de corta vida media (PC1) y regula la transcripción de los genes involucrados en el control del número de copias (*copS*) y de los sistemas de mantenimiento del plásmido ( $\delta$  y  $\omega$ - $\epsilon$ - $\zeta$ ). La proteína  $\delta_2$ , unida al ATP, tiene una unión inespecífica al ADN y forma complejos dinámicos (DC) en éste. El complejo PC1, tras la interacción con  $\delta_2$ , sufre una transición estructural que lleva a la formación de complejo de vida media larga (PC2, *parS*- $\omega_2$ ) y complejos de segregación (SC, *parS*- $\omega_2$ - $\delta_2$ ). El complejo  $\omega_2$ -*parS* facilita la reubicación de  $\delta_2$  hacia PC2 promoviendo la formación de complejos cuaternarios *parS*- $\omega_2$ - $\delta_2$ - $\omega_2$ -*parS* (BC, apareamiento de plásmidos mediado por los sitios *parS*) o *parS*- $\omega_2$ - $\delta_2$ -nsDNA (BC1, apareamiento plásmido-nucleoide). Relaciones equimolares de  $\omega_2$ : $\delta_2$  facilitan la transición estructural de  $\delta_2$  que desencadena la hidrólisis de ATP. En la forma ADP  $\delta_2$  disminuye su afinidad por el ADN y como resultado final el desensamblaje de los complejos de apareamiento. La unión cooperativa de  $\delta_2$  a diferentes zonas de la nucleoide genera un gradiente que dirige el posicionamiento y la partición de los plásmidos.

Los ciclos de ensamblaje y desensamblaje podrían atar los plásmidos al nucleoide de forma equidistante de para garantizar la segregación plasmídica mediante un mecanismo compatible con el “diffusion-ratchet” o el “DNA relay”.

Además,  $\omega_2$  uniéndose al promotor ( $P_\omega$ ) del operón  $\omega\epsilon\zeta$  facilita el reclutamiento de la RNA polimerasa de *Bacillus subtilis* (RNAP- $\sigma^A$ ) hacia el  $P_\omega$ . La ocupación parcial del promotor por parte de  $\omega_2$ , aumenta la transición de complejo cerrado (RP<sub>C</sub>) hacia complejo abierto (RP<sub>O</sub>) con mayor utilización de  $P_\omega$  por la RNAP- $\sigma^A$ . La ocupación total del promotor, en la cual  $\omega_2$  envuelve a  $P_\omega$  dejando el ADN de forma casi recta, facilita la formación de RP<sub>C</sub>, impidiendo la isomerización a la forma RP<sub>O</sub>. Las dos actividades de  $\omega_2$ , activador y represor de transcripción, requieren la interacción con el dominio N-terminal de la subunidad  $\beta'$  de la RNAP- $\sigma^A$ . Se describe un mecanismo poco caracterizado en el cual la proteína  $\omega_2$  controla la fluctuación del número de copias, la segregación activa del plásmido e indirectamente los genes de resistencia a los antibióticos mediante la estimulación o la inhibición de la formación de RP<sub>O</sub>.

### 3.4. Conclusiones.

- 1- El extremo C-terminal de la proteína  $\delta_2$  está implicado en la unión a ADN. Esta región no es esencial ni para la interacción entre  $\delta_2$ - $\omega_2$  o  $\delta_2$ - $\delta_2$  ni para la unión y la hidrólisis de ATP.
- 2- La interacción de  $\omega_2$  unida a *parS* con  $\delta_2$  facilita la transición estructural entre ambas proteínas y en relaciones de estequiometría, se estimula la actividad de ATPasa de  $\delta_2$ .
- 3- El extremo N-terminal de  $\omega_2$  interacciona con la región central de  $\delta_2$ . La región central de  $\delta_2$  también se requiere para la interacción  $\delta_2$ - $\delta_2$ . Los dominios de interacción de  $\omega_2$ - $\delta_2$  y  $\delta_2$ - $\delta_2$  se encuentran yuxtapuestos pero son distintos entre sí.
- 4- La formación de diferentes tipos de complejos cuaternarios *parS*- $\omega_2$ - $\delta_2$ -nsDNA requieren la unión de  $\delta_2$  a ATP pero no su hidrólisis. A concentraciones sub-estequiométricas, se promueve apareamiento entre plásmidos, pero a concentraciones estequiométricas se estimula la hidrólisis de ATP y el desensablaje del complejo cuaternario. La proteína  $\delta_2$  una vez intercambiado el ADP con ATP reformula de las estructuras de blobs en ADN.
- 5- La proteína  $\omega$ :YFP<sub>2</sub> se une a las regiones *parS* de los plásmidos formando focos discretos, mientras la proteína  $\delta$ :GFP<sub>2</sub> se asocia al ADN de manera no específica formando una nube de fluorescencia alrededor del nucleóide. La interacción entre  $\omega$ :YFP<sub>2</sub> unida a *parS* con  $\delta$ :GFP<sub>2</sub> facilita la captura y el apareamiento del plásmido con el nucleóide.
- 6- El ciclo continuo de la interacción  $\omega$ :YFP<sub>2</sub>- $\delta$ :GFP<sub>2</sub>, la hidrólisis de ATP y el desensablaje de los complejos apareados facilita la segregación de los plásmidos.

- 7- La región *parS* reconocida por  $\omega_2$  mapa aguas arriba de los promotores (P) de los genes *copS*,  $\delta$  y  $\omega$ . El complejo  $\omega_2$ -*parS* presenta dos propiedades: relaciones sub-estequiométricas activan mientras relaciones estequiométricas reprimen la transcripción del promotor.
- 8- La proteína  $\omega_2$  interacciona de manera cooperativa con el ADN del  $P_\omega$ ,  $\delta_2$  y RNAP- $\sigma^A$ . Las interacciones proteína-ADN y proteína-proteína son necesarias y suficientes para la activación y la represión de transcripción.
- 9- La proteína  $\omega_2$  promueve la formación de  $RP_C$  pero impide la isomerización a  $RP_O$ .
- 10- La proteína  $\omega_2$  unida al ADN del  $P_\omega$ , interacciona con la región N-terminal de la sub-unidad  $\beta'$  de la RNAP- $\sigma^A$ . Es el primer informe que describe este tipo de interacción.





## *References*



- Ah-Seng, Y., J. Rech, D. Lane & J. Y. Bouet (2013) Defining the role of ATP hydrolysis in mitotic segregation of bacterial plasmids. *PLoS Genet*, 9, e1003956.
- Aiyar, A. (2000) The use of CLUSTAL W and CLUSTAL X for multiple sequence alignment. *Methods Mol Biol*, 132, 221–41.
- Alonso, J. C., K. Shirahige & N. Ogasawara (1990) Molecular cloning, genetic characterization and DNA sequence analysis of the recM region of *Bacillus subtilis*. *Nucleic Acids Res*, 18, 6771–7.
- Alonso, J. C., A. C. Stiege, B. Dobrinski & R. Lurz (1993) Purification and properties of the RecR protein from *Bacillus subtilis* 168. *J Biol Chem*, 268, 1424–9.
- Anthony, L. C., I. Artsimovitch, V. Svetlov, R. Landick & R. R. Burgess (2000) Rapid purification of His(6)-tagged *Bacillus subtilis* core RNA polymerase. *Protein Expr Purif*, 19, 350–4.
- Arenson, T. A., O. V. Tsodikov & M. M. Cox (1999) Quantitative analysis of the kinetics of end-dependent disassembly of RecA filaments from ssDNA. *J Mol Biol*, 288, 391–401.
- Atmakuri, K., E. Cascales, O. T. Burton, L. M. Banta & P. J. Christie (2007) *Agrobacterium* ParA/MinD-like VirC1 spatially coordinates early conjugative DNA transfer reactions. *EMBO J*, 26, 2540–51.
- Aylett, C. H., Q. Wang, K. A. Michie, L. A. Amos & J. Lowe (2010) Filament structure of bacterial tubulin homologue TubZ. *Proc Natl Acad Sci U S A*, 107, 19766–71.
- Bae, B., E. Davis, D. Brown, E. A. Campbell, S. Wigneshweraraj & S. A. Darst (2013) Phage T7 Gp2 inhibition of *Escherichia coli* RNA polymerase involves misappropriation of sigma70 domain 1.1. *Proc Natl Acad Sci U S A*, 110, 19772–7.
- Barilla, D., E. Carmelo & F. Hayes (2007) The tail of the ParG DNA segregation protein remodels ParF polymers and enhances ATP hydrolysis via an arginine finger-like motif. *Proc Natl Acad Sci U S A*, 104, 1811–6.
- Barne, K. A., J. A. Bown, S. J. Busby & S. D. Minchin (1997) Region 2.5 of the *Escherichia coli* RNA polymerase sigma70 subunit is responsible for the recognition of the 'extended-10' motif at promoters. *EMBO J*, 16, 4034–40.
- Bartosik, A. A., K. Glabski, P. Jecz, K. Lasocki, M. Mikosa, D. Plochocka, C. M. Thomas & G. T. Jagura-Burdzy (2014) Dissection of the region of *Pseudomonas aeruginosa* ParA that is important for dimerization and interactions with its partner ParB. *Microbiology*.
- Behnke, D., H. Malke, M. Hartmann & F. Walter (1979) Post-transformational rearrangement of an in vitro reconstructed group-A streptococcal erythromycin resistance plasmid. *Plasmid*, 2, 605–16.
- Benoff, B., H. Yang, C. L. Lawson, G. Parkinson, J. Liu, E. Blatter, Y. W. Ebright, H. M. Berman & R. H. Ebright (2002) Structural basis of transcription activation: the CAP-alpha CTD-DNA complex. *Science*, 297, 1562–6.
- Bignell, C. & C. M. Thomas (2001) The bacterial ParA-ParB partitioning proteins. *J Biotechnol*, 91, 1–34.
- Bingle, L. E. & C. M. Thomas (2001) Regulatory circuits for plasmid survival. *Curr Opin Microbiol*, 4, 194–200.
- Birnboim, H. C. & J. Doly (1979) A rapid alkaline extraction procedure for screening recombinant plasmid DNA. *Nucleic Acids Res*, 7, 1513–23.
- Bochkareva, A. & N. Zenkin (2013) The sigma70 region 1.2 regulates promoter escape by unwinding DNA downstream of the transcription start site. *Nucleic Acids Res*, 41, 4565–72.
- Boeger, H., D. A. Bushnell, R. Davis, J. Griesenbeck, Y. Lorch, J. S. Strattan, K. D. Westover & R. D. Kornberg (2005) Structural basis of eukaryotic gene transcription. *FEBS Lett*, 579, 899–903.
- Bouet, J. Y. & D. Lane (2009) Molecular basis of the supercoil deficit induced by the mini-F plasmid partition complex. *J Biol Chem*, 284, 165–73.
- Brantl, S. & D. Behnke (1992a) Characterization of the minimal origin required for replication of the streptococcal plasmid pIP501 in *Bacillus subtilis*. *Mol Microbiol*, 6, 3501–10.
- Brantl, S. & D. Behnke (1992b) Copy number control of the streptococcal plasmid pIP501 occurs at three levels. *Nucleic Acids Res*, 20, 395–400.
- Brantl, S., D. Behnke & J. C. Alonso (1990) Molecular analysis of the replication region of the conjugative *Streptococcus agalactiae* plasmid pIP501 in *Bacillus subtilis*. Comparison with plasmids pAM beta 1 and pSM19035. *Nucleic Acids Res*, 18, 4783–90.
- Brantl, S., A. Nowak, D. Behnke & J. C. Alonso (1989) Revision of the nucleotide sequence of the *Streptococcus pyogenes* plasmid pSM19035 repS gene. *Nucleic Acids Res*, 17, 10110.
- Brantl, S. & E. G. Wagner (1994) Antisense RNA-mediated transcriptional attenuation occurs faster than stable antisense/target RNA pairing: an in vitro study of plasmid pIP501. *EMBO J*, 13, 3599–607.
- Brantl, S. & E. G. Wagner (1997) Dual function of the copR gene product of plasmid pIP501. *J Bacteriol*, 179, 7016–24.
- Breuner, A., R. B. Jensen, M. Dam, S. Pedersen & K. Gerdes (1996) The centromere-like parC locus of plasmid R1. *Mol Microbiol*, 20, 581–92.
- Browning, D. F. & S. J. Busby (2004) The regulation of bacterial transcription initiation. *Nat Rev Microbiol*, 2, 57–65.
- Bruand, C., S. D. Ehrlich & L. Janniere (1991) Unidirectional theta replication of the structurally stable *Enterococcus faecalis* plasmid pAM beta 1. *EMBO J*, 10, 2171–7.
- Bruand, C., S. D. Ehrlich & L. Janniere (1995) Primosome assembly site in *Bacillus subtilis*. *EMBO J*, 14, 2642–50.
- Bruand, C., E. Le Chatelier, S. D. Ehrlich & L. Janniere (1993) A fourth class of theta-replicating plasmids: the pAM beta 1 family from gram-positive bacteria. *Proc Natl Acad Sci U S A*, 90, 11668–72.
- Burgess, R. R., A. A. Travers, J. J. Dunn & E. K. Bautz (1969) Factor stimulating transcription by RNA polymerase. *Nature*, 221, 43–6.
- Camacho, A. G., R. Misselwitz, J. Behlke, S. Ayora, K. Welfle, A. Meinhart, B. Lara, W. Saenger, H. Welfle & J. C. Alonso (2002) In vitro and in vivo stability of the epsilon2zeta2 protein complex of the broad host-range *Streptococcus pyogenes* pSM19035 addiction system. *Biol Chem*, 383, 1701–13.
- Camara, B., M. Liu, J. Reynolds, A. Shadrin, B. Liu, K. Kwok, P. Simpson, R. Weinzierl, K. Severinov, E. Cota, S. Matthews & S. R. Wigneshweraraj (2010) T7 phage protein Gp2 inhibits the *Escherichia coli* RNA polymerase by antagonizing stable DNA strand separation near the transcription start site. *Proc Natl Acad Sci U S A*, 107, 2247–52.
- Campbell, E. A., O. Muzzin, M. Chlenov, J. L. Sun, C. A. Olson, O. Weinman, M. L. Trester-Zedlitz & S. A. Darst (2002) Structure of the bacterial RNA polymerase promoter specificity sigma subunit. *Mol Cell*, 9, 527–39.

- Carrasco, B., S. Ayora, R. Lurz & J. C. Alonso (2005) *Bacillus subtilis* RecU Holliday–junction resolvase modulates RecA activities. *Nucleic Acids Res*, 33, 3942–52.
- Castaing, J. P., J. Y. Bouet & D. Lane (2008) F plasmid partition depends on interaction of SopA with non–specific DNA. *Mol Microbiol*, 70, 1000–11.
- Ceglowski, P. & J. C. Alonso (1994) Gene organization of the *Streptococcus pyogenes* plasmid pDB101: sequence analysis of the *orf eta–copS* region. *Gene*, 145, 33–9.
- Ceglowski, P., A. Boitsov, N. Karamyan, S. Chai & J. C. Alonso (1993) Characterization of the effectors required for stable inheritance of *Streptococcus pyogenes* pSM19035–derived plasmids in *Bacillus subtilis*. *Mol Gen Genet*, 241, 579–85.
- Chen, Y. & H. P. Erickson (2008) In vitro assembly studies of FtsZ/tubulin–like proteins (TubZ) from *Bacillus* plasmids: evidence for a capping mechanism. *J Biol Chem*, 283, 8102–9.
- Chivers, P. T. & R. T. Sauer (2000) Regulation of high affinity nickel uptake in bacteria. Ni<sup>2+</sup>–Dependent interaction of NikR with wild–type and mutant operator sites. *J Biol Chem*, 275, 19735–41.
- Cramer, P., D. A. Bushnell & R. D. Kornberg (2001) Structural basis of transcription: RNA polymerase II at 2.8 angstrom resolution. *Science*, 292, 1863–76.
- Darst, S. A. (2001) Bacterial RNA polymerase. *Curr Opin Struct Biol*, 11, 155–62.
- Darst, S. A., N. Opalka, P. Chacon, A. Polyakov, C. Richter, G. Zhang & W. Wriggers (2002) Conformational flexibility of bacterial RNA polymerase. *Proc Natl Acad Sci U S A*, 99, 4296–301.
- de la Hoz, A. B., S. Ayora, I. Sitkiewicz, S. Fernandez, R. Pankiewicz, J. C. Alonso & P. Ceglowski (2000) Plasmid copy–number control and better–than–random segregation genes of pSM19035 share a common regulator. *Proc Natl Acad Sci U S A*, 97, 728–33.
- de la Hoz, A. B., F. Pratto, R. Misselwitz, C. Speck, W. Weihofen, K. Welfle, W. Saenger, H. Welfle & J. C. Alonso (2004) Recognition of DNA by omega protein from the broad–host range *Streptococcus pyogenes* plasmid pSM19035: analysis of binding to operator DNA with one to four heptad repeats. *Nucleic Acids Res*, 32, 3136–47.
- del Solar, G., J. C. Alonso, M. Espinosa & R. Diaz–Orejas (1996) Broad–host–range plasmid replication: an open question. *Mol Microbiol*, 21, 661–6.
- del Solar, G., A. M. Hernandez–Arriaga, F. X. Gomis–Ruth, M. Coll & M. Espinosa (2002) A genetically economical family of plasmid–encoded transcriptional repressors involved in control of plasmid copy number. *J Bacteriol*, 184, 4943–51.
- DeLano, F. A. (2002) The PyMol Molecular Graphics System [online] <http://www.pymol.org>.
- Dombroski, A. J., W. A. Walter, M. T. Record, Jr., D. A. Siegele & C. A. Gross (1992) Polypeptides containing highly conserved regions of transcription initiation factor sigma 70 exhibit specificity of binding to promoter DNA. *Cell*, 70, 501–12.
- Dove, S. L., S. A. Darst & A. Hochschild (2003) Region 4 of sigma as a target for transcription regulation. *Mol Microbiol*, 48, 863–74.
- Dunham, T. D., W. Xu, B. E. Funnell & M. A. Schumacher (2009) Structural basis for ADP–mediated transcriptional regulation by P1 and P7 ParA. *EMBO J*, 28, 1792–802.
- Dunny, G. M. & D. B. Clewell (1975) Transmissible toxin (hemolysin) plasmid in *Streptococcus faecalis* and its mobilization of a noninfectious drug resistance plasmid. *J Bacteriol*, 124, 784–90.
- Durkacz, B. W. & D. J. Sherratt (1973) Segregation kinetics of colicinogenic factor col E1 from a bacterial population temperature sensitive for DNA polymerase I. *Mol Gen Genet*, 121, 71–5.
- Ebersbach, G. & K. Gerdes (2005) Plasmid segregation mechanisms. *Annu Rev Genet*, 39, 453–79.
- Ebersbach, G., D. J. Sherratt & K. Gerdes (2005) Partition–associated incompatibility caused by random assortment of pure plasmid clusters. *Mol Microbiol*, 56, 1430–40.
- Ebright, R. H. (1993) Transcription activation at Class I CAP–dependent promoters. *Mol Microbiol*, 8, 797–802.
- Ebright, R. H. (2000) RNA polymerase: structural similarities between bacterial RNA polymerase and eukaryotic RNA polymerase II. *J Mol Biol*, 304, 687–98.
- Fogel, M. A. & M. K. Waldor (2006) A dynamic, mitotic–like mechanism for bacterial chromosome segregation. *Genes Dev*, 20, 3269–82.
- Fujita, M. & Y. Sadaie (1998) Rapid isolation of RNA polymerase from sporulating cells of *Bacillus subtilis*. *Gene*, 221, 185–90.
- Funnell, B. E. (2005) Partition–mediated plasmid pairing. *Plasmid*, 53, 119–25.
- Garner, E. C., C. S. Campbell & R. D. Mullins (2004) Dynamic instability in a DNA–segregating prokaryotic actin homolog. *Science*, 306, 1021–5.
- Garner, E. C., C. S. Campbell, D. B. Weibel & R. D. Mullins (2007) Reconstitution of DNA segregation driven by assembly of a prokaryotic actin homolog. *Science*, 315, 1270–4.
- Garner, M. M. & A. Revzin (1981) A gel electrophoresis method for quantifying the binding of proteins to specific DNA regions: application to components of the *Escherichia coli* lactose operon regulatory system. *Nucleic Acids Res*, 9, 3047–60.
- Gasteiger E., H. C., Gattiker A., Duvaud S., Wilkins M.R., Appel R.D., Bairoch A.; (2005) Protein Identification and Analysis Tools on the ExPASy Server; . (In) John M. Walker (ed): The Proteomics Protocols Handbook, Humana Press (2005). , pp. 571–607
- Gautier, R., D. Douguet, B. Antonny & G. Drin (2008) HELIQUEST: a web server to screen sequences with specific alpha–helical properties. *Bioinformatics*, 24, 2101–2.
- Gerdes, K., M. Howard & F. Szardenings (2010) Pushing and pulling in prokaryotic DNA segregation. *Cell*, 141, 927–42.
- Gerdes, K., J. Moller–Jensen & R. Bugge Jensen (2000) Plasmid and chromosome partitioning: surprises from phylogeny. *Mol Microbiol*, 37, 455–66.
- Ghasriani, H., T. Ducat, C. T. Hart, F. Hafizi, N. Chang, A. Al–Baldawi, S. H. Ayed, P. Lundstrom, J. A. Dillon & N. K. Goto (2010) Appropriation of the MinD protein–interaction motif by the dimeric interface of the bacterial cell division regulator MinE. *Proc Natl Acad Sci U S A*, 107, 18416–21.
- Ghosh, P., A. Ishihama & D. Chatterji (2001) *Escherichia coli* RNA polymerase subunit omega and its N–terminal domain bind full–length beta' to facilitate incorporation into the alpha2beta subassembly. *Eur J Biochem*, 268, 4621–7.

- Gnatt, A. L., P. Cramer, J. Fu, D. A. Bushnell & R. D. Kornberg (2001) Structural basis of transcription: an RNA polymerase II elongation complex at 3.3 Å resolution. *Science*, 292, 1876–82.
- Golovanov, A. P., D. Barilla, M. Golovanova, F. Hayes & L. Y. Lian (2003) ParG, a protein required for active partition of bacterial plasmids, has a dimeric ribbon–helix–helix structure. *Mol Microbiol*, 50, 1141–53.
- Gomis–Ruth, F. X., M. Sola, P. Acebo, A. Parraga, A. Guasch, R. Eritja, A. Gonzalez, M. Espinosa, G. del Solar & M. Coll (1998a) The structure of plasmid–encoded transcriptional repressor CopG unliganded and bound to its operator. *EMBO J*, 17, 7404–15.
- Gomis–Ruth, F. X., M. Sola, R. Perez–Luque, P. Acebo, M. T. Alda, A. Gonzalez, M. Espinosa, G. del Solar & M. Coll (1998b) Overexpression, purification, crystallization and preliminary X–ray diffraction analysis of the pMV158–encoded plasmid transcriptional repressor protein CopG. *FEBS Lett*, 425, 161–5.
- Gruber, S. & J. Errington (2009) Recruitment of condensin to replication origin regions by ParB/SpoOJ promotes chromosome segregation in *B. subtilis*. *Cell*, 137, 685–96.
- Gruber, T. M. & C. A. Gross (2003) Assay of *Escherichia coli* RNA polymerase: sigma–core interactions. *Methods Enzymol*, 370, 206–12.
- Gruber, T. M., D. Markov, M. M. Sharp, B. A. Young, C. Z. Lu, H. J. Zhong, I. Artsimovitch, K. M. Geszvain, T. M. Arthur, R. R. Burgess, R. Landick, K. Severinov & C. A. Gross (2001) Binding of the initiation factor sigma(70) to core RNA polymerase is a multistep process. *Mol Cell*, 8, 21–31.
- Hanahan, D. (1983) Studies on transformation of *Escherichia coli* with plasmids. *J Mol Biol*, 166, 557–80.
- Haugen, S. P., W. Ross & R. L. Gourse (2008) Advances in bacterial promoter recognition and its control by factors that do not bind DNA. *Nat Rev Microbiol*, 6, 507–19.
- Hayes, F. & D. Barilla (2006) The bacterial segrosome: a dynamic nucleoprotein machine for DNA trafficking and segregation. *Nat Rev Microbiol*, 4, 133–43.
- Heidrich, N. & S. Brantl (2007) Antisense RNA–mediated transcriptional attenuation in plasmid pIP501: the simultaneous interaction between two complementary loop pairs is required for efficient inhibition by the antisense RNA. *Microbiology*, 153, 420–7.
- Hellman, L. M. & M. G. Fried (2007) Electrophoretic mobility shift assay (EMSA) for detecting protein–nucleic acid interactions. *Nat Protoc*, 2, 1849–61.
- Hester, C. M. & J. Lutkenhaus (2007) Soj (ParA) DNA binding is mediated by conserved arginines and is essential for plasmid segregation. *Proc Natl Acad Sci U S A*, 104, 20326–31.
- Hochschild, A. & S. L. Dove (1998) Protein–protein contacts that activate and repress prokaryotic transcription. *Cell*, 92, 597–600.
- Holm, L. & P. Rosenstrom (2010) Dali server: conservation mapping in 3D. *Nucleic Acids Res*, 38, W545–9.
- Horodniceanu, T., D. H. Bouanchaud, G. Bieth & Y. A. Chabbert (1976) R plasmids in *Streptococcus agalactiae* (group B). *Antimicrob Agents Chemother*, 10, 795–801.
- Howard, M. & K. Gerdes (2010) What is the mechanism of ParA–mediated DNA movement? *Mol Microbiol*, 78, 9–12.
- Hu, Z., E. P. Gogol & J. Lutkenhaus (2002) Dynamic assembly of MinD on phospholipid vesicles regulated by ATP and MinE. *Proc Natl Acad Sci U S A*, 99, 6761–6.
- Hwang, L. C., A. G. Vecchiarelli, Y. W. Han, M. Mizuuchi, Y. Harada, B. E. Funnell & K. Mizuuchi (2013) ParA–mediated plasmid partition driven by protein pattern self–organization. *EMBO J*, 32, 1238–49.
- Igarashi, K. & A. Ishihama (1991) Bipartite functional map of the *E. coli* RNA polymerase alpha subunit: involvement of the C–terminal region in transcription activation by cAMP–CRP. *Cell*, 65, 1015–22.
- Ireton, K., N. W. t. Gunther & A. D. Grossman (1994) spoJ is required for normal chromosome segregation as well as the initiation of sporulation in *Bacillus subtilis*. *J Bacteriol*, 176, 5320–9.
- James, E., M. Liu, C. Sheppard, V. Mekler, B. Camara, B. Liu, P. Simpson, E. Cota, K. Severinov, S. Matthews & S. Wigneshweraraj (2012) Structural and mechanistic basis for the inhibition of *Escherichia coli* RNA polymerase by T7 Gp2. *Mol Cell*, 47, 755–66.
- Jensen, R. B., M. Dam & K. Gerdes (1994) Partitioning of plasmid R1. The parA operon is autoregulated by ParR and its transcription is highly stimulated by a downstream activating element. *J Mol Biol*, 236, 1299–309.
- Jensen, R. B., R. Lurz & K. Gerdes (1998) Mechanism of DNA segregation in prokaryotes: replicon pairing by parC of plasmid R1. *Proc Natl Acad Sci U S A*, 95, 8550–5.
- Jeon, Y. H., T. Yamazaki, T. Otomo, A. Ishihama & Y. Kyogoku (1997) Flexible linker in the RNA polymerase alpha subunit facilitates the independent motion of the C–terminal activator contact domain. *J Mol Biol*, 267, 953–62.
- Kammann, M., J. Laufs, J. Schell & B. Gronenborn (1989) Rapid insertional mutagenesis of DNA by polymerase chain reaction (PCR). *Nucleic Acids Res*, 17, 5404.
- Kang, G. B., H. E. Song, M. K. Kim, H. S. Youn, J. G. Lee, J. Y. An, J. S. Chun, H. Jeon & S. H. Eom (2010) Crystal structure of *Helicobacter pylori* MinE, a cell division topological specificity factor. *Mol Microbiol*, 76, 1222–31.
- Khoo, S. K., B. Loll, W. T. Chan, R. L. Shoeman, L. Ngoo, C. C. Yeo & A. Meinhart (2007) Molecular and structural characterization of the PezAT chromosomal toxin–antitoxin system of the human pathogen *Streptococcus pneumoniae*. *J Biol Chem*, 282, 19606–18.
- Kim, H. J., M. J. Calcutt, F. J. Schmidt & K. F. Chater (2000) Partitioning of the linear chromosome during sporulation of *Streptomyces coelicolor* A3(2) involves an oriC–linked parAB locus. *J Bacteriol*, 182, 1313–20.
- Kim, S. K. & J. Shim (1999) Interaction between F plasmid partition proteins SopA and SopB. *Biochem Biophys Res Commun*, 263, 113–7.
- King, G. F., Y. L. Shih, M. W. Maciejewski, N. P. Bains, B. Pan, S. L. Rowland, G. P. Mullen & L. I. Rothfield (2000) Structural basis for the topological specificity function of MinE. *Nat Struct Biol*, 7, 1013–7.
- Kovacic, R. T. (1987) The 0 degree C closed complexes between *Escherichia coli* RNA polymerase and two promoters, T7–A3 and lacUV5. *J Biol Chem*, 262, 13654–61.

- Kroos, L. & Y. T. Yu (2000) Regulation of sigma factor activity during *Bacillus subtilis* development. *Curr Opin Microbiol*, 3, 553–60.
- Krummel, B. & M. J. Chamberlin (1989) RNA chain initiation by *Escherichia coli* RNA polymerase. Structural transitions of the enzyme in early ternary complexes. *Biochemistry*, 28, 7829–42.
- Kulbachinskiy, A. & A. Mustaev (2006) Region 3.2 of the sigma subunit contributes to the binding of the 3'-initiating nucleotide in the RNA polymerase active center and facilitates promoter clearance during initiation. *J Biol Chem*, 281, 18273–6.
- Lane, W. J. & S. A. Darst (2010) Molecular evolution of multisubunit RNA polymerases: structural analysis. *J Mol Biol*, 395, 686–704.
- Larsen, R. A., C. Cusumano, A. Fujioka, G. Lim-Fong, P. Patterson & J. Pogliano (2007) Treadmilling of a prokaryotic tubulin-like protein, TubZ, required for plasmid stability in *Bacillus thuringiensis*. *Genes Dev*, 21, 1340–52.
- Le Chatelier, E., S. D. Ehrlich & L. Janniere (1994) The pAM beta 1 CopF repressor regulates plasmid copy number by controlling transcription of the repE gene. *Mol Microbiol*, 14, 463–71.
- Le Quere, B. & J. M. Ghigo (2009) BcsQ is an essential component of the *Escherichia coli* cellulose biosynthesis apparatus that localizes at the bacterial cell pole. *Mol Microbiol*, 72, 724–40.
- Lee, P. S. & A. D. Grossman (2006) The chromosome partitioning proteins Soj (ParA) and Spo0J (ParB) contribute to accurate chromosome partitioning, separation of replicated sister origins, and regulation of replication initiation in *Bacillus subtilis*. *Mol Microbiol*, 60, 853–69.
- Leipe, D. D., Y. I. Wolf, E. V. Koonin & L. Aravind (2002) Classification and evolution of P-loop GTPases and related ATPases. *J Mol Biol*, 317, 41–72.
- Leonard, T. A., P. J. Butler & J. Lowe (2005a) Bacterial chromosome segregation: structure and DNA binding of the Soj dimer—a conserved biological switch. *EMBO J*, 24, 270–82.
- Leonard, T. A., J. Moller-Jensen & J. Lowe (2005b) Towards understanding the molecular basis of bacterial DNA segregation. *Philos Trans R Soc Lond B Biol Sci*, 360, 523–35.
- Leplae, R., D. Geeraerts, R. Hallez, J. Guglielmini, P. Dreze & L. Van Melderen (2011) Diversity of bacterial type II toxin-antitoxin systems: a comprehensive search and functional analysis of novel families. *Nucleic Acids Res*, 39, 5513–25.
- Lewis, R. A., C. R. Bignell, W. Zeng, A. C. Jones & C. M. Thomas (2002) Chromosome loss from par mutants of *Pseudomonas putida* depends on growth medium and phase of growth. *Microbiology*, 148, 537–48.
- Licht, A., P. Freede & S. Brantl (2011) Transcriptional repressor CopR acts by inhibiting RNA polymerase binding. *Microbiology*, 157, 1000–8.
- Lim, H. C., I. V. Surovtsev, B. G. Beltran, F. Huang, J. Bewersdorf & C. Jacobs-Wagner (2014) Evidence for a DNA-relay mechanism in ParABS-mediated chromosome segregation. *Elife (Cambridge)*, 3, e02758.
- Lin, D. C. & A. D. Grossman (1998) Identification and characterization of a bacterial chromosome partitioning site. *Cell*, 92, 675–85.
- Lioy, V. S., C. Machon, M. Tabone, J. E. Gonzalez-Pastor, R. Daugelavicius, S. Ayora & J. C. Alonso (2012) The zeta toxin induces a set of protective responses and dormancy. *PLoS One*, 7, e30282.
- Lioy, V. S., M. T. Martin, A. G. Camacho, R. Lurz, H. Antelmann, M. Hecker, E. Hitchin, Y. Ridge, J. M. Wells & J. C. Alonso (2006) pSM19035-encoded zeta toxin induces stasis followed by death in a subpopulation of cells. *Microbiology*, 152, 2365–79.
- Lioy, V. S., F. Pratto, A. B. de la Hoz, S. Ayora & J. C. Alonso (2010a) Plasmid pSM19035, a model to study stable maintenance in Firmicutes. *Plasmid*, 64, 1–17.
- Lioy, V. S., O. Rey, D. Balsa, T. Pellicer & J. C. Alonso (2010b) A toxin-antitoxin module as a target for antimicrobial development. *Plasmid*, 63, 31–9.
- Liu, Y., Y. Wang, S. Schwarz, Y. Li, Z. Shen, Q. Zhang, C. Wu & J. Shen (2013) Transferable multiresistance plasmids carrying cfr in *Enterococcus* spp. from swine and farm environment. *Antimicrob Agents Chemother*, 57, 42–8.
- López Torrejón, G. 2002. Estudio de proteínas que intervienen en procesos de recombinación genética en bacterias LrpC y Hbsu de *Bacillus subtilis*, y las proteínas del plásmido pSM19035 de *Streptococcus pyogenes*. In *Ph.D. Universidad Autónoma de Madrid, Madrid*.
- Lutkenhaus, J. (2012) The ParA/MinD family puts things in their place. *Trends Microbiol*, 20, 411–8.
- Lutkenhaus, J. & M. Sundaramoorthy (2003) MinD and role of the deviant Walker A motif, dimerization and membrane binding in oscillation. *Mol Microbiol*, 48, 295–303.
- Lynch, A. S. & J. C. Wang (1995) SopB protein-mediated silencing of genes linked to the sopC locus of *Escherichia coli* F plasmid. *Proc Natl Acad Sci U S A*, 92, 1896–900.
- Ma, L. Y., G. King & L. Rothfield (2003) Mapping the MinE site involved in interaction with the MinD division site selection protein of *Escherichia coli*. *J Bacteriol*, 185, 4948–55.
- Majors, J. (1975) Initiation of in vitro mRNA synthesis from the wild-type lac promoter. *Proc Natl Acad Sci U S A*, 72, 4394–8.
- Malke, H. (1974) Genetics of resistance to macrolide antibiotics and lincomycin in natural isolates of *Streptococcus pyogenes*. *Mol Gen Genet*, 135, 349–67.
- Mateja, A., A. Szlachcic, M. E. Downing, M. Dobosz, M. Mariappan, R. S. Hegde & R. J. Keenan (2009) The structural basis of tail-anchored membrane protein recognition by Get3. *Nature*, 461, 361–6.
- Maxam, A. M. & W. Gilbert (1980) Sequencing end-labeled DNA with base-specific chemical cleavages. *Methods in enzymology*, 65, 499–560.
- McIntosh, J. R. (2012) Motors or dynamics: what really moves chromosomes? *Nat Cell Biol*, 14, 1234.
- Meinhart, A., C. Alings, N. Strater, A. G. Camacho, J. C. Alonso & W. Saenger (2001) Crystallization and preliminary X-ray diffraction studies of the epsilonzeta addiction system encoded by *Streptococcus pyogenes* plasmid pSM19035. *Acta Crystallogr D Biol Crystallogr*, 57, 745–7.
- Meinhart, A., J. C. Alonso, N. Strater & W. Saenger (2003) Crystal structure of the plasmid maintenance system epsilon/zeta: functional mechanism of toxin zeta and inactivation by epsilon 2 zeta 2 complex formation. *Proc Natl Acad Sci U S A*, 100, 1661–6.

- Miller, A., D. Wood, R. H. Ebricht & L. B. Rothman-Denes (1997) RNA polymerase beta' subunit: a target of DNA binding-independent activation. *Science*, 275, 1655–7.
- Miller, J. F. (1972) Molecular genetics; Experiments. *Cold Spring Harbor Laboratory (Cold Spring Harbor, N.Y.)*.
- Misselwitz, R., A. B. de la Hoz, S. Ayora, K. Welfle, J. Behlke, K. Murayama, W. Saenger, J. C. Alonso & H. Welfle (2001) Stability and DNA-binding properties of the omega regulator protein from the broad-host range *Streptococcus pyogenes* plasmid pSM19035. *FEBS letters*, 505, 436–40.
- Mohl, D. A. & J. W. Gober (1997) Cell cycle-dependent polar localization of chromosome partitioning proteins in *Caulobacter crescentus*. *Cell*, 88, 675–84.
- Moller-Jensen, J., J. Borch, M. Dam, R. B. Jensen, P. Roepstorff & K. Gerdes (2003) Bacterial mitosis: ParM of plasmid R1 moves plasmid DNA by an actin-like insertional polymerization mechanism. *Mol Cell*, 12, 1477–87.
- Monsalve, M., M. Mencia, F. Rojo & M. Salas (1996) Activation and repression of transcription at two different phage phi29 promoters are mediated by interaction of the same residues of regulatory protein p4 with RNA polymerase. *The EMBO journal*, 15, 383–91.
- Moritz, E. M. & P. J. Hergenrother (2007) Toxin-antitoxin systems are ubiquitous and plasmid-encoded in vancomycin-resistant enterococci. *Proc Natl Acad Sci U S A*, 104, 311–6.
- Motallebi-Veshareh, M., D. A. Rouch & C. M. Thomas (1990) A family of ATPases involved in active partitioning of diverse bacterial plasmids. *Mol Microbiol*, 4, 1455–63.
- Muller, J., S. Oehler & B. Muller-Hill (1996) Repression of lac promoter as a function of distance, phase and quality of an auxiliary lac operator. *J Mol Biol*, 257, 21–9.
- Murakami, K. S. & S. A. Darst (2003) Bacterial RNA polymerases: the whole story. *Curr Opin Struct Biol*, 13, 31–9.
- Murakami, K. S., S. Masuda, E. A. Campbell, O. Muzzin & S. A. Darst (2002a) Structural basis of transcription initiation: an RNA polymerase holoenzyme-DNA complex. *Science*, 296, 1285–90.
- Murakami, K. S., S. Masuda & S. A. Darst (2002b) Structural basis of transcription initiation: RNA polymerase holoenzyme at 4 Å resolution. *Science*, 296, 1280–4.
- Murakami, K. S., S. Masuda & S. A. Darst (2003) Crystallographic analysis of *Thermus aquaticus* RNA polymerase holoenzyme and a holoenzyme/promoter DNA complex. *Methods Enzymol*, 370, 42–53.
- Murayama, K., P. Orth, A. B. de la Hoz, J. C. Alonso & W. Saenger (2001a) Crystal structure of omega transcriptional repressor encoded by *Streptococcus pyogenes* plasmid pSM19035 at 1.5 Å resolution. *J Mol Biol*, 314, 789–96.
- Murayama, K., P. Orth, A. B. de la Hoz, J. C. Alonso & W. Saenger (2001b) Crystal structure of omega transcriptional repressor encoded by *Streptococcus pyogenes* plasmid pSM19035 at 1.5 Å resolution. *Journal of molecular biology*, 314, 789–96.
- Murray, H., H. Ferreira & J. Errington (2006) The bacterial chromosome segregation protein Spo0J spreads along DNA from parS nucleation sites. *Mol Microbiol*, 61, 1352–61.
- Mutschler, H., M. Gebhardt, R. L. Shoeman & A. Meinhart (2011) A novel mechanism of programmed cell death in bacteria by toxin-antitoxin systems corrupts peptidoglycan synthesis. *PLoS Biol*, 9, e1001033.
- Mutschler, H. & A. Meinhart (2011) epsilon/zeta systems: their role in resistance, virulence, and their potential for antibiotic development. *J Mol Med (Berl)*, 89, 1183–94.
- Ni, L., W. Xu, M. Kumaraswami & M. A. Schumacher (2010) Plasmid protein TubR uses a distinct mode of HTH-DNA binding and recruits the prokaryotic tubulin homolog TubZ to effect DNA partition. *Proc Natl Acad Sci U S A*, 107, 11763–8.
- Nordstrom, K. & S. J. Austin (1989) Mechanisms that contribute to the stable segregation of plasmids. *Annu Rev Genet*, 23, 37–69.
- Novick, R. P. (1987) Plasmid incompatibility. *Microbiol Rev*, 51, 381–95.
- O'Farrell, P. H. (1975) High resolution two-dimensional electrophoresis of proteins. *J Biol Chem*, 250, 4007–21.
- Ogden, T. H. & M. S. Rosenberg (2007) Alignment and topological accuracy of the direct optimization approach via POY and traditional phylogenetics via ClustalW + PAUP\*. *Syst Biol*, 56, 182–93.
- Park, K. T., W. Wu, K. P. Battaile, S. Lovell, T. Holyoak & J. Lutkenhaus (2011) The Min oscillator uses MinD-dependent conformational changes in MinE to spatially regulate cytokinesis. *Cell*, 146, 396–407.
- Park, K. T., W. Wu, S. Lovell & J. Lutkenhaus (2012) Mechanism of the asymmetric activation of the MinD ATPase by MinE. *Mol Microbiol*, 85, 271–81.
- Pedersen, K., S. K. Christensen & K. Gerdes (2002) Rapid induction and reversal of a bacteriostatic condition by controlled expression of toxins and antitoxins. *Mol Microbiol*, 45, 501–10.
- Perez-Cheeks, B. A., P. J. Planet, I. N. Sarkar, S. A. Clock, Q. Xu & D. H. Figurski (2012) The product of tadZ, a new member of the parA/minD superfamily, localizes to a pole in *Aggregatibacter actinomycetemcomitans*. *Mol Microbiol*, 83, 694–711.
- Perez-Rueda, E. & J. Collado-Vides (2000) The repertoire of DNA-binding transcriptional regulators in *Escherichia coli* K-12. *Nucleic Acids Res*, 28, 1838–47.
- Pettersen, E. F., T. D. Goddard, C. C. Huang, G. S. Couch, D. M. Greenblatt, E. C. Meng & T. E. Ferrin (2004) UCSF Chimera—a visualization system for exploratory research and analysis. *J Comput Chem*, 25, 1605–12.
- Pogliano, J., M. D. Sharp & K. Pogliano (2002) Partitioning of chromosomal DNA during establishment of cellular asymmetry in *Bacillus subtilis*. *J Bacteriol*, 184, 1743–9.
- Popp, D., W. Xu, A. Narita, A. J. Brzoska, R. A. Skurray, N. Firth, U. Ghoshdastider, Y. Maeda, R. C. Robinson & M. A. Schumacher (2010) Structure and filament dynamics of the pSK41 actin-like ParM protein: implications for plasmid DNA segregation. *J Biol Chem*, 285, 10130–40.
- Popp, D., A. Yamamoto, M. Iwasa, A. Narita, K. Maeda & Y. Maeda (2007) Concerning the dynamic instability of actin homolog ParM. *Biochem Biophys Res Commun*, 353, 109–14.
- Pratto, F. (2007) Análisis del sistema de partición activa del plásmido pSM19035 de *Streptococcus pyogenes*. *Ph.D. Universidad Autónoma de Madrid, Madrid*.

- Pratto, F., A. Cicek, W. A. Weihofen, R. Lurz, W. Saenger & J. C. Alonso (2008) Streptococcus pyogenes pSM19035 requires dynamic assembly of ATP-bound ParA and ParB on parS DNA during plasmid segregation. *Nucleic Acids Res*, 36, 3676–89.
- Pratto, F., Y. Suzuki, K. Takeyasu & J. C. Alonso (2009) Single-molecule analysis of protein-DNA complexes formed during partition of newly replicated plasmid molecules in Streptococcus pyogenes. *J Biol Chem*, 284, 30298–306.
- Pryor, E. E., Jr., E. A. Waligora, B. Xu, S. Dellos-Nolan, D. J. Wozniak & T. Hollis (2012) The transcription factor AmrZ utilizes multiple DNA binding modes to recognize activator and repressor sequences of Pseudomonas aeruginosa virulence genes. *PLoS Pathog*, 8, e1002648.
- Ptacin, J. L., S. F. Lee, E. C. Garner, E. Toro, M. Eckart, L. R. Comolli, W. E. Moerner & L. Shapiro (2010) A spindle-like apparatus guides bacterial chromosome segregation. *Nat Cell Biol*, 12, 791–8.
- Ptashne, M. (1986) Gene regulation by proteins acting nearby and at a distance. *Nature*, 322, 697–701.
- Pupov, D., N. Miropolskaya, A. Sevostyanova, I. Bass, I. Artsimovitch & A. Kulbachinskiy (2010) Multiple roles of the RNA polymerase {beta}' SW2 region in transcription initiation, promoter escape, and RNA elongation. *Nucleic Acids Res*, 38, 5784–96.
- Ramsey, D. M., P. J. Baynham & D. J. Wozniak (2005) Binding of Pseudomonas aeruginosa AlgZ to sites upstream of the algZ promoter leads to repression of transcription. *J Bacteriol*, 187, 4430–43.
- Raumann, B. E., M. A. Rould, C. O. Pabo & R. T. Sauer (1994) DNA recognition by beta-sheets in the Arc repressor-operator crystal structure. *Nature*, 367, 754–7.
- Ravin, N. V., J. Rech & D. Lane (2003) Mapping of functional domains in F plasmid partition proteins reveals a bipartite SopB-recognition domain in SopA. *J Mol Biol*, 329, 875–89.
- Reynolds, R. & M. J. Chamberlin (1992) Parameters affecting transcription termination by Escherichia coli RNA. II. Construction and analysis of hybrid terminators. *J Mol Biol*, 224, 53–63.
- Rhodiou, V. A. & S. J. Busby (1998) Positive activation of gene expression. *Curr Opin Microbiol*, 1, 152–9.
- Ringgaard, S., J. Lowe & K. Gerdes (2007) Centromere pairing by a plasmid-encoded type I ParB protein. *J Biol Chem*, 282, 28216–25.
- Ringgaard, S., K. Schirner, B. M. Davis & M. K. Waldor (2011) A family of ParA-like ATPases promotes cell pole maturation by facilitating polar localization of chemotaxis proteins. *Genes Dev*, 25, 1544–55.
- Ringgaard, S., J. van Zon, M. Howard & K. Gerdes (2009) Movement and equipositioning of plasmids by ParA filament disassembly. *Proc Natl Acad Sci U S A*, 106, 19369–74.
- Roberts, M. A., G. H. Wadhams, K. A. Hadfield, S. Tickner & J. P. Armitage (2012) ParA-like protein uses nonspecific chromosomal DNA binding to partition protein complexes. *Proc Natl Acad Sci U S A*, 109, 6698–703.
- Rodionov, O., M. Lobočka & M. Yarmolinsky (1999) Silencing of genes flanking the P1 plasmid centromere. *Science*, 283, 546–9.
- Rojo, F. & J. C. Alonso (1994) The beta recombinase from the Streptococcal plasmid pSM 19035 represses its own transcription by holding the RNA polymerase at the promoter region. *Nucleic Acids Res*, 22, 1855–60.
- Rost, B. (1996) PHD: predicting one-dimensional protein structure by profile-based neural networks. *Methods Enzymol*, 266, 525–39.
- Rosvoll, T. C., B. L. Lindstad, T. M. Lunde, K. Hegstad, B. Aasnaes, A. M. Hammerum, C. H. Lester, G. S. Simonsen, A. Sundsfjord & T. Pedersen (2012) Increased high-level gentamicin resistance in invasive Enterococcus faecium is associated with aac(6)Ie-aph(2)Ia-encoding transferable megaplasmids hosted by major hospital-adapted lineages. *FEMS Immunol Med Microbiol*, 66, 166–76.
- Roy, A., A. Kucukural & Y. Zhang (2010) I-TASSER: a unified platform for automated protein structure and function prediction. *Nat Protoc*, 5, 725–38.
- Saecker, R. M., M. T. Record, Jr. & P. L. Dehaseth (2011) Mechanism of bacterial transcription initiation: RNA polymerase – promoter binding, isomerization to initiation-competent open complexes, and initiation of RNA synthesis. *J Mol Biol*, 412, 754–71.
- Saecker, R. M., O. V. Tsodikov, K. L. McQuade, P. E. Schlux, Jr., M. W. Capp & M. T. Record, Jr. (2002) Kinetic studies and structural models of the association of E. coli sigma(70) RNA polymerase with the lambdaP(R) promoter: large scale conformational changes in forming the kinetically significant intermediates. *J Mol Biol*, 319, 649–71.
- Saint-Girons, I., N. Duchange, G. N. Cohen & M. M. Zakin (1984) Structure and autoregulation of the metJ regulatory gene in Escherichia coli. *J Biol Chem*, 259, 14282–5.
- Salje, J. (2010) Plasmid segregation: how to survive as an extra piece of DNA. *Crit Rev Biochem Mol Biol*, 45, 296–317.
- Sambrook J, F. E., Maniatis T (1989) Molecular cloning: a laboratory manual. Cold Spring Harbor Laboratory, Cold Spring Harbor, New York.
- Sambrook, J. & D. W. Russell (2006) SDS-Polyacrylamide Gel Electrophoresis of Proteins. *CSH Protoc*, 2006.
- Schindelin, H., C. Kisker, J. L. Schlessman, J. B. Howard & D. C. Rees (1997) Structure of ADP x AIF4(-)-stabilized nitrogenase complex and its implications for signal transduction. *Nature*, 387, 370–6.
- Schneider, C. A., W. S. Rasband & K. W. Eliceiri (2012) NIH Image to ImageJ: 25 years of image analysis. *Nat Methods*, 9, 671–5.
- Schofield, W. B., H. C. Lim & C. Jacobs-Wagner (2010) Cell cycle coordination and regulation of bacterial chromosome segregation dynamics by polarly localized proteins. *EMBO J*, 29, 3068–81.
- Schreiter, E. R. & C. L. Drennan (2007) Ribbon-helix-helix transcription factors: variations on a theme. *Nat Rev Microbiol*, 5, 710–20.
- Schreiter, E. R., M. D. Sintchak, Y. Guo, P. T. Chivers, R. T. Sauer & C. L. Drennan (2003) Crystal structure of the nickel-responsive transcription factor NikR. *Nat Struct Biol*, 10, 794–9.
- Schumacher, M. A. (2012) Bacterial plasmid partition machinery: a minimalist approach to survival. *Curr Opin Struct Biol*, 22, 72–9.



- Schumacher, M. A., T. C. Glover, A. J. Brzoska, S. O. Jensen, T. D. Dunham, R. A. Skurray & N. Firth (2007a) Segrosome structure revealed by a complex of ParR with centromere DNA. *Nature*, 450, 1268–71.
- Schumacher, M. A., A. Mansoor & B. E. Funnell (2007b) Structure of a four-way bridged ParB–DNA complex provides insight into P1 segrosome assembly. *J Biol Chem*, 282, 10456–64.
- Schumacher, M. A., K. M. Piro & W. Xu (2010) Insight into F plasmid DNA segregation revealed by structures of SopB and SopB–DNA complexes. *Nucleic Acids Res*, 38, 4514–26.
- Schumacher, M. A., Q. Ye, M. T. Barge, M. Zampini, D. Barilla & F. Hayes (2012) Structural mechanism of ATP-induced polymerization of the partition factor ParF: implications for DNA segregation. *J Biol Chem*, 287, 26146–54.
- Schwarz, F. V., V. Perreten & M. Teuber (2001) Sequence of the 50-kb conjugative multiresistance plasmid pRE25 from *Enterococcus faecalis* RE25. *Plasmid*, 46, 170–87.
- Sengupta, B., S. B. Laughlin & J. E. Niven (2010) Comparison of Langevin and Markov channel noise models for neuronal signal generation. *Phys Rev E Stat Nonlin Soft Matter Phys*, 81, 011918.
- Sharp, M. M., C. L. Chan, C. Z. Lu, M. T. Marr, S. Nechaev, E. W. Merritt, K. Severinov, J. W. Roberts & C. A. Gross (1999) The interface of sigma with core RNA polymerase is extensive, conserved, and functionally specialized. *Genes Dev*, 13, 3015–26.
- Sheridan, S. D., M. L. Opel & G. W. Hatfield (2001) Activation and repression of transcription initiation by a distant DNA structural transition. *Mol Microbiol*, 40, 684–90.
- Shin, M., S. Kang, S. J. Hyun, N. Fujita, A. Ishihama, P. Valentín-Hansen & H. E. Choy (2001) Repression of deoP2 in *Escherichia coli* by CytR: conversion of a transcription activator into a repressor. *EMBO J*, 20, 5392–9.
- Slatko, B. E. & L. M. Albright (2001) Denaturing gel electrophoresis for sequencing. *Curr Protoc Mol Biol*, Chapter 7, Unit 7.6.
- Sletvold, H., P. J. Johnsen, I. Hamre, G. S. Simonsen, A. Sundsfjord & K. M. Nielsen (2008) Complete sequence of *Enterococcus faecium* pVEF3 and the detection of an omega-epsilon-zeta toxin-antitoxin module and an ABC transporter. *Plasmid*, 60, 75–85.
- Sletvold, H., P. J. Johnsen, G. S. Simonsen, B. Aasnaes, A. Sundsfjord & K. M. Nielsen (2007) Comparative DNA analysis of two vanA plasmids from *Enterococcus faecium* strains isolated from poultry and a poultry farmer in Norway. *Antimicrob Agents Chemother*, 51, 736–9.
- Sletvold, H., P. J. Johnsen, O. G. Wikmark, G. S. Simonsen, A. Sundsfjord & K. M. Nielsen (2010) Tn1546 is part of a larger plasmid-encoded genetic unit horizontally disseminated among clonal *Enterococcus faecium* lineages. *J Antimicrob Chemother*, 65, 1894–906.
- Smith, T. L. & R. T. Sauer (1996) Dual regulation of open-complex formation and promoter clearance by Arc explains a novel repressor to activator switch. *Proc Natl Acad Sci U S A*, 93, 8868–72.
- Soberon, N. E., V. S. Liroy, F. Pratto, A. Volante & J. C. Alonso (2011) Molecular anatomy of the *Streptococcus pyogenes* pSM19035 partition and segrosome complexes. *Nucleic Acids Res*, 39, 2624–37.
- Somers, W. S. & S. E. Phillips (1992) Crystal structure of the met repressor-operator complex at 2.8 Å resolution reveals DNA recognition by beta-strands. *Nature*, 359, 387–93.
- Spiess, E. L., R. (1988) Electron Microscopic Analysis of Nucleic Acids and Nucleic Acid-Protein Complexes. *Methods in Microbiology*, Volume 20.
- Studier, F. W. (2005) Protein production by auto-induction in high density shaking cultures. *Protein Expr Purif*, 41, 207–34.
- Studier, F. W. & B. A. Moffatt (1986) Use of bacteriophage T7 RNA polymerase to direct selective high-level expression of cloned genes. *J Mol Biol*, 189, 113–30.
- Summers, D. K. (1991) The kinetics of plasmid loss. *Trends Biotechnol*, 9, 273–8.
- Surtees, J. A. & B. E. Funnell (2001) The DNA binding domains of P1 ParB and the architecture of the P1 plasmid partition complex. *J Biol Chem*, 276, 12385–94.
- Swapna, G., A. Chakraborty, V. Kumari, R. Sen & V. Nagaraja (2011) Mutations in beta' subunit of *Escherichia coli* RNA polymerase perturb the activator polymerase functional interaction required for promoter clearance. *Mol Microbiol*, 80, 1169–85.
- Szardenings, F., D. Guymer & K. Gerdes (2011) ParA ATPases can move and position DNA and subcellular structures. *Curr Opin Microbiol*, 14, 712–8.
- Taly, J. F., C. Magis, G. Bussotti, J. M. Chang, P. Di Tommaso, I. Erb, J. Espinosa-Carrasco, C. Kemena & C. Notredame (2011) Using the T-Coffee package to build multiple sequence alignments of protein, RNA, DNA sequences and 3D structures. *Nat Protoc*, 6, 1669–82.
- Tang, M., D. K. Bideshi, H. W. Park & B. A. Federici (2007) Iteron-binding ORF157 and FtsZ-like ORF156 proteins encoded by pBtoxis play a role in its replication in *Bacillus thuringiensis* subsp. israelensis. *J Bacteriol*, 189, 8053–8.
- Tovchigrechko, A. & I. A. Vakser (2006) GRAMM-X public web server for protein-protein docking. *Nucleic Acids Res*, 34, W310–4.
- Unterholzner, S. J., B. Poppenberger & W. Rozhon (2013) Toxin-antitoxin systems: Biology, identification, and application. *Mob Genet Elements*, 3, e26219.
- van den Ent, F., J. Møller-Jensen, L. A. Amos, K. Gerdes & J. Lowe (2002) F-actin-like filaments formed by plasmid segregation protein ParM. *EMBO J*, 21, 6935–43.
- van Vliet, A. H., F. D. Ernst & J. G. Kusters (2004) NikR-mediated regulation of *Helicobacter pylori* acid adaptation. *Trends Microbiol*, 12, 489–94.
- van Vliet, A. H., S. W. Poppelaars, B. J. Davies, J. Stoof, S. Bereswill, M. Kist, C. W. Penn, E. J. Kuipers & J. G. Kusters (2002) NikR mediates nickel-responsive transcriptional induction of urease expression in *Helicobacter pylori*. *Infect Immun*, 70, 2846–52.
- Vassilyev, D. G., S. Sekine, O. Laptenko, J. Lee, M. N. Vassilyeva, S. Borukhov & S. Yokoyama (2002) Crystal structure of a bacterial RNA polymerase holoenzyme at 2.6 Å resolution. *Nature*, 417, 712–9.
- Vassilyev, D. G., M. N. Vassilyeva, A. Perederina, T. H. Tahirov & I. Artsimovitch (2007a) Structural basis for transcription elongation by bacterial RNA polymerase. *Nature*, 448, 157–62.

- Vassilyev, D. G., M. N. Vassilyeva, J. Zhang, M. Palangat, I. Artsimovitch & R. Landick (2007b) Structural basis for substrate loading in bacterial RNA polymerase. *Nature*, 448, 163–8.
- Vecchiarelli, A. G. & B. E. Funnell (2013) Probing the N-terminus of ParB using cysteine-scanning mutagenesis and thiol modification. *Plasmid*, 70, 86–93.
- Vecchiarelli, A. G., Y. W. Han, X. Tan, M. Mizuuchi, R. Ghirlando, C. Biertumpfel, B. E. Funnell & K. Mizuuchi (2010) ATP control of dynamic P1 ParA–DNA interactions: a key role for the nucleoid in plasmid partition. *Mol Microbiol*, 78, 78–91.
- Vecchiarelli, A. G., L. C. Hwang & K. Mizuuchi (2013) Cell-free study of F plasmid partition provides evidence for cargo transport by a diffusion–ratchet mechanism. *Proc Natl Acad Sci U S A*, 110, E1390–7.
- Vecchiarelli, A. G., K. Mizuuchi & B. E. Funnell (2012) Surfing biological surfaces: exploiting the nucleoid for partition and transport in bacteria. *Mol Microbiol*, 86, 513–23.
- Vecchiarelli, A. G., M. A. Schumacher & B. E. Funnell (2007) P1 partition complex assembly involves several modes of protein–DNA recognition. *J Biol Chem*, 282, 10944–52.
- Vo, N. V., L. M. Hsu, C. M. Kane & M. J. Chamberlin (2003) In vitro studies of transcript initiation by Escherichia coli RNA polymerase. 3. Influences of individual DNA elements within the promoter recognition region on abortive initiation and promoter escape. *Biochemistry*, 42, 3798–811.
- Vogel, U. & K. F. Jensen (1994) The RNA chain elongation rate in Escherichia coli depends on the growth rate. *J Bacteriol*, 176, 2807–13.
- Volante, A., Soberón, N.E., Ayora, S. and Alonso, J.C. (2014) The interplay between different stability systems contributes to faithful segregation: Streptococcus pyogenes pSM19035 as a model. *Microbiol Spectrum*.
- Wang, J. D., M. E. Rokop, M. M. Barker, N. R. Hanson & A. D. Grossman (2004) Multicopy plasmids affect replisome positioning in Bacillus subtilis. *J Bacteriol*, 186, 7084–90.
- Waterhouse, A. M., J. B. Procter, D. M. Martin, M. Clamp & G. J. Barton (2009) Jalview Version 2—a multiple sequence alignment editor and analysis workbench. *Bioinformatics*, 25, 1189–91.
- Weihofen, W. A., A. Cicek, F. Pratto, J. C. Alonso & W. Saenger (2006) Structures of omega repressors bound to direct and inverted DNA repeats explain modulation of transcription. *Nucleic Acids Res*, 34, 1450–8.
- Welfle, K., F. Pratto, R. Misselwitz, J. Behlke, J. C. Alonso & H. Welfle (2005) Role of the N-terminal region and of beta-sheet residue Thr29 on the activity of the omega2 global regulator from the broad-host range Streptococcus pyogenes plasmid pSM19035. *Biol Chem*, 386, 881–94.
- Werner, F. (2007) Structure and function of archaeal RNA polymerases. *Mol Microbiol*, 65, 1395–404.
- Werner, F. (2008) Structural evolution of multisubunit RNA polymerases. *Trends Microbiol*, 16, 247–50.
- Werner, F. & D. Grohmann (2011) Evolution of multisubunit RNA polymerases in the three domains of life. *Nat Rev Microbiol*, 9, 85–98.
- Williams, D. R., D. P. Macartney & C. M. Thomas (1998) The partitioning activity of the RK2 central control region requires only incC, korB and KorB-binding site O(B)3 but other KorB-binding sites form destabilizing complexes in the absence of O(B)3. *Microbiology*, 144 ( Pt 12), 3369–78.
- Wilson, G. A. & K. F. Bott (1968) Nutritional factors influencing the development of competence in the Bacillus subtilis transformation system. *J Bacteriol*, 95, 1439–49.
- Wintjens, R. & M. Rooman (1996) Structural classification of HTH DNA-binding domains and protein–DNA interaction modes. *J Mol Biol*, 262, 294–313.
- Wittig, I., H. P. Braun & H. Schagger (2006) Blue native PAGE. *Nat Protoc*, 1, 418–28.
- Wu, W., K. T. Park, T. Holyoak & J. Lutkenhaus (2011) Determination of the structure of the MinD–ATP complex reveals the orientation of MinD on the membrane and the relative location of the binding sites for MinE and MinC. *Mol Microbiol*, 79, 1515–28.
- Wu, Y., Q. Li & X. Z. Chen (2007) Detecting protein–protein interactions by Far western blotting. *Nat Protoc*, 2, 3278–84.
- Yamaichi, Y. & H. Niki (2000) Active segregation by the Bacillus subtilis partitioning system in Escherichia coli. *Proc Natl Acad Sci U S A*, 97, 14656–61.
- Yanisch-Perron, C., J. Vieira & J. Messing (1985) Improved M13 phage cloning vectors and host strains: nucleotide sequences of the M13mp18 and pUC19 vectors. *Gene*, 33, 103–19.
- Youderian, P., S. Bouvier & M. M. Susskind (1982) Sequence determinants of promoter activity. *Cell*, 30, 843–53.
- Yuzenkova, Y., N. Zenkin & K. Severinov (2008) Mapping of RNA polymerase residues that interact with bacteriophage Xp10 transcription antitermination factor p7. *J Mol Biol*, 375, 29–35.
- Zhang, G., E. A. Campbell, L. Minakhin, C. Richter, K. Severinov & S. A. Darst (1999) Crystal structure of Thermus aquaticus core RNA polymerase at 3.3 Å resolution. *Cell*, 98, 811–24.
- Zhang, G. & S. A. Darst (1998) Structure of the Escherichia coli RNA polymerase alpha subunit amino-terminal domain. *Science*, 281, 262–6.
- Zhang, Y., Y. Feng, S. Chatterjee, S. Tuske, M. X. Ho, E. Arnold & R. H. Ebright (2012) Structural basis of transcription initiation. *Science*, 338, 1076–80.
- Zhu, W., N. C. Clark, L. K. McDougal, J. Hageman, L. C. McDonald & J. B. Patel (2008) Vancomycin-resistant Staphylococcus aureus isolates associated with Inc18-like vanA plasmids in Michigan. *Antimicrob Agents Chemother*, 52, 452–7.
- Zielenkiewicz, U. & P. Ceglowski (2005) The toxin–antitoxin system of the streptococcal plasmid pSM19035. *J Bacteriol*, 187, 6094–105.





**Cover inspired by Osvaldo Cavandoli**